Epigenetic Regulation of Osteoblast Differentiation

Dissertation

for the award of the degree

"Doctor of Philosophy (Ph.D)"

Division of Mathematics and Natural Sciences

of the Georg-August University Göttingen

within the doctoral program "Genes and Development"

of the Georg-August University School of Science (GAUSS)

Submitted by

Zeynab Najafova

born in Baku, Azerbaijan

Göttingen, 2016

Thesis Supervisor:

Prof. Dr. Steven A. Johnsen

Thesis Committee Members:

Prof. Dr. Steven A. Johnsen (Reviewer)
Clinic for General, Visceral and Pediatric Surgery
University Medical Center Göttingen

Prof. Dr. Matthias Dobbelstein (Reviewer)
Department of Molecular Oncology
University Medical Center Gottingen

Prof. Dr. Gregor Bucher
Department of Developmental Biology
Georg-August-University Göttingen

Date of oral examination: August 9, 2016

Affidavit

I hereby declare that the PhD thesis entitled “Epigenetic Regulation of Osteoblast Differentiation” has been written independently and with no other sources and aids than quoted.

_____

Zeynab Najafova

June, 2016

Göttingen

“To my Father, who seeded the love for science in me. He always encouraged me to follow my dreams and settle for nothing but the best”.

Table of Contents:

LIST OF FIGURES

ABBREVIATIONS

µCT	Micro-computer tomography
µg	Microgram
µl	Microliter
4OHT	4-hydroxy-tamoxifen
7sk snRNA	7SK small nuclear RNA (snRNA)
ALB1	Albumin 1 gene
ALPL	Alkaline phosphatase, liver/bone/kidney gene
AP-1	Activator protein-1
AR	Androgen receptor
ASBMR	American Society for Bone Mineral Research
ASF1A	Anti-silencing function 1 homolog A histone chaperone
ATP	Adenosine triphosphate
B.Pm	Bone perimeter
BD	Bromodomain
BET	Bromodomain and extraterminal domain family
BFR	Bone formation rate
BGLAP, OC	Bone gamma-carboxyglutamate protein or Osteocalcin
BID	Basic residue-enriched interaction domain
BMI1	B lymphoma Mo-MLV insertion region 1 homolog
BMP	Bone morphogenic protein
bp	base pair
BPO	Benzoylperoxid
BRD4	Bromodomain containing protein 4
BRG1	Brahma-related gene 1
BS	Bone surface
BV	Bone volume
C/EBP	CCAAT/enhancer binding protein

Ca2+	Calcium ion 2+
CDH11	Cadherin 11
CDK9	Cyclin-dependent kinase 9
CDKN1A	Cyclin-dependent kinase inhibitor 1
CEAS	Cis-regulatory Element Annotation System
c-FOS	Cellular Finkel-Biskis-Jinkins osteosarcoma gene
CGI	CpG island
CHD	Chromodomain-Helicase-DNA binding
ChIP	Chromatin immunoprecipitation
CO2	Carbon dioxide
COL10A1	Collagen type X alpha 1 chain
COL1A1	Collagen type I alpha 1
CpG	Cytosine and guanine separated by one phosphate dinucleotide
CRC	Chromatin remodeling complex
Cre	Causes recombination (recombinase)
DCN	Decorin
DEPC	Diethylpyrocarbonate
DESeq	Differential expression analysis for sequence count data
DI	Deionized
DIF	Differentiated state
DiffBind	Differential Binding Analysis of ChIP-Seq peak data
DLX5	Distal-Less Homeobox 5
DMEM	Dulbecco's Modified Eagle Medium
DMP1	Dentin matrix acidic phosphoprotein 1
DMSO	Dimethyl sulfoxide
DNA	Deoxyribonucleic acid
DNMT	DNA methyltransferase
dNTP	Deoxynucleotide Triphosphates
DOT1L	Disruptor of telomeric silencing 1-like

DRB	5,6-Dichloro-1-β-D-ribofuranosylbenzimidazole
DSIF	DRB Sensitivity Inducing Factor
DUB	Deubiquitinating enzymes
dUTP	Deoxyuridine Triphosphate
E2	Estradiol
EDTA	Ethylenediaminetetraacetic acid
ELN	Elastin
EpiCSeg	Epigenome Count-based Segmentation
ER	Estrogen receptor
ERK	Extracellular signal-regulated kinase
ERT2	Estrogen receptor that binds tamoxifen
ES cell	Embryonic stem cell
ET	Extraterminal
EZH2	Enhancer of zeste homolog 2
FA	Formaldehyde
FACT	Facilitates chromatin transcription
FBS	Fetal bovine serum
FCS	Fetal calf serum
FDR	False discovery rate
FGF	Fibroblast growth factor
Flox	Gene/DNA region flanked by two LoxP sites
FLP	Flippase
FOSL2	FOS-like antigen 2
FOXA1	Forkhead Box A1
FRT	Flippase recognition target
GATA-4	GATA-sequence binding protein-4
GC	Guanine-cytosine
Gcn5	General control of amino-acid synthesis, yeast, homolog-like 2
GLI1, 2, 3	Glioma-associated oncogene family zinc finger 1, 2, 3

GNAT	Gcn5-related N-acetyltransferases
GO	Gene ontology
GR	Glucocorticoid receptor
GRE	Glucocorticoid response element
GREAT	Genomic regions enrichment of annotations tool
GSEA	Gene set enrichment analysis
H2A	Histone H2A
H2B	Histone H2B
H2Bub1 (H2BK120ub1)	Histone H2B monoubiquitinated at lysine (K) 120 residue
H3	Histone H3
H3K27ac	Histone H3 acetylated at lysine (K) 27 residue
H4	Histone H4
hASC	Human adipose derived (mesenchymal) stem cells
HAT	Histone acetyltransferase
HDAC	Histone deacetylase
HDI	HDAC inhibitor
HDM	Histone demethylase
HET	Heterozygote
HEXIM	Hexamethylene bisacetamide Inducible protein
hFOB	Human fetal osteoblast
HIRA	histone cell cycle regulation-defective homolog A
HMT	Histone methylthansferase
HRP	Horseradish peroxidase
HSC	Hematopoietic stem cell
HTSeq	High-throughput sequencing data analysis
IBSP	Integrin-binding sialoprotein
IDG-SW3	Immortomouse/Dmp1-GFP-SW3
IgG	Immunoglobulin G
IGV	Integrative Genomics Viewer

Ihh	Indian hedgehog
IL-1	Interleukin-1
INO80	Inositol requiring mutant 80 (ATPase)
IP	Immunoprecipitation
ISWI	Imitation switch family of chromatin remodellers
JMJD6	Jumonji Domain Containing 6
JQ1	(S)-tert-butyl 2-(4-(4-chlorophenyl)-2,3,9-trimethyl-6H-thieno[3,2-f][1,2,4]triazolo[4,3-a][1,4]diazepin-6-yl)acetate, BET inhibitor
JUND	Jun D proto-oncogene
KAT	Lysine acetyltransferase
Kb	Kilobase pair
KDM4B	Lysine (K)-Specific Demethylase 4B
KO	Knockout
LacZ	Lactose operon Z (β-galactosidase gene product)
LARP7	La Ribonucleoprotein Domain Family, Member 7
lnRNA	long non-coding RNA
LoxP	Locus of Crossover in P1 (Cre recombinase recognition site)
LSD1	Lysine (K)-specific demethylase 1A
L-SOX5	SRY-box 5
MACS	Model-based analysis for ChIP-seq
MAR	Mineral apposition rate
MBP	Methyl-CpG binding proteins
MCF10A	Michigan Cancer Foundation-10A cells
MCF7	Michigan Cancer Foundation-7 cells
M-CSF	Macrophage colony-stimulating factor
MEF2c	Myocyte enhancer factor 2C
MEF2d	Myocyte enhancer factor 2d
MEM	Minimum Essential Medium Eagle
MEPE	Matrix extracellular phosphoglycoprotein
mg	milligram

min	minutes
miRNA	micro RNA
ml	milliliter
MMA	Methacrylate
MMP9	Matrix metallopeptidase 9
MOPS	3-(N-morpholino)propanesulfonic acid
MSC	Mesenchymal stem cells
MYST	Moz/Ybf2/Sas2/Tip60 histone acetyltransferase family
N.OC	Number of osteoclasts
Na	Sodium
ncRNA	Non-coding RNA
NELF	Negative elongation factor
Neo	Neomycin
NFATC1	Nuclear factor of activated T-cells 1
NF-kB	Nuclear factor 'kappa-light-chain-enhancer' of activated B-cells
NHOST	Normal human osteoblast
NPS	N-terminal cluster of phosphorylation sites
NSD3	Nuclear receptor SET domain -3
OB	Osteoblast
OC	Osteoclast
Oc.S	Osteoclast surface
OPG (TNFRFS11B)	Osteoprotegerin or Tumor necrosis factor receptor superfamily member 11B
OPN	Osteopontin
OSR2	Odd-skipped-related 2
OSX	Osterix gene
P/S	Penicillin/Streptomycin solution
P300/CBP	E1A (adenovirus early region 1A) binding protein p300 / cAMP-response element-binding protein
padj	P-value adjusted

PBS	Phosphate buffered saline
PCA	Principal component analysis
PCAF	p300/CBP-associated factor
PcG	Polycomb group proteins
PDID	Phosphorylation dependent interaction domain
PFA	Paraformaldehyde
Pi	Inorganic phosphate
PID	P-TEFb interaction domain
PKC-δ	Protein kinase C delta
PPARγ	Peroxisome proliferator-activated receptor gamma
PPi	Inorganic pyrophosphate
PRC	Polycomb repressive complex
pre-miRNA	Precursor miRNA
pri-miRNA	Primary miRNA
PRMT	Protein arginine methyltransferases
PRX1	Paired related homeobox 1
PTH	Parathyroid hormone
PTHrP	Parathyroid hormone-related protein
qRT-PCR	quantitative real-time poly chain reaction
RANK	Receptor activator of nuclear factor κ B
RANKL	Receptor activator of nuclear factor kappa-B ligand
RBP2	Retinol Binding Protein 2
RelA	V-Rel Avian Reticuloendotheliosis Viral Oncogene Homolog A
ReMap	Regulatory Map of Transcription Factor Binding Sites
RING1B	Ring Finger Protein 1B
RIPA	Radioimmunoprecipitation assay buffer
RNA	Ribonucleic acid
RNAi	RNA interference
RNAPII	RNA polymerase II

RNF20	Ring finger protein 20
RNF40	Ring finger protein 40
RPD3	Right parietal dorsal 3
RPKM	Reads per kilobase per million
RPLP0	Ribosomal Protein, Large, P0
rpm	Rounds per minute
RSAT	Regulatory Sequence Analysis Tools
RT	Room temperature
RUNX3	Runt related transcription factor 3
RXR	Retinoic x receptor
SAHA	Suberanilohydroxamic acid
SDS	Sodium dodecyl sulfate
sec	second
SET	Su(var)3-9, Enhancer of Zeste, Trithorax
siBRD4	siRNA targeting BRD4
siCNTR	non-targeting control riRNA
siRNA	small interfering RNA
SMAD	Signal transducers 'mothers against decapentaplegic homologues'
SOST	Sclerostin
SOX	SRY-box gene
SOX9	SRY (Sex Determining Region Y)-Box 9
ssRNA	single-stranded RNA
SSRP1	Structure-specific recognition protein-1
STAT5	Signal transducer and activator of transcription 5
SWI/SNF	SWItch/Sucrose Non-Fermentable
TAE	Tris-acetate-EDTA
Tb.N	Trabecular number
Tb.Sp	Trabecular separation
Tb.Th	Trabecular thicknes

TBS	Tris-buffered saline
TE	Tris-EDTA
TEAD1	TEA (transcriptional enhancer factor) domain transcription factor 1
TET	Ten-eleven translocation methylcytosine dioxygenase
TFF1	Trefoil factor 1
TGFBR2	Transforming Growth Factor, Beta Receptor II
TGF-β	Transforming growth factor beta
THBS2	Thrombospondin-2
TR	Transcribed region
TRAP	Tartrate-resistant acid phosphatase
TSS	Transcription start site
TTS	Transcription termination site
TV	Tissue volume
UND	Undifferentiated state
USP22	Ubiquitin-specific peptidase 22
UTR	Untranslated region
VDR	Vitamin D receptor
VDRE	Vitamin D response element
VEGF	Vascular endothelial growth factor
VEH	Vehicle
Wnt	Abbreviation from two words: Drosophila segment polarity gene Wingless and the vertebrate homolog, Integrated-1
WT	Wild-type

ACKNOWLEDGEMENTS

Over the four years of my thesis project I received encouragement, support and help from great number of people. I owe my gratitude to all those who made this dissertation possible.

I have been amazingly fortunate to have Prof. Dr. Steven A. Johnsen as my thesis supervisor, who continuously inspired me to dream and achieve more. His motivation and support helped me in all times of my research. He taught me to think critically and encouraged me to believe in my own ideas and skills.

I am grateful to Prof. Dr. Hans Will whose true passion for science, enthusiasm and wise advices continuously encouraged me to pursue the path of a scientist. He became more of a mentor and friend to me than a professor.

I would like to thank my committee members Prof. Dr. Matthias Dobbelstein and Prof Dr. Gregor Bucher for their support, helpful suggestions and insightful comments on my research project.

I would like to express my sincere gratitude to my collaborators without whom this project would not reach the point it has now. Roberto Tirado Magallanes under the guidance of Dr. Morgane Thomas-Chollier and Prof. Dr. Denis Thieffry substantially contributed to the bioinformatic analysis of the sequenced data. I truly appreciate his patience in teaching and introducing me the bioinformatic techniques. I also acknowledge Peng Liu, who under the guidance of Prof. Dr. Jan Tuckermann performed the analysis in mice skeletons. My gratitude also extends to Dr. John R. Hawse and Dr. Subramaniam Malayannan for their help with mouse osteocyte experiments. In addition, I would like to thank Dr. Hanna Taipaleenmäki and Dr.

Katharina Jähn from Prof. Dr. Dr. Eric Hesse's group, who patiently taught me how to handle the mice and perform the injections. I learned a lot and more importantly I gained generous friends through these partnerships.

I am also indebted to my former and present colleagues for creating a professional and fun atmosphere in the lab. I really enjoyed our vigorous discussions and get-togethers. Moreover, it was their great moral support and experience that helped me in the times of failures and doubts. I would like to thank in particular Dr. Florian Wegwitz for the assistance with the mice generation and experiments; Dr. Simon Baumgart and Dr. Tareq Hossan for their help with hFOB experiments; Dr. Sankari Nagarajan and Wanhua Xie for sharing with me their knowledge in bioinformatic analysis. On a special note, I would like to mention Dr. Vivek Kumar Mishra and Dr. Upasana Bedi for their readiness to help and for all the support and encouragement throughout my thesis project. More importantly, I would like to thank Dr. Oleksandra Karpiuk, who excellently guided me during the early steps of my project.

Finally, I would like to express my deepest gratitude to my parents and sisters for their unconditional love, support and unwavering belief in me. Without them I would not become the person I am now. They have been by my side no matter how difficult the things became. I owe them everything I have achieved in my life.

ABSTRACT

Proper temporal epigenetic regulation of gene expression is essential for cell fate determination and tissue development. However, epigenetic mechanisms involved in control of bone-specific transcriptional programs remain largely unexplored. In this study we focused on functional characterization of two epigenetic regulators – Bromodomain-containing Protein-4 (BRD4) and Ring Finger Protein 40 (RNF40) in development and maintenance of osteoblast fate. BRD4 was previously shown to control the transcription of defined subsets of genes in various cell systems. In this study we examined the role of BRD4 in promoting lineage-specific gene expression and show that BRD4 is essential for osteoblast differentiation. Genome-wide analyses show that BRD4 is recruited to the transcriptional start site of differentiation-induced genes. Unexpectedly, while promoter-proximal BRD4 occupancy correlated with gene expression, genes which displayed moderate expression and promoter-proximal BRD4 occupancy were most highly regulated during differentiation and sensitive to BRD4 inhibition. Therefore, we examined distal BRD4 occupancy and uncovered a specific co-localization of BRD4 with the transcription factors C/EBPb, TEAD1, FOSL2 and JUND at putative osteoblast-specific enhancers. These findings reveal the intricacies of lineage specification and provide new insight into the context-dependent functions of BRD4.

RNF40 forms with RNF20 the obligate E3 complex and mediates monoubiquitination of lysine 120 of histone H2B (H2Bub1). Despite its global correlation with active gene transcription, we previously demonstrated a specific role for H2Bub1 in controlling osteoblast (OB)-specific gene expression during OB differentiation of mesenchymal stem cells (Karpiuk et al., 2012, Mol Cell). To address the significance of H2Bub1 for bone development *in vivo*, we generated OB-specific Rnf40 conditional knockout

(KO) models. Given the crucial role of RUNX2 in osteoblast lineage commitment and chondrocyte hypertrophy, the Rnf40$^{Runx2\text{-}Cre}$ knockout mice developed achondroplastic-like phenotype with shorter bone sizes. Surprisingly, micro computed tomography (µCT) analysis showed increased bone mineral density (BMD) in these mice, a finding that could be associated with decreased osteoclast function and hence osteopetrosis-like phenotype. Remarkably, the Rnf40$^{Bglap\text{-}Cre}$ KO mice displayed only osteopetrotic-like phenotype with significant increase in bone mineral density without any further alterations in bone formation and apposition rate. This suggested the importance of H2Bub1 at the earlier stages of osteoblast commitment. Strikingly, the number of osteoclasts was substantially reduced in these mice suggesting the increased BMD to be associated with reduced bone resorption. *Ex vivo* differentiation studies confirmed a role for Rnf40 and H2Bub1 in OB differentiation as revealed by decreased alkaline phosphotase activity/expression, mineralization and expression of *Runx2* and *Sp7* in KO OBs. Consistently, Rnf40-deficient OBs showed significantly reduced *Rankl* expression and triggered less osteoclast formation as revealed by osteoblast and osteoclast co-culture experiments. Remarkably, the reverse effect in modulating osteoblast specific H2Bub1 levels in Ubiquitin-Specific Protease 22 (Usp22)$^{Runx2\text{-}Cre}$ KO mice did not have any impact on bone in mice. Altogether, these data indicate significance of H2Bub1 signaling in regulating the osteoblast lineage commitment. Moreover, H2Bub1 appears to act as defining epigenetic regulator of osteoblast-osteoclast “communication“ *in vivo* which provides a basis for future studies to investigate the potential of its regulatory pathway for the treatment of conditions such as aging-related osteoporosis.

INTRODUCTION

Bone Biology

Anatomic Structures

Bone is the major supportive tissue of the body. It is responsible for the individual body shape, enables body movement, provides protection for inner soft tissues and serves as a major storage of calcium and phosphate ions. Moreover, bones “host” bone marrow - the main source of blood cells in adults. These properties make bone a very dynamic organ that undergoes constant remodeling to adapt to daily mechanical changes placed upon it, which is also the key mechanism during bone fracture repair.

Four bone types can be characterized in an adult human. These include long (i.e. phalanges, femur), short (i.e. tarsal and carpal bones), flat (i.e. cranial bones) and irregular (vertebrae) bones (Buckwalter et al., 1995; Clarke, 2008). In a typical bone, the bones tissue is localized around the hematopoietic bone-marrow and is surrounded by periosteum, the connective-tissue membrane (Buck and Dumanian, 2012; Buckwalter et al., 1995). The medullary cavity is lined by endosteum. Based on the structural density, the bone tissue is further classified into two tissue types: compact (cortical) and cancellous (trabecular). Whereas the compact bone provides the resistance to the mechanical loading to the bone, the flexible trabecular structures enable the deformation of the bone in response to the same load. Despite the same composition, the trabecular bone is metabolically more active and displays higher rate of bone-turnover than the cortical bone. The ratio of cortical and trabecular tissue within the bones depends on the bone type. In the long bones, the cortical bone constitutes the substantial part of the central diaphysis. The diaphysis gradually transitions into metaphysis that is mainly made of cancellous bone. The metaphysis

underlies the epiphyseal growth plate consisting of proliferating chondrocytes involved in bone lengthening which in adults gets replaced by the bone tissue forming the epiphyseal line. The polar ends of the long bones called epiphysis most commonly form the joint surfaces and, hence, are covered by articular cartilage. The epiphysis similar to metaphysis are represented by trabecular tissue (Figure 1).

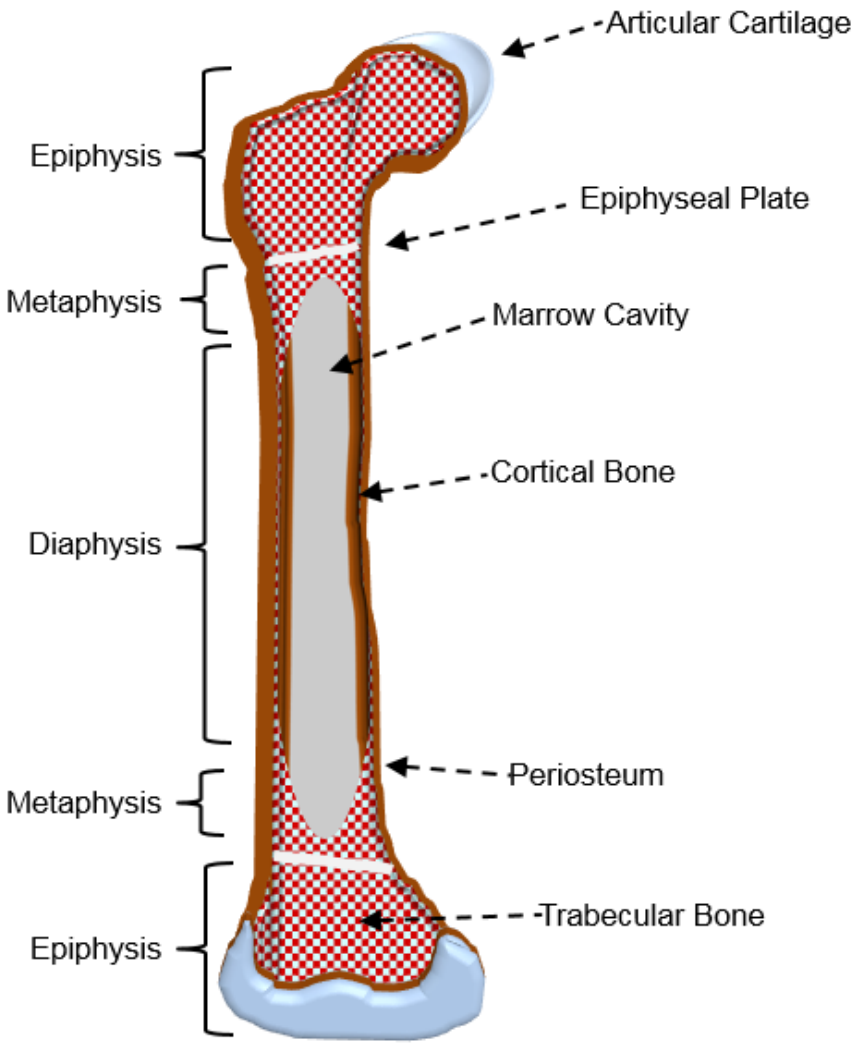

Figure 1. ***Schematic representation of anatomic structures of a long bone.***

Based on histological properties, bone tissue can be further classified into woven and lamellar bone. The first is characterized by the unorganized pattern of mineralization and fibrillary structure. Woven bone is evident in the embryonal skeleton and gradually gets replaced by more organized lamellar bone consisting of

densely packed collagen fibrils (Buck and Dumanian, 2012; Buckwalter et al., 1995; Clarke, 2008).

Both trabecular and cortical bone harbor osteons which are considered the functional units of the bone tissue. In the compact bone these are also known as Haversian systems. Given the concentric structure consisting of lamellae surrounding the blood vessel channels (Haversian Canal) that supply blood and nutrients to the bone cells, these units resemble the sequential order of bone formation. The Haversian Systems are usually oriented in parallel order to long axis of the bone. Besides the longitudinal channels, there are also so called Volkmanns Canals with transverse blood vessels connecting the osteons with the periosteum (Clarke, 2008).

In fact, highly vascularized outer fibrous layer of periosteum provides the substantial part of blood supply to the bone. Importantly, the inner layer of periosteum referred as cambium or osteogenic layer is densely populated by osteoprogenitor cells and differentiating osteoblasts contributing to radial growth of the bones (Dwek, 2010).

Bone cells

In general, bone formation and development, the normal bone functioning and homeostasis are controlled by coordinated play of three cell populations in the bone: osteoblasts, osteocytes and osteoclasts (Figure 2). Additionally, the chondrocytes are similarly considered the key players involved in endochondral ossification. While osteoclasts rise from hematopoietic progenitor cells, the rest of above mentioned cells involve one common progenitor cell type, i.e. the mesenchymal stem cells (Buck and Dumanian, 2012; Buckwalter et al., 1995).

Osteoblasts are mononucleated cells involved in bone matrix synthesis, deposition and responsible for its subsequent mineralization (Figure 2). The bone matrix

consists mainly of the inorganic component represented by hydroxyapatite, and the collagen rich organic component. In addition to collagen, some other non-collagenous proteins such as sialoproteins, proteoglycans and gla-containing proteins make up the content of the organic matrix. The process of hydroxyapatite formation starts within the intracellular vesicles of the osteoblasts. The presence of calcium binding bone sialoprotein and calbindin along with some phospholipids enable accumulation of the calcium ions within these vesicles. The phosphate enrichment within the vesicles is regulated by the activity of type III Na/Pi cotransporter. Once reaching the certain level of the ions, the solubility point of $CaPO_{4\ is}$ exceeded leading to the crystal formation. At this point, the hydroxyapatite crystals start extending into the extracellular matrix through the penetration of vesicular membranes. The concertation of Ca^{2+} ions and inorganic phosphate Pi within the extracellular fluid is critical for the continuation of the crystal formation. More importantly, it was shown that inorganic pyrophosphate (PPi) acts as inhibitor of mineralization. Therefore hydrolysis of PPi by alkaline phosphatase resulting in Pi formation is crucial in regulation of mineralization process by osteoblasts (Orimo, 2010).

Once trapped within the secreted matrix the osteoblasts become terminally differentiated forming the osteocytes. In fact, 90 percent of all bone cells is represented by osteocytes (Kini and Nandeesh, 2012). Osteocytes possess filapodial processes residing within the bone matrix canaliculi allowing nutritional and signaling exchange between the cells and blood vessels. Hence, the embedded osteocytes form the syncytium within the bone enabling interconnection of these cells with each other and with bone surface (Figure 2). Given the embedded location and high connection possibility, osteocytes display mechanosensory functions. In

response to mechanical loading, these cells coordinate the interaction of osteoblasts with osteoclasts by signaling molecules, and hence, control the bone homeostasis and remodeling. Moreover, these cells through the process of osteocytic osteolysis resulting in perilacunar remodeling can modulate their own environment (Prideaux et al., 2016). Osteoblasts also form the bone lining cells recognized as resting osteoblasts within endosteum on the surface of quiescent bone.

Osteoclasts differentiate from bone marrow macrophages (Figure 2). By fusing together they form multinucleated cells and are responsible for bone-matrix resorption (Buck and Dumanian, 2012; Buckwalter et al., 1995; Clarke, 2008). While macrophage colony-stimulating factor (M-CSF) signaling is required for control of cellular proliferation and survival of osteoclasts, the differentiation and resorptive activity of osteoclasts largely depend on receptor activator of nuclear factor kappa-B (RANK) signaling (Kim and Kim, 2016). The cells of osteoblastic lineage by producing activator of NF-jB ligand (RANKL) that binds to the RANK receptor on the surface of osteoclasts induce the differentiation of the latter from progenitors and subsequently their activation. On molecular level, the osteoclast formation and differentiation largely depend on RANKL induced activation of nuclear factor kappa-B (NF-kB), that controls the sequential expression of FBJ osteosarcoma oncogene (c-FOS) and nuclear factor of activated T cells, cytoplasmic, calcineurin dependent 1 (NFATC1) (Yamashita et al., 2007). The resorptive activity of osteoclasts can be further modulated by the secreted form of RANK receptor - osteoprotegerin (OPG). It is considered as decoy receptor that by binding to the RANKL inhibits it further interaction with RANK receptor on the surface of osteoclasts. Consistently, the RANKL/OPG ratio in the serum or bone marrow is important determinant of normal bone remodeling (Boyce and Xing, 2008). Upon activation signaling, osteoclasts

undergo extensive cytoskeleton reorganization and attach to the bone matrix through the actin rich podosomes. This results in formation of sealing zone that marks the future resorption site. Once the attachment is complete, osteoclasts start resorbing the matrix through ruffled border membrane that is actually characterized as the resorbing organ of the osteoclasts. At this point, fusion of highly acidic intracellular vesicles with the plasma membrane and subsequent release of the content of these vesicles into resorption lacuna results in partitioning and dissolution of hydroxyapatite crystals. The almost simultaneous release of cathepsin K leads to downstream degradation of matrix proteins. In addition to cathepsin K, osteoclast-specific tartrate resistant acid phosphatase (TRACP) is similarly involved in the matrix degradation process (Väänänen, 2005). Moreover, several matrix metalloproteases can contribute to the matrix resorption, however might not carry the limiting function in this process (Delaissé et al., 2003). At the same time the products of degradation along with calcium and phosphate ions are endocytosed back into osteoclasts and subsequently released into the extracellular fluid through the functional secretion domain of the osteoclasts. Presumably, after task completion osteoclasts undergo apoptosis (Väänänen, 2005).

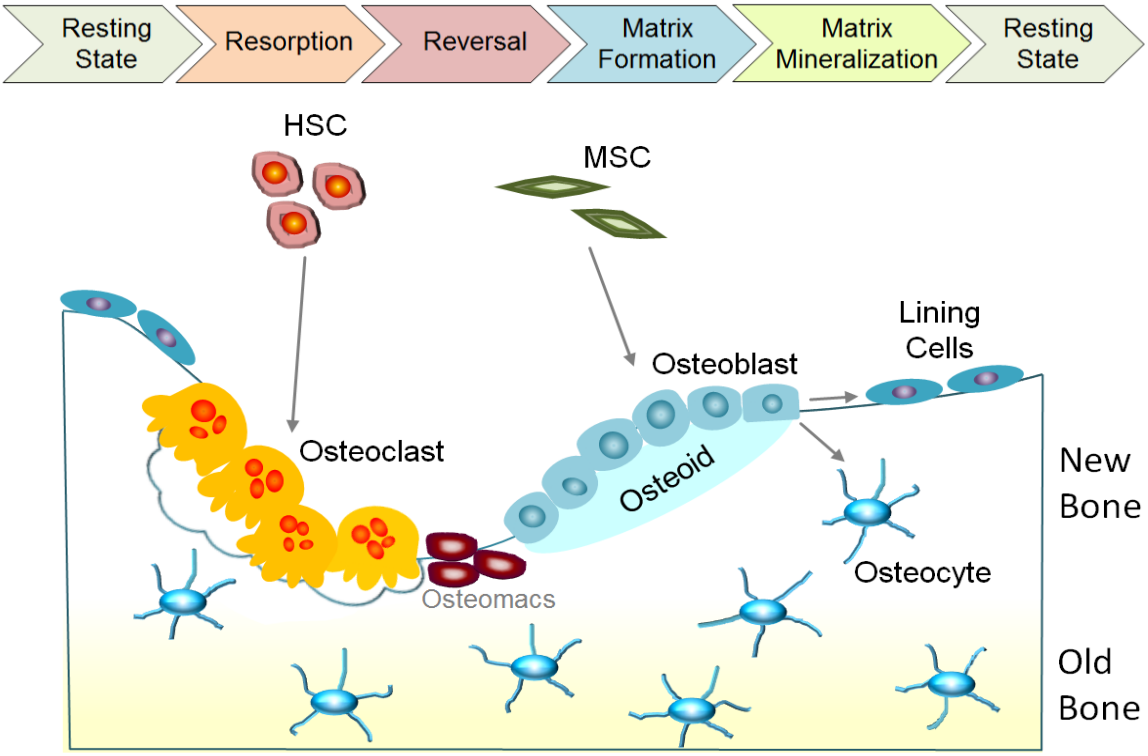

Figure 2.*The bone cells and bone remodeling process*. Bone undergoes continues remodeling within the discrete sites referred as Bone Remodeling Compartment (BRC). During this process upon activation, the osteoclasts derived from hematopoietic stem cells (HSC) start the bone resorption. Following resorption, the mononuclear macrophage-like cells of unknown origin (referred as osteomacs) coordinate the coupling of bone resorption by the following step of bone formation. This happens within the reversal phase. Consistently, the osteoblasts of mesenchymal origin (derived from mesenchymal stem cells, MSC) start producing the osteoid which subsequently undergoes mineralization. The osteoblasts imbedded in the bone matrix eventually mature and differentiate into osteocytes, which are also involved in coupling of bone resorption to bone formation. Osteoblasts also form the bone lining cells that cover the bone surfaces and thought to be involved in cellular communications with osteocytes. They also make the canopy over the remodeling sites.

Bone formation

The initial steps of osteogenesis require the formation of mesenchymal cell (MSC) condensations, location and shape of which are determined by the intricate network of signaling molecules. Depending on the character of patterning signals, the indicated mesenchymal condensations can directly differentiate into osteoblasts choosing the path of *intramembranous ossification*, or through formation of chondrocytes they enter the path of *endochondral ossification* (Hojo et al., 2015). In

fact, the primary skeleton is entirely made of cartilage and later during the fetal development and postnatal growth it gets replaced by the stiff bone tissue. The matter of lineage specification choice of bipotential osteo-chondroprogenitor cells depends on the subsequent expression of master regulators in response to signaling molecules. The initially SRY box-containing gene 9 (*SOX-9*) positive mesenchymal stem cells by subsequent co-expression of L-SOX5 and SOX-6 direct the chondrogenic differentiation of MSCs. The pre-cartilaginous cell condensations start expression of adhesion molecules such as N-cadherin, tenascin-C and others to enable the tight clustering of these cells within the nodules (Lefebvre and Bhattaram, 2010). In the next stage following the formation of condensed structures, the cells enter the stage of rapid proliferation forming the shafts of the bones and extensively produce extracellular matrix. Eventually, several layers of chondrocytes at different maturation steps form the growth plate (Figure 3) that is responsible for future bone lengthening. Within the staggered structure the proliferating chondrocytes stop dividing, increase in volume and become hypertrophic. Hypertrophic chondrocytes precede the layer of terminally differentiated matrix-mineralizing chondrocytes. Whereas all the previous forms of chondrocytes express collagen type 10a1 (COL10A1) the terminal chondrocytes start expressing more osteoblast-specific markers including Runt-related transcription factor 2 and 3 (RUNX2 and RUNX3). Additionally, MADS-box containing myocyte enhancer factor 2c and 2d transcription factors (MEF2c and MEF2d) are expressed, and along with RUNX2/3 they determine the terminal differentiation path of chondrocytes. Presumably, the terminally differentiated chondrocytes later undergo apoptosis. Following the death of chondrocytes a variety of cells invade the “liberated” space including the osteoblasts that start producing bone matrix, osteoclasts that remove the cartilaginous matrix,

stromal and hematopoietic cells that form the bone marrow (Figure 3). A number of factors produced by chondrocytes assist this process, such as VEGF that enables blood vessel formation by invading endothelial cells, matrix metalloproteases that in addition to osteoclast-specific enzymes (e.g. MMP9) resorb the matrix. Hence, the initial steps of bone formation within the diaphysis of the fetal bones are defined as primary ossification center. During the postnatal development secondary centers in the epiphyses arise. Eventually, in the adulthood the two ossification centers fuse upon the closure of the growth plate (Lefebvre and Bhattaram, 2010)

Intramembranous ossification is mainly characteristic for the formation of flat skull bones. The earlier expression of RUNX2 with subsequent induction of osterix (OSX) gene directs the MSCs along the osteogenic path (de Crombrugghe et al., 2001). In this case osteoblasts produce first the unmineralized bone matrix (osteoid) in radial direction forming the ossification center in the middle of the bones. Expression of Colagen type1a (COL1A1) and Alkaline Phosphatase (ALPL) is important event preceding the onset of mineralization. Eventually, the developing bones get connected by an elastic tissue referred as sutures. Infiltrated by undifferentiated osteoprogenitor cells, these mainly contribute to future bone growth. Within the first two years of life, these sutures eventually disappear leading to the fusion of skull bones.

Signaling networks in bone

Several pathways converge in the establishment, development, maintenance and specialization of osteo- and chondrocyte-specific cell types. Among them noteworthy is to mention the Indian Hedgehog (Ihh), Wnt-Wingless and the Transforming growth factor-beta (TGF-β) and bone morphogenic protein (BMP)

signaling pathways (TGF-β/BMP pathway) (Hojo et al., 2015). The crosstalk of these pathways coordinates the rather complex process of bone formation, development and homeostasis in a time-, stage and cell-type-specific manner.

The Ihh signaling is important for endochondral bone development by controlling the formation of RUNX2-expressing osteoblasts. Response to Ihh signaling is mediated through transcription factors GLI1, GLI2 and GLI3 (Hojo et al., 2015). Ihh through GLI1 regulates the expression of osteoblast-specific genes (Hojo et al., 2012). It was shown that by interacting with RUNX2, GLI2 positively affects the osteoblast differentiation of mesenchymal stem cells (Shimoyama et al., 2007). At the same time, Ihh signaling controls the proliferation and maturation of pre-hypertrophic chondrocytes through regulation of Parathyroid hormone related protein (PTHrP) expression in these cells. The PTHrP-deficient mice display inhibited proliferation and early maturation of hypertrophic chondrocytes leading to achondroplasia-like changes in mice (Karaplis et al., 1994). Similarly, Ihh inhibits the differentiation of chondrocytes in endochondral bone through the transcriptional repressor GLI3 (Koziel et al., 2005). In this context, the FGF signaling exerts opposite to Ihh effects in chondrocytes by blocking the proliferation of chondrocytes.

The role of Wnt-signaling acts mainly downstream of Ihh signaling and is indispensable for the healthy bone formation. Activated by a variety of glycoprotein ligands, canonical Wnt pathway mediates its signaling through the stabilization of β-catenin, whereas one of the noncanonical Wnt signaling pathways involves calcium-dependent regulation of cellular migration, and the noncanonical planar cell polarity pathway through the GTPases regulates the cytoskeleton that is responsible for cell shape (Kim et al., 2013b) . The canonical Wnt pathway is important at all the stages of osteoblast formation and differentiation (Baron and Kneissel, 2013). Importantly,

the Wnt-signaling activation supports the already osteoblast committed MSCs (expressing RUNX2) to further specialize into OSX positive cells (Hu et al., 2005) by blocking the chondrogenic potential of these cells. Moreover, the β-catenin signaling blocks the adipogenic commitment of MSCs (Case and Rubin, 2010). Little is known about the relevance of noncanonical Wnt-signaling in the regulation of bone formation. Nonetheless, noncanonical ligand Wnt7b was reported to promote osteoblast differentiation through G protein–coupled protein kinase C δ (PKC-δ) activation (Tu et al., 2007). Similarly, Wnt5b mediated activation of noncanonical Wnt signaling exhibited anti-adipogenic potential by repressing the expression of PPARγ and hence favoring the osteoblast lineage commitment of MSCs (Takada et al., 2007)

TGF-β/BMP pathway includes a large number of extracellular signaling molecules which have profound functions at all the steps of osteogenesis including mesenchymal stem cell condensations, bone morphogenesis, endochondral ossification and osteogenic differentiation (Wu et al., 2016). Binding of the ligands to the cell surface receptors, induces the receptor phosphorylation with subsequent cascade activation of signal transducers Mothers against decapentaplegic homologues (SMAD). The nuclear translocated SMAD complexes were shown to interact with osteoblast-specific transcription factors such as RUNX2 and OSX (Rahman et al., 2015). As indicated by their name, the BMPs have attracted great attention due to heterotopic and orthotopic bone formation ability upon administration. In general, BMPs support the differentiation of mesenchymal stem cells along the osteogenic and chondrogenic lineages (Liu et al., 2007; Rahman et al., 2015). Among many BMPs, BMP-2 and BMP-7 have been extensively

characterized given their high osteogenic potential. Moreover, recombinant forms of these proteins are in clinical trials of bone diseases and fracture healing.

Additionally, hormonal signaling has major impact on the bone cells and in general bone development and remodeling. Given its essential role in regulating the calcium homeostasis, parathyroid hormone (PTH) receptor signaling exerts dual effects on bone by stimulating bone resorption and bone formation. By promoting the expression of RANKL and hence affecting the RANKL/OPG ratio, PTH stimulates activation and differentiation of bone resorbing cells, i.e. osteoclasts. At the same time, the positive effect on the osteoblasts was found to be mainly mediated through the downregulation of WNT inhibitor sclerostin (SOST). Interestingly, the pro-osteoclastic effects of PTH is prominent during the continuous dosage of the hormone, whereas the intermittent administration results in bone anabolic effects (Silva and Bilezikian, 2015).

Vitamin D receptor signaling is important regulator of normal physiological functions of osteogenic and chondrogenic cells. Mesenchymal stem cells at the stage of cellular condensations already express VDR. Activated by the ligand, the VDR in a heterodimer complex with retinoic acid receptor (RXR) is involved in transcriptional activation of some of the osteoblastic genes such as osteocalcin (BGLAP), RANKL, osteopontin (OPN). Moreover, the physiological significance of Vitamin D is also explained by its essential role in controlling calcium and phosphate homeostasis (Imai et al., 2013).

Glucocorticoid receptor (GR) signaling exhibits adverse effects on bone which is also often observed in the patients developing osteoporosis after long treatments with glucocorticoids (GC). GRs has two isoforms which upon ligand activation translocate

to nucleus and in homodimerized complex bind the target GR elements (GRE) to induce direct transactivation or repression of the target genes. Moreover, GR can indirectly regulate gene expression by associating with other transcription factors such as activator protein-1 (AP-1), NF-κB, or signal transducer and activator of transcription 5 (STAT5). It has been demonstrated that GC can favor the adipogenic specialization of MSCs in cost of osteoblastic by directly inducing the expression of adipocyte-specific master regulator peroxisome proliferator-activated receptor γ2 (PPARγ2). Interestingly, the effects of GR signaling on osteoblasts are somehow contradictory. Many *in vitro* differentiation protocols for osteoblasts include glucocorticoid *per se* due to ability to increase expression of some of osteoblast-specific genes such as alkaline phosphatase (ALPL), osteopontin (OPN), osteocalcin (BGLAP,OC) and bone sialoprotein (IBSP) (Imai et al., 2013). Moreover, some studies have indicated the synergistic effect of GC with some of BMPs (Mikami et al., 2010). On the other side GC treatment was shown to block the proliferation and differentiation of osteoblasts and induce apoptosis in these cells The osteoblast specific deletion of GR in mice revealed that antiproliferative effect of GC is receptor dimerization dependent whereas the inhibitory effect on differentiation dimerization independent (Rauch et al., 2010). Monomeric GR was shown to inhibit the AP-1 mediated regulation of some cytokines that exhibit pro-osteoblastic effects. Hence, large amount of evidence suggests that the GC induced differences on the bone might in fact depend on the timing, dose and duration of the treatment.

Sex hormones play key role in bone growth especially during puberty accounting to gender differences in skeleton. These differences rise because of stimulatory effect of androgen on periosteal bone growth whereas estrogens act in opposite way (Oury, 2012). More importantly, sex hormones have a crucial role in bone mass

maintenance in adulthood mainly by affecting both the osteoblasts and osteoclasts. Estrogens mainly exert inhibitory action on osteoclasts by several mechanisms. The pro-apoptotic effect of estrogen on osteoclasts was found to be associated with estrogen mediated decrease in the production of M-CSF, interleukin 1 and 6 (IL-1, IL-6) known to inhibit osteoclast apoptosis. Moreover, estrogen positively affects expression of apoptosis inducing FAS cell surface death receptor ligand (*FASL*) in osteoblasts that by binding to its receptor on osteoclasts induces apoptosis in latter. Additionally, by promoting the OPG and inhibiting the RANKL expression in osteoblasts, estrogens contribute to decreased differentiation and activity of osteoclasts (Oury, 2012). Estrogen signaling has been shown to increase osteoblast lifespan and exhibit anti-apoptotic effects on these cells through the activation of extracellular signal-regulated kinases (ERK) signaling pathway (Kousteni et al., 2001). Interestingly, the osteoblast-specific deletion studies on mice of estrogen receptor alpha (ERα) have demonstrated controversial results. The early ablation of ERα in mesenchymal cells and osteoblast precursors ($ER\alpha^{PRX1\text{-}Cre}$ and $ER\alpha^{OSX\text{-}Cre}$ mouse models, respectively) resulted in low bone mineral density (BMD) in mice in addition to reduced cortical thickness. However, the deletion of ERα in osteoblast precursor cells ($ER\alpha^{Col1a1\text{-}Cre}$) under the control of Col1a1 did not lead to any prominent changes in the bone. However, the use of another mouse model for mature osteoblasts $ER\alpha^{OC\text{-}Cre}$ and $ER\alpha^{Dmp1\text{-}Cre}$ revealed reduction in both the cortical and trabecular bone parameters (Khalid and Krum, 2016). Androgens have similarly positive role in osteoblasts. By reducing the IL-6 production it was shown to inhibit the apoptosis of osteoblasts. Moreover, by modulating the OPG expression in osteoblasts, androgens decrease bone resorption through attenuation of osteoclast activity (Syed and Khosla, 2005).

Bone growth

As the individual's height increases the bones also grow in size both in length and diameter. The bones grow in length primarily through longitudinal enlargement of growth plate cartilage repeating the steps of endochondral ossification (Figure 3). Briefly, the chondrocytes of the growth plate by subsequent differentiation and maturation process form the columns of chondrocytes unidirectionally extending from epiphysis to bone metaphysis. As the unmineralized cartilage extends in length and reaches the metaphysis, special mononuclear cells referred as septoclasts or chondroclasts start resorbing the cartilage from the metaphysial end. Concomitantly, the invading blood vessels enable recruitment of bone cells. The remaining sites of the cartilage (septa) serve as potential sites of bone mineralization by osteoblasts forming this way the primary trabecular bone (primary spongiosa). Gradually, all the cartilage material of growth plate gets replaced by subsequent steps of bone turnover developing this way the secondary spongiosa. By distancing away from the growth plate, the metaphysial trabeculae get eventually resorbed, hence, not reaching the bone diaphysis. In contrast, given the pressure of mechanical loading on the bone, the metaphysial trabeculae on the periphery continue growing and get thicker eventually integrating into the metaphysial cortical bone (Rauch, 2005).

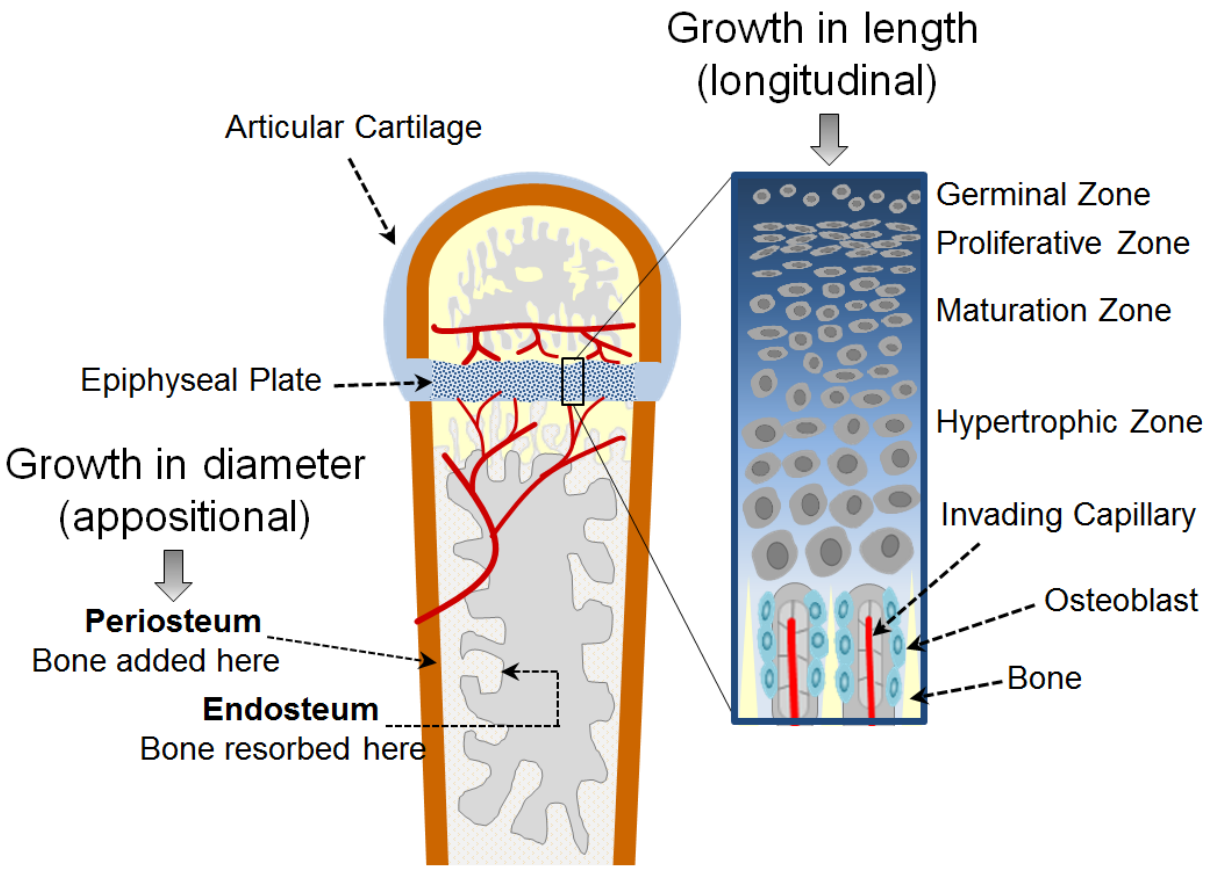

Figure 3. ***Model of bone growth.*** The bone grows in length due to proliferative activity of chondrocytes within the epiphyseal growth plate. Chondrocytes are formed in the germinal zone, after which they undergo proliferation and maturation. Once mature, the chondrocytes start becoming hypertrophic and lay down extracellular matrix. Eventually, the hypertrophic chondrocytes undergo apoptosis, and are replaced by osteoblasts brought in with the invading capillaries. The latter form more bone and are directly involved in matrix mineralization. Hence, the longitudinal bone growth follows the steps of endochondral ossification. The appositional growth of the bone in diameter is controlled by the osteogenic activity of cambium (osteogenic layer) of periosteum. Consistently, the bone is formed from outside and the old bone is resorbed from inside (endosteum) to maintain the bone marrow cavity.

Although bone growth in length stops in early adulthood culminating in the complete ossification of the epiphyseal growth plate and fusion of primary and secondary ossification centers, the bone growth in width can continue throughout the life (appositional growth) and is mainly controlled by the physiological signaling of sex hormones. It happens through the deposition of bone matrix by the osteoblasts of the osteogenic layer of periosteum around the diaphysis. Additionally, newly formed chondroblasts of the perichondrium surrounding the cartilage anlage are similarly involved in the thickening of the bone. Consistently, during the peripheral thickening of

the bone, matrix resorption mediated from the endosteal surface of the bone is important for the expansion of bone marrow cavity (Rauch, 2005).

Bone modelling and remodeling

Bone is a dynamic organ that undergoes constant adaptation through bone modelling and remodeling in response to mechanical loading and physical influences.

Bone modelling accounts for changes in the bone shape and structure to optimize the bone strength in response to biomechanical force. This is achieved through the independent processes of bone formation and bone resorption in the stress experiencing regions of the bone (Seeman, 2009).

Bone remodeling is a physiological process that has substantial role in bone mass maintenance and in regulation of serum calcium levels and, hence, bone homeostasis. By changing the structure of the bone, bone remodeling also minimizes and prevents the possibility and accumulation of micro damage occurrence. More importantly, bone remodeling is critical during fracture healing. The process of bone remodeling mainly happens on the endosteal surface of the bone, i.e. on the endocortical, trabecular and intracortical (Haversian systems) components. It is rarely observed on the periosteal surface (Seeman, 2009). Unlike bone modeling, bone remodeling is controlled by the balanced coupling of bone resorption to bone formation. Loss of balance and/or coupling of these processes serve as the basis for the most of the skeletal diseases. Indeed, bone loss associated with increased rate of bone resorption and/or reduced rate of bone formation is observed during osteoporosis, the most prevalent bone disease among aged population. Hence, the bone remodeling is dependent on the tightly synchronized activity of several cellular compartments of bone that form the “bone multicellular unit” (BMU) (Raggatt and Partridge, 2010). BMU is usually lined up with a

layer of so-called canopy cells, presumably the bone-lining cells that form the bone remodeling compartment (BRC). The process of bone remodeling starts with activation phase which involves the sensing of remodeling-initiating signal (Figure 2). Osteocytes play a key role in this process. By producing number of anabolic factors, osteocytes might coordinate the action of osteoblasts and osteoclast within the BRC. Moreover, damage associated apoptosis of osteocytes serves as a chemoattractant for osteoclast recruitment. Similarly, the PTH induced activation of osteoblasts can induce the release of factors by the latter such as RANKL that initiate differentiation of osteoclasts (Raggatt and Partridge, 2010). Following the signal detection and subsequent recruitment of osteoclasts to the sites of remodeling, the osteoclast mediated resorption of the bone matrix starts. At the end of the resorption phase, cells of yet unknown origin infiltrate the freshly formed resorption lacunae. These cells were proposed to be the osteoblast-specific macrophages, the so-called osteomacs, involved in the removal of collagenous debris. However, recent findings also suggested that these could be some kind of bone lining cells involved in the deposition of fresh collagenous matrix. In any case, the reversal cells most likely play important role in coupling of bone resorption to bone formation within the BRC (Raggatt and Partridge, 2010) . Moreover, osteoclasts were similarly shown to be involved in the regulation of coupling process. Namely, the expression of semaphorin 4D (Sema4D) by osteoclasts was shown to inhibit the bone formation process by osteoblasts which is required for initial step of bone resorption. In contrast, the expression of semaphorin 3A by osteoblasts was shown to inhibit the further action of osteoclasts. Moreover, the expression of membrane bound ephrinB2 by osteoclasts and ephrinB4 by osteoblasts were similarly shown to regulate the coupling of bone resorption to bone formation. The ephrinB2 binding of osteoclasts to the ephrinB4 on the surface of osteoblasts stimulates osteoblast differentiation whereas the

reverse case of the signaling inhibits osteoclastogenesis, suggesting ephrinB2/ephrinB4 signaling as important event in the termination of bone resorption and initiation of bone formation. Consistently, the bone resorption associated release of several signaling factors such as BMPs, TGF-β or insulin growth factor-1 (IGF-1) was found to trigger the osteoblast differentiation. Altogether, these signaling events lead to activation and differentiation of the osteoblasts that culminate the cycle of bone remodeling by subsequent phase of bone matrix formation (Figure 2). Osteoblasts and osteocytes then promote the subsequent mineralization of freshly formed matrix (Sims and Martin, 2014).

Epigenetic mechanisms in bone

As previously discussed, the development of “bony” skeleton involves a series of steps which includes lineage commitment of mesenchymal cells into osteochondroprogenitors and hematopoietic cells into macrophages, cellular expansion, differentiation and maturation of the specialized cells that contribute to formation of fully functional bone structures. Each stage of cellular progression and development is characterized by the specific, i.e. selective pattern of gene expression that is achieved by the orchestration of transcriptional and epigenetic regulatory networks in spatiotemporal manner. Epigenetic mechanisms contribute to the establishment and maintenance of gene expression patterns without altering the DNA sequence (Figure 4). The major mechanisms of epigenetic regulation include post-translational modifications of histones and DNA that subsequently lead to the changes in chromatin structure and accessibility to transcriptional regulators (Minarovits et al., 2016). In this context, protein complexes involved in histone exchange, chromatin reorganization and nucleosome positioning broaden the

spectra of epigenetic mechanisms affecting gene expression (Becker and Workman, 2013). Consistently, the evolution of several histone variants that affects the nucleosome structure and dynamics *per se* serves as an additional mechanism of epigenetic control. Finally, RNA interference (RNAi) pathways and long-noncoding RNAs (lnRNA) have emerged as additional epigenetic regulators of gene expression at post-transcriptional and pre-translational levels (Minarovits et al., 2016).

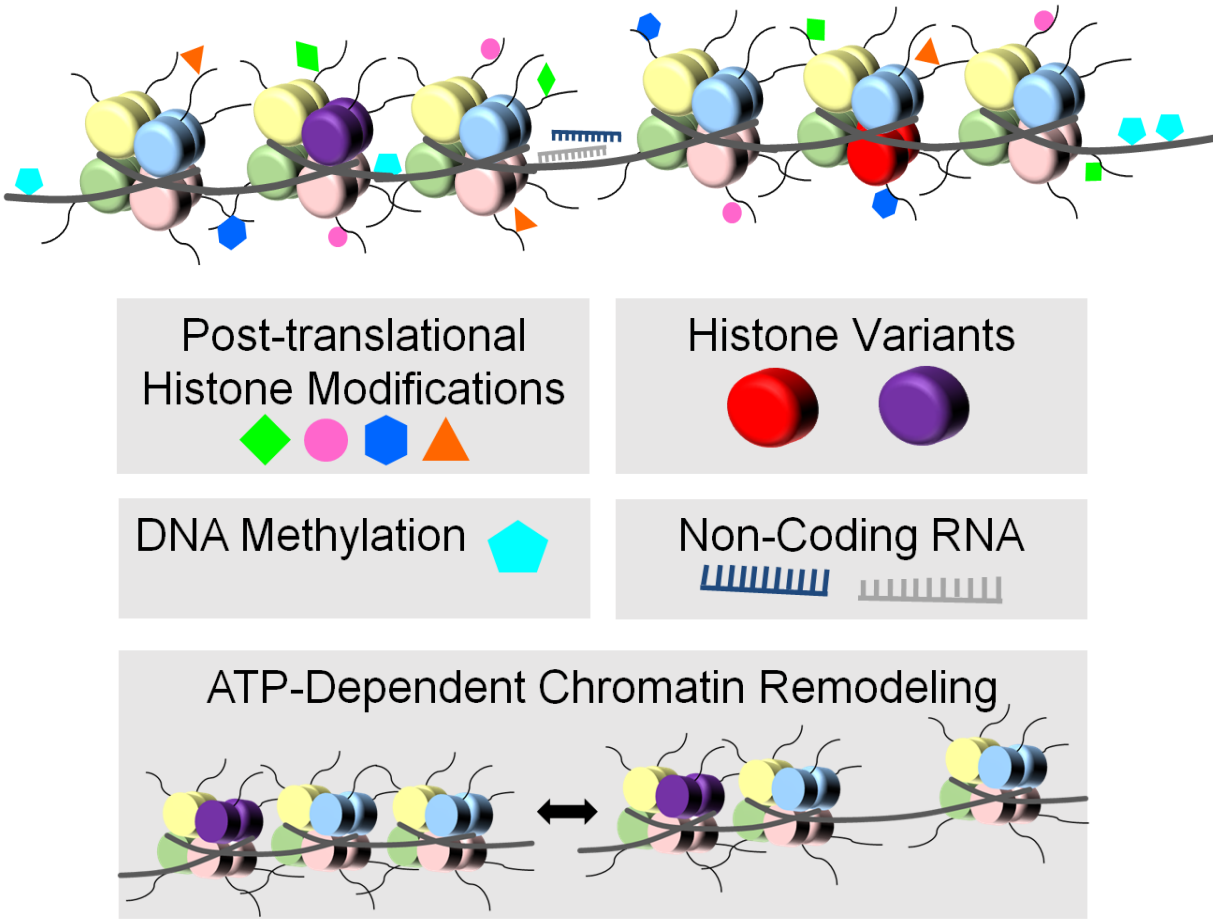

Figure 4. Epigenetic mechanisms of gene regulation. The term "epigenetics" literally means "above genetics" and refers to the heritable changes in chromatin organization affecting the gene expression regulation without altering the DNA code. This can be achieved by the post-translational modifications to DNA and histones which affect the chromatin structure and dynamics and provide the scaffold for the recruitment of other epigenetic and transcriptional regulators. Similarly, the histone variants can positively or negatively influence the nucleosomal stability. Consistently, the accessibility of DNA to transcriptional machinery is regulated by the activity of ATP-dependent chromatin remodelers. Additionally, the non-coding RNAs regulate expression by involving RNAi pathways are directly modulating the chromatin organization and transcriptional machinery.

Chromatin organization

In a eukaryotic cell DNA is condensed into highly organized chromatin structure. Such a chromatin structure is composed of basic repeating units, i.e. nucleosomes. Each nucleosome consists of a core particle with linker DNA. The core particle is made of an octamer of histone proteins H2A, H2B, H3 and H4, each present in two copies, and 147 bp long DNA fragment wrapped in 1.7 helical turn around the octamer. Each core particle is connected with the adjacent neighbors through the linker DNA. This way, the nucleosomal array structure “beads on the string” is arranged. The further condensation of nucleosomal array into 30nm fiber structure is partially mediated by linker histones H1 and H5 (Samara et al., 2010). Each of the core histones possess “histone-fold” and “histone-tail” (N-terminal) domains. The fold-domain is responsible for the interaction of histones heterodimers with each other. The histone dimers H3-H4 make a centrally located tetramer which is covered by the bundles of H2A-H2B heterodimer from both sides through H2B-H4 associations. The N-terminal histone tails along with histone H2A C-terminal tail protrude from the center of histone core. Moreover, the N-terminal tail of histone H4 was shown to contribute to chromatin condensation by building internucleosomal interaction with the highly acidic region (“acidic patch”) of histone dimer H2A-H2B that constitutes the binding surface for a variety of nucleosome binding proteins. Consistently, the latter can compete out the interaction of histone H4 N-terminal tail from this surface, thus affecting the stability and dynamics of the nucleosome as a whole (Kalashnikova et al., 2013). Moreover, the histone tails are subject to many histone post-translational modifications that may impose positive or negative functional consequences on gene expression. The pattern of the post-translational histone modifications is regulated by the enzymatic activity of proteins that can deposit

the specific modification - “writers”; the “erasers” that remove it, and the “readers” that recognize it and recruit the other “writers” and “erasers” along with transcription machinery to further influence gene expression. Histone modifications based on net charge change to the chromatin may influence the histone-DNA and histone-histone interactions. For a long time this was thought to be the main mechanism affecting the transcriptional regulation of a gene. However, more evidence suggests that specific combination and pattern of histone modifications form a distinct code (histone code) associated with a defined chromatin state. In this case, the “decryption” of the code by reader-domain containing proteins is the key step in the transmission of epigenetic information to the transcription regulatory networks (Strahl and Allis, 2000).

Post-translational histone modifications

Histone tails can undergo a variety of chemical modifications including methylation, acetylation, ubiquitination, phosphorylation, polyadenylation, ribosylation, glycosylation and crotonylation suggesting the vast diversity of histone code. Much research has been done on the histone methylation, acetylation and phosphorylation in context of transcriptional regulation of gene expression.

Histone acetylation is linked to active transcription. It is catalyzed by histone acetyltransferases (HAT, or KAT), enzymes responsible for transferring the acetyl residues from acetyl-CoA to the lysine ε-amino groups on the N-terminal tails of histones, mainly H3 and H4. Two main classes of HATs have been characterized so far. These include the Gcn5-related N-acetyltransferases (GNAT) and the MYST (Moz/Ybf2/Sas2/Tip60) families. E1A binding protein p300 and cAMP-response element-binding protein (CREB)-binding protein (p300/CBP) proteins have been considered as another family of HATs and play ubiquitous role as transcriptional

coactivators. The removal of the histone acetylation is carried out by histonedeacetylases (HDAC). In mammals, HDACs are classified into 4 groups: class I HDACs contains the right parietal dorsal 3 (RPD3)-like enzymes; class II, the HDA1-like enzymes; class III is represented by the sirtuins, whereas the class IV has only one characterized member – HDAC11. The most commonly investigated histone acetylation sites include H3 K9/14/27 and H4 K5/8/12/16 which were shown to be widespread marks associated with both active promoters and enhancers (Gordon et al., 2015; Verdone et al., 2005). Subsequently, the recognition of the acetylated histones is carried out by the bromodomain containing proteins (“readers”).

Histones methylation may lead to transcription activation or repression depending on the location, pattern and type of the methylation. Histones can be methylated on lysine and arginine residues. Methylation of lysine can be in mono-, di- and trimethylated form. Arginine can be either mono- or dimethylated, the latter in symmetric or assymetric form. The methylation involves transfer of methyl groups from S-adenosyl- L-methionine (SAM) to the ε-amino group by hitsone methyltransferases (HAT). These enzymes can be classified into three main groups: SET(Suppressor of variegation, Enhancer of zeste, Trithorax)-domain-containing proteins, DOT1(Disruptor of Telomeric silencing)-like proteins and arginine N-methyltransferases (PRMT). The latter are subdivided into two types based on asymmetric or symmetric dimethylation properties. The removal of methyl groups is catalyzed by demethylases (HDM) that can be grouped into two classes: amine oxidases and jumonji C (JmjC)-domain-containing dioxygenases (Gordon et al., 2015; Zhang and Reinberg, 2001). The recognition of methyl groups is carried out through the chromodomains of the proteins. The widely studied histone methylation sites include H3K4 – associated with active or poised promoters (K4me3) and enhancers (K4me1); H3K9 associated with heterochromatin, H3K27 involved in

gene silencing; H3K36, H3K79me2/3 – associated with actively transcribed genes and H4K20 associated with inactive state.

Histone phosphorylation can target all four histone molecules and occurs on serine, threonine or tyrosine residues of the latter. It is mediated by a wide range of kinases and can be subsequently removed by histone exchange or phosphatases. Among many, phosphorylation of histone variant H2AX on serine 139, referred as λH2AX, is of special importance given its role in DNA damage response. It is one of first events happening after damage induction and wide spreading of this mark serves as recruitment platform for a variety protein complexes involved in damage repair. Phosphorylation of serine 10 and 28 residues of histone H3 by Aurora kinase B has been linked to chromatin condensation during cellular division. In context of gene expression regulation, histone phosphorylation is associated with active transcription. Moreover, it has been reported that histone phosphorylation can be involved in histone cross-talk with histone acetylation. Namely, H3S28 phosphorylation was shown to displace the Polycomb Repressive Complex 2 (PRC2) from gene promoters leading to loss of H3K27me3 from these promoters with subsequent acetylation of H3K27 and gene activation (Lau and Cheung, 2011; Rossetto et al., 2012).

Among the 4 core histones, histone H2A and H2B are more abundantly subjected to ubiquitination. Unlike acetylation or methylation, ubiquitination involves conjugation of relatively larger, 76 amino acid long polypeptide molecule to the indicated histone tails certainly inducing steric changes in the nucleosome. The ubiquitin (ub) conjugation is a three step process involving ATP dependent ubiquitin activation by E1 enzyme, the conjugation of ubiquitin by E2 enzyme with subsequent ligation of ubiquitin to the lysine of the target protein through its C-terminal cysteine by E3 enzymes. Histone H2B and H2A are monoubiquitinated at positions K120 and K119, respectively (H2BK120 and

H2AK119). Polyubiquitination is also common, and was shown for histone H2A and its variant H2A.X during DNA damage induced signaling (Minarovits et al., 2016).

H2AK119ub1 is associated with Polycomb group (PcG) protein mediated gene silencing and is known to be catalyzed by Ring finger protein 1B (RING1B) E3 ligase of polycomb repressive complex 1 (PRC1). In addition, two other members of PRC1 – RING1 and B lymphoma Mo-MLV insertion region 1 homolog (BMI1) were shown to have supportive role in facilitating the E3 ligase activity of RING1B (Cao and Yan, 2012)

Monoubiquitination of histone H2B is carried out by E3 obligate heteromeric complex of ring finger proteins RNF20/RNF40 (Zhu et al., 2005). Genome-wide studies have revealed strong association of H2BK120ub1 with actively transcribed genes (Minsky et al., 2008). It promotes chromatin decompaction (Fierz et al., 2011) and facilitates transcriptional elongation of genes by RNA polymerase II (RNAPII) in part through the histone H2A/H2B dimer replacement by histone chaperon complex Facilitates Chromatin Transcription (FACT) (Pavri et al., 2006). Moreover, H2BK120ub1 appears to be involved in histone-crosstalk influencing methylation of histone H3K4 and H3K79 thereby supporting transcription activation (Kim et al., 2005).

Consistently, like any post-translational histone modification, ubiquitination can be reversible. This is achieved by the activity of deubiquitinating enzymes (DUBs). Whereas some DUBs preferentially target either H2AK119ub1 or H2BK120ub1, the others exhibit less specificity and can deubiquitinate both (Cao and Yan, 2012).

Histone modifications in bone

Cellular differentiation is accompanied by quantitative and qualitative changes in post-translational histone modifications. In general, the changes in activating histone modifications positively correlate with gene expression changes (Su et al., 2016).

Consistently, the same relationship was observed for some osteoblast-specific genes during the osteogenic differentiation of mesenchymal stem cells (MSC). For instance, Lee and colleagues identified differentiation linked increase of H3 and H4 promoter acetylation at osteocalcin (OC) and osterix (OSX) genes associated with decreased recruitment of HDAC1 and increased occupancy of p300 at these promoters (Lee et al., 2006). The spontaneous differentiation of human placental MSCs was similarly associated with increase of H3K9 and H3K14 acetylation at RUNX2 and ALPL promoters (Li et al., 2011).

Several histone acetyltransferases have been implicated in osteoblast-specific gene regulation, bone formation and remodeling. As previously mentioned the parathyroid hormone is important regulator of bone formation and remodeling. One of many genes regulated by PTH is matrix metalloprotease-13 (MMP13) expressed in osteoblasts and chondrocytes. It is a collagenase that has specific role during endochondral ossification. It was demonstrated that PTH induces MMP13 expression by promoting recruitment of p300/CBP-associated factor (PCAF) and p300 to the promoter of this gene in RUNX2 dependent manner. Consistently, the promoter acetylation of MMP13 increased consistently in response to PTH treatment. Moreover, the activity of PCAF was further augmented by p300 meditated acetylation of this protein (Lee and Partridge, 2010). Moreover, in the absence of PTH signaling, MMP13 is repressed through HDAC4 interacting with RUNX2 on the promoter of this gene (Shimizu et al., 2010).

Given the positive correlation of histone acetylation with osteoblast-specific gene expression, extensive research has been conducted on HDAC inhibition as potential approach for inducing osteogenesis in bone pathologies such as osteoporosis. The main effects of HDACs in bone biology can be attributed to their ability to inhibit RUNX2, the master regulator of osteoblast differentiation. They have been also found on the

promoters of other osteoblast-specific genes as well. Namely, this was shown for HDAC1 (Lee et al., 2006) and also for class II HDAC4 and HDAC5 (Jeon et al., 2006) . Moreover, some transcriptional repressors such as zinc finger protein 521 (Zfp521) by associating with HDAC3 repress the RUNX2 promoter activity hence modulating the stage dependent opposing role of RUNX2 in early and mature osteoblasts (Hesse et al., 2010). Although the HDACs share structural and some functional redundancy within their classes, they may also display some specific functions. This was particularly shown for HDAC8 where the germline deletion of this protein in mice lead to perinatal lethality due to skull abnormalities mainly through derepression of homeobox genes involved in patterning (Haberland et al., 2009). Although germline deletion of HDAC1 is also embryonically lethal, the death is caused mainly by proliferation defects (Lagger et al., 2002).

Based on therapeutic success of HDAC inhibitors (HDI) in epilepsy, bipolar disorder, and cancer, this class of drugs have been extensively studied by the scientific community. Out of many HDIs a few including suberoylanilide hydroxamic acid (SAHA) Valproate, Panobinostat, Belinostat and others have been already clinically approved. HDI have also displayed great anabolic features on bone. Many reports by different labs demonstrated increased osteoblast gene expression, mineralization, alkaline phosphatase activity and enhanced Runx2 transcriptional activity *in vitro* in different osteoblastic cell lines upon HDI treatments (Cho et al., 2005; Lee et al., 2009; Schroeder et al., 2007). Interestingly, clinical investigation of the patients treated with valproate revealed conflicting to *in vitro* data results associated with decreased bone mineral density. The *in vivo* studies in rodents also revealed somewhat unexpected results based on the background strain and immune system of the mice used for the studies (Senn et al., 2010).

Similarly, histone methylation has profound role in regulating the differentiation potential of MSCs towards osteoblastic lineage. For instance, MSC-specific deletion of SET domain containing histone methyltransferase (ESET, or SETDB1) for H3K9 inhibited differentiation of MSCs both *in vitro* and *in vivo*. It was demonstrated that ESET inhibits RUNX2 mediated transactivation which is important for osteoblast maturation. In agreement with this finding, MSC-specific ESET knockout mice displayed detrimental changes in trabecular bone volume and number of osteoblasts (Lawson et al., 2013). The role of PRC2 complex, namely H3K27 methyltransferase EZH2 has been also addressed in the context of osteoblastic differentiation. Genome-wide profiling of EZH2 binding sites in differentiating MSCs before and after osteoblastic induction revealed that differentiation lead to global disassociation of Enhancer of zeste homolog 2 (EZH2) from substantial amount of target genes. Namely, out of more than 4000 EZH2 bound genes, around 30 maintained EZH2 after osteogenic differentiation. Consistently, this was in line with reduced H3K27me3 levels at the promoters of the target genes including RUNX2 (Wei et al., 2011). Moreover, distinct class of histone demethylases were identified as critical regulators of osteogenic differentiation of human adipose derived mesenchymal cells (hASC). Recent findings demonstrated that osteogenic differentiation of these cells was associated with reduced binding of retinoblastoma binding protein 2 (RBP2) and lysine specific demethylase 1 (LSD1 or KDM1A) , the H3K4me demethylases at the promoter of OC and OSX genes with subsequent increase in methylated H3K4 levels. Furthermore, mice xenograft models with Bio-Oss collagen scaffolds seeded with demethylase depleted hASCs revealed increased mineralization compared to scaffolds with control hASCs (Ge et al., 2011, 2014). The critical role of histone demethylases in osteoblast differentiation was further strengthened by another study by Ye L. and colleagues (Ye et al., 2012b). The authors

identified two lysine(K)-specific demethylases KDM4B and KDM6B to be upregulated during BMP4/7 induced osteogenic differentiation of MSCs. KDM6B was shown to regulate BMP2, BMP4 and HOX gene expression by removing H3K27me3 whereas KDM4B promoted DLX5 (distal-less homeobox 5) expression through removal of H3K9me3. DLX5 has profound role in osteoblastogenesis by regulating activation of RUNX2 (Samee et al., 2008). Similarly, another H3K27me3 demethylase, i.e. KDM6A was shown to carry the same role by positively regulating differentiation of MSCs into osteoblasts by affecting the expression of master regulators (Hemming et al., 2014).

The mutations causing deletion within the histone H3 lysine 36 (H3K36) trimethyltransferase gene Whsc1 (Wolf-Hirschhorn Syndrome candidate 1) leads to the development of the syndrome with the same name. This pathology is associated with growth and mental retardation, and most notably, it leads to skeletal abnormalities. It was discovered later, that Whsc1 is important for interaction of RUNX2 with p300 and facilitates this way RUNX2 dependent transcriptional regulation of target osteoblast-specific genes such as COL1A1 (Lee et al., 2014)

Increasing body of evidence suggests that lineage-specific gene expression is mainly regulated by the activity of tissue-specific enhancers. The combination of histone modifications marking the enhancer regions can dictate the functional activity of the enhancer and its accessibility to transcription factor networks involved in lineage determination. Genome-wide profiling of a combination of histone marks, namely H3K36me3, H4K20me1, H3K4me1, H3K4me2, H3K4me3, H3K9ac, H3K27ac, H4K5ac and H3K9me3 in osteoblasts induced to differentiate into osteocytes revealed more quantitative changes in these modifications correlating with gene expression changes rather than qualitative. This suggests that most of the epigenetically active regions priming the osteoblast-specific regulatory elements were established at much earlier

stages of osteoblast establishment. Moreover, vitamin D induced increase in VDR/RXR binding events in the osteocytes were mainly localized to enhancer regions enriched by H3K4me1, H3K27ac, H3K9ac and H4K5ac (St John et al., 2014). Consistently, a similar enrichment pattern was observed for co-bound RUNX2 and C/EBPb enhancer sites in mouse osteoblasts (Meyer et al., 2014a)

We previously showed that monoubiquitination of histone H2B positively affects also differentiation of human mesenchymal stem cells into the osteoblastic lineage (Karpiuk et al., 2012). H2Bub1 was shown to control expression of differentiation induced genes and differentiation of MSCs was largely impaired if cells were depleted for RNF40 or RNF20.

BET proteins

As briefly mentioned before, the histone acetylation marks are recognized by reader proteins via bromodomains. In humans, there are approximately 46 bromodomain harboring proteins which are categorized into eight families based on structure and sequence homology. The discovery of small-molecule inhibitors of Bromodomain and Extra-Terminal (BET) family proteins with high anti-tumorigenic potential made a breakthrough in the field of “epigenetic chemotherapy” of a variety of cancer subtypes and, as such, made a strong basis for extensive research in the field of BET proteins biology. The BET family includes bromodomain containing protein 2 (BRD2), BRD3, BRD4 and testis-specific BRDT. These proteins are characterized by two N-terminal bromodomain modules (BD1, BD2), one conserved extraterminal domain (ET), and additionally BRD4 and BRDT possess a C-terminal P-TEFb interaction domain (PID) (Figure 5). The modular structure of BET proteins facilitates multiple interaction possibilities for these proteins stimulating the transcriptional

activation. The binding of bromodomains to diacetylated lysine sequences, preferentially to H3 K9/K14 and H4 K5/8/12/16 enables tethering of the BETs to the active chromatin (Filippakopoulos et al., 2012) through its bromodomains (Figure 5). Moreover, the bromodomains of BRD4 can bind with acetylated non-histone proteins. For instance, the second bromodomain (BD2) of BRD4 was shown to actively bind the triacetylated cyclin T1 whereas the PID of BRD4 accounted for disassociation of HEXIM from P-TEFb this way leading to its release (Schröder et al., 2012). The latter are known to facilitate activation of RNA Polymerase II and hence the transcriptional elongation of downstream genes. The interaction of BRD4 with diacetylated TWIST was similarly shown to be dependent on BD2 (Shi et al., 2014). Moreover, both bromodomains exhibit binding ability towards acetylated v-rel avian reticuloendotheliosis viral oncogene homolog A (RelA) protein and hence are required for NF-kB activity (Huang et al., 2009). Furthermore, based on the ability of erythroid transcription factor GATA-1 to bind the BET proteins and subsequent identification of BRD3 BD1 to be responsible for this interaction, it was suggested that the same would be true for BRD4 (Lamonica et al., 2011; Stonestrom et al., 2015). A recent finding also discovered the BD1 dependent interaction of ERG with BRD4 (Blee et al., 2016). However, the function of BETs in transcriptional regulation is not only acetylation dependent. In fact, BRD4 was shown to interact with a number of transcription factors in an acetylation-independent manner (Roe et al., 2015). Consistently, proteomic analysis revealed the ability of ET domain of BRD4 to interact with some chromatin remodelers like nuclear-receptor binding SET domain protein 3 (NSD3), Chromodomain Helicase DNA Binding Protein 4 (CHD4) and Jumonji Domain Containing pretin 6 (JMJD6) (Liu et al., 2013; Rahman et al., 2011). Interestingly, BRD4 was also shown to interact with p53 which was dependent on the

phosphorylation events within the NPS (N-terminal cluster of phosphorylation sites) that controlled the conformational switch between phosphorylation dependent interaction domain (PDID) and basic residue enriched interaction (BID) (Figure 5). Namely, in the absence of phosphorylation, p53 binds the BID whereas the PDID masks the BD2 from binding to acetylated chromatin. Upon phosphorylation, the PDID interacts with BID this way unmasking the BD2 and facilitating recruitment of BRD4-p53 complex to the chromatin (Wu et al., 2013). The function of SEED (Ser/Glu/Asp-rich region) domain remains unknown, however the earlier studies on BRD2 suggested that it may be involved in the interaction with transcriptional regulators of cell cycle E2F1 and E2F2 (Denis et al., 2000).

The role of BRD4 in transcriptional regulation was further supported by the genome-wide analysis which revealed association of BRD4 with non-coding eRNA production from enhancers (Di Micco et al., 2014; Kanno et al., 2014; Liu et al., 2013; Nagarajan et al., 2014; Zhang et al., 2012). Further studies also suggested role of BRD4 in maintaining the chromatin organization (Wang et al., 2012). Similar functions were also shown for BRDT during male germ cell differentiation (Gaucher et al., 2012).

Given their crucial role in transcriptional regulation of gene expression, BET proteins were also shown to promote oncogene induced aberrant gene expression in various human malignancies. In this context, the BET inhibition was shown to induce anti-tumorigenic effects in a variety of MYC driven cancers, such as in hematological malignancies (Coudé et al., 2015; Filippakopoulos et al., 2010; Mertz et al., 2011), in brain tumors medulloblastoma (Venkataraman et al., 2014) and glioblastoma (Rajagopalan et al., 2014), in lung adenocarcinoma (Tsai et al., 2015), castration resistant prostate cancer (Asangani et al., 2014), estrogen positive breast cancer (Bihani et al., 2014), ovarian cancer (Baratta et al., 2015) and so on. Consistently,

BRD4 inhibition potently inhibited MYC driven osteosarcoma (Lamoureux et al., 2014). Moreover, the BET inhibitor JQ1 was shown to block the differentiation of both osteoblasts and osteoclasts by directly targeting the transcriptional networks involved in lineage determination (Lamoureux et al., 2014; Park-Min et al., 2014). Namely, BETi blocked the expression of RUNX2 in osteoblasts and RANKL mediated MYC-NFAT axis involved in osteoclast differentiation and activation.

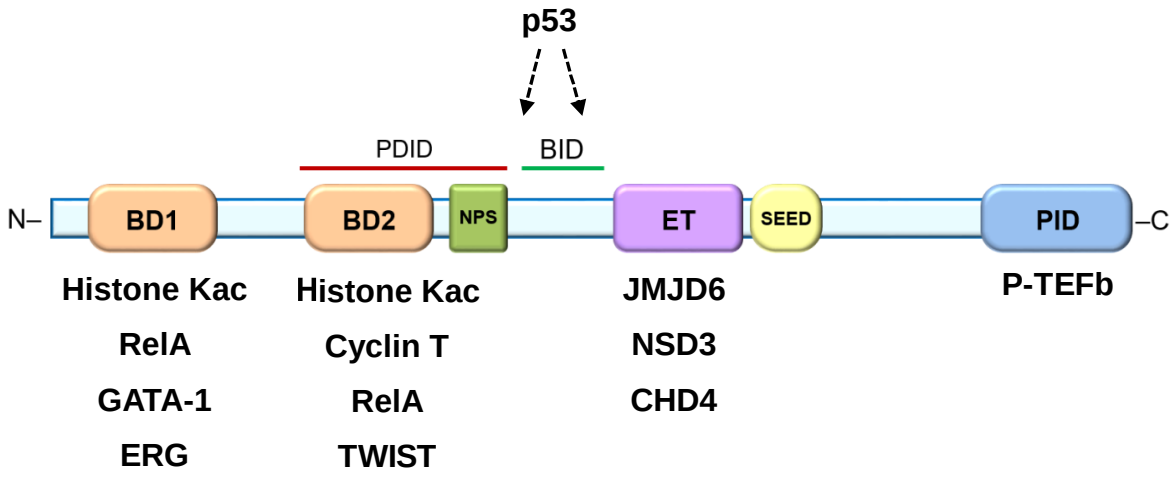

Figure 5. ***Structure and interaction partners of BRD4 protein***. BRD4 protein has several functional domains which are BD1 (bromodomain I); BD2 (bromodomain 2); PDID (phosphorylation dependent interaction domain) including NPS (N-terminal cluster of phosphorylation sites); BID (basic residue enriched interaction); ET (extra-terminal domain); SEED (Ser/Glu/Asp-rich region); PID (P-TEFb interacting domain within its C-terminal domain (CTD)).

DNA methylation

In general, DNA methylation is a reversible process associated with gene repression. It is carried out by DNA methyltransferases (DNMT) and occurs on the fifth carbon of cytosine bases (5mC). DNA methylation is most commonly observed on the palindromic dinucleotide repeats within the CpG islands (CGI). Almost 70% of human gene promoters were identified to be CGI rich. In particular, these include most of the housekeeping genes and some tissue-specifc genes (Larsen et al., 1992; Zhu et al., 2008). During the replication, the DNA methylation pattern of

parental strands is passed on to the newly formed daughter strands by the DNMT1 enzyme. After replication, de novo methylation sites are established by DNMT3A and DNMT3B enzymes. Despite its inheritable nature, DNA methylation was at the same time shown to be a very dynamic feature rapidly changing in many biological settings. The dynamic cycle of DNA methylation involves cytosine methylation, oxidation of methyl group by the family of Ten-eleven Translocation (TET) dioxygenases with subsequent formation of 5-hydroxymethylcytosine (5hmC), and restoration of unmethylated cytosines by either replication-dependent dilution or DNA glycosylase-initiated base excision repair by TDG (thymine-DNA glyosylase) (Wu and Zhang, 2014). Methylated DNA can be recognized by methyl-CpG binding proteins (MBP) that by recruiting histone modifying enzymes lead to formation of chromatin repressive signatures associated with gene inactivation. The group of zink finger-CxxC domain (ZF-CxxC domain) containing proteins was, in contrast, shown to maintain the unmethylated DNA structure within the CpG islands by recruiting the H3K4 methyltransferases and DNA demethylases (Minarovits et al., 2016). Consistently, given its broad function in regulating gene expression, DNA methylation has profound functions in bone development. In fact, differentiation of MSCs into osteoblasts is accompanied by the promoter methylation events at stemness genes (Dansranjavin et al., 2009). Active promoter DNA demethylation was consistently observed on DLX5, RUNX2, BGLAP, and OSX genes upon osteogenic induction of hASCs (Zhang et al., 2011a). The expression of SOST was also shown to be dependent on promoter methylation which decreased during transition of osteoblasts to osteocytes (Delgado-Calle et al., 2012a). Consistently, CpG island methylation was associated with decreased expression of RANKL and OPG genes in patients with osteoarthritis and osteoporosis (Delgado-Calle et al.,

2012b). The reduced expression of RANKL in response to vitamin D treatment in mouse stromal cells ST2 was in part associated with recruitment of methyl-CpG-binding protein 2 (MeCP2) to the methylated CpG island which then blocked the bindindg of TATA binding protein (TBP) required for gene activation (Kitazawa and Kitazawa, 2007).

Epigenetic contributions of non-coding RNAs

Increasing body of evidence suggests key regulatory functions of non-coding RNAs (ncRNAs) in gene expression regulation. The ncRNAs are classified into two categories based on their size. The small RNAs stand out as integral players of RNA interference pathway and are mainly involved in gene silencing due to RNA degradation and translational repression. Moreover, some of them can incorporate function of histone and DNA methyltransferases to achieve gene silencing on chromatin level. The long ncRNAs (lnRNA) can affect gene expression by acting as tethers and scaffolds for chromatin modifying enzymes, contributing to changes in chromatin structure (Holoch and Moazed, 2015). In addition, the discovery of enhancer RNAs revealed additional functions of lnRNAs in controlling gene expression by assisting enhancer-promoter looping, choromatin accessibility at defined regions, RNAPII transcriptional elongation by releasing the negative elongation factor (NELF) and activating positive transcription elongation factor (P-TEFb) (Hsieh et al., 2014; Li et al., 2013; Mousavi et al., 2013; Schaukowitch et al., 2014; Zhao et al., 2016)

Based on the action and formation mode, the small RNAs are further grouped into three categories: micro RNAs (miRNA), short interfering RNAs (siRNA) and Piwi-interacting RNAs (piRNA). Among these the miRNAs are the most widely studied

class of non-coding RNAs. miRNA are initially produced as single stranded RNA (ssRNA), referred as pri-miRNA molecules via transcription of miRNA coding genes or during splicing events from introns. They can be produced in sense and antisense orientiation. The ssRNA in turn forms imperfect double-stranded structure through hairpin-looping. The pri-miRNA is recognized b Microprocessor complex consisting of “Pasha” and “Drosha” proteins that contribute to liberation of the hairpins from initial pri-miRNA through the RNAse III activity of the “Drosha” protein. This results in formation of precursor miRNA (pre-miRNA). These then are transported to the cytoplasm by the shuttler proteins where they are subjected to endonuclease processing by Dicer enzyme. This results in formation of miRNA duplex molecule one strand of which is integrated to the RNA-induced silencing complex (RISC), which then binds to a specific target mRNA to induce its cleavage. miRNA can also induce translational repression with subsequent degradation due to deadenylation of the pol(A) tail of target mRNA (Eulalio et al., 2009; Holoch and Moazed, 2015; Jeltsch, 2011).

miRNAs were shown to play crucial role at every stage of bone formation, development and remodeling. Since mesenchymal stem cells have the multilineage potential to differentiate into adipocytes, osteoblasts, chondrocyte and myoblasts, it is of great importance to decipher the molecular mechanisms that would act some kind of “switches” modulating the lineage determination of MSCs into favored direction. As such, targeting specific transcription factors, i.e. master regulators involved in one lineage can be in fact used to modulate the differentiation choice of MCSs. At least, 19 miRNAs were discovered to target 3’-UTR region of RUNX2 in different cells of mesenchymal origin. In contrast, miR-27a and 27-b by inhibiting PPARγ were shown to promote osteoblastogenesis (Hassan et al., 2015; Vrtačnik et

al., 2014). The anabolic effect of miRNAs in bone was further demonstrated on the example of potentiating effects of miRNAs on Wnt signaling. Namely, miR-29a, miR-218 and miR-335-5p were shown to target and hence downregulate the expression of Wnt inhibitors (Hassan et al., 2012; Vrtačnik et al., 2014). A recent study in humans discovered association of high miR-214 with reduced bone formation rate in aged patients with osteoporosis. This was most likely due to direct inhibition of ATF4, the transcription regulator of osteoblastogenesis, by miR-214 (Wang et al., 2013). Furthermore, as in many other cellular systems, miRNAs were reported to impose positive or negative effects on osteoclastogenesis. For instance, miR-21 by targeting programmed cell death 4 (PDCD4) resulted in derepression of c-FOS required for differentiation of osteoclasts and in enhanced expression of miR-21 itself (Sugatani et al., 2011). At the same time, estrogen induced apoptosis of the osteoclasts was in part shown to be achieved by downregulating the expression of miR-21 that targets the FasL, the known inducer of apoptosis in osteoclasts (Sugatani and Hruska, 2013). These findings altogether suggest that the use of miRNA antisense inhibitors could be considered as a potential strategy to modulate bone remodeling during bone diseases.

Moreover, the recent advances in high-throughput sequencing techniques resulted in identification of vast number of long non-coding RNAs controlling general and tissue-specific cellular events during normal and diseased states. However, up to now very little is known about the lnRNA and their function in bone. 116 lnRNAs were found to be differentially regulated in BMP-2 induced mesenchymal stem cells differentiating into osteoblasts (Zuo et al., 2013). In human fetal osteoblasts (hFOBs) lncRNA-ANCR (anti-differentiation ncRNA) was shown to be downregulated during differentiation. Moreover, the authors discovered association of ANCR with EZH2 as

mechanistic basis to promote RUNX2 promoter H3K27 trimethylation (Zhu and Xu, 2013).

ATP-dependent chromatin remodelers, histone variants and histone chaperones

The level of chromatin compaction and nucleosome dynamics has a direct consequence on the transcriptional activity of the genes. ATP-dependent chromatin remodeler complexes (CRC) by using ATP-hydrolysis alter DNA-histone interactions hence controlling the accessibility of DNA to transcriptional regulators. Currently, the CRCs are classified into 4 groups: switching defective/sucrose nonfermenting (SWI/SNF) family; imitation switch (ISWI) family; chromodomain, helicase, DNA binding (CHD) family and inositol requiring 80 (INO80) family. All of these CRCs share some common features associated with their structure, namely the conserved ATPase domain that is required for remodeling through destabilization of DNA-histone connections; domains that recognize specific histone modifications; domains/proteins responsible for interaction with transcription factors and other chromatin remodelers; and proteins/domain that regulate the ATPase activity. Several mechanisms were suggested explaining the remodeling function of the CRCs. The currently accepted model is the “loop recapture” model which speaks for formation of a DNA loop structure on the surface of the core octamer which would propagate in wave-like manner over the surface of core octamer. Additionally, the ISWI group of CRCs can achieve chromatin remodeling in a different way. They bind the nucleosome in two copies and facilitate bidirectional sliding of DNA over the nucleosome (Clapier and Cairns, 2009; Hargreaves and Crabtree, 2011).

The components of SWI/SNF complex were shown to have crucial role in bone development as well. For instance, the expression of Brahma Related Gene 1 (BRG1) is dependent on BMP2 induced RUNX2 expression. Moreover, BRG1 can control the BGLAP expression by being directly recruited to its promoter by CCAAT/Enhancer Binding Protein beta (C/EBPb) transcription factor. Furthermore, OSX can utilize activity of BRG1 to facilitate target gene expression (Chen et al., 2015). The CHARGE syndrome in humans (combination coloboma of the eye, heart defects, atresia of the nasal choanae, retardation of growth and/or development, genital and/or urinary abnormalities, and ear abnormalities and deafness) is caused by the mutations in CHD7 chromatin remodeler. Consistently, these patients also show craniofacial abnormalities. Moreover, it was previously shown that CHD7 favors osteogenic differentiation of MSCs over adipogenic by facilitating Wnt5 induced inactivation of PPARγ (Takada et al., 2007).

The transcriptional activity can be further affected by the composition of core octamer and hence the activity of histone chaperones involved in nucleosome assembly and incorporation of different histone variants. Genome-wide studies have revealed positive correlation of histone variant H2A.Z with active enhancers (Brunelle et al., 2015). Interestingly, another report, however, suggested an inhibitory function of H2A.Z on transcriptional regulation due to enhanced chromatin compaction. Here authors also displayed histone H3.3 to be associated with active enhancer (Chen et al., 2013). Multiple histone chaperones have been identified to be involved in replication independent incorporation of histone variants into nucleosomes and/or nucleosome assembly/reassembly. For instance, histone cell cycle regulator (HIRA) is known as classical histone chaperone involved in assembly of H3.3-H4. The FACT complex was shown to mediate the nucleosomal H2A-H2B to

H2A.X–H2B exchange. Moreover, the FACT also facilitates H2A-H2B exchange in H2BK120-dependent manner (Pavri et al., 2006). The incorporation of H2A.Z was shown to be dependent on the chromatin remodeler complex SWI/SNF subunit p400 whereas recent finding discovered histone chaperone Acidic (Leucine-Rich) Nuclear Phosphoprotein 32 Family, Member E (ANP32E) to be responsible for removal of H2A.Z during DNA double-strand breaks (Gursoy-Yuzugullu et al., 2015; Xu et al., 2012).

Up to now very little is known about the histone variants and chaperones during osteogenesis. Interestingly, the differentiation of mouse myoblastic cells C2C12 into osteoblasts was shown to be dependent on histone chaperone activity of HIRA and Anti-Silencing Function 1A (ASF1A) and hence on histone H3.3 variant (Song et al., 2012). Moreover, a recent discovery from our group revealed the positive function of FACT subunit structure-specific recognition protein-1 (SSRP1) in promoting osteogenic differentiation. It was demonstrated that SSRP1 regulates expression of Wnt signaling target genes by specifically affecting the β-catenin transclocation to nucleus (Hossan et al., 2016). However, the “histone chaperone” activity of SSRP1 has been not examined yet in the context of osteoblastic gene expression regulation.

Epigenetic priming and pioneer transcription factors

The differential pattern of gene expression defining specific cellular phenotype is established and maintained by the state of the chromatin architecture. Consistently, the chromatin remodeling plays a major role in controlling the accessibility of lineage “compatible” genes to the transcriptional machinery through dynamic regulation of chromatin compaction and decompaction. Since chromatin regulators *per se* do not have DNA sequence binding specificity, the recruitment of these factors to the

“required” genomic sites is regulated by the activity of DNA sequence-specific transcription factors (TF). In fact, transcription factors play the key role in the defining the future of cell fate reprogramming. They do so by directly binding their target sequences within the promoter, enhancer and other regulatory DNA elements. Given their broad properties in transcriptional control, these factors can be categorized in two groups of general and tissue/lineage-specific TFs (TTF). Moreover, the repertoire of enhancers co-bound by several TFs establish the cell identity-specific activation of target genes. More importantly, the epigenetic marking of enhancers seems to happen prior the activation of promoter-coupled events (Drouin, 2014) .

The TFs require the accessibility of target DNA sequence to be able to bind it. This suggests that initial epigenetic priming of the TF binding regions may set up the permissive environment for lineage-specific transcription factors. Such an event of epigenetic pre-patterning has been established in embryonic stem (ES) cells. For instance, the cis-element within the immunoglobulin lambda-like polypeptide 1 (*Igll1*)–pre-B lymphocyte gene 1 (*VpreB1*) locus was initially marked by histone H3ac and H3K4me2 in undifferentiated ES cells. Upon differentiation into pre-B lymphocytes, this region expanded and became localized by TFs that resulted in subsequent activation of *Igll1 and VpreB1* genes (Szutorisz et al., 2005). Similarly, in undifferentiated ventral foregut endoderm cells with bipotential choice to either differentiate into hepatoblasts or pancreas cells, the histone modification H3K9/K14ac and H3K27me3 seemed to play important role in decision making. Namely, in undifferentiated state the H3K9/K14ac and H3K27me3 was preferentially enriched at the pancreas-specific pancreatic and duodenal homeobox 1 (Pdx1) elements whereas the liver-specific regulatory elements were substantially devoid of this marks. The differentiation into hepatoblasts was consistently associated with

increase in H3K9/K14 ac at these elements whereas the pancreatic elements remained silent because of H3K27me3 (Xu et al., 2011).

The recent advances in genome-wide studies further revealed that epigenetic marking of enhancers with specific histone variants such as H2A.Z or H3.3 can similarly serve the purpose of chromatin pre-patterning for downstream activation of enhancers and target genes (Zaret and Carroll, 2011).

Given the fact that epigenetic priming and transcription factors might be important in the establishment of lineage specifying regulatory origins, it still remains unclear how these TFs, chromatin regulators and histone modifications get localized to specific genomic sites in the silent chromatin. This all suggested existence of some additional mechanisms that would control the exposure of DNA for the regulatory circuits. Indeed, based on earlier ChIP and *in vivo* footprinting studies, a specific subtype of transcription factors was discovered that in historic terms of view appear to be first in accessing the silent condensed chromatin and initiate downstream events of transcriptional activation (Cirillo et al., 2002; Zaret and Carroll, 2011). These “pioneer” transcription factors (PTF) were shown to possess the intrinsic ability to engage their target sequences on the nucleosomes within the compact chromatin. Later studies revealed two modes of action for PTFs. In an active mode, given their intrinsic ability to bind DNA and histones, binding of PTF can affect the nucleosome positioning and disrupt internucleosomal interactions which ultimately lead to chromatin unfolding. In passive mode, the primary PTF binding to regulatory regions primes these sites for further binding of other TFs thus resulting in subsequent acceleration of transcriptional response (Zaret and Carroll, 2011). The first PTFs identified were Forkhead Box A1 (FOXA) and GATA-sequence binding TF-4 (GATA-4) involved in albumin 1 (ALB1) enhancer activation in liver precursor

endodermal cells (Cirillo et al., 2002). Interestingly, GATA-4 was shown to precede binding of estrogen receptor α (ERα) to osteoblast-specific enhancers of RUNX2, ALPL and FASL during estrogen stimulation of osteosarcoma cell lines U2OS (Miranda-Carboni et al., 2011).

The PTFs also play important role in mesenchymal stem cells. As such, the cooperative binding of CCAAT-enhancer-binding proteins (C/EBP) β and -δ, glucocorticoid receptor (GR), retinoid X receptor (RXR), signal transducer and activator of transcription 5 (Stat5a) within few hours of adipocyte differentiation of MSCs coincided with extensive changes in chromatin landscape. Moreover, most of this TF “hotspots” localized in the vicinity of PPARγ binding sites, priming these sites for subsequent binding of PPARγ at relatively later stages of adipocyte differentiation. Notably, among these TFs, C/EBPb was identified as key player binding to these “hotspots” already before the differentiation induction (Siersbæk et al., 2011). Given the important function of GR, RXR and C/EBP factors in osteogenesis (Gutierrez et al., 2002; Imai et al., 2013; Meyer et al., 2014a; Mikami et al., 2010), it is more likely that these TFs would also display “pioneer” functions during lineage commitment of OBs. In fact, most of RUNX2 binding sites in differentiating mouse osteoblasts were co-bound by C/EBPb. Most of these sites were localized to regions epigenetically marked to be enhancers. Moreover, upon vitamin D stimulation, the VDR/RxR binding also coincided with most of the RUNX2 and C/EBPb binding sites. Consistently, RUNX2 and C/EBPb binding in these cells preceded the vitamin D induced VDR binding (Meyer et al., 2014b; Pike et al., 2015).

Aim of Study

Epigenetic mechanisms are key regulatory elements during formation, establishment and maintenance of tissue-specific gene expression patterns. Acquirement of a specific cell state is always accompanied by extensive remodeling of epigenome and transitions between the states, and hence, cellular plasticity depends on the versatile interaction of several layers of epigenetic hierarchy. Consistently, the deregulation of these mechanisms contributes to the initiation, progression and maintenance of aberrant gene expression. Fortunately, the reversibility of epigenetic processes has laid the basis for the emergence of the new field of epigenetic therapy. Currently, epigenetic therapy is rapidly progressing especially in the field of cancer treatment and several epigenetic inhibitors have already entered clinical trials. The recent advances in sequencing techniques and substantial amount of sequenced data greatly enhanced our understanding of epigenetic mechanisms controlling gene expression. However, despite the growing field of cancer epigenetics, much less has been undertaken in the field of bone biology.

In the current study we sought to deepen our understanding of epigenetic mechanisms contributing to the normal process of osteoblast differentiation. Based on our previous observations, the differentiation of human mesenchymal stem cells (MSC) to the osteoblastic lineage was dependent on the global levels of histone H2B monoubiquitination at lysine 120 (H2Bub1) (Karpiuk et al., 2012). Moreover, we established the CDK9-WAC-RNF20/RNF40 axis to equally contribute to the regulation of global H2Bub1 levels and hence the differentiation of MSCs into osteoblasts (Figure 6). Cyclin-dependent kinsase 9 (CDK9) is a component of Positive transcription elongation factor b (P-TEFb) which in addition contains one of

three cyclin T molecules. P-TEFb activity is stringently regulated by the inhibitory complex consisting of the 7SK small nuclear ribonucleoprotein complex, La Related Protein-7 (LARP7) and Hexamethylene bisacetamide Inducible protein (HEXIM). In this complex 7SK snRNA mediates the interaction of P-TEFb with HEXIM which in turn blocks the kinase activity of CDK9. LARP7 was shown to associate with 7SK snRNA and control its stability (He et al., 2008; Li et al., 2005). Upon activation and disassociation from the inactive complex, P-TEFb stimulates RNA Polymerase II (RNAPII) mediated transcriptional elongation. During transcriptional activation, RNAPII is paused shortly after transcription initiation by negative transcription elongation factors (NELF) in complex with 5,6-dichloro-1-β-d-ribofuranosylbenzimidazole (DRB) - sensitivity inducing factor (DSIF). This event is considered as promoter proximal pausing of RNAPII which is also required for efficient generation of full length mRNA transcripts. During P-TEFb mediated activation NELF-E and DSIF subunit suppressor of Ty 5 homolog (SUPTH5) are subjected to phosphorylation which leads to release of NELF from the RNA molecule. At the same time, P-TEFb also phosphorylates the Ser2 residues within the RNAPII C-terminal heptapeptide repeats YSPTSPS leading to pause release of RNAPII (Yamaguchi et al., 1999, 2013). Moreover, CDK9-mediated phosphorylation of the ubiquitin-conjugating enzyme E2A (UBE2A) leads to its activation and, hence, contributes to downstream monoubiquitination of histone H2B as well (Pirngruber et al., 2009; Shchebet et al., 2012). The coupling of histone H2B monoubiquitination to transcriptional elongation was further supported by the ability of WW domain containing adaptor with coiled-coil (WAC) to directly associate the RNF20/RNF40 complex to Ser2 phosphorylated RNAPII (Zhang and Yu, 2011). Consistently, loss of both CDK9 and WAC exhibited similar effects by downregulating osteoblast-specific

genes in MSCs most likely through global decrease in H2Bub1 levels (Karpiuk et al., 2012).

The association of P-TEFb with the inhibitory complex also suggested a requirement for activator proteins to mediate its release once required. As such, the BET protein BRD4 was shown to associate with the active pool of P-TEFb and mediate its recruitment to acetylated chromatin (Jang et al., 2005; Patel et al., 2013; Schröder et al., 2012; Yang et al., 2005). Given its role in P-TEFb activation, we hypothesized that BRD4 may similarly regulate the expression of osteogenic genes through directly acting upstream of CDK9-WAC-RNF20/40 axis (Figure 6). We therefore decided to elucidate its function during osteoblastogenesis. In line with this, we also intended to analyze the epigenetic landscape associated with differentiation induced changes in gene expression. Moreover, given its role as a epigenetic reader, we further sought to decipher the transcription factors that could potentially utilize BRD4 to regulate the osteoblast-specific gene expression.

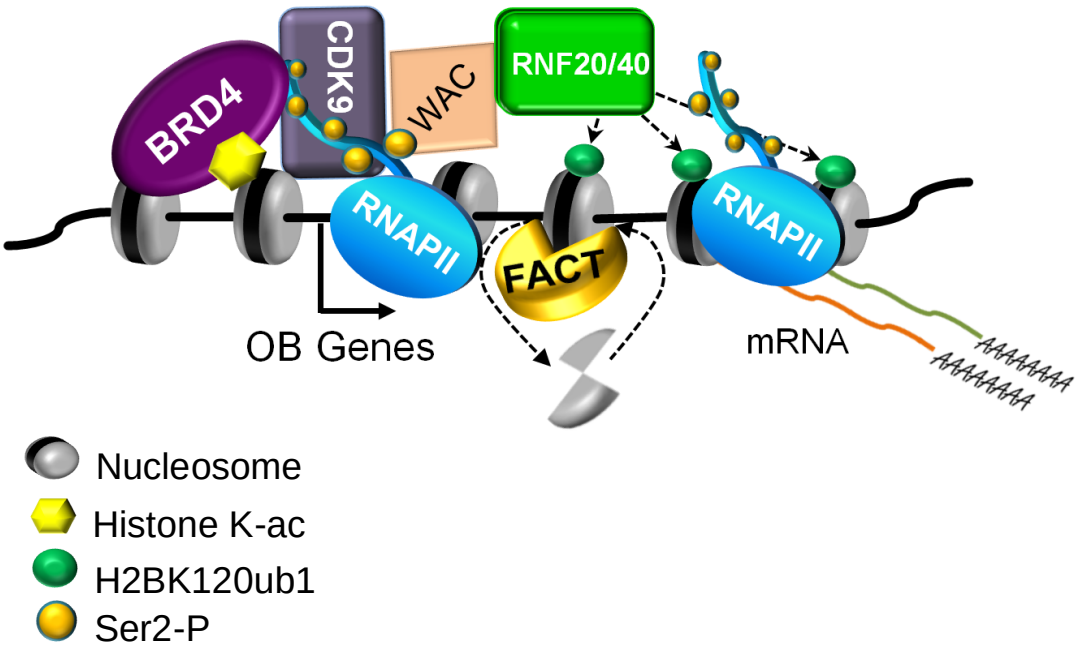

Figure 6. ***The model of BRD4-CDK9-WAC-RNF20/40 axis in regulation of osteoblast-specific gene expression***. Shortly after transcription initiation, RNAPII is paused at the promoter. Given the lineage-specific signal induction, BRD4 mediates the release of P-TEFB (CDK9) from inactive complex. CDK9 phosphorylates then the paused RNAPII at Ser2 residues of C-terminal tail. The Ser2P is recognized by adaptor protein WAC that links RNF20/40 to activated RNAPII on the chromatin. The subsequent monoubiquitination of H2B by this E3 ligase complex further stimulates transcriptional elongation by RNAPII, for example by facilitating the histone H2A-H2B exchange by FACT, hence easing the passage of RNAPII through "bulky" nucleosomes.

Furthermore, based on the function of RNF20/RNF40 induced H2B monoubiquitination in controlling the osteogenic differentiation we decided to determine its function during normal bone development in mice as well. Proceeding from our *in vitro* experience, we hypothesized that mice with conditional loss of H2Bub1 would not develop functionally normal bones. Moreover, we assumed that through modulation of H2Bub1 levels in mice, namely through the osteoblast-specific deletion of the H2Bub1-specific DUB - ubiquitin-specific protein 22 (USP22), we could achieve increased bone formation. This would imply an anabolic potential of USP22 inhibitors and as such, offer a new strategy for epigenetic therapy of bone loss associated diseases, such as osteoporosis.

MATERIALS AND METHODS

Materials

Equipment

-150 °C Freezer (MDF-C2156VAN)	Panasonic, Kadoma, Japan
-20 °C Freezer	Liebherr GmbH, Biberach
-80 °C Freezer “Hera freeze”	Thermo Fisher Scientific, Waltham, USA
2100 Bioanalyzer	Agilent Technology, Santa Clara, USA
Agarose gel chamber	Harnischmacher Labortechnik, Kassel
Balance	Sartorius AG, Göttingen
Bandelin Sonoplus Sonicator	Bandelin electr. GmbH & Co. KG, Berlin
Biological Safety Cabinet “Safe 2020”	Thermo Fisher Scientific, Waltham, USA
Bioruptor ® Plus sonication device	Diagenode SA, Liège, Belgium
Bioruptor ® Pico sonication device	Diagenode SA, Liège, Belgium
Centrifuge (Megafuge 1.OR)	Thermo Fisher Scientific, Waltham, USA
Centrifuge 4 °C (5417R)	Eppendorf AG, Hamburg
Centrifuge 4 °C (Fesco 21)	Thermo Fisher Scientific, Waltham, USA
Counting chamber (Neubauer)	Brand GmbH & Co. KG, Wertheim
DynaMag TM 2	LifeTechnology, Carlsbad, USA
DynaMag TM 96 Side	LifeTechnology, Carlsbad, USA
Eclipse TS100	Nikon, Tokio, Japan
Electrophoresis & Electrotransfer Unit	GE Healthcare Europe GmbH, München
Gel iX Imager	Intas Science Imaging GmbH, Göttingen
HERAcell 150i CO 2 Incubator	Thermo Fisher Scientific, Waltham, USA
Imager Western Blot	Bio-Rad Laboratories, Hercules, USA
Inverse Microscope “Axiovert 40 CFL”	Carl Zeiss MicroImaging GmbH, Göttingen
Isotemp ® water bath	Thermo Fisher Scientific, Waltham, USA

Magnet stirrer “MR3001”	Heidolph GmbH & Co. KG, Schwabach
Microcentrifuge C1413-VWR230	VWR, Radnor, USA
Microscope Axio Scope.A1 equipped with an AxioCam MRc	Carl Zeiss MicroImaging GmbH, Göttingen
Microscope Axiovert 100	Carl Zeiss MicroImaging GmbH, Göttingen
Microwave	Clatronic International GmbH, Kempen
Mini Trans-Blot TM Cell	Bio-Rad Laboratories, Hercules, USA
Mini-PROTEAN Tetra Cell	Bio-Rad Laboratories, Hercules, USA
Mr. Frosty ® Cryo Freezing Container	Thermo Fisher Scientific, Waltham, USA
Nano Drop ® ND-1000	Peqlab Biotechnology GmbH, Erlangen
Optical Reaction Module CFX96 TM	Bio-Rad Laboratories, Hercules, USA
pH meter inoLab ®	WTW GmbH, Weilheim
Pipette Aid ® portable XP	Drummond Scientific Co., Broomall, USA
Pipettes “Research” Series	Eppendorf AG, Hamburg
PowerLyzer™ 24 (Bead-Based Homogenizer)	MO BIO Lab., QIAGEN, USA
Power supply Power Pack P25T	Biometra GmbH, Göttingen
PowerPac TM Basic Power Supply	Bio-Rad Laboratories, Hercules, USA
PowerPac TM HC Power Supply	Bio-Rad Laboratories, Hercules, USA
Qubit ® 2.0 Fluorometer	Invitrogen GmbH, Karlsruhe
Refrigerator	Liebherr GmbH, Biberach
Scanner Epson V700 Photo	Seiko Epson, Suwa, Japan
Shaker “Rocky”	Schütt Labortechnik GmbH, Göttingen
Test tube rotator	Schütt Labortechnik GmbH, Göttingen
Thermal Cycler T100 TM	Bio-Rad Laboratories, Hercules, USA
Thermo mixer C	Eppendorf AG, Wessling-Berzdorf
Vortex-Genie 2	Electro Scietific Industr. Inc., Portland, USA

Consumable Materials

96-well Multiplate ® PCR plate, white	Bio-Rad Laboratories, Hercules, USA
Bioruptor Microtubes (0.1, 0.65, 1.5 ml)	Diagenode SA, Liège, Belgium
CA-Membrane 0.2 and 0.45µm filters	TH. Geyer, Wesertal
Cell scraper (16 cm, 25 cm)	Sarstedt AG & Co., Nümbrecht
Cellstar 6- ,12-well cell culture plates	Greiner Bio-One GmbH, Frickenhausen
Cellstar PP-tube 15 and 50 ml	Greiner Bio-One GmbH, Frickenhausen
Cellstar tissue culture dish 100×20 mm	Greiner Bio-One GmbH, Frickenhausen
Cellstar tissue culture dish 145×20 mm	Greiner Bio-One GmbH, Frickenhausen
Cryo Tube Vial (1.8 ml)	Thermo Fisher Scientific, Waltham, USA
Disposable Safety Scalpel	FEATHER Safety Razor Co., Osaka Japan
DNA loBinding Tube 1.5 and 0.5 ml	Eppendorf AG, Wessling-Berzdorf
Fine-ject 27Gx3/4 (Nr 20) Needles	Henke-Sass Wolf, Tuttlingen
Gel blotting paper (Whatman paper)	Sartorius AG, Göttingen
Hybond^{TM}-PVDF Transfer Membrane	GE Healthcare Europe GmbH, München
Injekt-F 1ml single-up syringe	B.Braun Melsungen, Melsungen
Lysing Matrix Tubes with beads	MP Biomedicals, Eschwege
Microtube 1.5 ml and 2 ml	Sarstedt AG & Co., Nümbrecht
Parafilm ® “M”	Pechiney Plastic Packaging, Chicago, USA
PCR-Strips	Biozyme, St. Joseph, USA
Pipette filter tips	Sarstedt AG & Co., Nümbrecht
Pipette tips	Greiner Bio-One GmbH, Frickenhausen
Soft-Ject® Syringes 10 and 20ml	Henke-Sass Wolf, Tuttlingen

Chemicals and Reagents

α,α-Trehalose (+)	AppliChem GmbH, Darmstadt
Agarose	Carl Roth GmbH & Co. KG, Karlsruhe
Agencourt ® AMPure ® XP Beads	Beckman Coulter Inc. Brea USA
Albumin Fraction V (Protease and Fatty Acid free)	SERVA, Heidelberg

Alizarin Red S	Sigma-Aldrich Co., St. Louis, USA
Ammonium persulfate	Carl Roth GmbH & Co. KG, Karlsruhe
Ammonium sulfate	Carl Roth GmbH & Co. KG, Karlsruhe
Antibiotic-Antimycotic	LifeTechnology, Carlsbad, USA
Aprotinin	Carl Roth GmbH & Co. KG, Karlsruhe
Ascorbic acid	Sigma-Aldrich Co., St. Louis, USA
BET inhibitor (+)JQ1 ($C_{23}H_{25}ClN_4O_2S$)	provided by Stefan Knapp from Goethe-University Frankfurt am Main
Bromophenol blue	Sigma-Aldrich Co., St. Louis, USA
Calcein	Sigma-Aldrich Co., St. Louis, USA
Calcitriol (1α,25-dihydroxy Vit D3)	Biomol GmbH, Hamburg
Calcium Chloride	Carl Roth GmbH & Co. KG, Karlsruhe
Chloroform	Carl Roth GmbH & Co. KG, Karlsruhe
Dexamethasone	Sigma-Aldrich Co, St. Louis, USA
Diethylpyrocarbonate dihydrate	Carl Roth GmbH & Co. KG, Karlsruhe
Dimethyl sulfoxide	AppliChem GmbH, Darmstadt
di-Sodium hydrogen phosphate	Carl Roth GmbH & Co. KG, Karlsruhe
Dithiothreitol	Carl Roth GmbH & Co. KG, Karlsruhe
DMEM	LifeTechnology, Carlsbad, USA
DMEM/F12	LifeTechnology, Carlsbad, USA
dNTP Bundle	Jena Bioscience, Jena
Ethanol absolute	Th. Geyer GmbH & Co. KG, Renningen
Ethidium bromide	Carl Roth GmbH & Co. KG, Karlsruhe
Ethylenediaminetetraacetic acid	Carl Roth GmbH & Co. KG, Karlsruhe
Fetal Bovine Serum	Thermo Scientific HyClone, Logan,USA
Formaldehyde	Sigma-Aldrich Co., St. Louis, USA
Formamide	Carl Roth GmbH & Co. KG, Karlsruhe
Glycerol	Carl Roth GmbH & Co. KG, Karlsruhe
Glycine	Carl Roth GmbH & Co. KG, Karlsruhe

HD Green Plus DNA Stain	INTAS, Science Imaging, Göttingen
Hydrochloric acid	Carl Roth GmbH & Co. KG, Karlsruhe
Immobilon TM Western HRP substrate	Merck Millipore KGaA, Darmstadt
Iodoacetamide	Sigma-Aldrich Co, St. Louis, USA
Isopropanol	Carl Roth GmbH & Co. KG, Karlsruhe
L-Ascorbic acid	Sigma-Aldrich Co, St. Louis, USA
Lithium Chloride	Sigma-Aldrich Co, St. Louis, USA
Leupeptin	Carl Roth GmbH & Co. KG, Karlsruhe
Linear Acrylamide	Ambion, USA
Magnesium chloride	Carl Roth GmbH & Co. KG, Karlsruhe
MEM α powder	LifeTechnologies AG, Carlsbad, US
Methanol	Carl Roth GmbH & Co. KG, Karlsruhe
Monopotassium phosphate	Carl Roth GmbH & Co. KG, Karlsruhe
MOPS 3-(N-Morpholino)-propansulfonic acid sodium salt	Carl Roth GmbH & Co. KG, Karlsruhe
N,N-Dimethylformamide	Sigma-Aldrich Co., St. Louis, USA
N-ethylmaleimide	Sigma-Aldrich Co., St. Louis, USA
Nonidept TM P40	Sigma-Aldrich Co., St. Louis, USA
Opti-MEM	LifeTechnology, Carlsbad, USA
Paraformaldehyde	Carl Roth GmbH & Co. KG, Karlsruhe
PBS tablets	LifeTechnology, Carlsbad, USA
Pefabloc SC	Carl Roth GmbH & Co. KG, Karlsruhe
Penicillin-Streptomycin solution	Sigma-Aldrich Co., St. Louis, USA
Polybrene	Sigma-Aldrich, St. Louis, USA
Potassium acetate	Carl Roth GmbH & Co. KG, Karlsruhe
Potassium chloride	AppliChem GmbH, Darmstadt
Potassium dihydrogen phosphate	Carl Roth GmbH & Co. KG, Karlsruhe
Propidium iodide solution	Sigma-Aldrich Co., St. Louis, USA
Protein A Sepharose TM CL-4B	GE Healthcare, Uppsala, Sweden

QIAzol® Lysis Reagent	Qiagen, Maryland, USA
RNAiMAX	LifeTechnology, Carlsbad, USA
Roti ® -Phenol	Carl Roth GmbH & Co. KG, Karlsruhe
Rotiphorese ® Gel 30	Carl Roth GmbH & Co. KG, Karlsruhe
Rotipuran ® Chloroform	Carl Roth GmbH & Co. KG, Karlsruhe
Rotipuran ® Isoamylalcohol	Carl Roth GmbH & Co. KG, Karlsruhe
Sepharose TM CL-4B	GE Healthcare, Uppsala, Sweden
Skim milk powder	Carl Roth GmbH & Co. KG, Karlsruhe
Sodium acetate	Carl Roth GmbH & Co. KG, Karlsruhe
Sodium azide	Sigma-Aldrich Co., St. Louis, USA
Sodium chloride	Carl Roth GmbH & Co. KG, Karlsruhe
Sodium deoxycholate	AppliChem GmbH, Darmstadt
Sodium dodecylsulfate (SDS)	Carl Roth GmbH & Co. KG, Karlsruhe
Sodium hydrogen carbonate	Carl Roth GmbH & Co. KG, Karlsruhe
Sodium hydroxide	Carl Roth GmbH & Co. KG, Karlsruhe
ß-Glycerolphosphate	Sigma-Aldrich Co., St. Louis, USA
SYBR Green	Roche Diagnostics GmbH, Mannheim
TEMED	Carl Roth GmbH & Co. KG, Karlsruhe
Tris	Carl Roth GmbH & Co. KG, Karlsruhe
Triton X-100	AppliChem GmbH, Darmstadt
Trypsin-EDTA	LifeTechnology, Carlsbad, USA
Tween-20	AppliChem GmbH, Darmstadt

Kits and reagents

Alkaline phosphatase leukocyte kit	Sigma-Aldrich Co., St. Louis, USA
Agilent High Sensitivity DNA Kit	Agilent Technology, Santa Clara, USA
HOT FIREPol® DNA Polymerase Set	Solis BioDyne, Estonia
Lipofectamine TM RNAiMAX	LifeTechnology, Carlsbad, USA
NEXTflex Rapid Directional RNA-Seq Kit	Bioo Scientific, Austin, USA

MicroPlex Library Preparation TM	Diagenode SA, Liège, Belgium
Qubit dsDNA HS Assay	LifeTechnology, Carlsbad, USA
Immobilon Western Chemiluminiscent HRP substrate	Millipore, Billerica, USA
SuperSignal ® West Femto Maximum	Thermo Fisher Scientific, Waltham, USA

Enzymes

Colleganase A	Roche Diagnostics, Mannheim
Dispase	Gibco, Life Technologies, USA
Proteinase K	LifeTechnology, Carlsbad, USA
Reverse Transcriptase (M-MuLV)	New England Biolabs, FFM
RNase A	Qiagen GmbH, Hilden
RNase inhibitor	New England Biolabs, FFM
Taq DNA Polymerase	Primetech, Minsk, Belarus

Molecular weight standards

Gene RulerTM DNA-Ladder	Fermentas GmbH, St. Leon-Rot
PageRulerTM Prestained Protein Ladder	Fermentas GmbH, St. Leon-Rot

Cells

Name	Origin	Source
hFOB 1.19	Human	T. Spelsberg, Mayo Clinic, USA (Harris et al., 1995)
IDG-SW3	Mouse	Malayannan Subramaniam and John R. Hawse, Mayo Clinic, USA (Woo et al., 2011)
Primary long bone OBs	Mouse	This Study
Primary calvarial OBs	Mouse	This Study

Oligonucleotides

siRNAs

TARGET	SEQUENCE (5' à 3')	SOURCE	Catalogue Nr.
Non-targeting siRNA#2 (ON-TARGETplus)	UGGUUUACAUGUUGUGUGA	Dharmacon (Lafayette, USA)	D-001810-02
BRD4 siRNA#2 (siGENOME)	GAACCUCCCUGAUUACUAU	Dharmacon (Lafayette, USA)	D-004937-02
BRD4 siRNA#3 (siGENOME)	UAAAUGAGCUACCCACAGA	Dharmacon (Lafayette, USA)	D-004937-03
BRD4 siRNA#4 (siGENOME)	UGAGAAAUCUGCCAGUAAU	Dharmacon (Lafayette, USA)	D-004937-04
BRD4 siRNA#5 (siGENOME)	AGCUGAACCUCCCUGAUUA	Dharmacon (Lafayette, USA)	D-004937-05

Primers

Primers were designed using the NCBI primer designing tool (http://www.ncbi.nlm.nih.gov/tools/primer-blast/) and ordered from Sigma-Aldrich Co., St. Louis, USA .

- *ChIP Primers*

TARGET	SEQUENCE (5' à 3')	REFERENCE
chr10:4705151-4705651 F	TGAGTAAACACTTAACAGGGCGT	This Study
chr10:4705151-4705651 R	CATCCACGTGTTCTGCATGATT	This Study
chr12:46886451-46886951 F	GCAGAAGAGTTCAGCCTCACC	This Study
chr12:46886451-46886951 R	CATTCAAATACAGTGAACCCAGACC	This Study
chr3: 16101551-16102051 F	ACTCATCTTCAGGAATGGGCA	This Study
chr3: 16101551-16102051 R	TGTTTGTGTCAACCACCAAAGG	This Study

COL1A1 TSS F	CACGTCTCGTTTTAAGCCGC	This Study
COL1A1 TSS R	GCCAAGAGGAAGGCCAAGTC	This Study
HNRNPK +BRD4 site F	TCCACGAGGTCCCTAGTTCC	(Nagarajan et al., 2015)
HNRNPK +BRD4 site R	GCCATTTCCCTGAGCGTGTA	(Nagarajan et al., 2015)
OLIG2 +H3K27me3 Site	GTCACCAACGCTCCCTGAAAT	This Study
OLIG2 +H3K27me3 Site	TTGCATGAGAGCAGAGGGGA	This Study
CDKN1A TR F	CCAGGGCCTTCCTTGTATCTCT	(Gomes and Espinosa, 2010)
CDKN1A TR R	ACATCCCCAGCCGGTTCT	Gomes and Espinosa, 2010)
CDKN1A TSS	GGGGCGGTTGTATATCAGG	(Pirngruber et al., 2009)
CDKN1A TSS	GGCTCCACAAGGAACTGACTTC	(Gomes et al., 2006)
RPLP0_TSS R	CTTCGCGACCCTACTTAAAGG	(Nagarajan et al., 2015)
RPLP0_TSS F	CAATCAGAAACCGCGGATAG	(Nagarajan et al., 2015)
SOST +H3K27me3 Site F	GAGTGCCTGGAACCTGTTTCT	This Study
SOST +H3K27me3 Site R	CACCGGACACTCTATGCTGG	This Study
TFF1+6KB F	CAGGCTTCTCCCTTGATGAAT	(Pirngruber and Johnsen, 2010)
TFF1+6KB R	ACACCCACCTTCCACAACAC	(Pirngruber and Johnsen, 2010)

- ***Gene Expression Primers***

TARGET	SEQUENCE (5’ à 3’)	REFERENCE
ALPL F	TGGGCCAAGGACGCTGGGAA	(Karpiuk et al., 2012)
ALPL R	AAGGCCTCAGGGGGCATCTCG	(Karpiuk et al., 2012)
BGLAP F	ATGAGAGCCCTCACACTCCT	This Study

BGLAP R	GCTTGGACACAAAGGCTGCAC	This Study
BMP1 F	GTTCTGAGAAGCCCGAGGTC	This Study
BMP1 R	AGAGCTGGCCTCTTTTCTGAG	This Study
BRD4 F	GCCGTCCACACTGCGTGAGC	(Nagarajan et al., 2014)
BRD4 R	TCCCGGGGTGCCCCTTCTTT	(Nagarajan et al., 2014)
CDH11 F	CCCTCAAGGGCCCCAGAAAT	This Study
CDH11 R	CGTCCCCAGTTAGCTTCTTCT	This Study
DCN F	GGGATAGGCCCAGAAGTTCC	This Study
DCN R	GATGGCATTGACAGCGGAAG	This Study
ELN F	TCCCGGGAGTTGGCATTTC	S.Baumgart, WG Johnsen
ELN R	ACTGGGCGGCTTTGGC	S.Baumgart, WG Johnsen
RPLP0	GATTGGCTACCCAACTGTTG	(Fritah et al., 2005)
RPLP0	CAGGGGCAGCAGCCACAAA	(Fritah et al., 2005)
RUNX2	TCGGAGAGGTACCAGATGGG	This Study
RUNX2	CATTCCGGAGCTCAGCAGAA	This Study
TGFBR2 F	CATGAGCAACTGCAGCATCAC	This Study
TGFBR2 R	CTTTCTCCATACAGCCACACAGA	This Study
THBS2 F	CCAGGGAGCTGAGATCAACG	This Study
THBS2 R	CCACCAATGAGCTCCCAGAG	This Study
TNFRSF11B F	GCGCTCGTGTTTCTGGACATC	This Study
TNFRSF11B R	CACACGGTCTTCCACTTTGC	This Study
mAlpl F	GGGCAATGAGGTCACATCCA	S.Baumgart, WG Johnsen
mAlpl R	GTGGTTACCCGAGTGGTAG	S.Baumgart, WG Johnsen
mBglap F	CCTGAGTCTGACAAAGCCTTCA	This Study

mBglap R	GCCGGAGTCTGTTCACTACCTT	This Study
mDmp1 F	TGCTCTCCCAGTTGCCAGAT	(Gingery et al., 2014)
mDmp1 R	AATCACCCGTCCTCTCTTCAGA	(Gingery et al., 2014)
mGapdh F	CACTTGAAGGGTGGAGCCAA	W. Xie, WG Johnsen
mGapdh R	GGTCATGAGCCCTTCCACAA	W. Xie, WG Johnsen
mMepe F	TGCTGCCCTCCTCAGAAATATC	(Gingery et al., 2014)
mMepe R	GTTCGGCCCCAGTCACTAGA	(Gingery et al., 2014)
mRnf40 (exon3) F	GCCACACTCCTCATCGTCAA	W. Xie, WG Johnsen
mRnf40(exon4) R	CTGGGAGAGGAGTCCCATCA	W. Xie, WG Johnsen
mRunx2 F	ATCCCATCCATCCACTCCA	S.Baumgart, WG Johnsen
mRunx2 R	GCCAGAGGCAGAAGTCAGAG	S.Baumgart, WG Johnsen
mSp7 F	GCAAAGGCCTGAGAGGAGTT	S.Baumgart, WG Johnsen
mSp7 R	GGGCTCTCTCTGTTCCCCTA	S.Baumgart, WG Johnsen

- ***Genotyping Primers***

Target	**Sequence (5' à 3')**	**Reference**	**Product Size**
Rnf40 F	GCGAAAGTCACATTTGGCCT	This Study	WT - 229 bp, LoxP/LoxP - 297 bp
Rnf40 R	CTTCACATTCCGTTCCTGCC		
Usp22 F	TGTGCCCTGGTTGCCCAGTGA	This Study	WT -322 bp, LoxP/LoxP- 470 bp
Usp22 R	GCACCACCACAGCCGTCCTT		
Runx2-Cre_24	CCAGGAAGACTGCAAGAAGG	(Movérare-Skrtic et al., 2014)	+Cre - 600 bp, WT - 780 bp
Runx2-Cre_25	TGGCTTGCAGGTACAGGAG		
Runx2-Cre_30	GGAGCTGCCGAGTCAATAAC		
Bglap-Cre F (general Cre)	CGCGGTCTGGCAGTAAAAACTAT	JAX® Mice and Services	+Cre - 332bp
Bglap-Cre R (generic Cre)	CCCACCGTCAGTACGTGAGATAT		
Rosa-CreERT2 wt F	AAAGTCGCTCTGAGTTGTTAT	(Ventura et al., 2007)	CreERT2 - 825bp ; WT - 650bp
Rosa-CreERT2 wt R	GGAGCGGGAGAAATGGATATG		

Rosa-CreERT2 mut R	CCTGATCCTGGCAATTTCG		

Antibodies

Primary Antibodies

The primary antibody dilutions were prepared in 5% skim milk in TBS-T and supplemented with 0.01% sodium azide.

Target Protein	ChIP	WB	Clone	Source	Cat. Nr
BRD4		1:1000		Abcam	ab128874
BRD4 (N-term)	3µl			Wu et al., 2006	
CEBP/β	1.5µg		C-19	Santa Cruz	sc-150
FOSL2	1.5µg		Q-20	Santa Cruz	sc-604
H2B		1:10000		Abcam	ab1790
H2Bub1	1µl		D11	Cell Signalling	5546
H2Bub1		1:10	7B4	Prenzel et al., 2011	
H3K27ac	1µg	1:1000		Diagenode	C15410196
H3K27me3	1µg			Diagenode	C15410195
HSC70		1:20000	B-6	Santa Cruz	sc 7298
IgG	1µg			Abcam	ab37415
JUND	1.5µg		329	Santa Cruz	sc-74
RNA Polymerase II	1.2µg	1:1000	N-20	Santa Cruz	sc-899
RNF40		1:500	S-12	Santa Cruz	sc-132079
STAT3	1.5µg		C-20	Santa Cruz	sc-482
TEAD1	1.5µg		31/TEF-1	BD Biosciences	610922

Secondary Antibodies

Name	WB	Source	Cat. Nr.
goat anti-mouse (IgG)-HRP	1:10000	Santa Cruz	sc-2004
goat anti-rabbit (IgG)-HRP	1:10000	Santa Cruz	sc-2005
donkey anti-goat (IgG)-HRP	1:5000	Santa Cruz	sc-2020

Buffers and Media

Alizarin Red staining solution: 2% Alizarin Red in DI H2O, pH 4.1-4.3 adjusted with HCl

Blocking solution: 1× PBS-T, 5% (w/v) milk

Calcein Solution: 0.4% (w/v) calcein, 0.4% sodium hydrogen carbonate prepared in PBS, filtered before injections.

DEPC water: 0.1% (v/v) DEPC in DI H2O

Formaldehyde (FA) gel buffer (10x): 200mM 3-[N-morpholino]propanesulfonic acid(MOPS) (free acid), 50mM sodium acetate, 10mM EDTA, pH 7 prepared in RNAse free water.

FA gel running buffer: 10% (v/v) 10xFA gel buffer, 0.74% Formaldehyde, prepared in RNAse free water.

Gomes Lysis Buffer: 150 mM NaCl, 1% (v/v) NP-40, 0.5% (w/v) sodium deoxycholate, 50 mM Tris-HCl (pH 8), 20 mM EDTA, 20 mM NaF, ± 0.1-0.5% (w/v) SDS

Gomes Wash Buffer: 100 mM Tris-HCl (pH 8.5), 500 mM LiCl, 1% (v/v) NP-40, 1% (w/v) sodium deoxycholate, 20 mM EDTA, 20 mM NaF

Inhibitor cocktail (1×): 1 mM Pefabloc, 1 ng/µl Aprotinin/Leupeptin, 10 mM BGP, 1 mM N-ethylmaleimide, 10 µM iodoacetamide

Lämmli buffer (6×): 0.35 M Tris (pH 6.8), 30% (v/v) glycerol, 10% (w/v) SDS, 9.3% (w/v) DTT, 0.02% (w/v) bromphenol blue

Nelson Lysis Buffer: 150 mM NaCl, 20 mM EDTA (pH 8), 50 mM Tris (pH 7.5), 0.5% (v/v) NP-40, 1% (v/v) Triton X-100, 20 mM NaF.

PBS (1×): 137 mM NaCl, 2.68 mM KCl, 4.29 mM $Na_2HPO4×2H2O$, 1.47 mM KH_2PO4, pH 7.4

PBS-T: PBS with 0.1% (v/v) Tween-20

PBS for cell culture: 1 PBS tablet per 500 ml ddH2O

PFA (4%): 4% paraformaldehyde powder prepared in PBS

qRT-PCR mix: 75 mM Tris-HCl (pH 8.8), 20 mM $(NH4)_2SO4$, 0.01% Tween-20, 3 mM MgCl2, 200 µM dNTPs, 0.5 U/reaction Taq DNA Polymerase, 0.25% Triton X-100, 1:80,000 SYBR Green I, 300 mM Trehalose

RIPA buffer: 1× PBS, 1% (v/v) NP-40, 0.5% (w/v) sodium deoxychelate, 0.1% (w/v) SDS

RNA loading dye (5x):0.16% brophenol blue solution, 4mM EDTA, 2.7% formaldehyde, 20% (v/v) glycerol, 30.84% (v/v) formamide,40% (v/v) FA gel buffer (10x), prepared in RNAse free water.

SDS separating gel (X%): X%(v/v) acrylamide, 375mM Tris-HCl (pH 8.8), 0.1% (w/v) SDS, 0.1% (w/v) APS, 0.04% (v/v) TEMED

SDS stacking gel: 5% (v/v) acrylamide, 125.5 mM Tris-HCl (pH 6.8), 0.1% (w/v) SDS, 0.1% (w/v) APS, 0.1% (v/v) TEMED

TAE buffer (50×): 2 M Tris, 1 M Acetic acid, 0.1 M EDTA

TBS: 150 mM NaCl, 2.68 mM KCl, 4.29 mM Na2HPO4×2H2O, 1.47 mM KH2PO4, (pH 7.4)

TBS-T: TBS with 0.1% (v/v) Tween-20

TE buffer: 10 mM Tris-HCl, 1 mM EDTA, pH to 8.0

Transfer buffer: 10% (v/v) 10× Western salts, 1% (v/v) Methanol

Tris-glycine electrophoresis buffer: 25 mM Tris, 200 mM Glycine, 0.1% (w/v) SDS

Weinmann buffer: 50mM Tris-HCl (pH 8), 10mM EDTA and 1 % SDS

Western salts (10x): 1.92 M Glycine, 250 mM Tris-HCl (pH 8.3), 0.02% (w/v) SDS

Media:

αMEM culture medium: phenol red, L-glutamine, supplemented with 10% FBS, 1% Penicillin-Streptomycin solution (100 U/ml penicillin, 100 µg/ml streptomycin).

DMEM-F12 cell culture medium: phenol red-free, high-glucose, supplemented with 10% FBS, 1% Penicillin-Streptomycin solution (100 U/ml penicillin, 100 µg/ml streptomycin)

Cell freezing medium: 42% corresponding culture medium, 50% FBS, 8% DMSO

Mouse Lines

Name	Description, Source
Bglap-Cre: B6N.FVB-Tg(BGLAP-cre)$^{1Clem/J}$	These mice harbor Cre-recombinase under the control of Bglap promoter (Zhang et al., 2002) http://jaxmice.jax.org/strain/019509.html
Rosa26-Cre/ERT2: ROSA26(Cre-ERT2)^{tmBock}	In these mice the fused Cre-recombinase with mutated form of estrogen receptor (ERT2) was inserted into ubiquitously expressed Gt(ROSA)26Sor Locus. The fused Cre gets translocated to the nucleous upon 4-hydroxytamoxifen treatment. (Ventura et al., 2007) http://jaxmice.jax.org/strain/008463.html
Rnf40$^{fl/fl}$ Rnf40^{Tm1Saj}	The exon 3 and 4 of Rnf40 gene are floxed with LoxP sequences in these mice. (Source: This Study, WG Johnsen)
Runx2-cre:	These mice express Cre-recombinase under the

Tg(Runx2-icre)^{1Jtuc}	control of second Runx2 promoter (Rauch et al., 2010) http://www.informatics.jax.org/allele/MGI:4455015
Usp22$^{fl/fl}$: Usp22$^{tm1a(KOMP)Wtsi}$	In this mouse line, the Usp22 gene exon2 is flanked from both sites with LoxP sequences. http://www.mousephenotype.org/martsearch_ikmc_project/martsearch/ikmc_project/35107

High-throughput sequencing data used in the study

Dataset	Type	Database	Accession Number	Source
hFOB DIF_BRD4	ChIP-Seq	GEO	GSE82297	This Study
hFOB DIF_H2Bub1	ChIP-Seq	GEO	GSE82297	This Study
hFOB DIF_H3K27ac	ChIP-Seq	GEO	GSE82297	This Study
hFOB DIF_H3K27me3	ChIP-Seq	GEO	GSE82297	This Study
hFOB DIF_INPUT	ChIP-Seq	GEO	GSE82297	This Study
hFOB DIF_RNAPII	ChIP-Seq	GEO	GSE82297	This Study
hFOB DIF+JQ1_H2Bub1	ChIP-Seq	GEO	GSE82297	This Study
hFOB DIF+JQ1_H3K27ac	ChIP-Seq	GEO	GSE82297	This Study
hFOB DIF+JQ1_H3K27me3	ChIP-Seq	GEO	GSE82297	This Study
hFOB DIF+JQ1_INPUT	ChIP-Seq	GEO	GSE82297	This Study
hFOB UND_BRD4	ChIP-Seq	GEO	GSE82297	This Study
hFOB UND_H2Bub1	ChIP-Seq	GEO	GSE82297	This Study
hFOB UND_H3K27ac	ChIP-Seq	GEO	GSE82297	This Study
hFOB UND_H3K27me3	ChIP-Seq	GEO	GSE82297	This Study
hFOB UND_INPUT	ChIP-Seq	GEO	GSE82297	This Study
hFOB UND_RNAPII	ChIP-Seq	GEO	GSE82297	This Study
L3.6 BRD4	ChIP-Seq	GEO	GSE82297	V. K. Mishra, WG Johnsen
L3.6 INPUT	ChIP-Seq	GEO	GSE82297	V.K. Mishra, WG Johnsen
MCF10A BRD4	ChIP-Seq	GEO	GSE72931	Sankari Nagarajan et al., 2016
MCF10A INPUT	ChIP-Seq	GEO	GSE65886	Sankari Nagarajan et al., 2015
MCF7+E2 BRD4	ChIP-Seq	GEO	GSE55923	Sankari Nagarajan et al., 2014
MCF7+E2 INPUT	ChIP-Seq	GEO	GSE55923	Sankari Nagarajan et al., 2014
NHOST H3K27ac	ChIP-Seq	GEO	GSE29611	ENCODE (Bradley

				Bernstein Lab)
NHOST H3K27me3	ChIP-Seq	GEO	GSE29611	ENCODE (Bradley Bernstein Lab)
NHOST H3K4me1	ChIP-Seq	GEO	GSE29611	ENCODE (Bradley Bernstein Lab)
NHOST H3K4me3	ChIP-Seq	GEO	GSE29611	ENCODE (Bradley Bernstein Lab)
NHOST RUNX2	ChIP-Seq	ENA	ERP003787	Anne-Mari Hakelien et al., 2014
NHOST DNAse-Hypersensitivity	DNAse-Seq	GEO	GSE32970	ENCODE (Gregory Crawford Lab)
hFOB DIF_DMSO	mRNA-Seq	GEO	GSE82297	This Study
hFOB DIF_JQ1	mRNA-Seq	GEO	GSE82297	This Study
hFOB DIF_siBRD4 #3	mRNA-Seq	GEO	GSE82297	This Study
hFOB DIF_siBRD4 #4	mRNA-Seq	GEO	GSE82297	This Study
hFOB DIF_siCNTR	mRNA-Seq	GEO	GSE82297	This Study
hFOB UND_DMSO	mRNA-Seq	GEO	GSE82297	This Study
hFOB UND_siCNTR	mRNA-Seq	GEO	GSE82297	This Study
Mouse_DIF_4OHT	mRNA-Seq	Unpublished		This Study
Mouse_DIF_VEH	mRNA-Seq			This Study
Mouse_UND_4OHT	mRNA-Seq			This Study
Mouse_UND_VEH	mRNA-Seq			This Study

Software and tools

Name	Version	Developer, Source
Bio-Rad CFX Manager	3.1	Bio-Rad Laboratories, Hercules, USA
Cistrome Galaxy Server · CEAS · MACS2 · Multiple wiggle files correlation · SitePro	 1.0.0 2.1.0.20140616.0 1.0.0 1.0.0	(Liu et al., 2011) (Shin et al., 2009) (Zhang et al., 2008) (Liu et al., 2011) (Shin et al., 2009)
Deeptool Galaxy Server · bamCoverage · computeMatrix	 1.1.4; 1.5.9.1; .2.2.2 1.5.9.1; 2.2.2	 (Ramírez et al., 2014)

· multiBamSummary · plotCorrelation · plotHeatmap · plotProfile	2.2.2 2.0.1 1.5.9.1; 2.2.2 1.5.9.1; 2.2.2	
EpiCSeg		(Mammana and Chung, 2015)
GREAT	3.0.0	(McLean et al., 2010)
GSEA		(Mootha et al., 2003; Subramanian et al., 2005)
HTSeq	0.6.0	(Anders et al., 2015)
Image Lab	5.2 build 14	Bio-Rad Laboratories, Hercules, USA
Integrative Genome Viewer	2	(Robinson et al., 2011; Thorvaldsdóttir et al., 2013)
MarkDuplicates Picard Tools	1.140	http://broadinstitute.github.io/picard/
Primer designing tool NCBI/Primer-BLAST		(Ye et al., 2012a)
ReMap		(Griffon et al., 2015)
REVIGO		(Supek et al., 2011)
RSAT		(Medina-Rivera et al., 2015; Thomas-Chollier et al., 2011, 2012)
Samtools	0.1.19	(Li, 2011; Li et al., 2009)
Statistical software R Packages: · DESeq2 · DiffBind · ggplot2 · gplots · qoseq · VennDiagram	3.2.2	R Development Core Team (2008). http://www.R-project.org (Love et al., 2014) (Ross-Innes et al., 2012; Stark R and Brown G, 2011) (Wickham, 2009) (Warnes et al., 2015) (Young et al., 2010) (Chen and Boutros, 2011)
UCSC Table Browser		(Karolchik et al., 2004)
useGalaxy Server · Bowtie2 · FastQC · RmDup(Samtools) · TopHat	15.07 2.1.0; 2.2.6 0.63; 0.64 2.0 2.0.14	(Blankenberg et al., 2010; Giardine et al., 2005; Goecks et al., 2010) (Langmead and Salzberg, 2012) S. Andrews (Babraham Institute) (Li et al., 2009) (Kim et al., 2013a)

Methods

Cell Culture

Immortalized cell lines and treatments

Human fetal osteoblast (hFOB 1.19) cells were maintained in 5% CO_2/atmosphere incubator in phenol red-free high-glucose Dulbecco's modified Eagle's media (DMEM/F12) supplemented with 10% fetal bovine serum (FBS) and 1% penicillin/streptomycin (P/S). Cells were pretreated with JQ1 (250nM) 1 hour before the induction of differentiation and then the inhibitor or equal volume of DMSO was added with every media change (every second day). For induction of differentiation, after reaching the confluency cells were treated with differentiation cocktail: 10 mM β-glycerophosphate, 0.2 mM ascorbate, 10 nM calcitriol and 100 nM dexamethasone and shifted to 39^0C incubator. Cells were differentiated for 5 days. For undifferentiated time point, cells were harvested prior differentiation induction and temperature change.

The experiments with IDG-SW3 osteocytes cells were performed by John R. Hawse and Malayannan Subramaniam from Department of Biochemistry and Molecular Biology in Mayo Clinic, USA. In brief, cells were maintained at 34^0C in collagen coated plates. For the experiment, cells were plated onto 12 well plates at 50% density and allowed to grow for additional 3-4 days to reach confluency. At this point the differentiation was induced and cells were transferred to 37'C incubator as described in (Woo et al., 2011). The JQ1 (250nM) treatment was also started. For Day 0 harvest, the cells were kept in differentiation media and treated with DMSO for 24 hours at 37'C. For long term treatment, differentiation media was replaced every third day with fresh treatments of DMSO and JQ1 (250nM). The cells were harvested

following 14 and 26 days of treatment for RNA or subjected to stainings. The harvested RNA was sent to us.

- ***siRNA Transfections***

For transient knockdown of genes cells were transfected with small interfering RNA (siRNA) using the Lipofectamine® RNAiMAX reagent according to the manufacturers' protocol. Namely, 15-20 pmol of siRNA were mixed with 5 µl RNAiMAX reagent in 500 µl of optiMEM (counted for a well of 6-well plates) and incubated for 20 min at room temperature. Meanwhile, the cells were trypsinized, counted and in amount of 220000-250000 cells in 1.5 ml of complete media without antibiotics were seeded into plates. Following the incubation, the transfection mix was added to the cells. The media was replaced to normal media after 6-12 hours post-transfection. If required, the differentiation was induced 24 hours following the transfection. The transfections were repeated after 72 hours following the forward transfection protocol recommended by the manufacturer.

- ***Alkaline phosphatase staining***

The alkaline phosphatase staining was performed using the Alkaline phosphatase leukocyte kit (Sigma) following manufacturer's instructions. Namely, after PBS wash cells were fixed for 30 s with Citrate fixing solution containing (for 98 ml): 65 ml acetone, 25 ml Citrate solution (Sigma-Aldrich Co., St. Louis, USA), 8 ml 37% formaldehyde. Following fixation, cells were washed with DI H2O for 40 s and incubated for 15 min with fresh diazonium salt solution. For preparation of diazonium salt solution 1 ml of FRV-Alkaline solution was mixed with 1 ml of sodium nitrate solution and incubated for 2 min, which was then added to 45 ml of DI H2O along with 1 ml of Naphtol AS-BI Alkaline solution. After 15 min, the staining solution

was removed and the wells are washed 2-3 x with DI H2O and dried. Pictures of the stained cells were taken under Microscope Axio Scope.A1equipped with an AxioCam MRc using 2.5x magnification or the whole plates were scanned.

- ***Alizarin Red staining***

After the PBS wash, the cells were fixed for 15 min with 4.2 % Formaldehyde in PBS. Following fixation, the cells were washed twice with DI water and stained with Alizarin Red staining solution for 15 min. Subsequently, the dye solution was removed and the wells were washed trice with DI H2O. For visualization, the plates were scanned.

Primary Cells

- ***Isolation of long bone cells***

The mouse long bone primary osteoblasts were isolated from $Rnf40^{Rosa\text{-}CreERT2}$ mutant mice (with “floxed” Rnf40 gene on both alleles) at age of 6 weeks. Following the sacrification, the femora and tibia from the mouse, partially freed from skin and underlying muscles were placed into PBS with 5% P/S. The lower extremities in PBS were then transferred to the cell culture hood. The muscles and periosteum were removed and carefully scraped off. The bones then were transferred into dishes with fresh PBS with 5% P/S. The bone epiphyses were cut off and the bone-marrow was flushed off with PBS by using 27G needles on the 1ml syringe. The clean bones were cut into smaller pieces and distributed into 3 eppendorf tubes (per mouse) with collagenase solution (α-MEM + 2mg/ml Collagenase A). The tubes with the bone pieces were incubated for 2 hours on shaking (1000rpm) thermal mixer set to 37ºC. In-between, the tubes were once vigorously shaked by hand. Following the 2 hours

incubation, the digestion solution was removed and the bone pieces were washed 3 times with complete α-MEM (+10% FBS, 1% P/S) medium. The bone pieces were then transferred into culture dishes with complete medium where they were minced by scalpel into finer pieces. The media with bone pieces was then transferred into 6cm cell culture dishes which were placed into 37ºC incubator. Within the first three days the plates were not moved allowing the cells to grow out the bone pieces.

- ***Isolation of primary calvarial osteoblasts***

The 1-3 days old pups of $Rnf40^{Rosa\text{-}CreERT2}$ mice were placed into cell culture hood where the heads of these animals were cut off with sharp scissors. The heads were shortly dipped into 70% ethanol and immediately transferred into dishes with PBS (+ 1% P/S). At the same time the tail tips were cut for subsequent genotyping. By holding the head with forceps, the skin was carefully peeled off (without damaging the calvaria). The exposed calvaria was cut (in shape of beetle head) and subsequently cleared off from soft tissues including the parts of side and hind calvaria. The calvaria was then placed into tubes with α-MEM digestion solution containing 2mg/ml Dispase and 1mg/ml Collagenase A. The calvaria were digested for 10 min on the thermal shaker (1000 rpm) set to 37ºC and after first incubation the digestion solution was discarded. The calvaria were subjected to 4 rounds of digestion in the same conditions (1000 rpm, 37ºC, 10 min) every time with fresh α-MEM digestion solution. After each round, the digestion solution was accumulated in 15ml falcons additionally containing 2 ml of the complete α-MEM media (10% FBS, 1% P/S) and stored on ice until the completion of 4^{th} round. After the last round, the accumulated digestion solution was centrifuged for 3-5 min at 300g to obtain the cell

pellet. The pellet was resuspended in complete α-MEM media and the cells were transferred to cell culture dishes. The cells were maintained in 37ºC incubators.

- ***The differentiation and treatments of primary mouse bone cells***

The primary mouse osteoblasts isolated from Rnf40$^{Rosa\text{-}CreERT2}$ mice were maintained in α-MEM supplemented with 10% (FBS) and 1% (P/S). For induction of Cre-recombinase mediated deletion of Rnf40 gene the cells were treated for 7 days with 250nM of 4-hydroxy-tamoxifen (4OHT) or equal volume of 100% ethanol. Then the cells were washed twice to remove the 4OHT and further maintained 2 additional days in the plain media with no 4OHT. At this timepoint cells of the undifferentiated (defined as day 0 in the study) state were harvested. For the differentiation, the rest of the cells were treated with 5 mM β-glycerophosphate, 0.2 mM ascorbate and 10 nM dexamethasone (the last only the first 3 media changes). The media was replaced every second day.

The osteoblast-osteoclast co-culture experiment

This experiment with prior osteoclast isolation and subsequent TRAP staining was performed by Peng Liu from Jan Tuckerman's group at Insitute of Comparative Molecular Endocrinology (CME), University of Ulm as briefly described below**.**

- ***Osteoclast Isolation***

The osteoclasts were isolated form 6-8 week old mice. The bones of the mice were dissected and cleared off the muscle tissues. The epiphyses were cut and the bone marrow was flushed off into 15 ml tubes with complete α-MEM (Gibco) medium with 10 % fetal calf serum (FCS from Gibco). After collecting the bone marrow flushes, the tubes were centrifuged at 1000 rpm for 5 min. The cellular pellet was

resuspended in 9 ml of cold water by pipetting up and down for 5 tiimes and one time in 10x PBS to lyse the red blood cells. The remaining cells were pelleted by another round of centrifugation and subsequently resuspended in 10 ml of α-MEM complete medium with 30ng/ml macrophage colony-stimulating factor (M-CSF from R&D Systems). The 5 ml of the resuspended cells was transferred into 100mmx20mm Corning non-treated suspension culture dishes where the stromal cells and lymphocytes can't adhere. Following 2-3 days, the macrophages (the osteoclast progenitors) were ready to use for co-culture experiment.

- ***The co-culture experiment***

At day 0, 4000 calvarial osteoblast cells from mutant Rnf40$^{Rosa\text{-}CreERT2}$ mice were seeded into 96-well plates in α-MEM complete medium containing 10nM vitamin D (Sigma). The next day, 200000 osteoclast progenitor cells from wild-type animals were seeded into osteoblast containing wells. On day 4 and 7 the media was refreshed with addition of vitamin D. On day 10, cells were fixed and subjected to tartrate-resistant acid phosphatase (TRAP) staining.

- ***TRAP Staining***

The cells of co-culture experiment were stained for TRAP activity with Acid Phosphotase Leukocyte Kit (Sigma). Namely, the cells were fixed for 30 seconds with fixative solution consisting of 25.51% (v/v) citrate solution, 66.32 % (v/v) acetone and 8.17% (v/v) formaldehyde (37%). Following the fixation, cells were washed with PBS and further maintained in PBS. Prior the fixation, the TRAP staining solution was prepared. For that 0.5 ml of Fast Garnet GBC Base Solution and 0.5 ml of Sodium Nitrite Solution were mixed softly by inversion for 30 seconds and incubated for 2 minutes. This mix was then added to another consisting of 45 ml

of prewarmed DI water (37° C), 0.5 ml Naphthol AS-Bl Phosphate Solution, Acetate Solution 2.0 ml and 1.0 ml Tartrate Solution. Right after fixation, the fresh prepared TRAP solution was added to the cells and cells were incubated for 1 hour in 37° C incubator protected from light. Cells were washed with PBS and maintained in PBS for visualization and counting performed under 40xmagnification with Leica DMI6000B microscope. The number of TRAP positive multinucleated cells was estimated in three replicates. Moreover, the expression of Opg and Rankl were identified in these cells with qRT-PCR. Student T-test was used for statistical evaluation.

Molecular Biology Methods

RNA Isolation

Isolation of RNA from cells was performed using the Trizol extraction protocol. In brief, cells were washed once with PBS and treated with QIAzol reagent in a volume of 500µl for a well of 6-well plate. Plates were incubated 3 min at RT on a shaker and transferred onto ice. Cells were scraped and transferred to eppendorf tubes. The primary mouse osteoblasts rich in extracellular matrix were additionally subjected to homogenization with the beads. Samples were subsequently twice extracted with 100µl of chloroform each time vortexed for 30 s and centrifuged at 4º C for 20 min, 10000 rpm. After combining the aqueous supernatants, isopropanol (1:1) was added and the RNA was precipitated overnight at -20º C. Following the 30 min centrifugation at 4º C, 12000 rpm, the pellets were twice washed with 70% ethanol and after last wash air-dried and diluted in 30 µl of DEPC treated nuclease free water. The concentration of obtained RNA was evaluated on Nanodrop.

Reverse Transcription (cDNA synthesis)

1µg of RNA in 10µl of nuclease free water was mixed with 2µl of 15µM 9mer random primer and 4µl of 2.5nM dNTP bundle mix and subjected to 5 min of incubation at 70º C. Then, a master mix containing of 1.625 µl of nuclease free water, 2µl of 10x reverse-transcription buffer, 0.125 µl of 25 U MMLV-reverse transcription enzyme and 0.25 µl of 10 U Murine RNase-Inhibitor was added to the RNA mix from previous step and the reaction mix was incubated for 1 hr at 42º C and subsequently at 95º C for 5 min to inactivate the enzyme. After cooling, the sample volume was brought to 50µl with nuclease free water.

Quantitative Real-Time PCR (qRT-PCR)

The qRT-PCR was performed in 25µl reaction volume. Namely, 1 µl of cDNA or ChIP isolated DNA were mixed with a 24 µl of master mix containing 14µl of qRT-PCR mix, 8.5 µl DI H2O and 1.5 µl of 5µM forward and reverse primer mix. The PCR reaction was performed using two-step protocol:

Temperature	Time	Cycles
95º C	2 min	1
95º C	15 sec	40-45 cycles
60º C	1 min	

The melting curve was recorded from 70 °C to 95 °C with the plate read every 0.5 °C. The relative DNA amount was quantified based on standard curve made from serial (1:4) dilutions of control (Input in case of ChIP) samples. All qRT-PCR samples were normalized to an internal reference gene and displayed relative to the control sample. Statistical analysis was done with Student's T-test.

Chromatin Immunoprecipitation

- ***Fixation and nuclear extraction***

Cells grown in 15cm cell culture plates were fixed at RT for 20 min with 12 ml of 1% formaldehyde in PBS. The formaldehyde was quenched for 5 min at RT with 1.3 ml of 1.25M Glycine. The cells were washed twice with ice-cold PBS and 1.5 ml Nelson Buffer with the protease inhibitor cocktail was added. Plates were placed onto ice and after 5 min of incubation, the cells were scraped, resuspended well with pipetting up-down and the cell extracts were transferred into 1.5ml eppendorf tubes. The samples were centrifuged at 4º C for 2 min at 2000g and the nuclear pellet was once again resuspended in Nelson Buffer with inhibitors and the centrifugation was repeated. The nuclear pellet was either snap-frozen at this point or subjected to sonication.

- ***Sonication***

The nuclear pellet was resuspended in 250-300µl of Gomes Lysis Buffer containing either 0.1% SDS - for BRD4, RNAPII, transcription factor ChIPs, or 0.5% SDS – for histone modification ChIPs. Usually because of the bigger volume of nuclear pellet, extracts from one plate were diluted in higher volume of Gomes Lysis Buffer and split then into 2-3 parts for shearing (not more than 300µl of chromatin sample per tube). After incubation of 15 min on a rotating wheel at 4º C, the nuclear extracts from hFOB cells were subjected to 18-25 cycles of sonication on Bioruptor Pico with 30 sec ON/OFF duty time. Before proceeding into IP 20-30 µl of extracts were taken for shearing test whereas the rest was snap-frozen at this point.

- ***Shearing test***

After shearing 20-30 µl of chromatin extract was subjected to phenol-chloroform-isoamyl DNA extraction procedure. Namely, the chromatin extracts were diluted with 100µl of Weinmann Buffer supplemented with 1µl of proteinase K (20µg/µl) and incubated for at least 4 hr at 65 °C. 100µl of 10mM TRIS (pH 8) mixed with 10µl of LiCl (8M) and 4 µl of linear polyacrylamide (2µg/µl) were added to the samples. The samples then were mixed in 1:1 ratio with phenol-chloroform-isoamyl solution and thoroughly vortexed for 30 s. Following the centrifugation for 2 min at full speed the aqueous phase was transferred into new tubes whereas the rest was subjected for back-extraction of remaining DNA by addition of 200µl buffer containing 10mM TRIS (pH 8) and 0.4 M LiCl. The second aqueous phase was added to the first after the second round of centrifugation. The DNA was precipitated with 2.5 volumes of 100% ethanol for at least 2hr at -80 °C and centrifuged at full speed for 30 min. The DNA pellet was washed twice with 70% ethanol and the pellets were air-dried and dissolved in 15 µl of DI H2O. All the steps of DNA isolation were performed at RT. The dissolved DNA samples were ran on 1-1.5% agarose gel. The size distribution of sheared chromatin extracts were confirmed to be in a range of 1500-1000 bp reaching up to 250 bp (optimal size range 500-300bp). In other case the shearing was repeated.

- ***Preclearing and IP***

After confirming the efficiency of sonication, the snap-frozen chromatin extracts were thawed on ice and precleared with 50% slurry of sepharose beads prepared in Gomes Lysis buffer with inhibitors. After one hour of incubation on rotating wheel at 4 °C the samples were centrifuged at 12000 g for 2 min. The supernatant was split

into corresponding number of IP samples required including also the negative IgG control. Specific ratio to IP samples was taken for input DNA (usually 1/5-1/10 to IP amount). The IP samples were brought to a final volume of minimum 500µl by a Gomes Lysis Buffer with inhibitors. At this point, if the SDS concentration in the samples was higher than 0.1%, the samples were diluted with Gomes Lysis Buffer without SDS. 1-2µg antibody was added to diluted chromatin extracts and the IP samples were incubated overnight at 4º C on a rotating wheel. Meanwhile, the solution of blocked protein A sepharose beads was prepared. Namely, the Protein A sepharose beads (≈ 0.5ml volume in 15ml tube) were mixed with 0.5g BSA in Gomes Lysis Buffer, incubated overnight at 4°C to allow the swelling. The next day the swollen sepharose was washed 3 times with Gomes Lysis Buffer (centrifugation 2min, 1000g) and finally the 50% slurry was made in Gomes Lysis Buffer with protease inhibitors. The blocked protein A beads were then added to the IP samples, and the incubation was continued for another 2 hours. The IP complexes then were subjected to a series of 7 washes: once with Gomes Lysis buffer, twice with Gomes Wash buffer, twice again with Gomes Lysis buffer and, finally, twice with TE buffer. For washing the beads were always centrifuged at 4 °C for 2 min at 2000g.

- ***DNA Isolation and confirmation of IP-efficiency***

The input samples and the beads after the last step of washes were resuspended in 50µl of 10mM TRIS (pH 8) with 0.2µg/µl RNAse and incubated for 30 min on a shaker at 37 °C. Then, 50µl of 2x Weinmann Buffer with 1µl of proteinase K (20µg/µl) was added to the beads, and the samples were incubated overnight on a shaker at 65 °C. The rest of the steps were repeated as described for shearing test. Namely,

the DNA was isolated similarly with phenol-chloroform-isoamyl extraction procedure. The DNA was diluted in 20µl of DI H2O and thoroughly mixed. Some of the sample was taken and further diluted to confirm the efficiency of immunoprecipitation by qRT-PCR on positive and negative sites. The PCR signals of the IP samples were normalized to Input DNA (taking into account the ratio of IP chromatin extract to Input), respectively and displayed as enrichment over Input in percent. The background signal was estimated using DNA from IgG immunoprecipitated DNA. If necessary, DNA was then subjected to library preparation for subsequent sequencing.

Genotyping

The mouse tail or ear biopsies were subjected to overnight digestion with 60-100mg/ml Proteinase K. The DNA was isolated following isopropanol precipitation with subsequent washes in 70% ethanol and final dilution of DNA in 50µl DI water. The DNA concentration was verified and in amount of 50ng was used for the PCR reactions by using the HOT FIREPol® DNA Polymerase Kit with following reaction conditions:

Reagents	Volume (µl)
H2O	14.8
10x HotFire Buffer	2.5
2mM dNTP mix	2.5
25mM MgCl2	2
5µM Primer F	1
5µM Primer R	1
HotFire Pol	0.15-0.2
DNA	1

In case there were three primers used for genotyping (such as for Runx2-Cre or Rosa-CreERT2), then the 1µl of the third primer was added to the reaction with respective reduction in the volume of water used. The PCR conditions used for genotyping are indicated below:

Temperature	Time	Cycles
95°C	15 min	1x
95°C	30 sec	35x
T °C (see below)	30-45 sec	
72°C	1 min	
72°C	10 min	1x
4°C	∞	O/N

Temperatures used for different targets were as follows: Rnf40/LoxP - 62^0 C (45 sec); Usp22/LoxP - 67^0 C (30 sec); Runx2-Cre - 60^0 C (30 sec); Bglap-Cre (generic Cre) – 62 ^{0}C (45 sec) and Rosa-CreERT2 - 55^0C (45 sec).

Protein Analysis

- ***Protein Isolation***

Following the PBS wash, the RIPA buffer with protease inhibitors was added to the cells, and the plates were incubated on the ice on a shaker to allow the cell detachment and lysis. The cells were scraped after 5 min of incubation. The cellular lysate was then subjected to sonication on Bioruptor for 10 cycles with 30 sec ON/OFF settings. The protein samples from primary mouse osteoblasts were additionally homogenized for 5 sec and also subjected to manual sonication for 10 cycles (5% power), 2 rounds on Bandelin Sonoplus Sonicator because of high content of viscous extracellular matrix.

- ***Western Blot Analysis***

Protein samples were separated via sodium dodecylsulfate polyacrylamide gel electrophoresis (SDS-PAGE). Namely, the SDS gels with required percentage were prepared and the sheared protein samples boiled with Laemmli buffer at 95º C for 5-10 min, were then loaded onto the gel. The gel was run with SDS Running Buffer at 10-15 mA. The separated proteins were transferred onto the PVDF Transfer Membrane in Transfer Buffer at 100 V for 90 min. The membrane was blocked for 30-45 min in 5% milk solution in TBS-T. Following the blocking, the membrane was incubated with primary antibody solutions at 4º C. The next day, the membrane was washed 3 times with TBS-T for 10 min and subjected for 1 hour incubation with HRP-coupled secondary antibody solutions in 5 % milk in TBS-T at RT. After the second incubation, the membranes were washed again 3 times. Subsequently, the membranes were developed with Immobilon Western Chemiluminiscent HRP substrate or SuperSignal West Femto Maximum (for weaker signals) and the chemiluminescence was detected on gel imaging system.

Next Generation Sequencing

ChIP DNA Library Preparation

The ChIP DNA was subjected to 30-40 cycles of sonication on Bioruptor Pico with 30 sec ON/OFF settings. The DNA was then directly used for library preparation by MicroPlex™ Library Preparation Kit following the manufacturer's instructions based on three basic steps of end repair, adaptor ligation and the last step of library amplification. The ChIP libraries were mainly prepared in triplicates. After purifying the amplified libraries with Ampure XP magnetic beads, the concentration of DNA was measured on Qubit and 2-4ng of DNA in 1µl was loaded onto High Sensitivity

DNA microfluidic chips and the average size distribution of the libraries were analyzed on Bioanalyzer.

RNA Library Preparation

- ***Verification of RNA Integrity on Gel***

500-1000ng of whole cell RNA, mixed with RNA Loading Dye was ran in FA running buffer on 1.2% agarose gel prepared in FA gel buffer with extra addition of 37% formaldehyde to a final concentration of 0.66%. The RNA integrity was evaluated based on the sharpness and ratio of 28sRNA (≈5 kb size) and 18sRNA (≈2 kb size) bands (28s should be twice intense than 18sRNA).

- ***mRNA Library Preparation***

The whole cell RNA in amount of 1µg from hFOBs and 4 µg from mouse primary cells were used for library preparation by using the NEXTflex Rapid Directional RNA-Seq Kit according to manufacturer's protocol. In brief, following the mRNA enrichment by Poly(A) magnetic beads, the mRNA was fragmented and subjected to first and then to second cDNA strand synthesis with addition of dUTPs. Consistently, the ends of the DNA were repaired and adapters were ligated. The adapter ligated DNA was subjected to amplification with simultaneous use of Uracil DNA Glycosylase in reaction mix, to allow the degradation of second cDNA strand and subsequent amplification of first strand. The concentration and size of amplified libraries were estimated similarly as for ChIP DNA library.

Sequencing and Data Analysis

Pooled libraries were used for cluster generation on cBot following 51 bp single-end sequencing on HiSeq 2000 from Illumina performed by the Transcriptome Analysis

Laboratory (TAL) in Goettingen, Germany. The sequencing BaseCaller bcl output files were further demultiplexed to FASTQ files using CASAVA 1.8.2 by TAL.

- ***ChIP-Sequencing Bioinformatic Analysis***

After verification of the quality of FASTQ files by FastQC, the FASTQ files were mapped to the human reference genome assembly hg19 using Bowtie2 (Langmead and Salzberg, 2012) with very-sensitive presets in end-to-end mode. For visualization the corresponding BAM files of the replicates were merged within each condition. For visualization in the genome browser and to generate the heatmaps, all the BAM files were filtered on MAPQ >=10 (MAPQ>=2 for TF ChIPs) with removal of duplicates and normalized to fragments (reads) per kilobase per million (RPKM) using the bamcoverage tool on deepTools (Ramírez et al., 2014) (Galaxy Version 1.1.4 and later for TF BAMs 1.5.9.1.0). The visualization was performed using the Integrative Genomics Viewer (Thorvaldsdóttir et al., 2013). For the differential binding analysis and chromatin segmentation, only the reads with MAPQ >=2 (Samtools 0.1.19) were retained for each BAM file and the BAM files were further deduplicated with MarkDuplicates Picard Tools (version 1.140). Heatmaps were generated using deepTools, the profile and correlation plots were made with deepTools and Cistrome Galaxy. The annotation file containing the genomic coordinates for all the human genes (assembly hg19) and CGI content within ± 1kb TSS regions were downloaded from the UCSC Table Browser (Karolchik et al., 2004). For correlations of ChIP-Seq signal with gene expression, duplicate TSS (from different transcripts) were removed. Based on gene expression values from hFOB RNA-Seq data, genes with DESeq “average baseMean” values < 20 and gene length < 1000bp were further removed from the analysis. Moreover, for genes

bearing more than one TSS, the TSS bearing the highest BRD4 signal was considered.

The peak calling step was performed with Model-based Analysis of ChIP-Seq 2 (MACS2) (Zhang et al., 2008) on Galaxy Cistrome (version 2.1.0.20140616.0) using default settings with q-cutoff <0.05. For BRD4, H3K27ac, H3K27me3, H2Bub1 and RNAPII –broad option was used, whereas for TF ChIP the narrow peak option was utilized. For each condition the corresponding input samples were used as control.

To determine osteoblast-specific BRD4 binding regions differential binding analysis of all the BRD4 binding sites and regions among four different cell lines (differentiated hFOB, MCF7, MCF10A and L3.6) was performed by using “DiffBind” (Ross-Innes et al., 2012) R package version 3.2.2. To determine the regions bound by BRD4 that are specific to differentiated hFOB the DiffBind thresholds were set to: Fold Concentration Change (hFOB vs the rest of the cell lines) >1 and FDR<0.05. These specific regions were further subdivided via Epigenome Count-based Segmentation (EpiCSeg) (Mammana and Chung, 2015) software. The states were determined based on the combination of five histone modifications H3K27ac, H3K27me3, H3K79me2, H3K4me3, H3K4me1 from normal human osteoblasts (NHOST) (Encode Consortium, 2012) as well as H3K27ac, H3K27me3 from differentiated hFOBs. Segments 3 and 4 were used as potential enhancer sites (marked by BRD4, H3K27ac and H3K4me1). Consecutive segments 3 and 4 were joined and considered as one region using Bedtools (Quinlan and Hall, 2010) merge (book end option). The resulting region file was analyzed using the Genomic Regions Enrichment of Annotations Tool (GREAT) (McLean et al., 2010) to identify genes associated with these putative enhancers and perform GO enrichment analysis (biological processes) on these genes. The same file was used as input for

ReMap (Regulatory Map of Transcription Factor Binding Sites) (Griffon et al., 2015) to calculate the enrichment of TFs based on publically available ChIP-seq data. Because of the larger size of some of the segments, we further intersected this file with DNAse-seq bed file from NHOST (ENCODE) to obtain the center of the regions (based on DNAse summits). We then performed *de novo* motif discovery using peak-motifs from Regulatory Sequence Analysis Tool (RSAT) suite (Medina-Rivera et al., 2015; Thomas-Chollier et al., 2012) on the regions flanking ±250 bp around the identified centers of "Segment 3+4". The differential mode was used between "Segment 3+4" versus "Segment 1+2+5" using oligo-analysis 6nt and 7nt outputting 5 motifs.

The BRD4 RPKM values, identified using the "reference-point" mode of computeMatrix tool on deepTools Galaxy (version 1.5.9.1.0), flanking ±500bp around the TSS of genes in differentiated hFOBs were used to group the genes into "Very Low" – $\log_2$BRD4 RPKM < 2.3; "Low" – 2.3 < $\log_2$BRD4 RPKM < 2.8; "Medium" – 2.8 < $\log_2$BRD4 RPKM < 3.3; "High" – $\log_2$BRD4 RPKM >3.3. The H3K27ac values within the groups were similarly identified on the same regions as BRD4. For RNAPII, regions ranging from TSS to +300 bp downstream were used. The H2Bub1 occupancy values were identified on the whole gene bodies (using the "scale-regions" mode of computeMatrix tool on deepTools Galaxy).

- ***RNA-Sequencing Bioinformatic Analysis***

For RNA-Seq the FASTQ files were mapped to the human genome (assembly hg19) using TopHat Gapped-read mapper (Kim et al., 2013a) for RNA-seq data with very sensitive Bowtie2 settings on Galaxy Platform (Version 0.9) (Goecks et al., 2010). The read counting was performed via HTSeq (Anders et al., 2015) (version 0.6.0)

with following parameters: -f bam -r pos -s reverse -a 10 -t exon -m union. The count files were subsequently subjected for differential analysis using the DESeq2 Package (Love et al., 2014) on R (Bioconductor version 3.2.2). For hFOB RNA-Seq, the Wald Test was utilized for a comparison of one-factor conditions (in case of DIF_JQ1 or DIF_siBRD4 #3+#4 vs DIF_DMSO or DIF_siCNTR, respectively), whereas for differential analysis of conditions differing by 2 factors (in case of DIF_DMSO + DIF_siCNTR vs UND_DMSO + UND_siCNTR) Likelihood Ratio Test reduced by “treatment” was used. The same model was implemented in case of comparison across all conditions and samples for estimation of sample-to-sample distances depicted in PCA plot. The similar settings were used for analysis of mRNA-Seq data from mouse primary calvarial cells.

The differentiation induced changes in hFOBs showed the same tendency and variance both in siCNTR as well as DMSO treated conditions between undifferentiated and differentiated states on mRNA level (Figure 10), respectively. Therefore, for the differential analysis, the siCNTR and DMSO conditions were combined within the same state and treated as replicates of one state. The PCA analysis also revealed a high level of similarity between both siRNAs used against BRD4 (Figure 10). For that reason, gene expression counts of the both conditions (siBRD4 #3 and 4) were combined and treated as replicates of one treatment. The threshold values to determine the differentially expressed genes during differentiation (DIF_siCNTR+DIF_DMSO vs UND_siCNTR+UND_DMSO) were as follows: DESeq2 “average baseMean” > 20, abs(log2fold change) >=1 and FDR < 0.05. For differentiation-unregulated genes the thresholds were set to abs(log_2 fold change value) <=0.2 and FDR >0.8. For JQ1 regulated genes (DIF_JQ1 vs DIF_DMSO) the thresholds were set to “average baseMean” >20, abs(log_2 fold

change) >=0.8, FDR < 0.05 and abs(log_2 fold change) <=0.2 and FDR >0.85 in case of unregulated genes. For siBRD4 regulated genes (DIF_siBRD4 #3 + #4 vs DIF_siCNTR), following thresholds were used: “average baseMean” >20, abs(log_2 fold change) >=0.7, FDR <0.05 and in case of siBRD4 unregulated genes the same thresholds as for JQ1 unregulated genes were used. The overlap of the regulated genes and subsequent venn diagrams were performed on R (3.2.2) by using the VennDiagram package(Chen and Boutros, 2011).

For mouse mRNA-Seq analysis, the following thresholds of gene regulation were used: for differentiation regulated genes (DIF_VEH vs UND_VEH) “average baseMean” >20, abs(log2fold change) >=0.9 and FDR <0.05, for Rnf40 regulated genes in differentiated state (DIF_4OHT vs DIF_VEH)) “average baseMean” >20, abs(log2fold change) >=1 and FDR <0.05; for Rnf40 regulated genes in undifferentiated state (UND_4OHT vs UND_VEH) “average baseMean” >20, abs(log2fold change) >=1 and FDR <0.05.

The Gene Ontology (GO) analysis was performed using the “goseq” (Young et al., 2010) Bioconductor package version 3.2.2. The significantly enriched GO categories were identified based on the FDR values < 0.05 using the Benjamini and Hochberg test. The resulting list of GO categories and the corresponding “bubble plots” were further synthesized using REVIGO (Supek et al., 2011) which clusters the categories based on semantics.

For the gene set enrichment analysis (GSEA) (Subramanian et al., 2005) the variance stabilization transformed read counts obtained through DESeq2 analysis were used. GSEA was performed with default settings (1000 permutations of gene

sets, Signal2Noise ranking metric). For enrichment analysis gene ontology sets (C5.all) were used.

The RNA-Seq heatmaps were performed with heatmap.2 from gplots R package (Warnes et al., 2015).

Animal Studies

The mouse lines

All the animal studies were performed in accordance with the Institutional Animal Care and Use Committee and the Institutional Guidelines for Humane Use of Animals in Research. The initially designed RNF40 construct (with two loxP sites flanking exons 3 and 4 of the *Rnf40* gene and two short flippase recognition target (FRT) sites around the neomycin (*Neo*) selection cassette) were electroporated in 129Sv/Pas-derived MPI II ES cells. The targeted clones were subsequently verified by quantitative and long-range PCR. Germ line chimeras were obtained by morulae aggregation (Kordowich et al., 2012). Following germ line transmission, the neomycin cassette was removed by crossing the $Rnf40^{loxPNeo}$ mice to a mouse strain expressing the FLP recombinase under the control of the Rosa26 promoter (Farley et al., 2000). The resulting mutant $Rnf40^{LoxP}$ mice ($Rnf40^{Tm1Saj}$) were crossed back for nearly 5 generations with C57/BL6 mice.

The $USP22^{LoxP}$ mice were generated using a “knockout first” approach. The embryonic stem cell line ($Usp22^{tm1a(KOMP)Wtsi}$ C57Bl6) were ordered from the University of California-Davis Knockout Mouse Project (KOMP) Repository. In these mice, the USP22 second is flanked by LoxP sites. Moreover, the first intron of the USP22 gene carries LacZ and neomycin resistance cassettes flanked by FRT sites. Since the lacZ and *Neo* cassetes are followed by polyadenylation sequences this

results in subsequent truncation of Usp22 gene (USP22 KO). The KO construct was originally put in C57/BL6-N which were later back-crossed to C57/BL6-J for at least for 5 generations. The $Usp22^{tm1a(KOMP)Wtsi}$ mice were then crossed with Rosa26 FLP recombinase mice to obtain the $USP22^{LoxP}$ mice.

The Rosa-CreERT2 and Bglap-Cre mice were obtained from JAX® Mice and Services. The generation of the mouse lines is described by Ventura et al., 2007 and Zhang et al., 2002, respectively. The Runx2-Cre mice were provided by Jan Tuckerman from Institute of Comparative Molecular Endocrinology (CME), University of Ulm (Rauch et al., 2010).

Mouse skeletal preparation

The mice were double injected with calcein solution (10µl/g of body weight) 9 and 2 day before the sacrification. Mice were euthanized with carbon dioxide. The skin and inner organs of the animals were removed. The skeleton with muscles were fixed for 3 days in 4% PFA solution, after which the skeletons were washed with tap water and transferred into 70% ethanol for long term storage.

The skeletons were sent to our collaborators Peng Liu from Jan Tuckerman's group at Institute of Comparative Molecular Endocrinology (CME), University of Ulm who performed the rest of analysis with mouse bones.

µCT Analysis

This analysis was performed by Peng Liu from Jan Tuckerman's group at Insitute of Comparative Molecular Endocrinology (CME), University of Ulm.

The bones (femora and vertebrae) were analyzed using a Skyscan 1176 in vivo micro CT (Bruker, Billerica, USA) equipped with an X-ray tube working at 50-80

kV/100 µA. Resolution was 9 µm, rotation step was set at 1°, and a 0.5 mm aluminum filter was used. For reconstruction of femora, region of interest was defined 0.3 mm apart from the distal growth plate into the diaphysis spanning 1.8 mm. Trabecular bone volume/tissue volume (BV/TV), trabecular thickness (Tb.Th.), trabecular separation (Tb.Sp.), trabecular number (Tb.N.) and cortical bone perimeter (B.Pm) were determined according to guidelines by ASBMR Histomorphometry Nomenclature Committee (Dempster et al., 2013). The size parameters of the bones were identified as follows: for torso - the length from the atlas to the sacrum; for femur - the length from the fovea capitis to the patella; for vertebra - the length of L5 vertebral body. Student T-test was used for statistical evaluation (comparison versus WT).

Bone Histomorphometry

The bone histomorphometric analysis including the paraffin and plastic embedding of the bones, the estimation of bone formation rate and osteoclast numbers was performed by Peng Liu from Jan Tuckerman's group at Insitute of Comparative Molecular Endocrinology (CME), University of Ulm

- ***Embedding of bones into plastic***

The mouse bones were placed into histological cassette which were subjected to a series of following treatments: 2-4 hours incubation at RT in 90% ethanol; 2 times 2-4 hours each incubation at RT in 100% ethanol; 2 times 24 hours each incubation at RT again in 100% ethanol; 3-4 days incubation at RT in infiltration solution I followed by 7-10 days incubation in infiltration solution II consisting of 100ml destabilized Methacrylate (MMA from Merck), 0.33 g Benzoylperoxid (BPO, Sigma) and 10ml Nonylphenyl (Merck); finally the cassettes with bones were incubated overnight

at 4º C in polymerization solution containing 100ml destabilized Methacrylate (MMA from Merck), 0.66 g Benzoylperoxid (BPO, Sigma) and 10ml Nonylphenyl (Merck) 0.5ml N,N-Dimethyl-p-toluidin (Merck).

- ***Embedding of bones into paraffin***

The PFA fixed bones were washed with DI water for 2 hours and subjected to decalcification in duration of 10 days at 37º C in EDTA (pH 7.2 set by NaOH and HCl) in a shaking incubator (125 rpm). The EDTA was refreshed every 2-3 days. The decalcified bones were washed for 2 hours in DI water and then embedded into liquid paraffin.

- ***Bone formation rate***

The dual calcein labeled bones embedded into plastic were utilized for measurement of bone formation rate (BFR) and mineral apposition rate (MAR) based on the width of the two green lines which is indicative of bone growth between two injection time points (7 days). The analysis and evaluation were performed by Osteomeasure Software (Osteometrics, Decatur, USA). Student T-test was used for statistical evaluation (comparison versus WT).

- ***Osteoclast number estimation***

The paraffin embedded bones were subjected to deparaffinization with xylol for 5 min twice. Subsequently, the decalcified bones were rehydrated by series of incubation in 100% ETOH - 5 min, 96% Ethanol - 2 min, 80% Ethanol - 2 min, 50% Ethanol - 2 min and DI H2O - 2 min. The rehydrated bones were incubated for 10 min in TRAP-buffer consisting of 0.328% (w/v) Sodium-acetate (Sigma) and 0.23% (w/v) Di-Sodium-tartrate (AppliChem) with pH 5 adjusted with HCl. Subsequently, the slides

were incubated for 2-4 hours at 37° C in TRAP-staining solution consisting of 10% (w/v) Naphthol-AS-BI-Phosphate (Sigma) and 1% (v/v) Dimethylformamid (DMF, Sigma) mixed with subsequent addition of TRAP-buffer, 60% (w/v) Fast Red Violett LB Salt (Sigma) and 0.5% (v/v) Triton X 100. The slides were washed with DI water and stained with Hämalaun for 3 min at RT (diluted with DI H2O in 1:5 ratio). After shortly rinsing in DI H2O, the slides were shortly immersed shortly for 2-3 times into 1.2% (v/v) water diluted HCl. The slides were immediately washed in tap water, and incubated in lukewarm tap water for another 10 min. The slides were then covered with Aquatex (Merck). The number of osteoclasts identified by red-pink color with blue-violet nucleus and osteoclast surface was identified on Osteomeasure Software (Osteometrics, Decatur, USA). Student T-test was used for statistical evaluation (comparison versus WT).

RESULTS

Role of BRD4 in osteoblast differentiation

BRD4 is indispensable for osteoblast differentiation

Cellular differentiation is a complex process involving coordinated network of transcription factors and epigenetic modifiers acting on cis- as well as trans-regulatory elements to selectively regulate lineage-specific gene expression. In this study we decided to elucidate role of epigenetic reader BRD4 in formation and maintenance of osteoblastic phenotype. Functional relevance of BRD4 in the regulation of bone formation was addressed in several *in vitro* models of osteoblast differentiation, namely in human fetal osteoblasts (hFOB) and in mouse IDG-SW3 osteocyte cells. hFOBs immortalized with temperature-sensitive SV40 T-antigen (Harris et al., 1995) are defined as early osteoblasts whereas similarly immortalized IDG-SW3 cells can be characterized as late-stage osteoblasts/osteocytes with mineralization potential (Woo et al., 2011). To determine the involvement of BRD4 at earlier steps of osteoblast differentiation we used siRNA mediated depletion as well as small molecule induced inhibition of BRD4 protein by JQ1 following 5 days of differentiation in hFOBs. Two single siRNAs in addition to siRNA smartpool were used for knockdowns to exclude the off-target effects (Figure 7A,B). Alkaline phosphatase staining of the cells used to assess the differentiation efficiency of osteoblastic lineage revealed decreased activity of the enzyme following the BRD4 inhibition or knockdown (Figure 7C).

In order to test our hypothesis we also looked at the global H2Bub1 protein levels following BRD4 inhibition/depletion. However, despite the differentiation induced

increase in H2Bub1 consistent with our previous finding (Karpiuk et al., 2012), loss of BRD4 function did not impact the H2Bub1 levels on a global scale (Figure 7B).

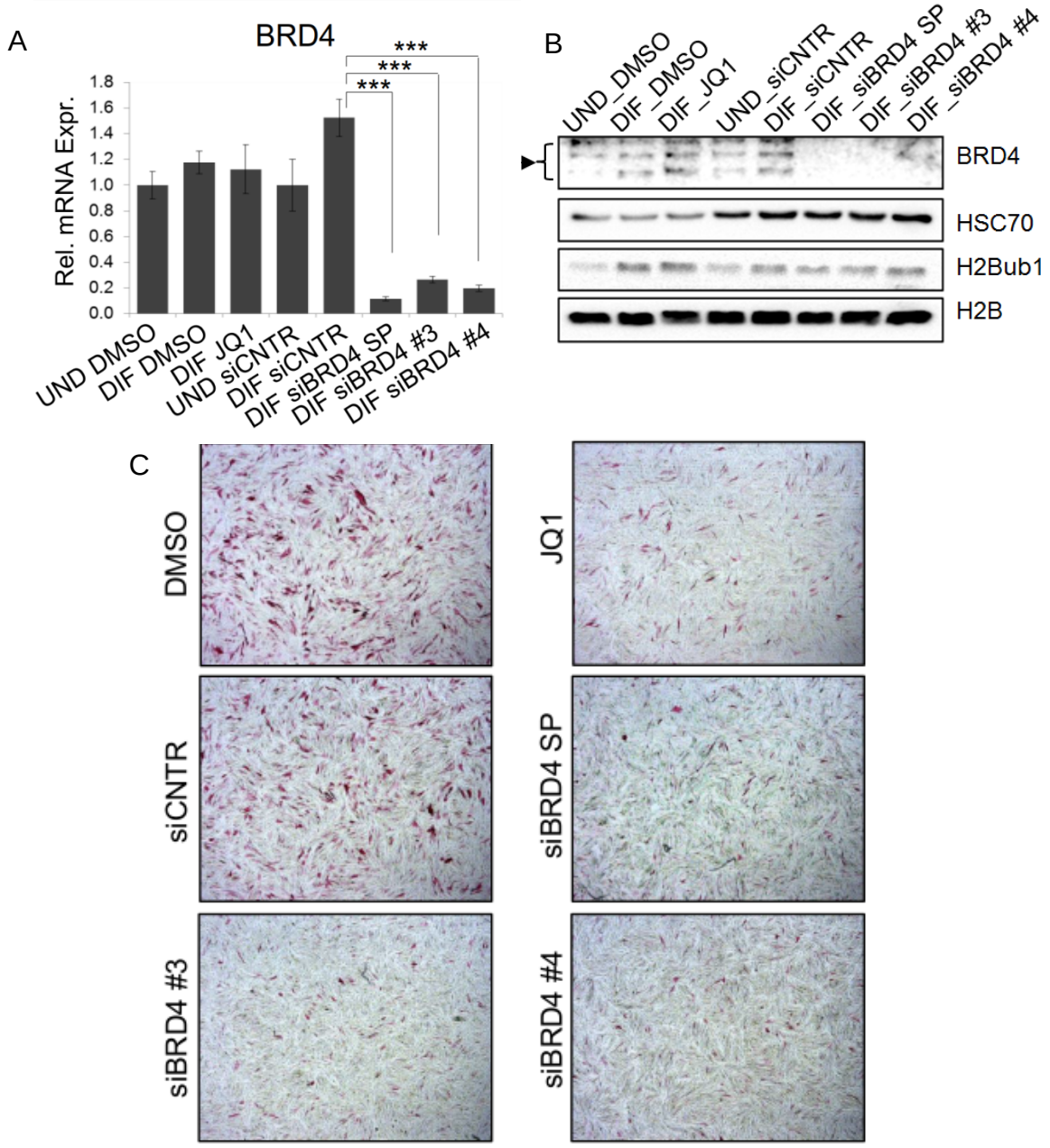

Figure 7. ***Loss of BRD4 results in impaired hFOB differentiation*** **A.** Western Blot analysis of BRD4 and H2Bub1 levels in whole cell protein extracts in hFOBs undifferentiated or osteoblast differentiated for 5 days following treatment with DMSO or JQ1, or non-targeting control siRNA (siCNTR) or BRD4 siRNA smartpool (siBRD4 SP) or two single siRNAs (siBRD4 #3 and #4). HSC70 and H2B were used as loading controls. **B**. Relative BRD4 gene expression assessed by qRT-PCR in hFOBs treated similarly as in (A). Gene expression was normalized to RPLP0 levels in undifferentiated controls, respectively. Mean±SD, n=3. Student t-test was performed for statistical analysis where ***p<0.001, **p<0.01, *p<0.05. C. Alkaline Phosphatase staining of differentiated hFOBs treated similarly as in A.

Nonethelles, targeting BRD4 by JQ1 or siRNA reduced the differentiation-induced expression of osteoblast-specific marker genes such as *RUNX2*, *ALPL* and Opg (*TNFRSF11B*) (Figure 8).

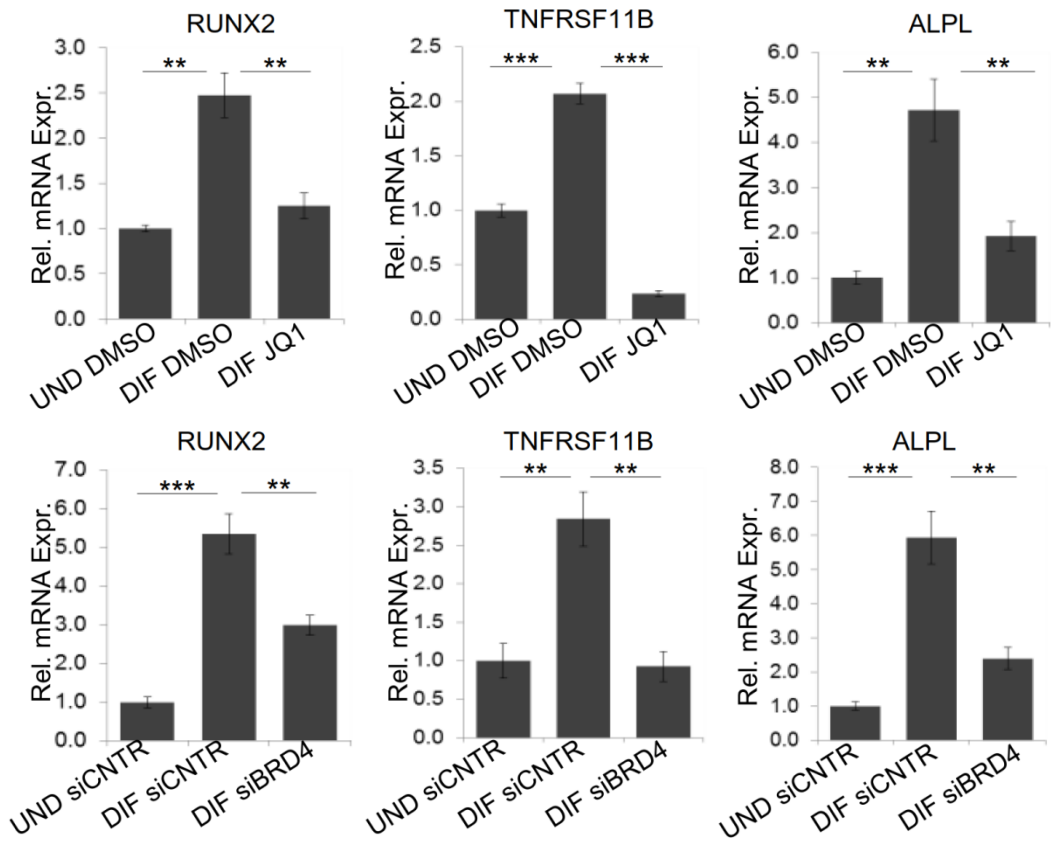

Figure 8. ***BRD4 is required for the expression of osteoblast-specific genes.*** hFOBs were differentiated for 5 days following DMSO or JQ1 (upper panels) or Control (siCNTR) or BRD4 (siBRD4) siRNA treatments (lower panels). The relative expression of osteoblast marker genes was evaluated via qRT-PCR analysis and normalized to expression level of RPLP0 housekeeping gene in undifferentiated state. Mean±SD, n=3. Student t-test was performed for statistical analysis where ***p<0.001, **p<0.01, *p<0.05.

Furthermore, we tested the effect of BRD4 inhibition on mineralization capacity of mouse IDG-SW3 osteocytes. These cells completely failed to mineralize after 14 days of differentiation in presence of JQ1 and showed reduced mineralization after 26 days of differentiation (Figure 9A). Similarly, the expression of marker genes *Mepe*, *Bglap* and *Dmp1* was also significantly reduced upon BRD4 inhibition compared to differentiated control cells (Figure 9B)

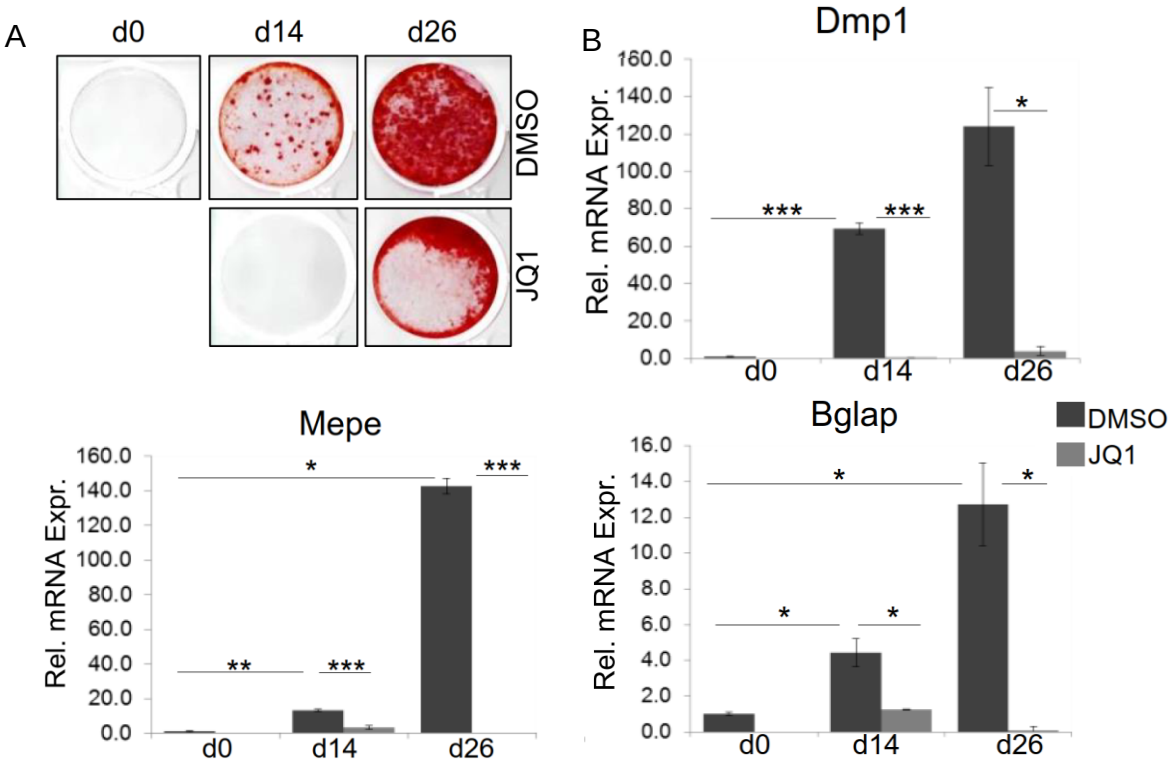

Figure 9. ***BRD4 is important for the mineralization of mouse osteocytes*.** The mouse IDG-SW3 osteocyte cells were differentiated for 14 and 26 days following DMSO or JQ1 treatment. **A**. The cells were stained with Alizarin red for detection of mineralized nodules. **B**. The relative expression of mouse osteocyte marker genes was evaluated via qRT-PCR and normalized to mouse Gapdh housekeeping gene in undifferentiated state. Mean±SD, n=3. Student t-test was performed for statistical analysis where ***p<0.001, **p<0.01, *p<0.05

Taken together, these results show that the BRD4 is indispensable for osteoblast lineage commitment independent of differentiation stage. Moreover, these effects do not seem to be mediated through the regulation of H2Bub1 levels.

Transcriptome wide effects of BRD4 perturbation

To determine the BRD4 mediated global control on gene expression and associated pathways we performed transcriptome sequencing in hFOBs following differentiation with subsequent BRD4 inhibition by JQ1 or depletion by two independent siRNAs (#3 and #4) (Figure 10).

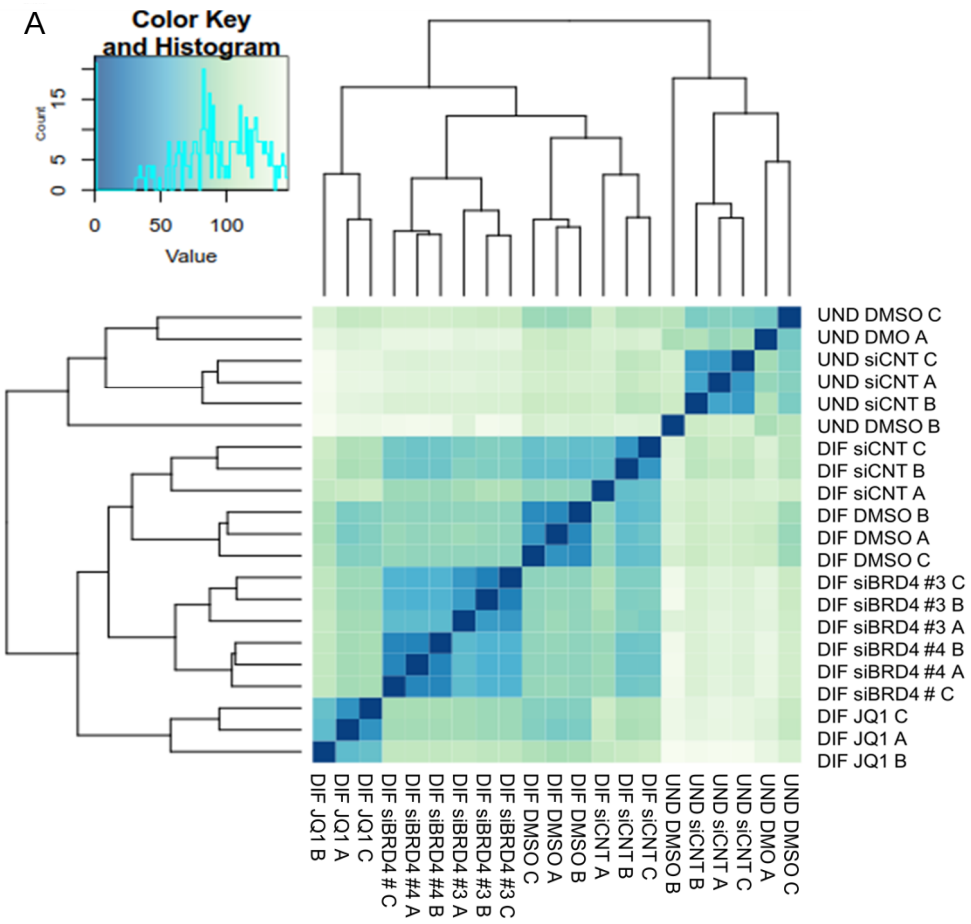
A
Color Key and Histogram
Count
0
5
15
0
50
100
Value
UND DMSO C
UND DMO A
UND siCNT C
UND siCNT A
UND siCNT B
UND DMSO B
DIF siCNT C
DIF siCNT B
DIF siCNT A
DIF DMSO B
DIF DMSO A
DIF DMSO C
DIF siBRD4 #3 C
DIF siBRD4 #3 B
DIF siBRD4 #3 A
DIF siBRD4 #4 B
DIF siBRD4 #4 A
DIF siBRD4 # C
DIF JQ1 C
DIF JQ1 A
DIF JQ1 B
DIF JQ1 B
DIF JQ1 A
DIF JQ1 C
DIF siBRD4 # C
DIF siBRD4 #4 A
DIF siBRD4 #4 B
DIF siBRD4 #3 A
DIF siBRD4 #3 B
DIF siBRD4 #3 C
DIF DMSO C
DIF DMSO A
DIF DMSO B
DIF siCNT A
DIF siCNT B
DIF siCNT C
UND DMSO B
UND siCNT B
UND siCNT A
UND siCNT C
UND DMO A
UND DMSO C

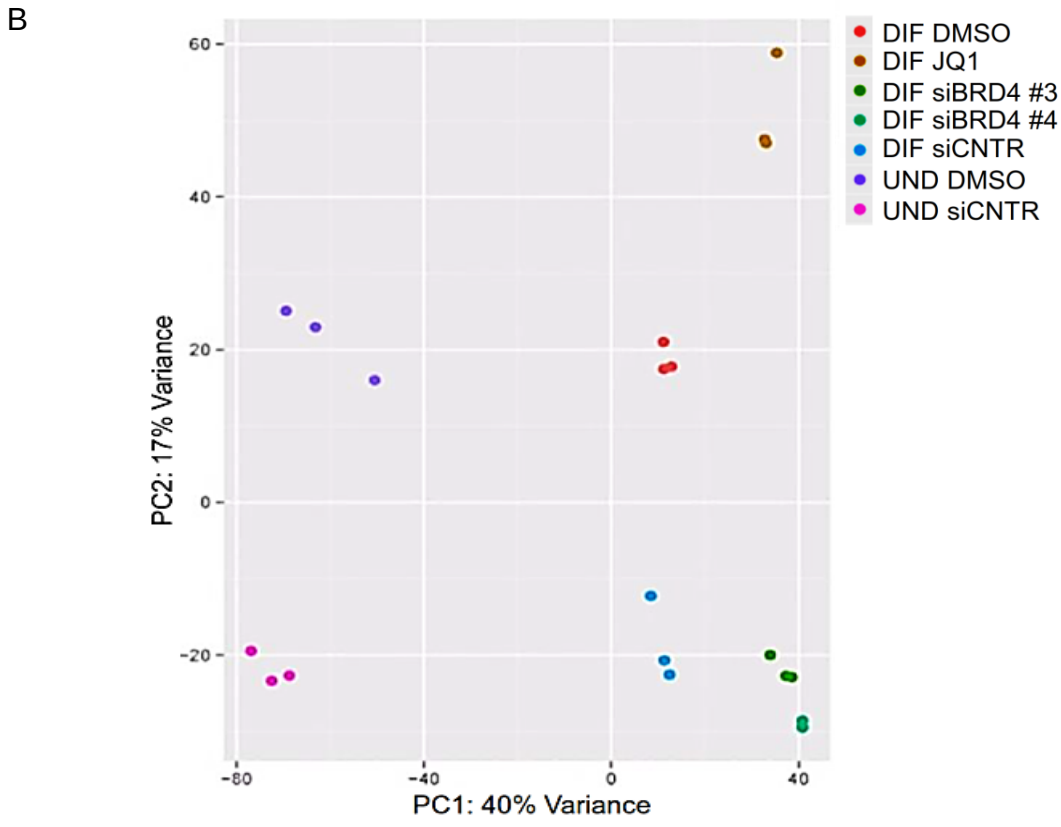
B
DIF DMSO
DIF JQ1
DIF siBRD4 #3
DIF siBRD4 #4
DIF siCNTR
UND DMSO
UND siCNTR
60
40
20
0
-20
PC2: 17% Variance
-80
-40
0
40
PC1: 40% Variance

Figure 10. ***Quality diagnostics of RNA-Seq data from hFOBs*****. A.** Heatmap of hierarchical clustering of Elucidean sample distances and **B**. Principal Component Analysis (PCA) of the mRNA-Seq data after variance stabilized transformation

The data quality was assessed by hierarchical sample clustering along with principal component analysis on variance stabilized transformation of mRNA-Seq data. As revealed by the clustering analysis, replicates clustered together within each condition verifying the similarity between these samples (Figure 10A). Interestingly, the differences induced by differentiation were similar within each condition (compare undifferentiated with the respective differentiated controls), whereas DMSO or siCNTR treatment induced on their own clear differences (Figure 10B). Moreover, two BRD4 siRNAs showed highest level of similarity in their actions, which seemed quite different from those induced by JQ1.

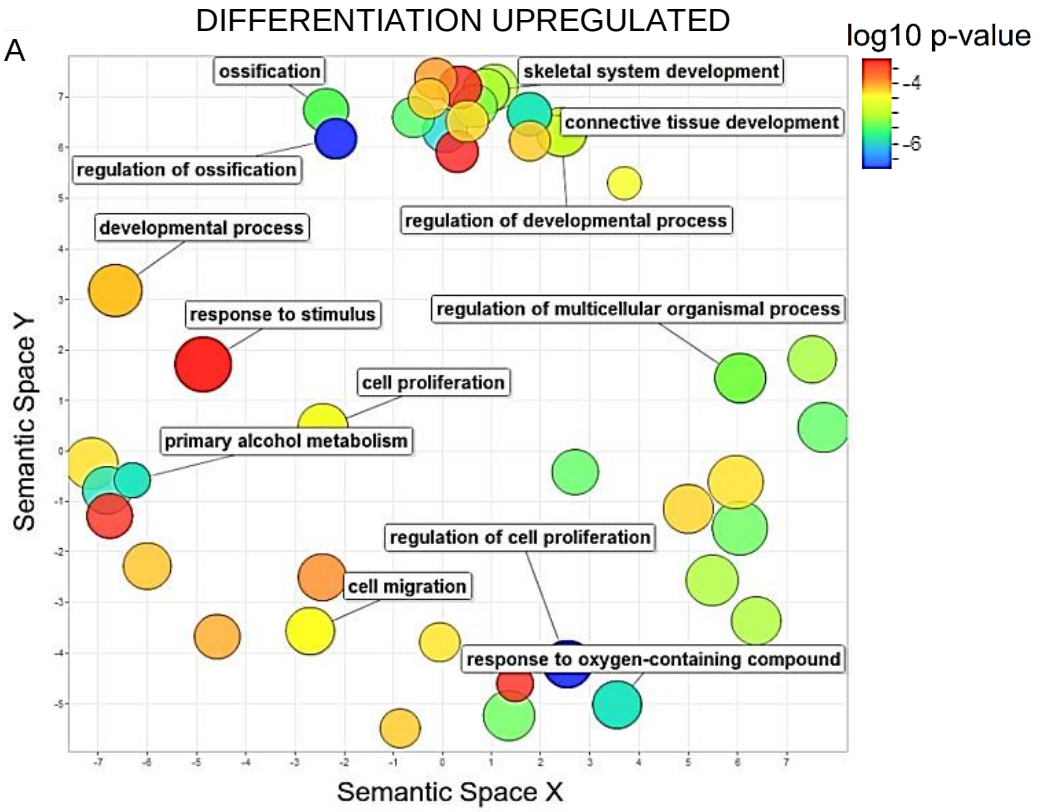

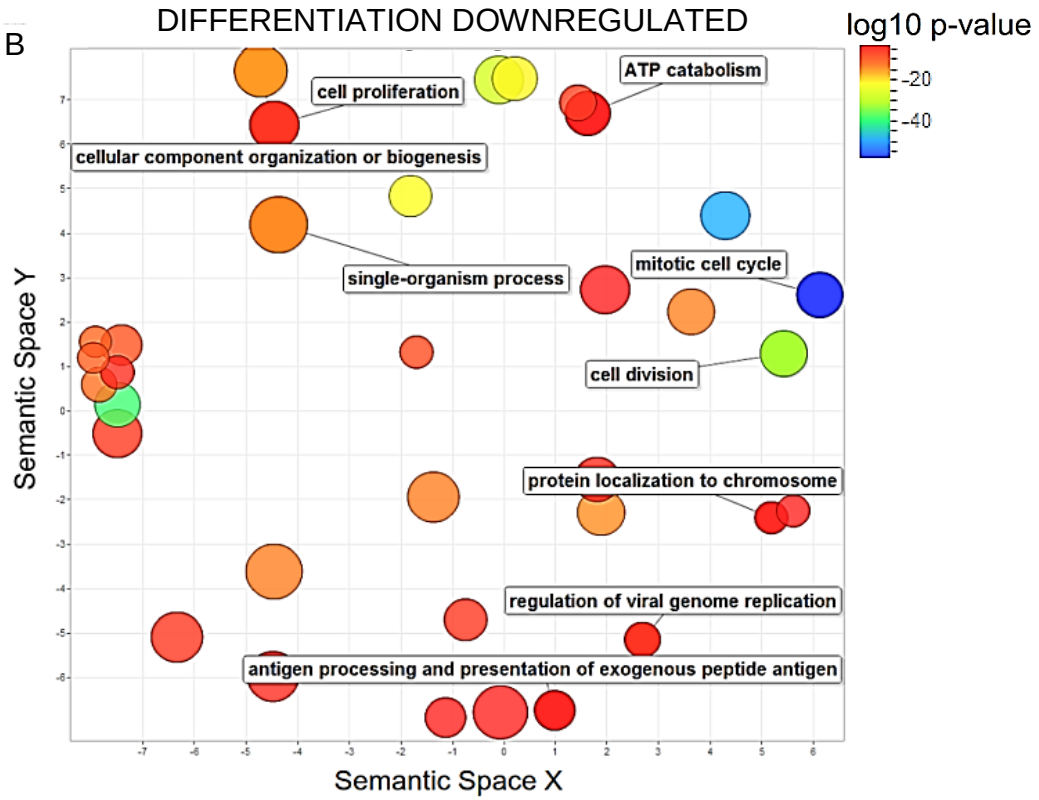

Figure 11. ***Gene Ontology on differentiation regulated genes*****.** Functional Classification Summary of GO terms associated with **A**. differentiation upregulated genes (log2fold change ≥1, FDR<0.05) and **B**. differentiation downregulated genes (log2fold change ≤-1, FDR<0.05), created by GO visualization tool REVGO. The color code depicts the log10 p-values of enriched GO term clusters.

As expected, the differential analysis of gene expression changes revealed that differentiation upregulated genes are significantly enriched in gene ontology (GO) terms involved in skeletal development (Figure 11A). Genes downregulated with differentiation were mainly associated with cell division and cell cycle (Figure 11B) pathways which is consistent with the notion that before differentiation cells undergo cell cycle arrest (Funato et al., 2001).

Notably, BRD4 knockdown and inhibition blocked the differentiation induced changes but to a different extend (Figure 12A, B). The overlap between JQ1 and siBRD4 regulated genes was not high and seemed different. Consistent with the positive role of BET proteins in gene transcription, we observed higher number of downregulated genes than number of induced genes following JQ1 or siBRD4 treatments (Figure

12). Interestingly, a large fraction of BRD4-regulated genes were also differentially regulated during osteoblast differentiation, further supporting a lineage-specific function of BRD4 in osteoblast differentiation.

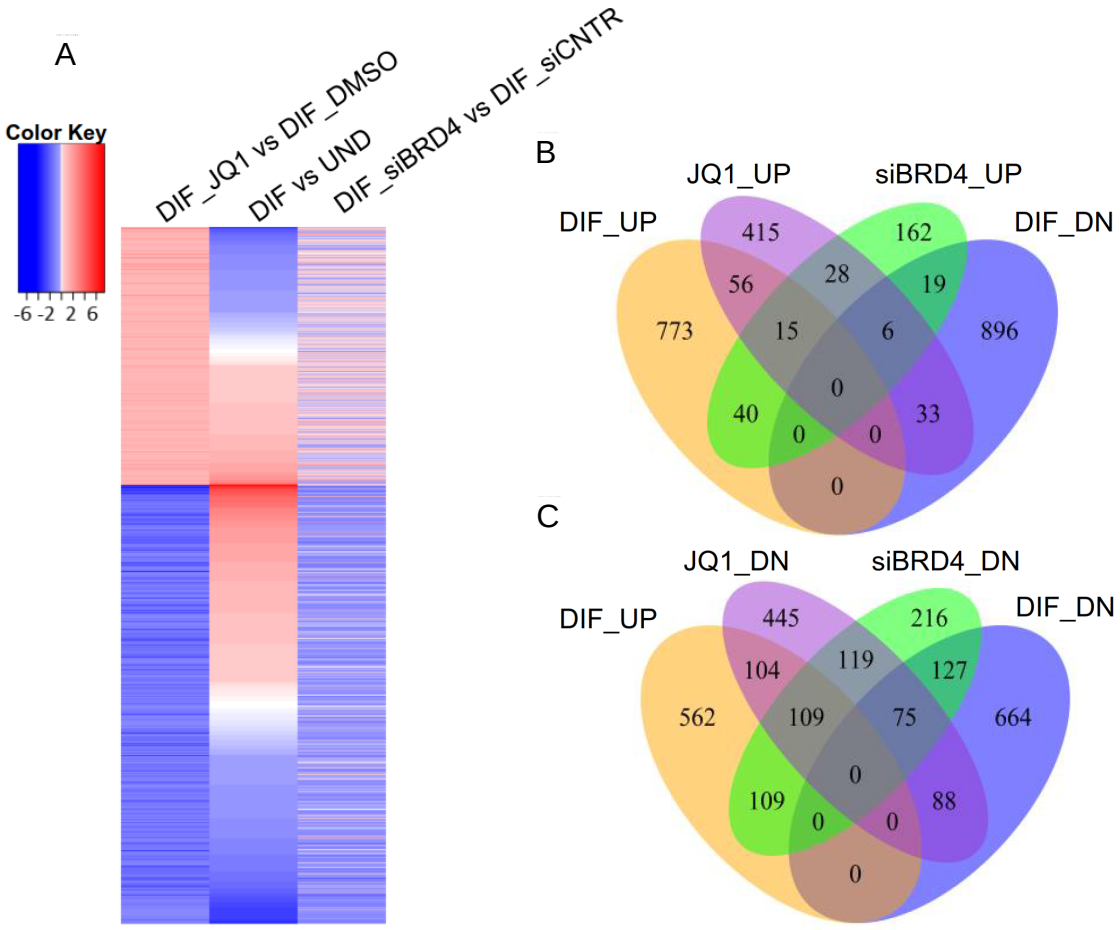

Figure 12. ***Transcriptome wide effects of BRD4 perturbation***. **A**. Heatmap depicting log2fold change values of mRNA-Seq data from hFOBs: (left) of JQ1 versus DMSO treated hFOBs in differentiated state; (middle) of control (siCNTR+DMSO) hFOBs in differentiated versus undifferentiated state; (right) of siBRD4 (#3 & #4) versus siCNTR treated hFOBs in differentiated state. Each row represents single gene. Genes up- (log2fold change value ≥0.8, padj≤0.05) and downregulated (log2fold change value ≤-0.8, padj≤0.05) in JQ1 versus DMSO treated hFOBs in differentiated state were selected for the heatmap. **B-C**. Venn Diagramms showing overlap of significantly regulated genes with following thresholds: in DIF_UP – differentiation upregulated genes (log2fold change value ≥1, padj≤0.05); in DIF_DN – differentiation downregulated genes (log2fold change value ≤-1, padj≤0.05); in JQ1_UP – JQ1 upregulated genes (log2fold change value ≥0.8, padj≤0.05); in JQ1_DN – JQ1 downregulated genes (log2fold change value ≤-0.8, padj≤0.05); in siBRD4_UP – siBRD4 (#3 & #4) upregulated genes (log2fold change value ≥0.7, padj≤0.05); in siBRD4_DN – siBRD4 downregulated genes (log2fold change value ≤-0.7, padj≤0.05).

Although BRD4 loss mediated effects extended beyond the list of differentiation regulated genes, the gene set enrichment analysis (GSEA) on the downregulated by siBRD4 (log2fold change<-0.7, padj<0.05) genes indicated enrichment for the GO

pathways associated with extracellular matrix, collagen and skeletal development (Table 1), In the case of JQ1 downregulated genes (log2fold change<-0.8, padj<0.05) effects seemed broader involving different developmental pathways in general including the skeletal system as well (Table 2).

Table 1. *GSEA report on siBRD4 downregulated genes*.

NAME	ES	NES	FDR q-val
EXTRACELLULAR_REGION	0.57	2.18	0.00000
EXTRACELLULAR_REGION_PART	0.57	2.15	0.00053
EXTRACELLULAR_MATRIX_PART	0.68	2.14	0.00035
VOLTAGE_GATED_CATION_CHANNEL_ACTIVITY	0.65	2.09	0.00026
EXTRACELLULAR_MATRIX	0.61	2.07	0.00021
COLLAGEN	0.79	2.07	0.00018
VOLTAGE_GATED_CHANNEL_ACTIVITY	0.63	2.07	0.00030
PROTEINACEOUS_EXTRACELLULAR_MATRIX	0.61	2.06	0.00026
GATED_CHANNEL_ACTIVITY	0.59	2.05	0.00046
CATION_CHANNEL_ACTIVITY	0.58	2.03	0.00042
REGULATION_OF_HEART_CONTRACTION	0.75	2.02	0.00057
SUBSTRATE_SPECIFIC_CHANNEL_ACTIVITY	0.56	2.01	0.00061
ION_CHANNEL_ACTIVITY	0.56	1.99	0.00073
SKELETAL_DEVELOPMENT	0.59	1.99	0.00068

Table 2. *GSEA report on JQ1 downregulated genes.*

NAME	ES	NES	FDR q-val
CYTOKINE_ACTIVITY	0.71	2.21	0.0000
CHEMOKINE_ACTIVITY	0.81	2.18	0.0000
CHEMOKINE_RECEPTOR_BINDING	0.80	2.17	0.0000
G_PROTEIN_COUPLED_RECEPTOR_BINDING	0.74	2.12	0.0000
LOCOMOTORY_BEHAVIOR	0.68	2.09	0.0000
REGULATION_OF_RESPONSE_TO_EXTERNAL_STIMUL	0.88	1.98	0.0013
EXTRACELLULAR_REGION_PART	0.55	1.90	0.0049
HEMATOPOIETIN_INTERFERON_CLASSD200_DOMAIN _CYTOKINE_RECEPTOR_BINDING	0.74	1.90	0.0053
BEHAVIOR	0.57	1.89	0.0064
EXTRACELLULAR_REGION	0.53	1.88	0.0068
EXTRACELLULAR_SPACE	0.55	1.87	0.0073
IMMUNE_RESPONSE	0.54	1.85	0.0102
RESPONSE_TO_EXTERNAL_STIMULUS	0.54	1.84	0.0109
HUMORAL_IMMUNE_RESPONSE	0.69	1.80	0.0231
LEUKOCYTE_MIGRATION	0.79	1.79	0.0268
COLLAGEN	0.73	1.79	0.0265
VASCULATURE_DEVELOPMENT	0.60	1.72	0.0409
MUSCLE_DEVELOPMENT	0.51	1.57	0.1346
ECTODERM_DEVELOPMENT	0.50	1.53	0.1555
SKELETAL_MUSCLE_DEVELOPMENT	0.59	1.52	0.1613
SKELETAL_DEVELOPMENT	0.46	1.46	0.2259

Taken together, these results uncover role of BRD4 in directing and maintaining the osteoblast-specific lineage determination by regulating the expression of genes involved in skeletal development, ossification, extracellular matrix organization

Differentiation induced genes recruit more BRD4 at TSS

It has been shown previously, that CDK9 controls differentiation of human mesenchymal stem cells (hMSC) into osteoblast linage through regulation of phosphorylation of RNA Polymerase II (RNAPII) and the downstream monoubiquitination of histone H2B (H2Bub1) which marks the lineage-specific gene transcription (Karpiuk et al., 2012). In accordance with this notion we decided to look for genome-wide localization of BRD4 along with H2Bub1 and RNAPII II to elucidate BRD4 associated molecular signatures involved in osteoblast lineage determination. Moreover, since very often BRD4 occupation correlates with histone H3 K27 acetylation (H3K27ac) (Nagarajan et al., 2014, 2015; Zhang et al., 2012), we also sought to look for global changes in H3K27ac levels in the context of differentiation regulation. Hence, chromatin immunoprecipitation followed by high-throughput sequencing (ChIP-Seq) of BRD4, RNAP II, H3K27ac and H2Bub1 was performed on undifferentiated and differentiated hFOBs. Additionally, to study the genome wide consequences of BRD4 inhibition on transcriptional regulation, H3K27ac and H2Bub1 ChIP-Seq, as marker of active transcription and elongation, respectively, were performed following JQ1 treatment. The efficiency of ChIP was verified by qRT-PCR on positive as well as negative genomic sites prior the sequencing (Figure 13).

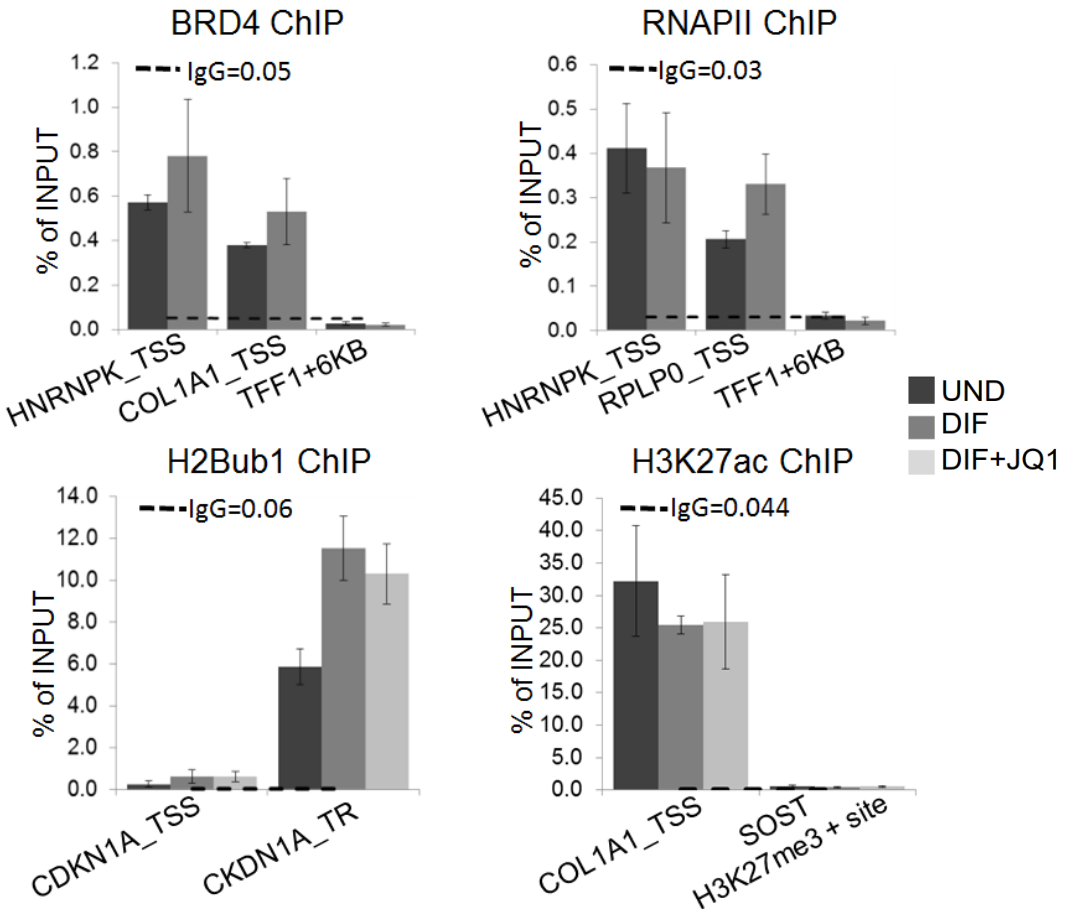

Figure 13.*Confirmation of ChIP efficiency in hFOBs.* Undiffirentiated or osteoblast differentiated hFOBs with or without JQ1 treatment were subjected to BRD4, RNAPII, H2Bub1 and H3K27ac chromatin immunoprecipitation (ChIP). qRT-PCR was used to verify the efficiency of immunoprecipitation on the positive as well as negative sites (note : different sites were used for different proteins). For background estimation IgG ChIPs were used. The ChIP efficiency is displayed as enrichment over Input in percent. Mean±SD, n=3**.**

In general, BRD4 correlated with RNAPII and H3K27ac levels on all the genomic regions (Figure 14). As expected, the correlation with H2Bub1 was almost not apparent since H2Bub1 is known to mainly localize to transcribed regions of the genes (Minsky et al., 2008) and other genomic regions are devoid of H2Bub1.

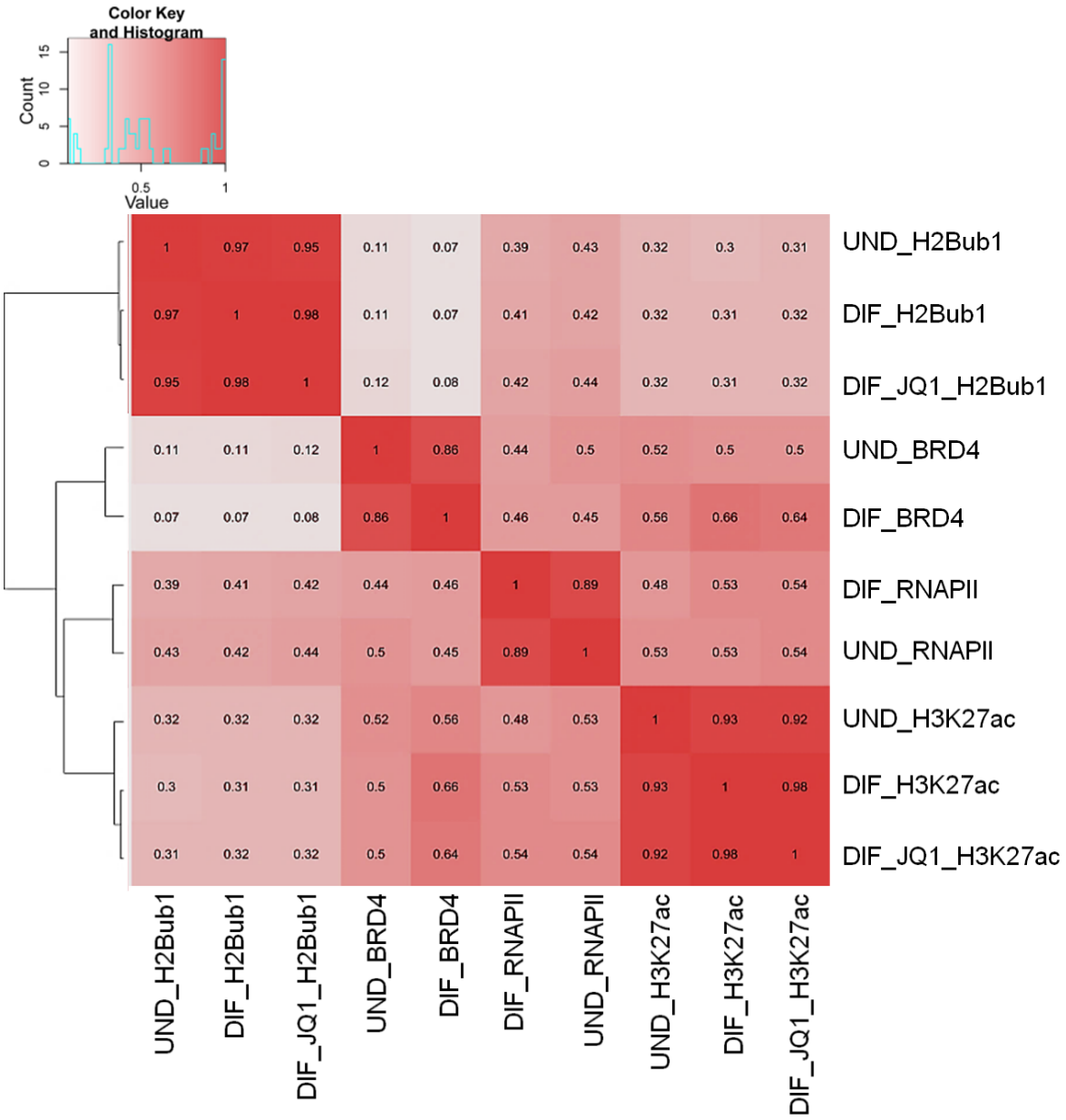

Figure 14. ***Genome wide correlation heatmap of BRD4, RNAPII, H3K27ac and H2Bub1 ChIP Signals.*** Normalized ChIP-Seq coverage files (bigwig files) of BRD4, RNAPII in undifferentiated and differentiated hFOBs, H3K27ac and H2Bub1 in undifferentiated, differentiated hFOBs treated with DMSO or JQ1, respectively were used to compute average coverages over 10KB bins for each condition and treatment. The Pearson correlations were evaluated for the given datasets on all the genomic regions.

In order to elucidate how BRD4 regulates differentiation on transcriptional level we sought to analyze the correlation of BRD4 occupancy around the transcription start site (TSS) of differentiation regulated genes with the respective changes in gene expression. Significantly upregulated during differentiation osteoblast-specific genes, such as matrix proteoglycan Decorin (*DCN*) (Takeuchi et al., 1994) and Odd-

Skipped Related 2 (*OSR2*) (Kawai et al., 2007) showed increased binding of BRD4 around the TSS (Figure 15). Consistently, RNAPII and H2Bub1 occupancy raised on the gene bodies indicating elevated transcriptional elongation (Figure 15).

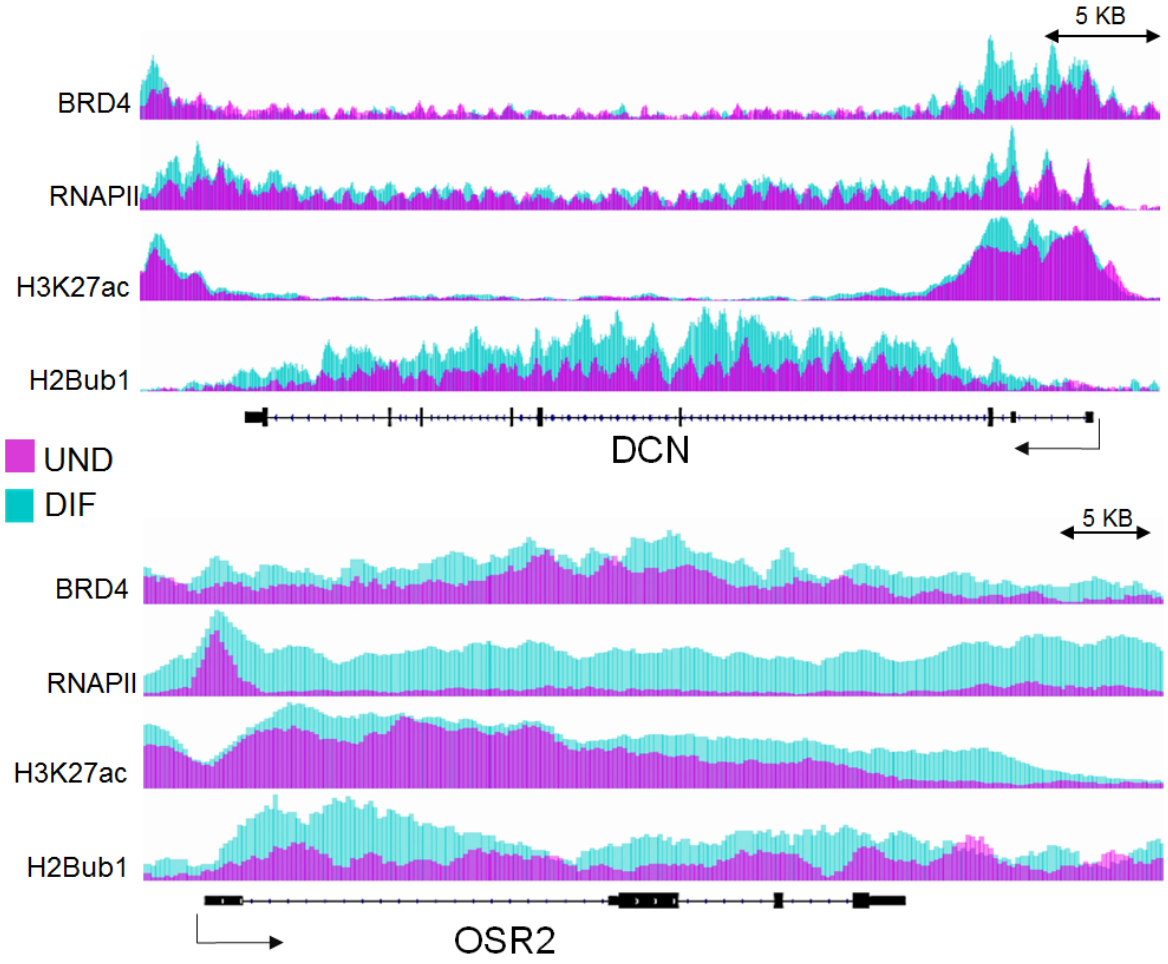

Figure 15. ***Differentiation induced genes exhibit higher enrichment of BRD4 around the TSS upon differentiation***. IGV profiles for 2 genes (top-DCN, bottom-OSR2) picked from the RNA-Seq list of differentiation upregulated genes (DIF_UP). Each lane represents normalized average occupancy (in RPKM) for BRD4, RNAPII, H3K27ac, and H2Bub1 in undifferentiated (pink) and differentiated (cyan) hFOBs, respectively. Grouped autoscale was used for each condition.

To get the overall picture of BRD4 involvement in transcriptional control of osteoblast phenotype, we grouped the genes into three groups based on the regulation as follows: differentiation induced genes (DIF_UP, log2fold change ≥1, padj<0.05), downregulated genes (DIF_DN, log2fold change ≤ -1, padj<0.05) and unregulated genes (abs(log2fold change) < 0.2, padj>0.8) and mapped BRD4 around the

promoter regions of these genes. In general, the BRD4 binding increased upon differentiation around the TSS of all the indicated groups, however, the genes of DIF_UP group exhibited highest increase (Figure 16 and 17).

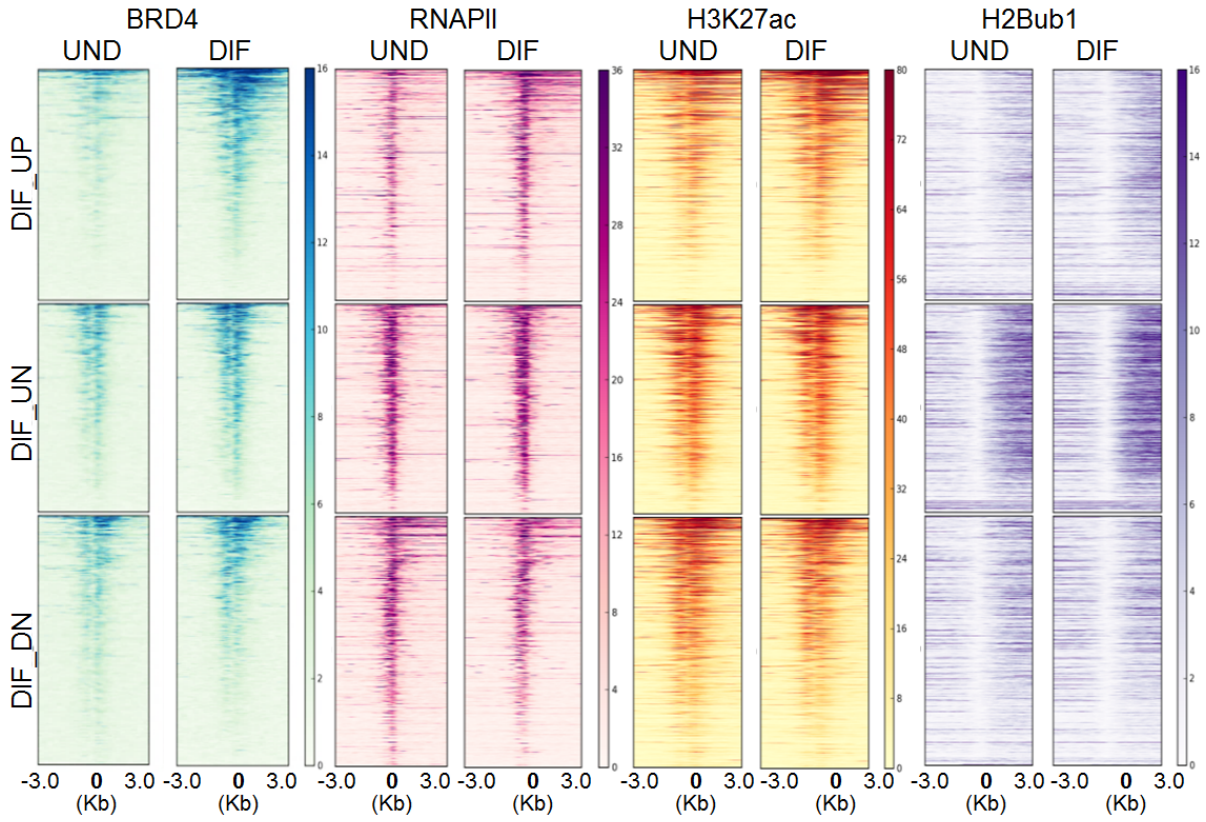

Figure 16. ***BRD4, RNAPII, H3K27ac and H2Bub1 show highest increase on osteoblast-specific genes upon differentiation*****.** Heatmaps depicting occupancy (RPKM values) of BRD4, RNAPII, H3K27ac and H2Bub1 in undifferentiated and differentiated hFOBs, respectively around the TSS (±3KB) of genes upregulated (DIF_UP), unregulated (DIF_UN) and downregulated (DIF_DN) during differentiation. Each row in the heatmaps represents one gene. The gene order in heatmaps was sorted from high to low based on BRD4 levels in differentiated state. The ordering was maintained the same for RNAPII, H3K27ac and H2Bub1, respectively. "0" defines the transcription start site of each gene.

Similarly, differentiation induced genes accumulated more RNAPII, H3K27ac and H2Bub1 around the TSS. However, almost no difference in occupancy was observed in the case of differentiation unregulated or downregulated genes (Figure16 and 17). In general, differentiation induced gene expression changes correlated well with the change in BRD4, RNAPII, H3K27ac and H2bub1 levels, especially in the case of differentiation upregulated genes (Figure 18).

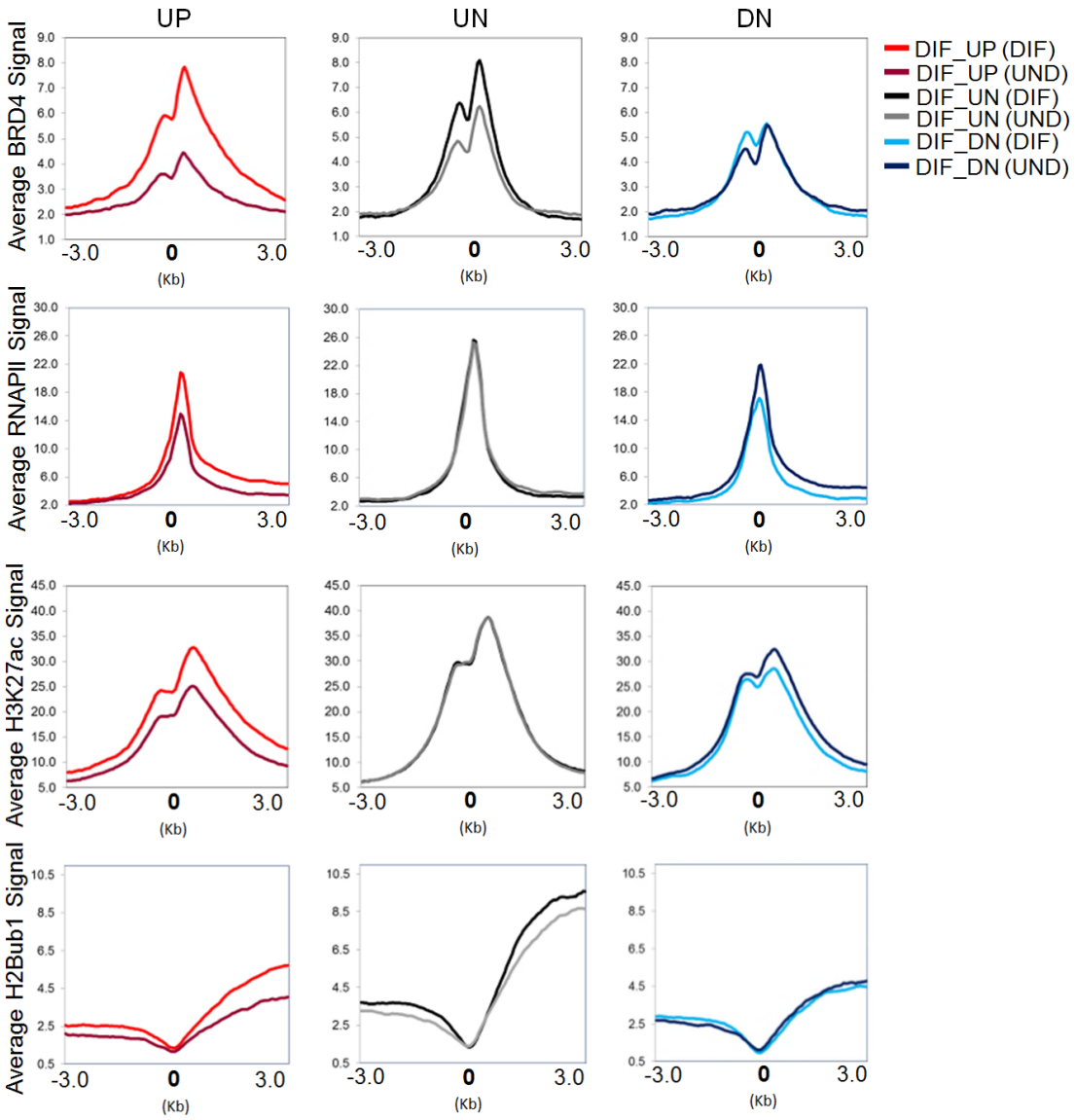

Figure 17. *Osteoblast-specific genes are the least marked genes in undifferentiated hFOBs*. Average enrichment profiles (in RPKM values) of RNAPII, H3K27ac, BRD4 and H2Bub1 in undifferentiated and differentiated hFOBs, respectively on the same genomic regions used for heatmaps in (Figure 16). The profiles are depicted for differentiation upregulated (DIF_UP), unregulated (DIF_UN) and downregulated (DIF_DN) genes separately for undifferentiated (UND) and differentiated (DIF) state. "0" defines the transcription start site.

Interestingly, while upregulated genes exhibited relatively low levels of BRD4 along with RNAPII, H3K27ac and H2Bub1 in undifferentiated state, differentiation unregulated genes were initially highly marked by all of the four indicated marks (compare DIF_UP with DIF_UN group, Figure 16 and 17). Since higher occupancy of "positive" histone modifications at the promoters correlates with higher gene

expression (Su et al., 2016), we decided to see whether the same could be observed in the case of differentiation unregulated genes.

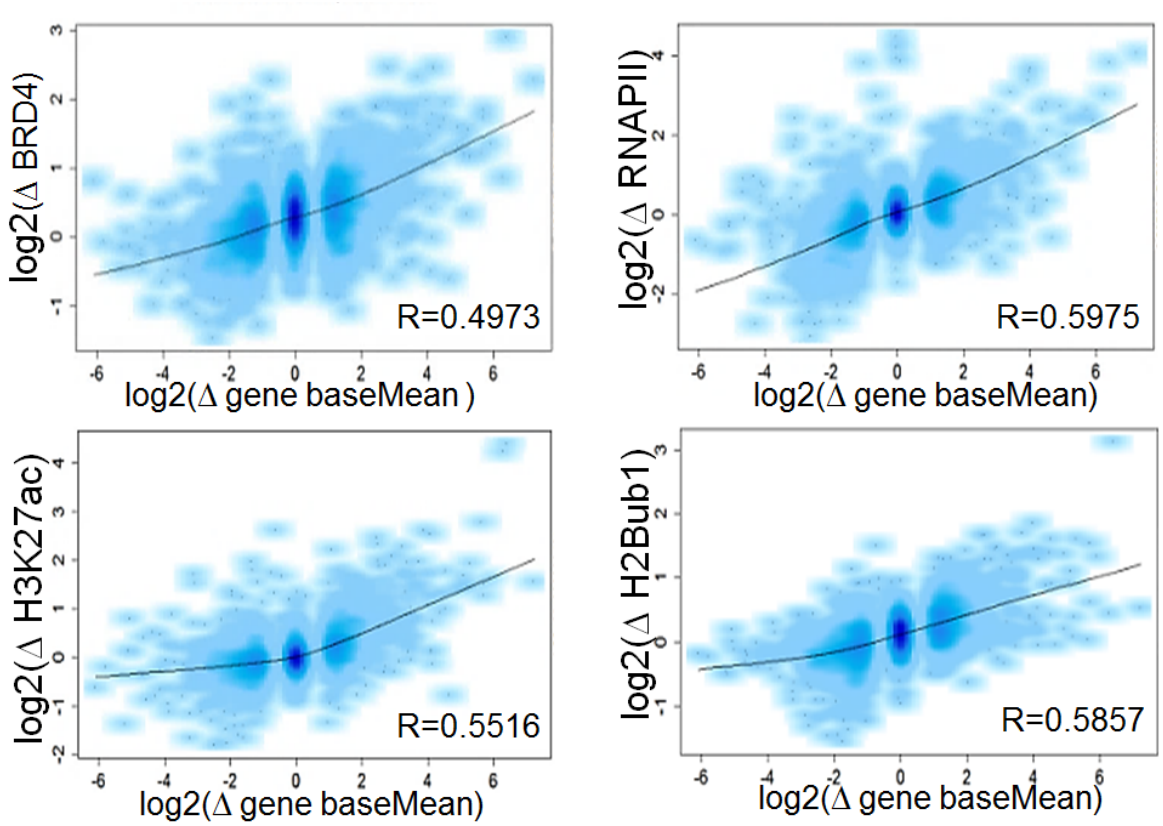

Figure 18. ***Correlation of differentiation induced gene expression change with BRD4, RNAPII, H3K27ac and H2Bub1 change*****.** Density scatter plots depict on the y-axis log2 fold change values of normalized ChIP-Seq signal occupancy in RPKM in differentiated hFOBs versus undifferentiated hFOBs at ± 500bp around the TSS for BRD4 and H3K27ac; 300 bp downstream of TSS – for RNAPII and on the gene body (TSS to TTS)– for H2Bub1. The x-axis represents log2fold change values of baseMean counts (differentiated hFOB vs undifferentiated) altogether of genes from all the three groups abovementioned. The R stands for Pearson Correlation coefficient.

Indeed, when we compared the baseMean counts of the genes from each group it turned out that the unregulated genes are highly expressed in undifferentiated hFOBs (Figure 19). Consistently, the upregulated genes were initially the least expressed genes when compared to downregulated or unregulated group of genes. Upon differentiation, the baseMean counts of upregulated genes reached the same level as for unchanged genes, while downregulated genes became less expressed dropping to similar level as upregulated genes showed in undifferentiated state.

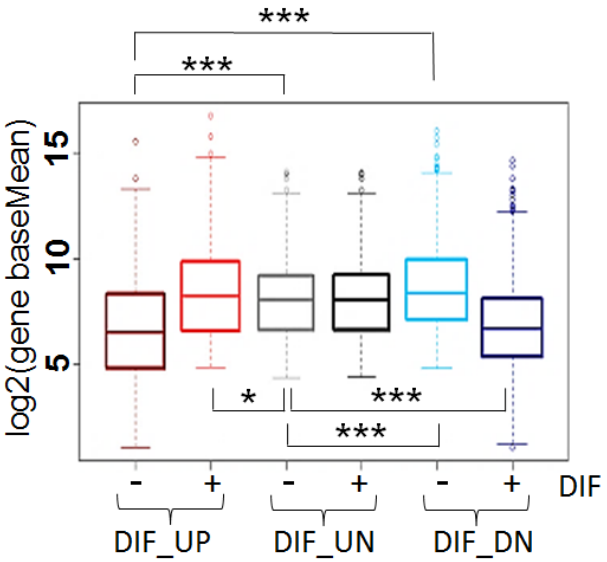

Figure 19. ***Differentiation unregulated genes are highly expressed genes.*** Boxplots showing log2fold gene expression counts (baseMean values) for genes upregulated (DIF_UP), unregulated (DIF_UN) and downregulated (DIF_DN) with differentiation in undifferentiated and differentiated hFOBs, respectively. The gene expression counts were obtained from differential gene expression analysis of RNA-Seq data with DESeq2 package. For statistical analysis Wilcoxon Rank Sum test was performed where ***p<0.001, **p<0.01, *p<0.05

Interestingly, the gene ontology analysis on the differentiation unregulated genes revealed enrichment for cellular metabolic processes which suggests "housekeeping" functions of these genes (Table 3)

Table 3. *Gene Ontology Analysis on differentiation unregulated (DIF_UN) genes*

CATEGORY	TERM	FDR
GO:0044260	*cellular macromolecule metabolic process*	2.31E-05
GO:0044237	*cellular metabolic process*	1.65E-04
GO:0010467	*gene expression*	1.65E-04
GO:0043170	*macromolecule metabolic process*	5.79E-04
GO:0044238	*primary metabolic process*	6.64E-04
GO:0008152	*metabolic process*	6.95E-04
GO:0016070	*RNA metabolic process*	2.53E-03
GO:0010468	*regulation of gene expression*	7.07E-03
GO:0071704	*organic substance metabolic process*	7.89E-03
GO:0006139	*nucleobase-containing compound metabolic process*	8.51E-03
GO:0046483	*heterocycle metabolic process*	1.15E-02
GO:0006807	*nitrogen compound metabolic process*	1.23E-02
GO:0006725	*cellular aromatic compound metabolic process*	1.92E-02
GO:0090304	*nucleic acid metabolic process*	2.30E-02
GO:0034641	*cellular nitrogen compound metabolic process*	4.25E-02

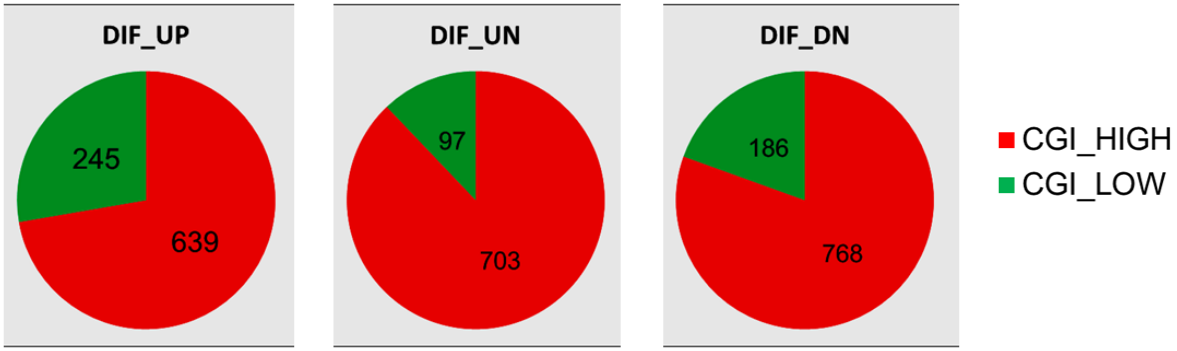

Figure 20. ***Promoter CGI content doesn't define the outcome of transcriptional regulation during differentiation.*** Pie charts represent the CGI (CpG Island) content within the promoter region (±1KB TSS) of differentiation upregulated (DIFF_UP), unregulated (DIF_UN) and downregulated genes. "CGI_HIGH" promoters are considered those with the sequences length at least 200 bp and with a G + C content of 50% and a CpG frequency (observed/expected; [*o*/*e*]) of 0.6 (Larsen et al., 1992).

Given the positive correlation between the highly expressed housekeeping genes with promoter CpG island (CGI) content (Larsen et al., 1992; Zhu et al., 2008), we questioned whether differentiation dependent genes would exhibit difference in promoter CGI content that would define the outcome of BRD4 dependent transcriptional regulation. Although, most of the differentiation unregulated genes were high CGI genes (≈87%), the distribution of differentiation upregulated or downregulated genes within CGI "HIGH" or "LOW" was not much different (≈80% and 72%, respectively) suggesting CGI content independent regulation of gene expression by BRD4 during differentiation (Figure 20).

Altogether, these findings indicate that increased transcription of osteoblast lineage defining genes correlates with elevated recruitment of BRD4 around the TSS of these genes. Moreover, the promoter CGI content most likely does not define the outcome of the differentiation dependent differential regulation of gene expression.

BRD4 marked genes differently respond to JQ1 treatment

JQ1 inhibition of BRD4 is mediated through its direct interaction with acetyl-lysine binding pockets of bromodomains disabling these from binding to acetylated chromatin. This means the observed effects of JQ1 treatment on transcriptional regulation involves genes that are or should be initially BRD4 marked. Indeed, osteoblast-specific genes – *DCN* and elastin (*ELN*) (Twine et al., 2014) downregulated with JQ1 treatment show substantial enrichment of BRD4 at the promoter regions (Figure 21). These genes are similarly marked by H3K27ac, RNAPII and H2Bub1 in differentiated state. Consistently, H2Bub1 levels as a readout of transcriptional elongation dropped with JQ1 treatment.

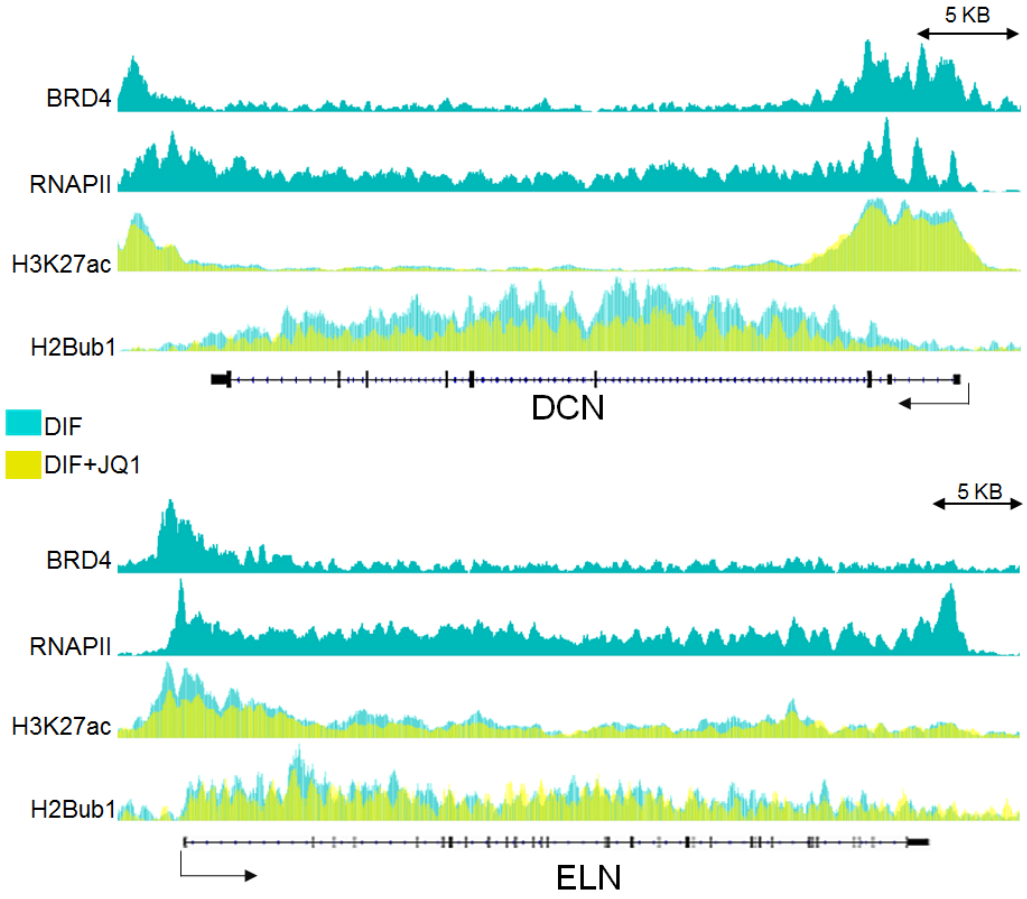

Figure 21. ***JQ1 dependent genes are BRD4 marked genes.*** **IGV profiles for 2 genes (top – DCN, bottom – ELN) picked from the RNA-Seq list of JQ1 downregulated genes.** Each lane represents normalized average occupancy (in RPKM) for BRD4, RNAPII, H3K27ac and H2Bub1 in differentiated hFOBs treated with DMSO (cyan) or JQ1 (yellow), respectively. Group autoscale option was used for DMSO and JQ1 treated H2Bub1 and H3K27ac profiles.

Interestingly, a reduction was also observed in H3K27ac levels upon JQ1 treatment. We therefore tested whether this effect was due to overall changes in protein levels of H3K27ac. Indeed, JQ1 induced decrease in differentiated hFOBs in H3K27ac levels, whereas siRNA mediated knockdown of BRD4 did not exhibit similar effect (Figure 22).

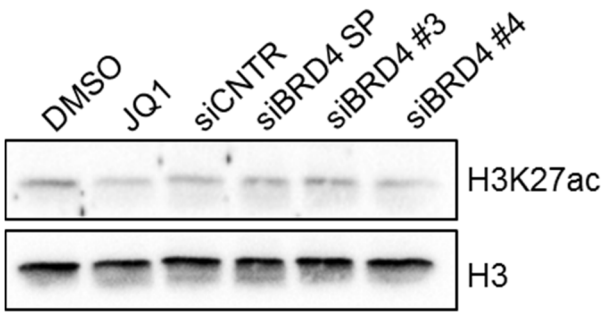

Figure 22. *JQ1 affects global H3K27ac protein levels*. Western Blot analysis of H3K27ac levels in whole cell protein extracts in differentiated for 5 days hFOBs following treatment with DMSO or JQ1, or non-targeting control siRNA (siCNTR) or BRD4 siRNA smartpool (siBRD4 SP) or two single siRNAs (siBRD4 #3 and #4). H3 were used as loading control.

To elucidate how promoter associated BRD4 occupancy accounts to transcriptional regulation of target genes, we grouped genes into three groups based on the effect of JQ1 treatment in differentiated hFOBs: up- (log2fold change >0.8, padj<0.05), un- (abs(log2fold change) <|0.2|, padj>0.85) and downregulated (log2fold change <-0.8, padj<0.05) and identified occupancy of BRD4 as well as RNAPII, H3K27ac and H2Bub1 around the TSS (± 3 KB) of these genes.

As expected JQ1 downregulated genes were highly BRD4 enriched which also correlated with high H3K27ac levels around the promoter regions (Figure 23). However, this was not consistent with RNAP II and H2Bub1 levels around the TSS of these genes. On contrary, JQ1 downregulated genes exhibited least amount of RNAPII and H2Bub1 occupancy when compared to the other two groups of genes (Figure 23 and 24). Consistently, H2Bub1 levels dropped across the JQ1 downregulated genes and JQ1 upregulated genes gained more H2Bub1. Given the global reduction of H3K27ac protein levels upon JQ1 treatment (Figure 22), the

genes of all three groups showed decreased levels of H3K27ac around the promoters.

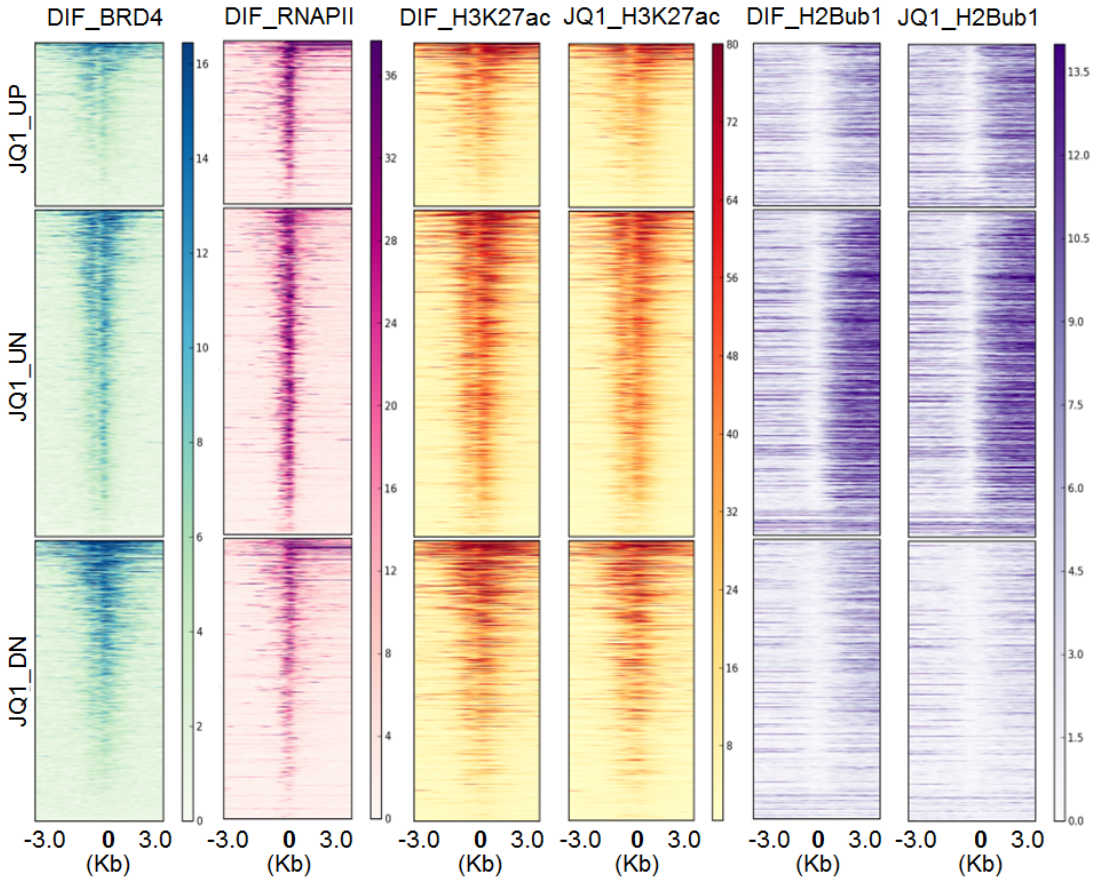

Figure 23. ***JQ1 downregulated genes are highly BRD4 bound*.** Heatmaps depicting occupancy (in RPKM) of BRD4, RNAPII in differentiated hFOBs and H3K27ac and H2Bub1 in differentiated hFOBs with DMSO or JQ1 treatment, respectively. Each row represents ±3KB region around the TSS of genes upregulated (JQ1_UP, log2fold change ≥0.8, FDR<0.05), unregulated (JQ1_UN, abs(log2fold change) ≤0.2, FDR>0.85) and downregulated (JQ1_DN, log2fold change ≤-0.8, FDR<0.05) upon JQ1 versus DMSO treatment in differentiated hFOBs. The gene order in heatmaps was sorted from high to low based on BRD4 levels in differentiated state. The ordering was maintained the same for RNAPII, H3K27ac and H2Bub1 heatmaps, respectively. "0" defines the transcription start site of each gene.

As in the case with differentiation unregulated genes JQ1 unaffected genes were highly BRD4, RNAPII, H3K27ac and H2Bub1 enriched suggesting higher gene expression (Figure 23 and Fugure 24). Indeed, the estimated gene expression counts were the highest for JQ1 unregulated genes in differentiated control hFOBs. Interestingly, JQ1 upregulated genes were the least expressed genes (Figure 25)

although harbored relatively higher levels of RNAPII (Figure 24) compared to other two groups indicating to perhaps “poised” state of polymerase on these genes

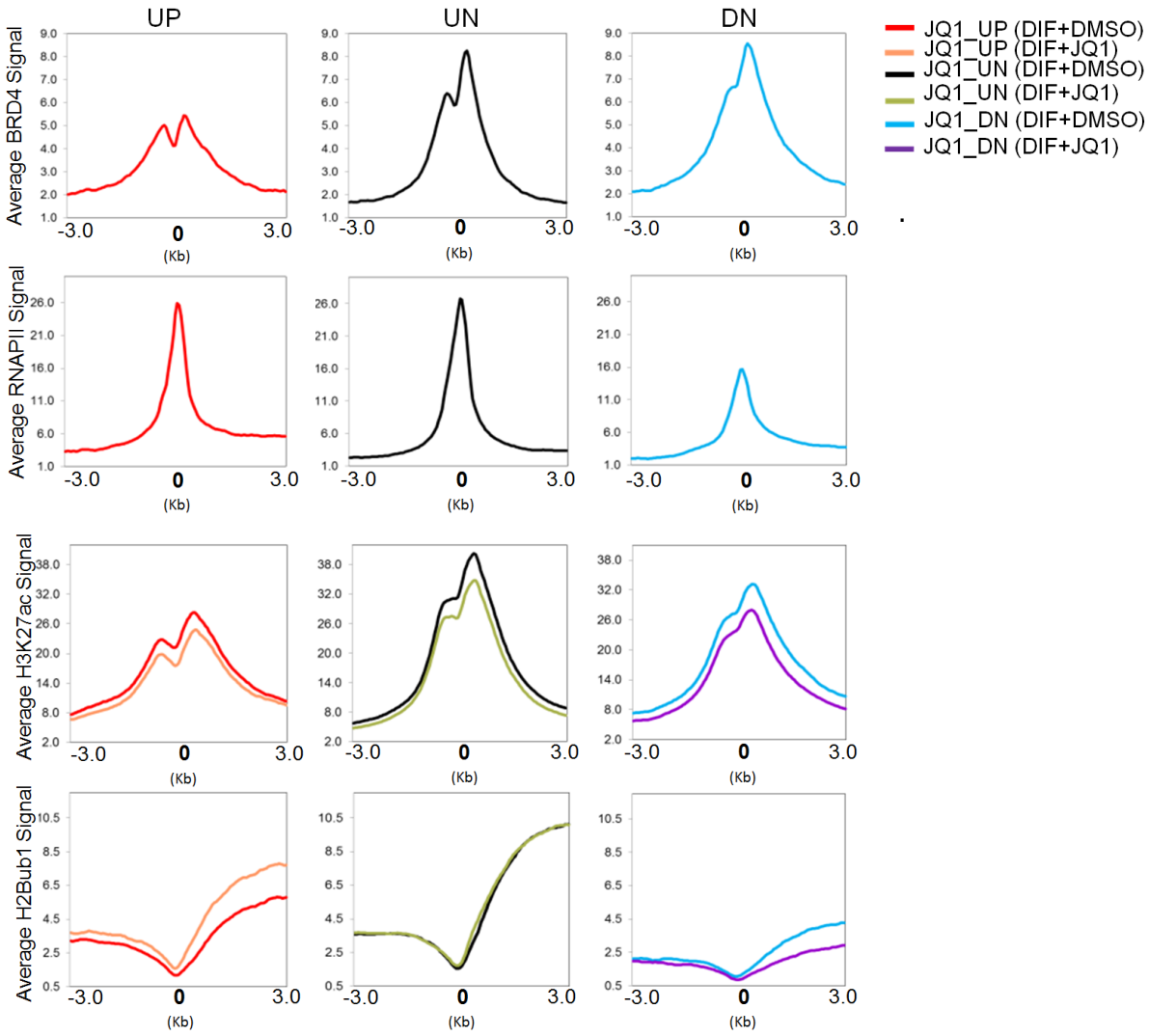

Figure 24. ***H2Bub1 Levels Change Consistently with Gene Expression Change induced by JQ1.*** Average enrichment profiles (in RPKM) of BRD4, RNAPII in differentiated hFOBs and H3K27ac and H2Bub1 in differentiated hFOBs with DMSO or JQ1 treatment, respectively, on the same genomic regions used for heatmaps in (Figure 23). The profiles are depicted for JQ1 upregulated (JQ1_UP), unregulated (JQ1_UN) and downregulated (JQ1_DN) genes, separately for DMSO or JQ1 treated state. “0” defines the transcription start site.

In this case BRD4 levels were more predictive of gene expression status. Therefore we sorted all the genes into four groups based on BRD4 levels, namely we defined 4 groups depending on the log2 BRD4 RPKM values around the TSS(±500) of the genes in differentiated control state: “Very Low” (<2.3), “Low”(2.3-2.8), “Medium” (2.8-3.3) and “High” (>3.3) (Figure 26) and looked for gene expression pattern within

each group. Similarly, RNAPII, H3K27ac and H2Bub1 signals showed the same tendency gradually increasing from “Very Low” to “High” group.

.

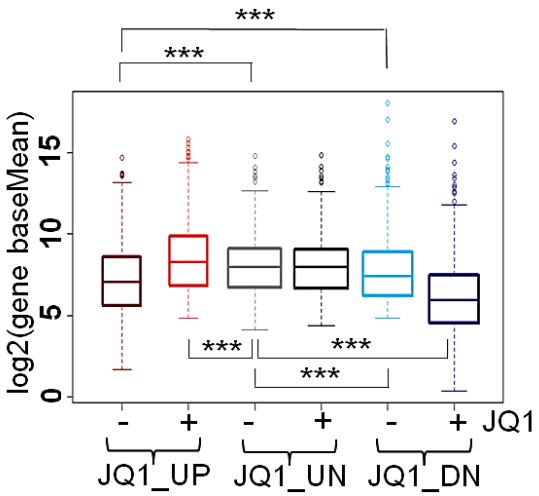

Figure 25. ***BRD4 dependent genes are highly expressed genes*.** Boxplots showing log2fold gene expression counts (baseMean values) for genes upregulated (JQ1_UP), unregulated (JQ1_UN) and downregulated (JQ1_DN) with JQ1 treatment in DMSO or JQ1 treated differentiated hFOBs, respectively. The gene expression counts were obtained from differential gene expression analysis of RNA-Seq data with DESeq2 package. For statistical analysis Wilcoxon Rank Sum test was performed where ***p<0.001, **p<0.01, *p<0.05

The quantified gene expression counts estimated in baseMean values also increased in accordance with BRD4 levels from “Very Low” to “High” group (Figure 27).

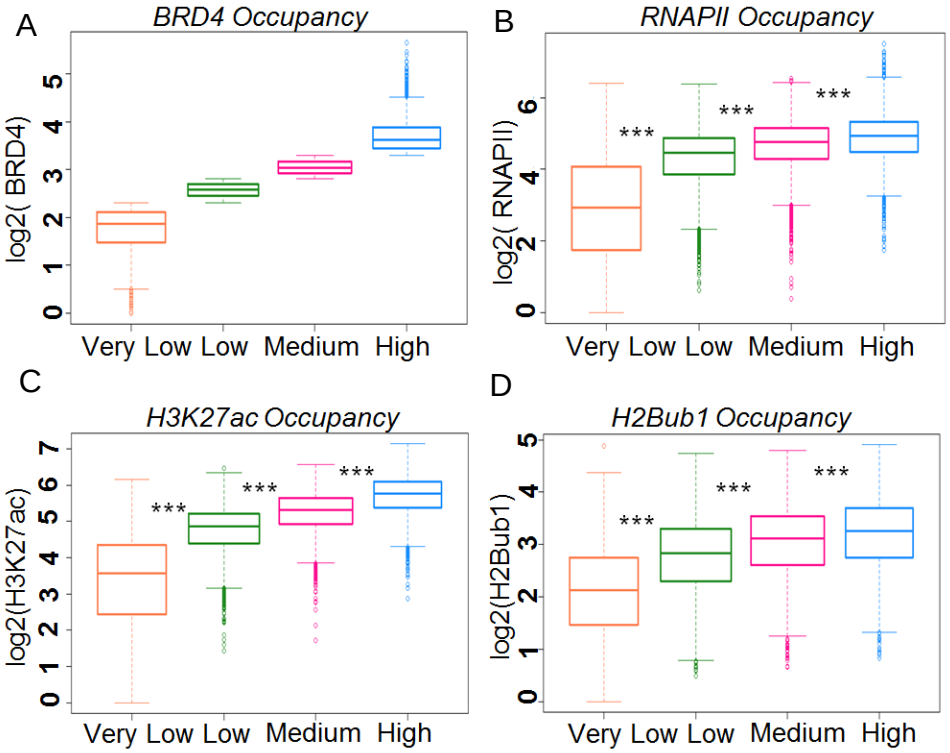

Figure 26. ***RNAPII, H3K27ac and H2Bub1 levels correlate with BRD4 levels*****. A**. Boxplots showing log2 RPKM values of BRD4 ±500bp around the TSS of genes in differentiated hFOBs treated with DMSO. Based on the BRD4 values genes were grouped in 4 classes: "Very Low" – log2 BRD4 RPKM< 2.3; "Low" – 2.3 < log2 BRD4 RPKM < 2.8; "Medium" – 2.8 < log2 BRD4 RPKM < 3.3; "High" – log2 BRD4 RPKM >3.3. **B-D.** Boxplots showing log2 RPKM values of RNAPII (300 bp downstream of TSS), H3K27ac (±500bp around the TSS) and H2Bub1 (on the gene body from TSS to TTS) occupancy, respectively in differentiated hFOBs within "Very Low", "Low", "Medium" and "High" BRD4 groups identified in (A). For statistical analysis Wilcoxon Rank Sum test was performed where ***p<0.001, **p<0.01, *p<0.05

Surprisingly, the absolute gene expression change induced by JQ1 treatment in differentiated hFOBs was the highest in the "Very Low" group (Figure 27). This indicated that lowly expressed and low BRD4 marked genes appeared to be more sensitive to JQ1 inhibition.

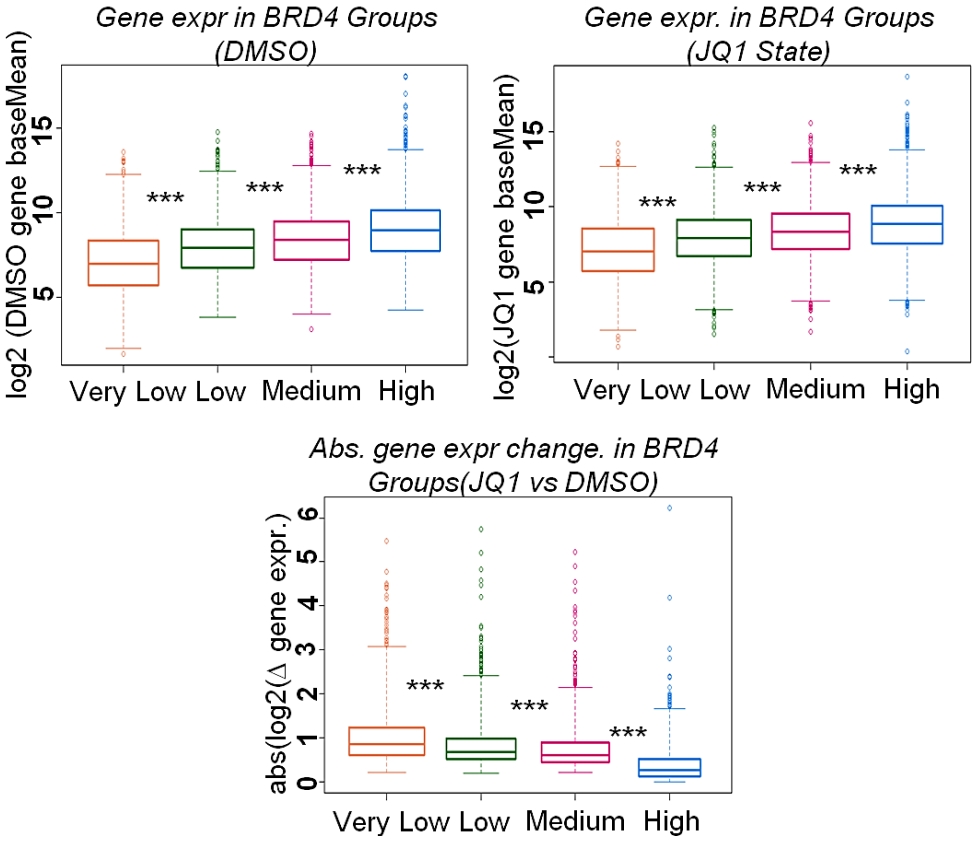

Figure 27. ***Gene expression correlates with BRD4 occupancy at TSS*****.** Boxplots showing log2 values of gene expression counts (baseMean values) in (UP left) differentiated hFOBs treated with DMSO, (UP right) in differentiated hFOBs treated with JQ1 and (DOWN) log2fold gene expression change induced by JQ1 versus DMSO in differentiated hFOBs within "Very Low", "Low", "Medium" and "High" BRD4 groups. For statistical analysis Wilcoxon Rank Sum test was performed where ***p<0.001, **p<0.01, *p<0.05.

Nonetheless, not all of the JQ1 regulated genes, as mentioned before, were low expressed and low marked genes. Interestingly, only 27% of JQ1 downregulated

genes belonged to the BRD4 “High” group whereas 32 % of these genes were found within the “Very Low” group (Table 4). In case of JQ1 upregulated genes almost half was comprised of BRD4 “Very Low” group genes, speaking for indirect mechanisms of gene expression regulation in this case. The distribution of JQ1 unchanged genes within the groups was more or less even among all of them.

Table 4. *Distribution of JQ1 group genes within the BRD4 groups*

	Very_Low (2627)	Low (2787)	Medium (3025)	High (2556)
JQ1_UP (553)	278	138	77	60
JQ1_UN (1092)	241	278	330	243
JQ1_DN (940)	302	205	178	255

As in case with differentiation unregulated genes, JQ1 unaffected genes were similarly enriched for GO terms associated with metabolic pathways (Table 5).

Table 5. *Gene Ontology Analysis on JQ1 unregulated (JQ1_UN) genes (top 15 hits)*

CATEGORY	TERM	FDR
GO:0044237	*cellular metabolic process*	2.25E-18
GO:0044260	*cellular macromolecule metabolic process*	1.40E-17
GO:0006139	*nucleobase-containing compound metabolic process*	4.10E-16
GO:0034641	*cellular nitrogen compound metabolic process*	9.78E-16
GO:0046483	*heterocycle metabolic process*	1.11E-15
GO:0010467	*gene expression*	1.70E-15
GO:0090304	*nucleic acid metabolic process*	3.48E-15
GO:0006725	*cellular aromatic compound metabolic process*	6.28E-15
GO:0044238	*primary metabolic process*	7.17E-15
GO:0006807	*nitrogen compound metabolic process*	1.37E-14
GO:0071704	*organic substance metabolic process*	3.93E-14
GO:0043170	*macromolecule metabolic process*	3.93E-14
GO:0008152	*metabolic process*	4.78E-14
GO:1901360	*organic cyclic compound metabolic process*	1.40E-13
GO:0016070	*RNA metabolic process*	4.78E-13

However, also here the promoter CGI content of the genes in all the three JQ1 groups was not much different between the groups (Figure 28) indicating CGI independent responsiveness to JQ1 inhibition of BRD4.

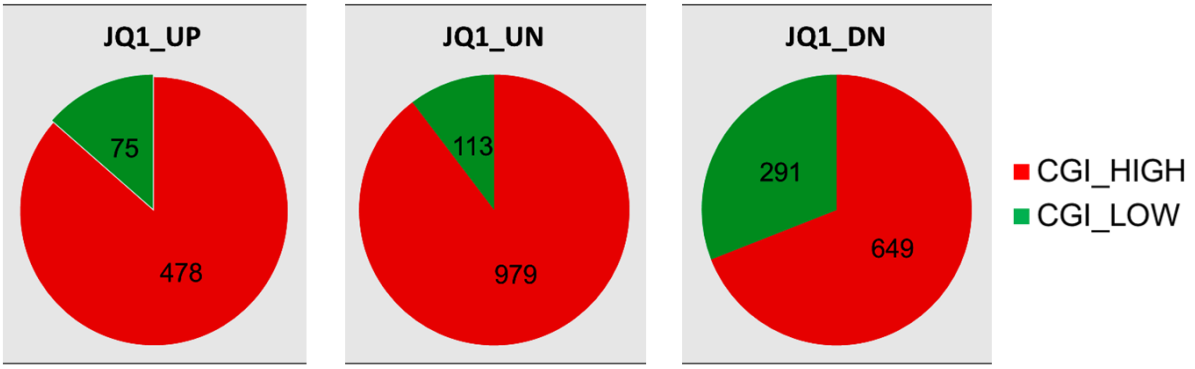

Figure 28. ***JQ1 Sensitivity Doesn't Depend on Promoter CGI Content***. Pie charts represent the CGI (CpG Island) content within the promoter region (±1KB TSS) of JQ1 upregulated (JQ1_UP), unregulated (JQ1_UN) and downregulated genes (JQ1_DN). "CGI_HIGH" promoters are considered those with the sequences length at least 200 bp and with a G + C content of 50% and a CpG frequency (observed/expected; [*o*/*e*]) of 0.6 (Larsen et al., 1992)

Altogether, these results indicate that TSS-associated BRD4 occupancy generally correlates with gene expression levels but only partially explains the extent of its requirement for gene expression, suggesting that additional mechanisms of transcriptional control may determine the effects of BRD4 inhibition or loss. Moreover, promoter CGI content does not define the outcome of promoter mediated transcriptional regulation by BRD4.

Identification of osteoblast-specific BRD4 bound putative enhancers

The transcriptional regulation of a gene is achieved by a cooperation of promoter- and enhancer-mediated events. BRD4 is known to occupy enhancers and facilitate enhancer RNA production (Di Micco et al., 2014; Kanno et al., 2014; Nagarajan et al., 2014; Zhang et al., 2012). Consistent with a proposed function at both enhancers and promoter proximal regions, nearly half of BRD4-enriched regions (45.3%) were localized to distal intergenic regions (Figure 29). Moreover, BRD4 occupancy

markedly correlated with RNAPII and H3K27ac on all the genomic regions (Figure 24). These findings support the notion that distal BRD4-bound regions might serve as transcribed enhancers responsible for the establishment and maintenance of an osteoblast-specific transcriptional program

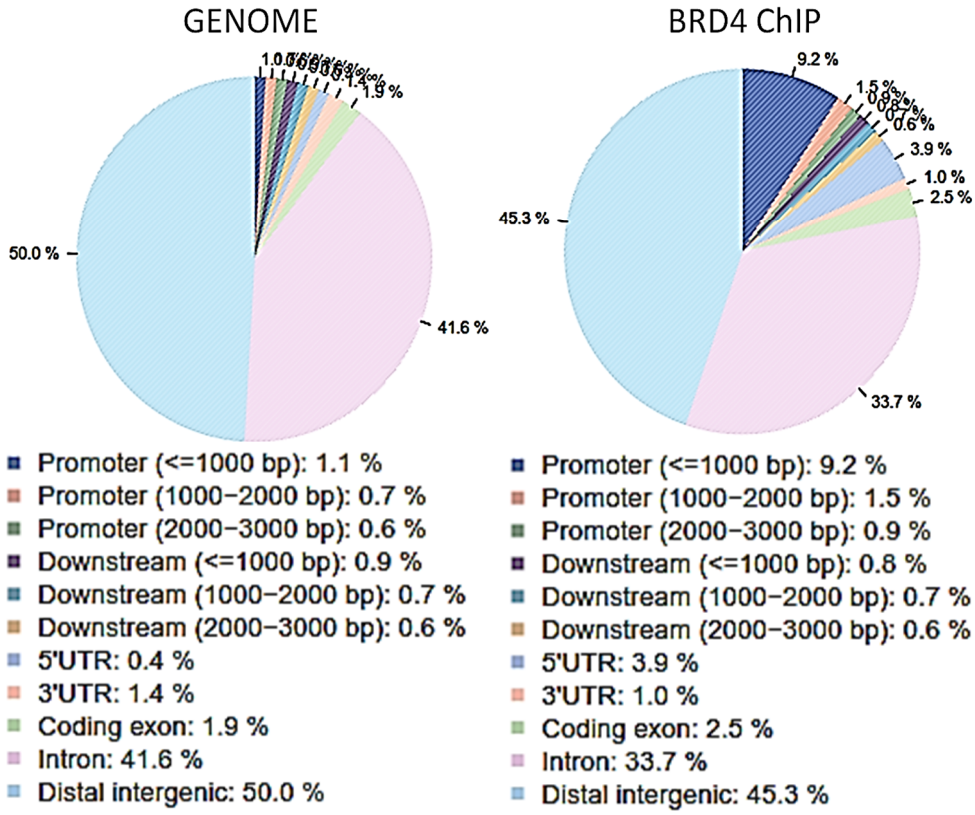

Figure 29. ***Genome wide distribution statistics of BRD4 in differentiated hFOBs*****.** CEAS (Cis-regulatory Element Annotation System) statistics in differentiated hFOBs at important genomic regions (left) showing the distribution of the given genomic features for the genomic input DNA and (right) for BRD4 ChIP.

We therefore sought to determine whether “promoter unrelated” BRD4 could be linked with the enhancers involved in osteoblast fate determination and maintenance. To find exclusively osteoblast-specific BRD4 bound regions we sought to identify and exclude BRD4 occupied sites that could be common between different tissues. Although there is considerable amount of ChIP-Seq data available online on BRD4, we decided to use for comparative analysis the datasets produced in our lab with the same conditions and antibody to avoid the variations that could be due to

choice of antibody and protocols used. Namely, we used datasets generated from 4 different cell lines: MCF10A, MCF7 treated with Estradiol (+E2), L3.6 and differentiated hFOBs. As shown (Figure 30), all 4 of these cell lines used had more distinct clusters of BRD4 bound regions than number of commonly shared sites.

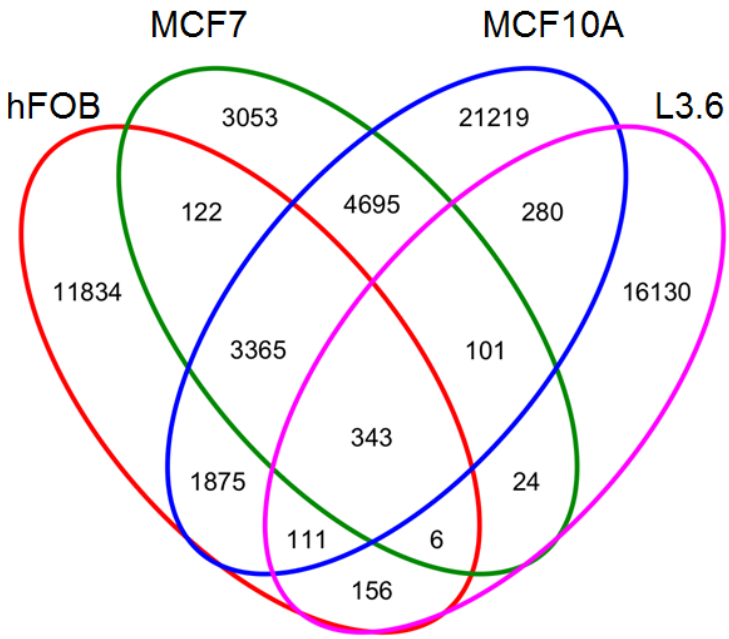

Figure 30. ***Cell type specific distribution of BRD4.*** Venn Diagramm showing the overlap of BRD4 peaks between the four cell lines: differentiated hFOBs (DIF_FOB), MCF10A, MCF7 treated with Estradiol (+E2) and L3.6 cells.

To find osteoblast-specific BRD4 regions we performed differential binding analysis between these cell lines and obtained 7822 differentially occupied regions which showed at least 2 fold higher BRD4 binding with FDR<0.05 in hFOBs. Since active enhancers can be identified based on the combination of active histone marks we performed chromatin segmentation analysis using Epigenome Count-based Segmentation (EpiCSeq) (Mammana and Chung, 2015) to further characterize osteoblast-specific BRD4-enriched regions. Based on high degree of epigenetic similarity of hFOB cells and Normal Human Osteoblast (NHOST) cells as identified through the high correlation of H3K27ac and H3K27me3 profiles between these two cell lines (Figure 31), we also utilized published H3K4me3, H3K4me1, H3K79me2,

H3K27me3 and H3K27ac occupancy profiles from NHOST cells along with H3K27ac and H3K27me3 from hFOBs to identify chromatin states which subdivide osteoblast-specific BRD4-bound regions

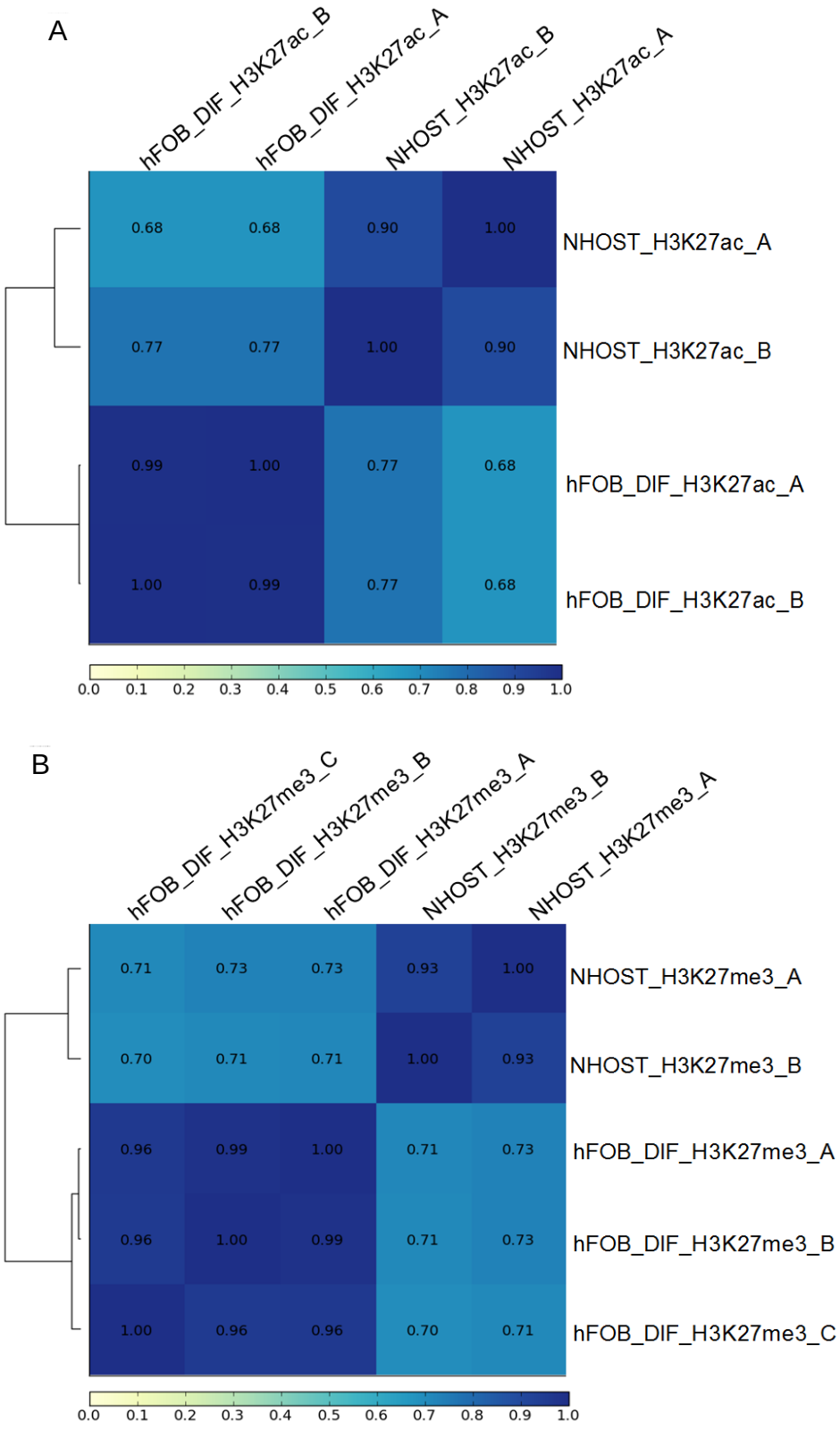

Figure 31. ***Correlation of H3K27ac and H3K27me3 profiles between hFOBs and NHOST cells*****.** Heatmaps depict Pearson correlation coefficients of A. H3K27ac in differentiated hFOBs with H3K27ac in NHOST and B. H3K27me3 in differentiated hFOBs with H3k27me3 in NHOST. BAM files were used to compute average coverages over 10KB bins for each condition. The correlations were evaluated on all the genomic regions.

Based on the segmentation analysis, 5 chromatin states were identified on these regions (Figure 32). States 1 and 2 were most likely associated with actively transcribed promoter regions as revealed by the combination of H3K27ac, H3K4me3 and H3K79me2 occupancy, where H3K4me3 is particularly associated with TSS-proximal regions and H3K79me2 with the proximal transcribed region of active genes. States 3 and 4 appear to represent putative enhancers based on the presence of both H3K27ac and H3K4me1 marks, both known to be associated with active enhancer regions. State 5 was only positive for H3K27ac, and specific for hFOBs, possibly indicating that these regions may be specific for the hFOB system and therefore less informative about general mechanisms related to osteoblast lineage-specification.

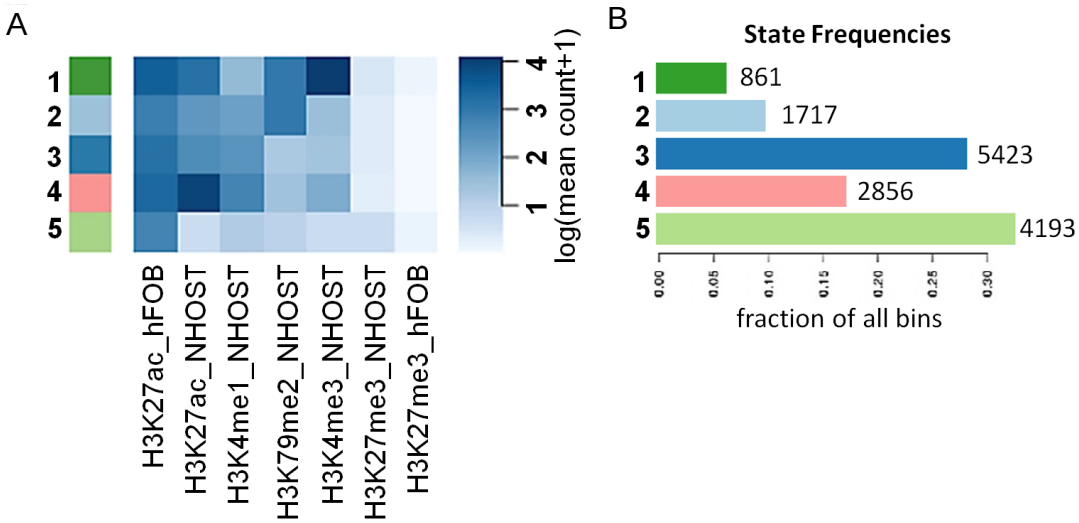

Figure 32. ***Chromatin segmentation of differentially BRD4 bound osteoblast-specific sites*****. A.** hFOB-specific differentially BRD4 bound regions (log2fold change>1 versus the other cell lines, FDR>0.05) were subjected to EpiCSeg segmentation analysis. 5 histone modifications from NHOST cells – H3K27ac, H3K4me1, H3K79me2, H3K4me3 and H3K27me3 and 2 from hFOBs – H3K27ac and H3K27me3 were used to identify chromatin states associated with selected BRD4 sites. The heatmap shows 5 chromatin states which were identified based on the combination and enrichment intensity (normalized counts) of used histone modifications. **B**. Bar chart showing the fraction of bins within each state identified from EpiCSeg analysis on differentially bound differentiated hFOB-specific BRD4 regions. The values next to the bars depict the number of regions (peaks) within each state.

Therefore we focused subsequent analysis on states 3 and 4. Consistently, the majority of “Segment 3+4” constituted distal intergenic regions or introns (Figure 33).

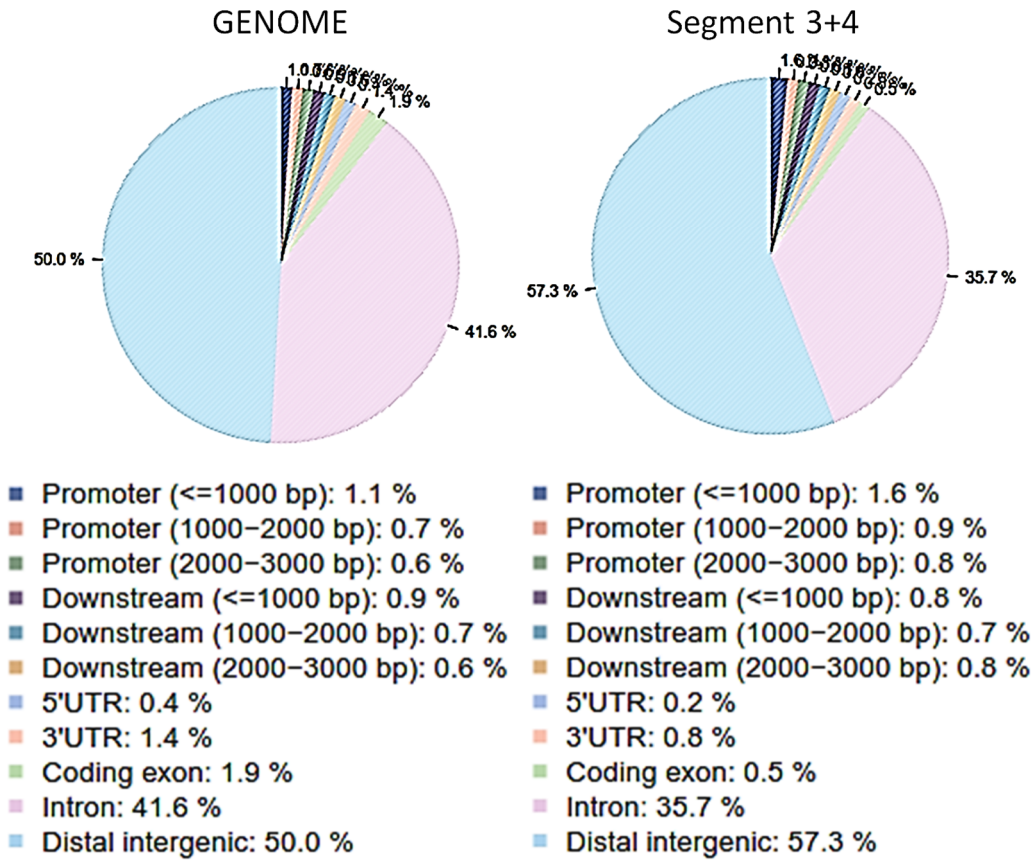

Figure 33. ***Genomic Distribution statistics on BRD4 bound sites within “Segment 3+4”.*** CEAS (Cis-regulatory Element Annotation System) statistics in differentiated hFOBs at important genomic regions (left) showing the distribution of the given genomic features for the genomic DNA and (right) for BRD4 signal on Segment 3+4.

Indeed, the IGV visualization of all the data for hFOB, NHOST, MCF7, MCF10A and L3.6 in this case shown for the osteoblast-specific genes - tumor necrosis factor receptor superfamily member 11b, or osteoprotegerin (*TNFRSF11B*) (Simonet et al., 1997) and collagen type I alpha 1 (*COL1a1*) (Komori, 2009), confirms the distal localization and osteoblast specificity of identified segments 3 and 4 (Figure 34). We also aligned all the available hFOB and NHOST ChIP-Seq data on the regions of “Segment 3+4”. Interestingly, upon differentiation the BRD4 signal substantially

increased on these regions implying involvement of these putative enhancers in the osteoblast fate determination (Figure 35).

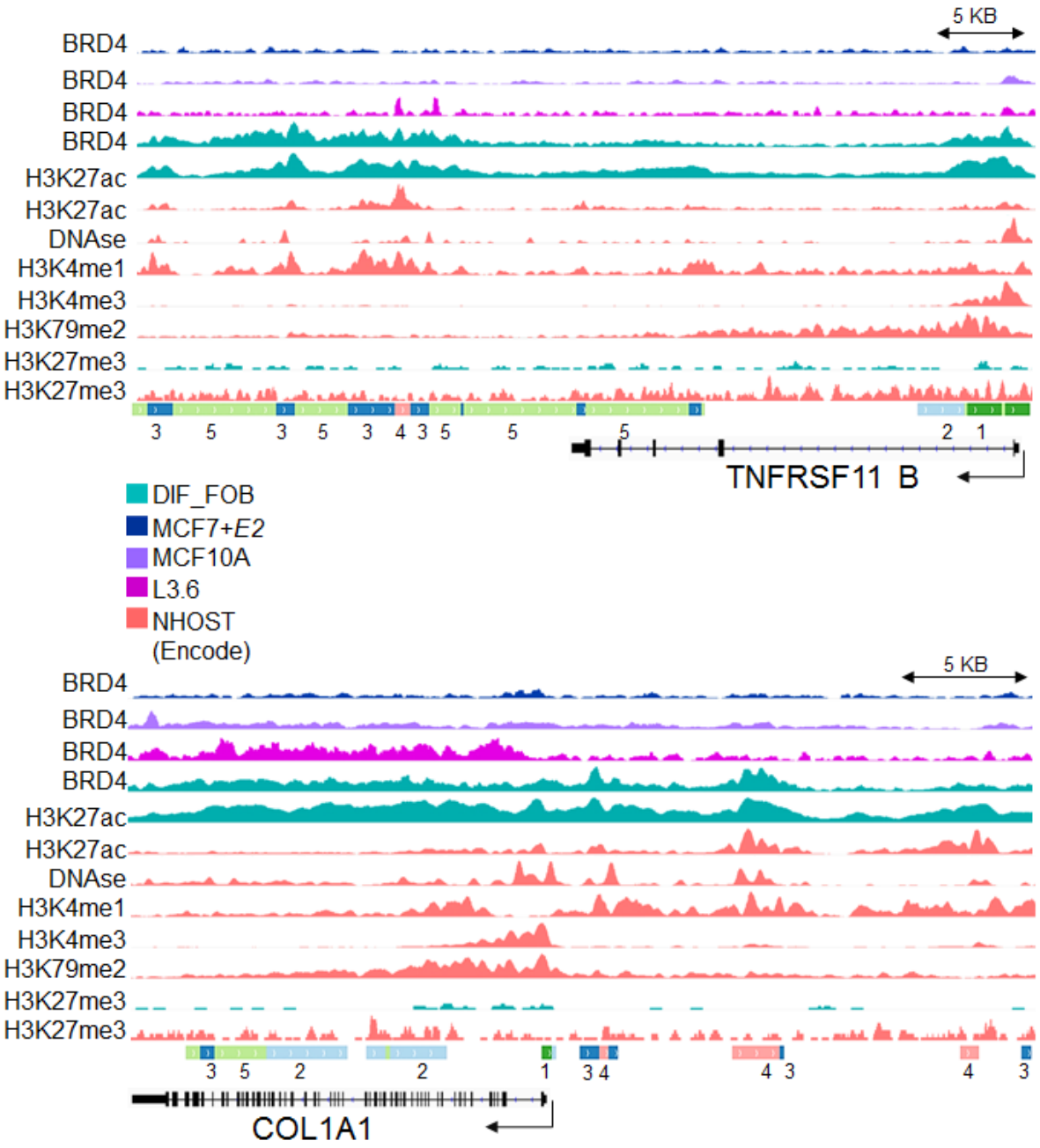

Figure 34. ***Segments 3 and 4 possess "putative" enhancer marks and are in close proximity to osteoblast-specific genes.*** IGV profile showing the distribution of segments around the osteoblast-specific *TNFRSF11B* (up) and *COL1A1* (down) gene. Each lane represents normalized occupancy of BRD4 in MCF7+E2 (darkblue), in MCF10A (purple), in L3.6 (magenta); BRD4, H3K27ac and H3K27me3 in differentiated hFOBs (cyan); H3K27ac, H3K4me1,DNAse-Seq, H3K4me3, H3K79me2 and H3K27me3 in NHOST (coral). The profiles were autoscaled on IGV.

Moreover, H3K27ac and RNAPII levels slightly increased on these regions during differentiation suggesting the possibility of transcription from these enhancers

(Figure 35). Certainly, all of these regions were enriched with H3K27ac and H3K4me1 in NHOST cells.

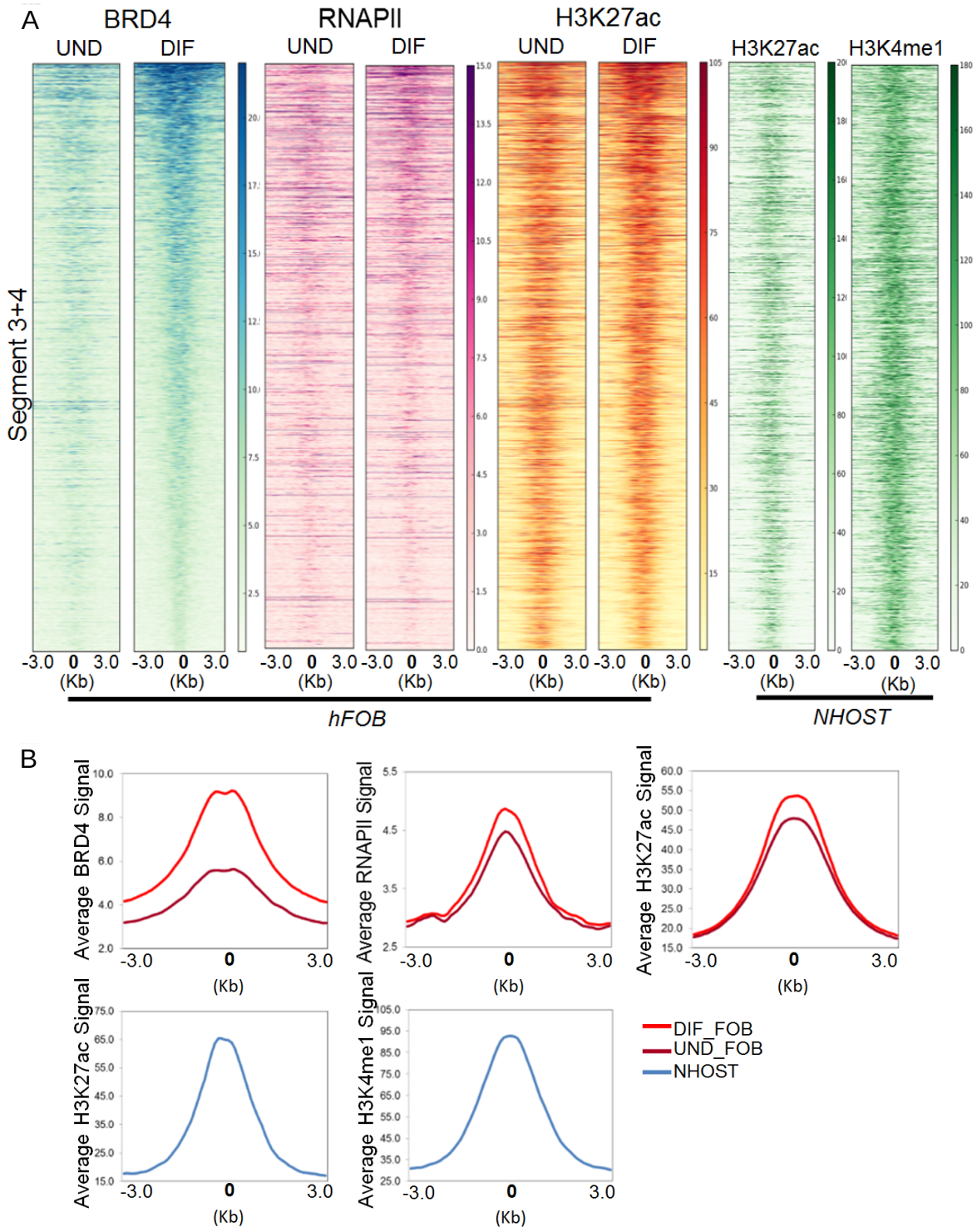

Figure 35. ***Segment 3+4 gain more BRD4, RNAPII and H3K27ac upon differentiation*****. A**. Heatmaps and **B**. Average enrichment profiles (in RPKM) showing BRD4, RNAPII, H3K27ac in undifferentiated and differentiated hFOBs, respectively and H3K27ac, H3K4me1 signal in NHOST ± 3KB around the center of identified from EpiCSeg "Segment3+4" (defined by "0" here). The segments in heatmaps are ordered from high to low based on BRD4 levels in differentiated state.

We also aligned the DNAse-seq data from NHOST on these sites. Notably, “Segment 3+4” demonstrated also high DNAse hypersensitivity (Figure 36) which is supporting the activity (“openness”) of the given regions. Thus, with the help of differential binding and chromatin segmentation analysis, we were able to identify putative osteoblast-specific enhancers potentially involved in lineage determination

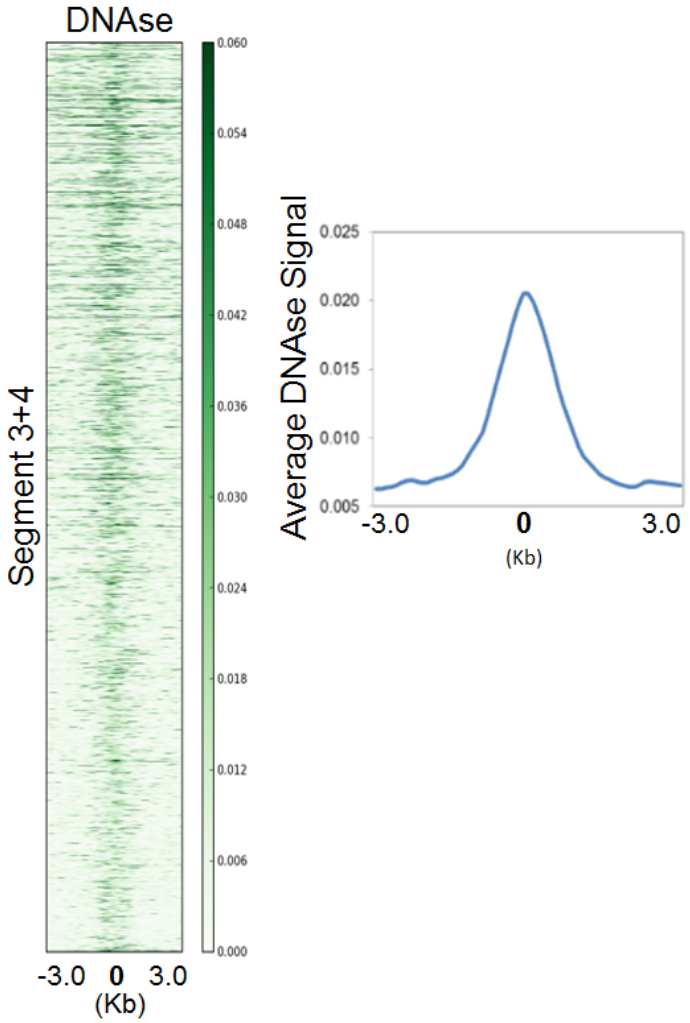

Figure 36. ***“Segment 3+4” display high DNAse signal in the related NHOST cells***. DNAse **A**. heatmap and **B**. average enrichment profile (in RPKM) in NHOST ± 3KB around the center (defined by “0” here) of “Segment 3+4”. The segments in heatmaps are ordered from high to low based on BRD4 levels in differentiated hFOBs.

Osteoblast-specific BRD4 bound putative enhancers show selective enrichment for distinct TFs.

Enhancers can regulate target gene expression in distance independent manner. To find out which possible genes are associated with the enhancers from “Segment 3+4” we used “Genomic Regions Enrichment of Annotations Tool” (GREAT).

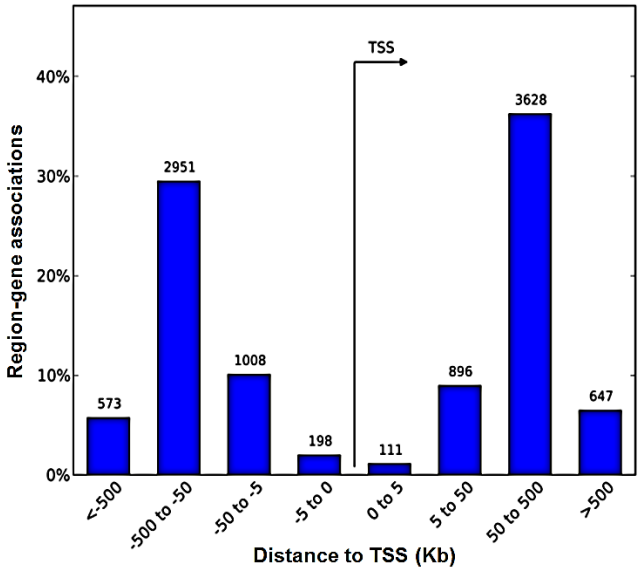

Figure 37. ***“Segment 3+4” associated BRD4 putative enhancers are mainly distally localized to any given gene TSS*****.** Bar chart from GREAT analysis depicting the distance and orientation of “Segement 3+4” regions from the nearest TSS.

Interestingly, the majority of these enhancers were found to be 50 to 500 kb away from known gene-specific TSS regions (Figure 37). Consistent with their specific enrichment in hFOB cells, these genes were enriched for pathways associated with skeletal development and extracellular matrix organization (Figure 38). However, not all of these genes were regulated with differentiation and not all were responsive to JQ1 (Figure 38B-D). Nonetheless, some of osteoblast essential genes were also found within this list and were mainly downregulated by JQ1 treatment (Figure 38E).

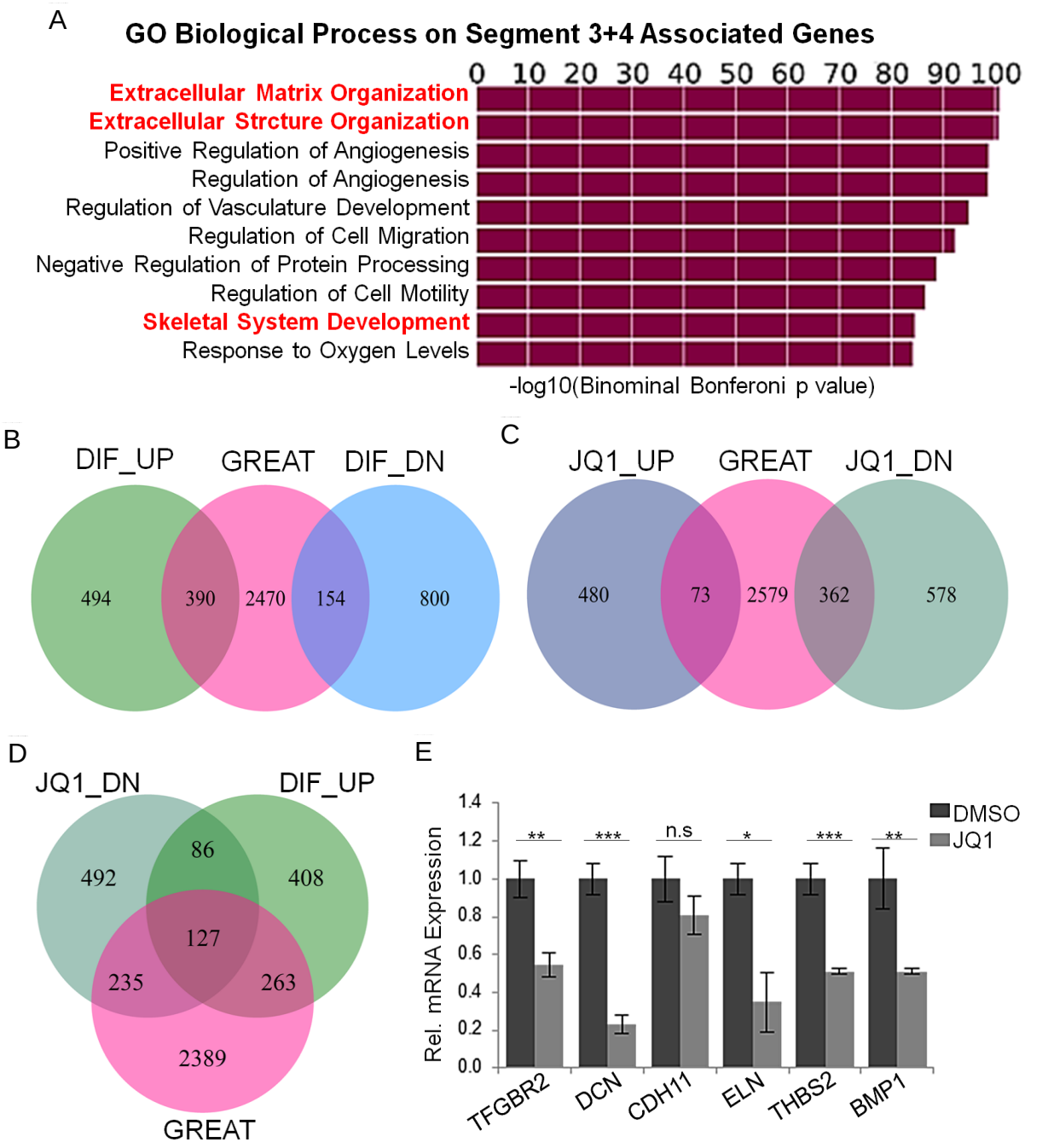

Figure 38. ***Genes associated with putative enhancers from Segment 3+4 are enriched with bone related pathways.*** **A.**Biological Process gene ontology analysis output of genes associated with putative enhancers from „Segment 3+4“ identified by GREAT. The bars represent the –log10 Binominal Bonferoni p value of the indicated pathways. **B-D**. Venn diagrams depicting the overlap of differentiation up- (DIF_UP, log2fold change ≥1, FDR<0.05) and downregulated (DIF_DN, log2fold change ≤-1, FDR<0.05) genes (B), JQ1 up- - (JQ1_UP, log2fold change ≥0.8, FDR<0.05) and downregulated (JQ1_DN, log2fold change ≤-0.8, FDR<0.05) genes (C), and differentiation upregulated with JQ1 downregulated genes (D), respectively with the genes associated with “Segment 3+4” obtained by GREAT analysis. **E**. Some of the osteoblast related genes were selected from the GREAT list and verified by qRT-PCR on the dependence to JQ1 regulation in differentiated hFOBs. The relative expression of the genes was normalized to the expression level of RPLP0 housekeeping gene in differentiated state. Mean±SD, n=3. Student t-test was performed for statistical analysis where ***p<0.001, **p<0.01, *p<0.05.

The functional activity of an enhancer is dependent on the transcription factors bound to it at a given time. The high DNAse hypersensitivity within the putative enhancers from “Segment 3+4” in NHOST cells (Figure 36) suggested the presence of nucleosome free regions that could serve as potential binding sites for tissue-specific transcription factors (TF). One of the main transcription factors involved in the osteoblast differentiation is the Runt-related transcription factor 2 (RUNX2) (Otto et al., 1997). Strikingly, “Segment 3+4” was found to be enriched with RUNX2 in NHOST (Figure 39).

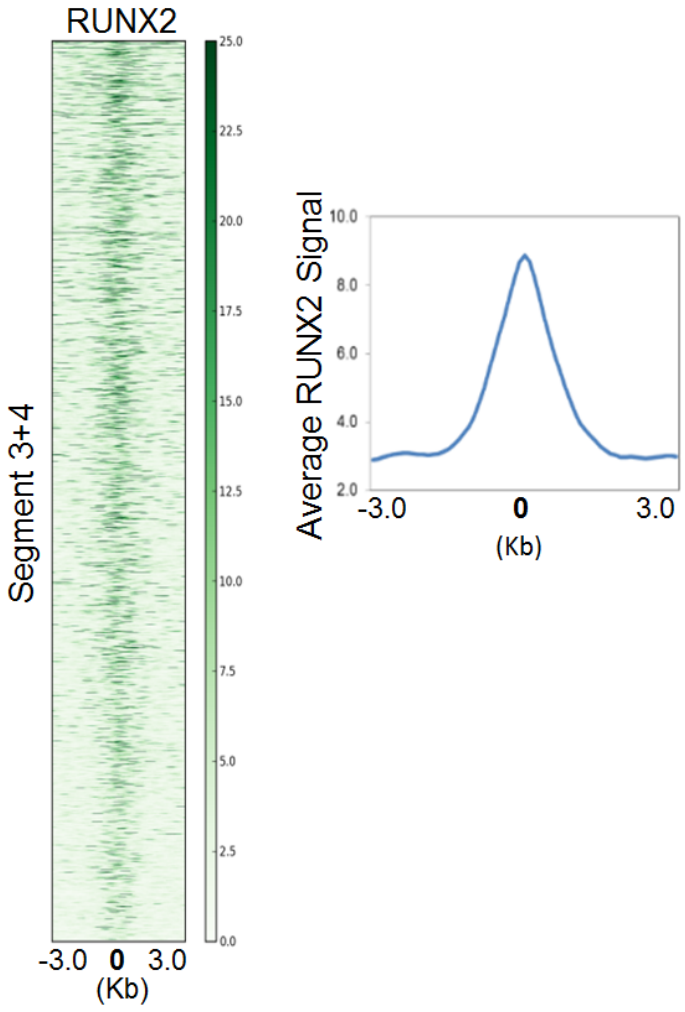

Figure 39. ***RUNX2 is enriched at putative enhancers of “Segment 3+4”.*** RUNX2 A. heatmap and B. average enrichment profiles (in RPKM) in NHOST ± 3KB around the center of “Segment3+4” (defined by “0” here).The segments in heatmaps are ordered from high to low based on BRD4 levels in differentiated hFOB cells.

To identify additional transcription factor binding motifs enriched in these regions, we performed differential motif analysis of “Segment 3+4” versus the “Segments 1+2+5”. We observed an enrichment of consensus sequences for the Activator protein-1 (AP1) transcription factor family as well as the Hippo/YAP-regulated Transcriptional enhancer factor TEF-1 (TEAD1) within the osteoblast-specific BRD4-bound regions of “Segment3+4” (Table 6).

Table 6. RSAT short summary on "Segment 3+4" vs "Segment 1+2+5"

Motif	Logo	3 Top Hits (Jaspar_Core_Vertebrates)
Oligos_6nt_m1	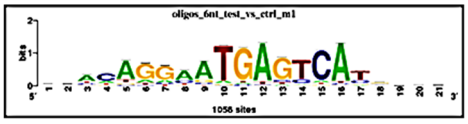	FOSL2, JUNB, BATF::JUN
Oligos_6nt_m2	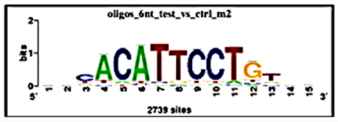	TEAD1, SPIB
Oligos_6nt_m3	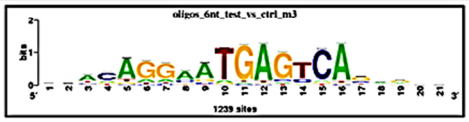	FOS, JUND, BATF::JUN
Oligos_6nt_m4	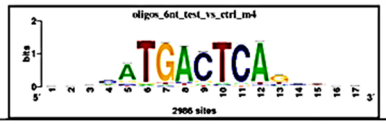	FOSL2, FOS, JUN_(var.2)
Oligos_6nt_m5		TEAD1, Hand1::Tcfe2a
Oligos_7nt_m1	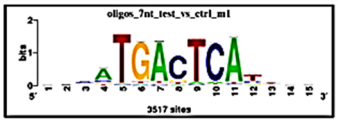	FOSL2, JUNB, JUN_(var.2)
Oligos_7nt_m2	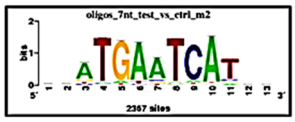	FOS, BATF::JUN, JUND
Oligos_7nt_m3	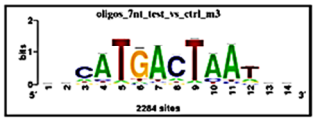	BATF::JUN, NFE2L1::MafG, JUN_(var.2)
Oligos_7nt_m4	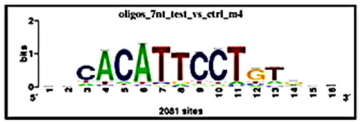	TEAD1
Oligos_7nt_m5	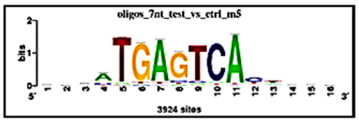	JUND, FOSL1, JUN::FOS

Moreover, an enrichment analysis within “Segment 3+4” of a large number of publically available datasets for the occupancy of various transcription factors and cofactors was performed using Regulatory Map of Transcription Factor Binding Sites (ReMap)(Griffon et al., 2015).These analyses confirmed the significant enrichment of AP1-bound regions on “Segment 3+4” (Figure 40) and further identified a significant overlap with additional transcription factors including Signal Transducer and Activator of Transcription 3 (STAT3) and CCAAT/Enhancer-Binding Protein-beta (C/EBPb).

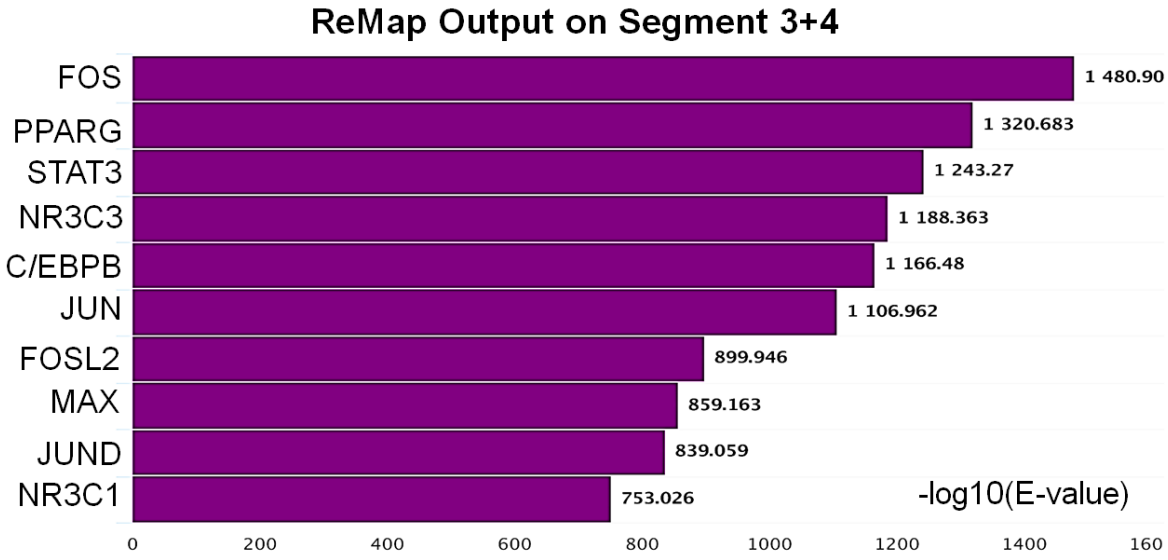

Figure 40. ***Overlap of BRD4 bound “Segment 3+4” with the transcription factor binding sites from different cell systems.*** Top 10 hits according to ReMap results performed on „Segment 3+4“.The bar charts depict the –log10 E-value (significance) of the overlap of BRD4 sites within the Segment 3+4 with the indicated transcription factor binding sites.

In addition, according to ReMap, peroxisome proliferator-activated receptor gamma (PPARG), nuclear receptor subfamily 3 group C member 3 (NR3C3) – progesterone receptor and nuclear receptor subfamily 3 group C member 1 (NR3C1) – glucocorticoid receptor and myc-associated factor X (MAX) transcription factor binding sites were similarly enriched within the “Segment 3+4”.

Based on previously discovered functions in osteoblasts (Gutierrez et al., 2002; Mahoney et al., 2005; Nicolaidou et al., 2012; Sabatakos et al., 2000; Stein et al., 2015; Zhou et al., 2011), out of the computationally predicted transcription factors we sought to characterize the potential involvement of AP-1 factors (FOSL2 and JUND), C/EBPb, STAT3 and TEAD1 on the osteoblast-specific "putative" enhancers of "Segment 3+4. Notably, based on RNA-seq data, all the identified transcription factors were highly expressed in hFOBs and only *RUNX2* and *FOSL2* expression were dependent on BRD4 (Figure 41), suggesting that these factors may serve as central mediators to facilitate BRD4 recruitment to osteoblast-specific enhancer regions.

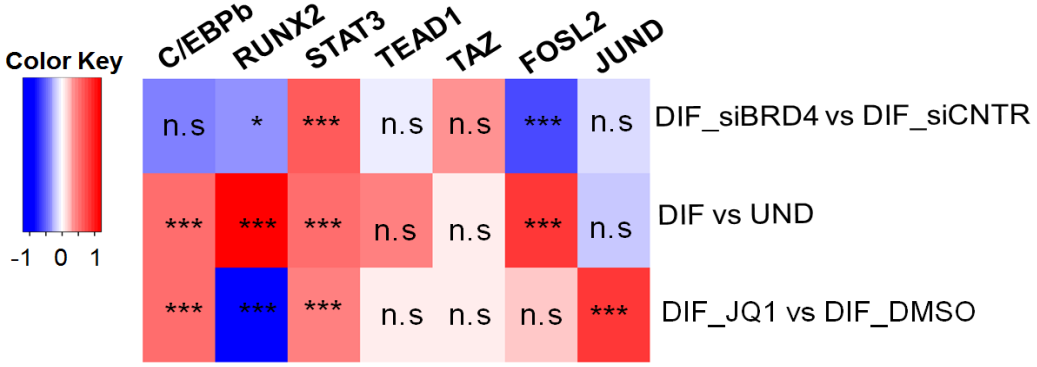

Figure 41. ***The expression profile and regulation of TF genes in hFOBs.*** The differentiation and siBRD4(#3 + #4) or JQ1 treatment induced relative gene expression change of the transcription factors associated with "Segment 3+4" identified from RSAT and REMAP tools, were evaluated from the RNA-Seq analysis of the hFOBs as described in Figure 12. Each column represents log2fold change values for the indicated conditions with padj = ***p<0.001; **p<0.01; *p<0.05.

After obtaining the regions of intersection of BRD4 with transcription factors from ReMap we performed ChIP-qPCR for C/EBPb, TEAD1, STAT3, JUND and FOSL2. Strikingly, almost all of the picked regions were enriched to some degree for the mentioned transcription factor signals (Figure 42). H3K27me3 marked OLIG2 gene showed similar to IgG enrichment for all the TF signals and was used as a negative control.

Thus, we performed additional genome-wide occupancy studies of all five transcription factors in hFOB cells to examine their overlap with osteoblast-specific BRD4-enriched regions. Interestingly, these transcription factors displayed differential binding patterns in hFOBs, where a significant number of C/EBPb-bound regions were largely devoid of other factors (Figure 43A). A number of sites displayed similar TEAD1, JUND and FOSL2 occupancy, while strongly enriched STAT3-bound regions lacked binding of the other factors.

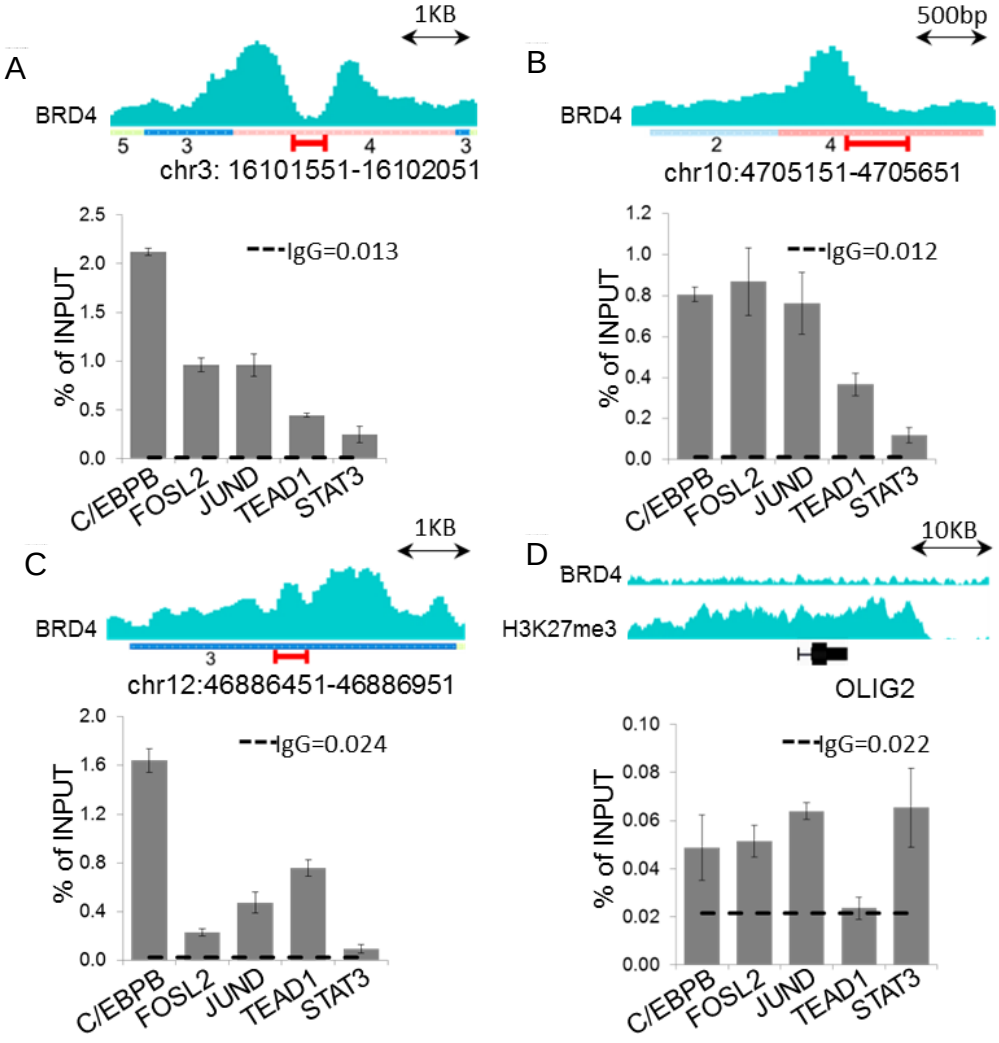

Figure 42. ***The qPCR verification of C/EBPb, TEAD1, FOSL2, JUND and STAT3 ChIP on "Segment 3+4".*** The efficiency of TF ChIPs was confirmed on 3 "potential" positive regions (A-C) obtained from REMAP intersection bed file and (D) on a HK27me3 marked OLIG2 gene which was used as a negative site. For background estimation IgG ChIPs were used. The ChIP efficiency is displayed as enrichment over Input in percent. Mean±SD, n=3. The IGV profiles show the "Segment 3+4" and BRD4 enrichment on these regions with the red segments indicating the localization of the qPCR primers designed for the given regions. For the negative OLIG2 genes H3K27me3 binding profile is also shown along with BRD4 to confirm the "repressed state" of the gene.

Notably, BRD4 exhibited differential binding profiles at the transcription factor bound regions, where C/EBPb-, JUND- and FOSL2-enriched sites displayed higher binding of BRD4, compared to TEAD1- and STAT3-enriched regions, which showed moderate and low levels of BRD4 occupancy, respectively (Figure 43B).

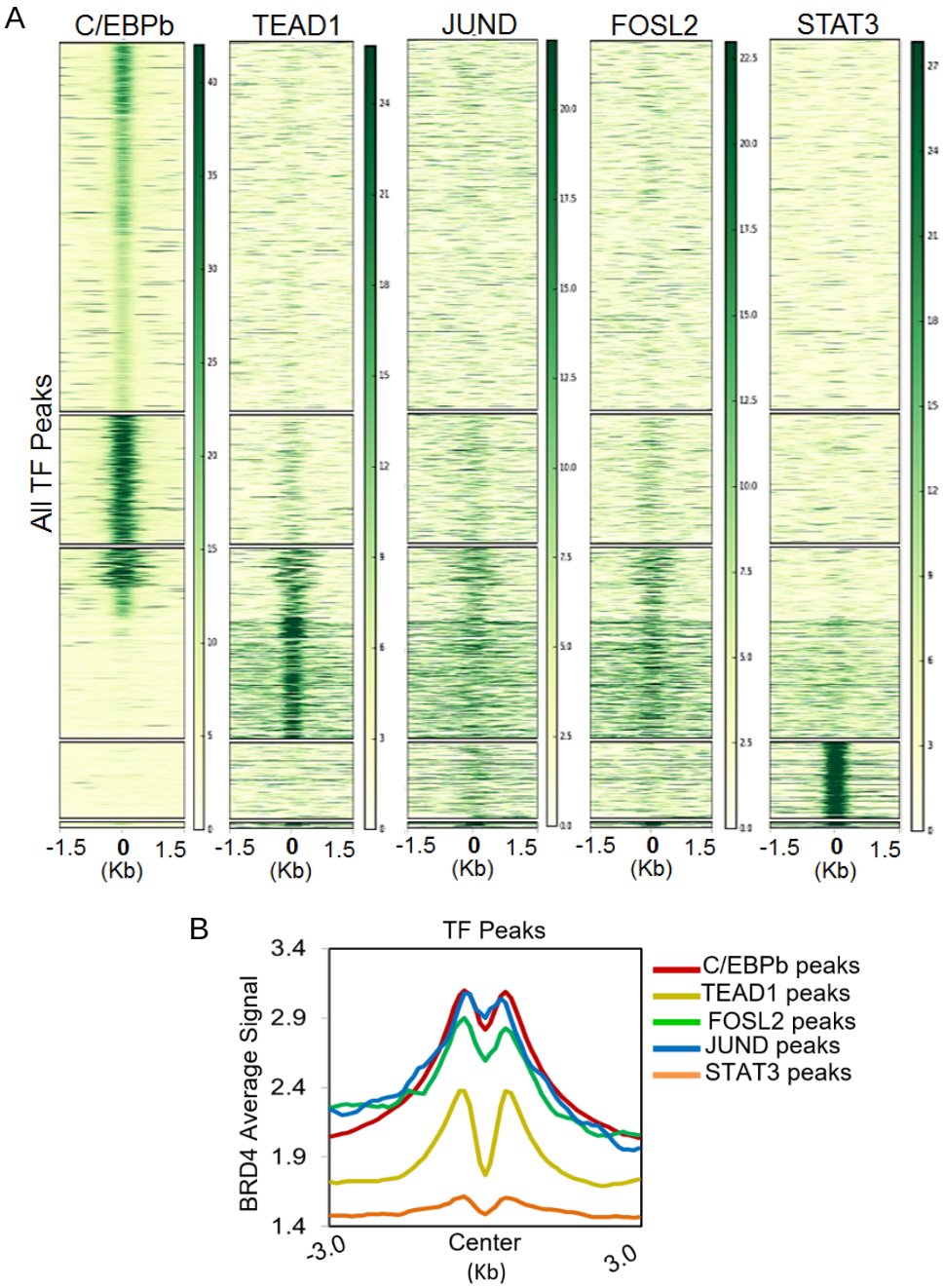

Figure 43. ***C/EBPb, TEAD1, FOSL, JUND and STAT3 display distinct biding pattern in hFOBs.*** **A.**The heatmaps depict linear k-means clustering of normalized coverage signals (RPKM) of C/EBPb, TEAD1, FOSL, JUND and STAT3 binding ±1.5KB around the center (defined here as "0") of the merged transcription factor peaks. **B**. Average binding profile of BRD4 (in RPKM) in differentiated hFOBs ±3KB around the center of C/EBPb, TEAD1, FOSL2, JUND and STAT3 peaks.

Remarkably, “Segment 3+4” displayed substantial binding of C/EBPb, TEAD1, FOSL2 and JUND whereas almost no STAT3 signal was detected on these regions (Figure 44).

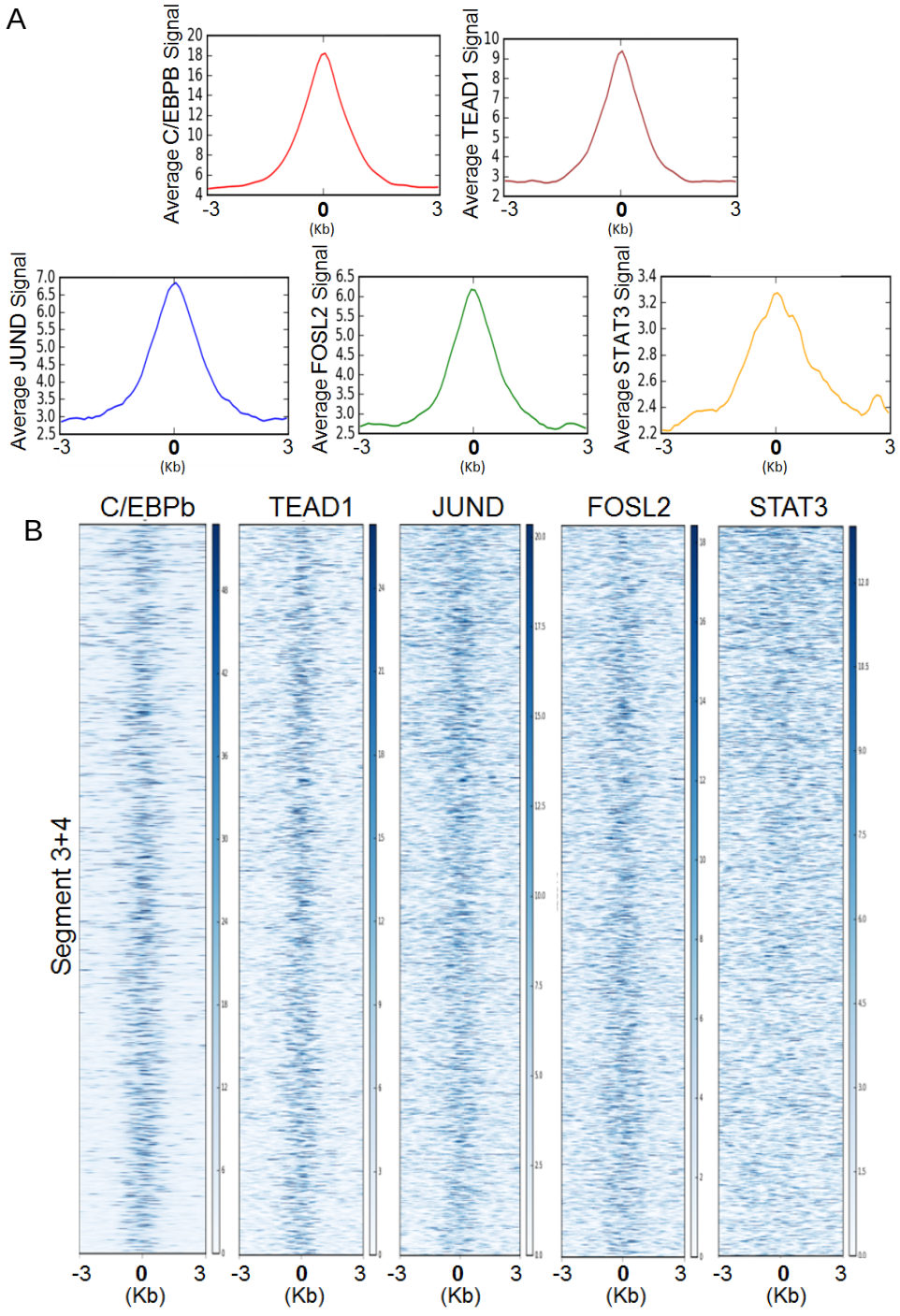

Figure 44. ***Occupancy of C/EBPb, TEAD1, FOSL2, JUND and STAT3 on the “Segment 3+4”.*** **A**. Average signal profiles and **B**. heatmaps depicting occupancy (in RPKM) of C/EBPb, TEAD1, FOSL2, JUND and STAT3 ±3KB around the center (defined as “0” here) of „Segment 3+4“, respectively. In the heatmaps each row represents one segment and is ordered from high to low based on signal intensity for each TF independently.

Interestingly, some “Segment 3+4” regions showed co-occupancy of all TFs (Figure 45) while many osteoblast-specific genes such as *ELN* and *DCN* showed distinct occupancy of the identified transcription factors at putative enhancer sites located within 50 kb of the genes.

As a result, by using genomic methods and a set of bioinformatic tools we identified osteoblast-specific BRD4 bound putative enhancers and transcription factors that could associate with BRD4 on these regions to induce and maintain the lineage-specific gene expression. Namely, 5 candidate transcription factors were found to be enriched at these enhancer segments: C/EBPb, AP1 factors JUND and FOSL2, TEAD1 and STAT3. Moreover, according to GREAT analysis these potential enhancers were associated with genes enriched for bone related GO terms. Notably, some of these genes were also dependent on functional activity of BRD4 which supported its role in regulating gene expression by assisting promoter and enhancer mediated transcriptional events.

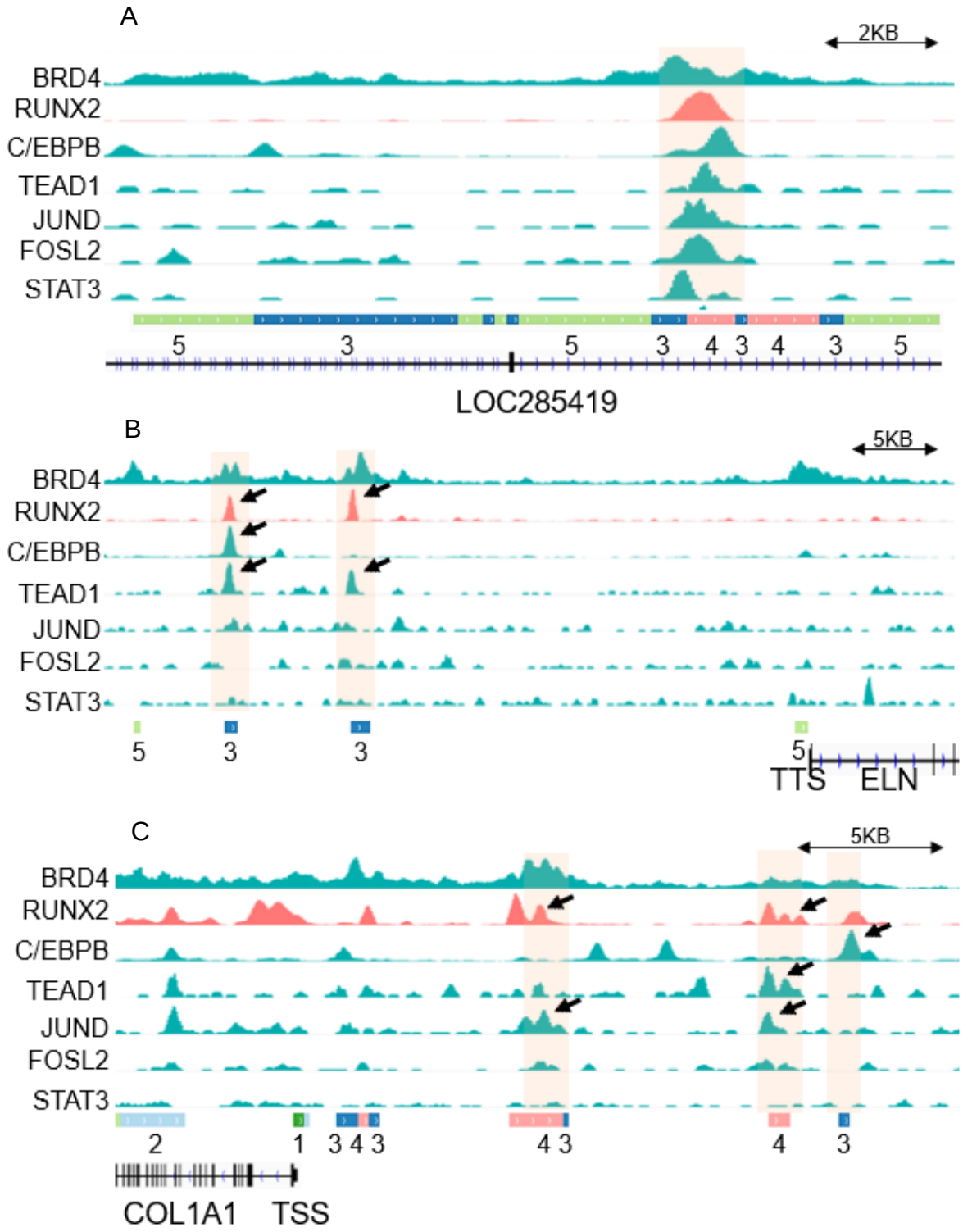

Figure 45. ***Localization of different TF peaks at "Segment 3+4" around the osteoblast-specific genes.*** IGV profiles depicting binding of C/EBPb, TEAD1, FOSL2, JUND and STAT3 in differentiated hFOBs (cyan) and RUNX2 in NHOST (coral) on the BRD4 occupied sites along with DNAse signal within "Segment 3+4": **A** – one common site with co-localization of all the TFs; **B-C** – on the putative "enhancers" proximal to osteoblast-specific genes ELN and COL1A1, respectively.

Role of H2Bub1 in osteogenesis

Conditional Rnf40$^{Runx2\text{-}Cre}$ mice show complex bone phenotype

In order to understand the biological significance of H2Bub1 during the skeletal development *in vivo*, we decided to use conditional knockout approach in mouse models since the complete knockout of RNF20 were shown to be embryonically lethal (Tarcic et al., 2016). Namely, we decided to elucidate what impact would the bone-specific deletion of RNF40 protein have in the developing mice. For that, we crossed the Runx2-Cre-recombinase expressing mice (Rauch et al., 2010) with Rnf40 floxed mice (Figure 46).

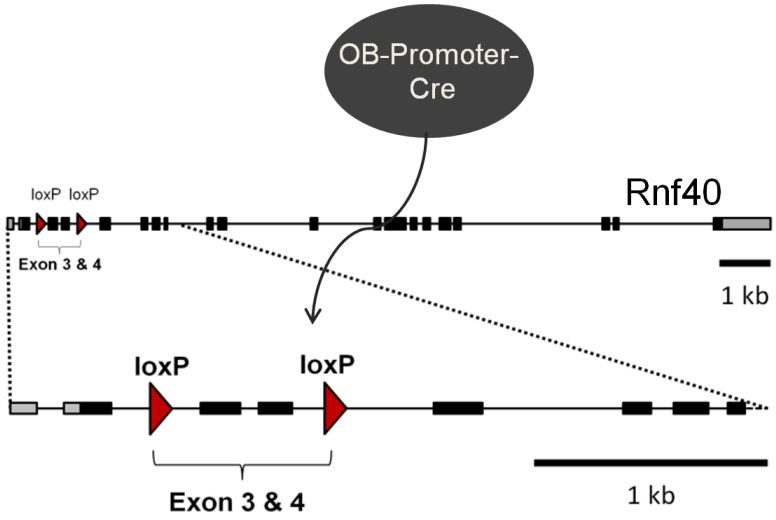

Figure 46. ***Generation of conditional bone-specific Rnf40 knockout mouse line.*** The expression of Cre is under the control of an osteoblast-specific (Runx2) promoter. The floxed Rnf40 mouse line contains loxP sites flanking the exon 3 and 4 of RNF40 gene. When the two mouse lines are bred together, the Cre enzyme recognizes the loxP sites and deletes the intervening DNA sequence only in the Cre expressing tissues.

The criteria for selecting Runx2 as the driver of Rnf40 deletion was its crucial role as a master regulator of bone formation (Komori, 2009; Otto et al., 1997). Runx2 is a transcription factor involved in skeletal development and is important at earlier stages of osteoblastic commitment of mesenchymal stem cells. Moreover, it plays as essential role during the terminal differentiation stages of chondrocytes (Komori, 2009).

The effect of Runx2-mediated deletion of Rnf40 in mice was, indeed, very striking. The knockout (KO) mice were much smaller in size (shorter bones) and hence lighter in weight compared to their wild-type (WT) and heterozygous (HZ) littermates (Figure 47) suggesting Rnf40 loss induced defects in bone formation/growth that could be due to functional impairment of osteoblasts. Moreover, given the significant role of chondrocytes during bone lengthening one could assume the shorter bones size may be similarly the result of defective chondrocyte hypertrophy and osteoblasts. Consistently, the phenotypic observation was not gender specific.

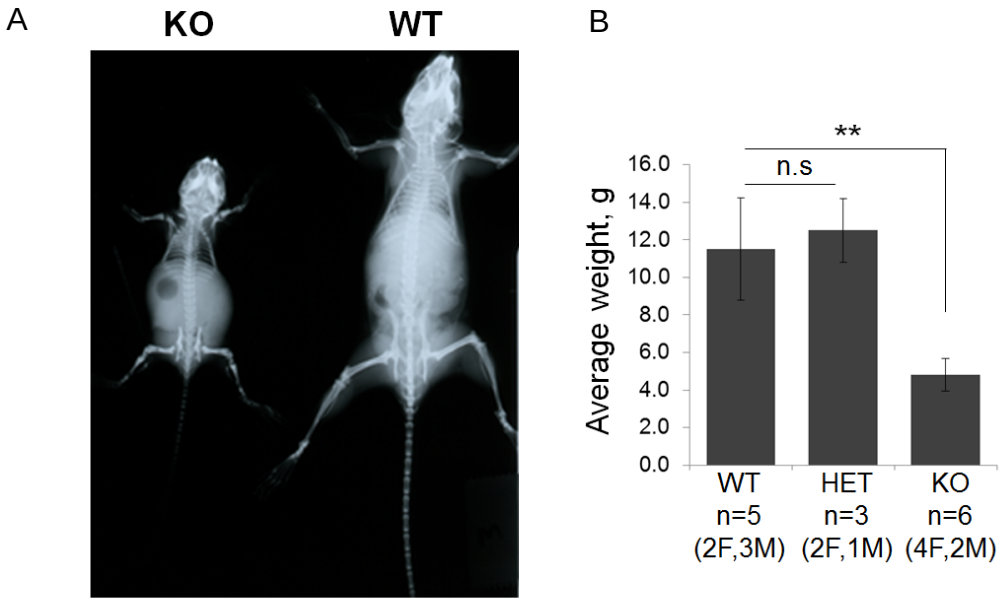

Figure 47. *Runx2 mediated deletion of Rnf40 in mouse skeleton leads to "dwarf"-like phenotype.* A. Representative X-ray scan images of conditional Rnf40$^{Runx2\text{-}Cre}$ KO and WT male mice at age of 7 weeks. B. Average weight of conditional Rnf40$^{Runx2\text{-}Cre}$ WT, HET and KO mice in both genders (female=F, male=M) at 3.5-4 weeks of age.

In order to evaluate the morphometric parameters of the bones from Rnf40 conditional mice (Table 7) the whole body skeleton of mice were subjected to µCT analysis performed by Prof. Dr. Jan Tuckermann's group at the University of Ulm, Germany.

Table 7. *Conditional Rnf40$^{Runx2\text{-}Cre}$ mice used in the study for µCT analysis*

.

Mouse #	Gender	Runx2-Cre	Rnf40/LoxP	Genotype	Age (weeks)	Weight
1	F	-	+/+	*WT*	3.5	8.9
2	F	-	+/+	*WT*	4	16.1
3	F	+	+/-	*HET*	3.5	10.6
4	F	+	+/-	*HET*	4	13.1
5	F	+	+/+	*KO*	3.5	4.6
6	F	+	+/+	*KO*	3.5	3.87
7	F	+	+/+	*KO*	4	
8	F	+	+/+	*KO*	4	5.6
9	F	+	+/+	*KO*	4	4.3
10	M	-	+/+	*WT*	3.5	11.2
11	M	-	+/+	*WT*	3.5	11
12	M	-	+/+	*WT*	3.5	10.3
13	M	+	+/-	*HET*	4	13.8
14	M	+	+/+	*KO*	3.5	4.31
15	M	+	+/+	*KO*	4	6.1

To our surprise, although the bones of conditional Rnf40$^{Runx2\text{-}Cre}$ knockout mice were much shorter in size, the bones of these mice showed increased mineral density which implied increased bone matrix formation (Figure 48). Consistently, the morphometric parameters of trabecular bone quantified in femurs and vertebrae, such as number of trabeculae (Tb.N) as well as thickness were significantly higher in the knockouts in both genders (Figure 49). These findings, however, were not consistent with our expectations based on *in vitro* studies were loss of H2Bub1 impaired the differentiation of human mesenchymal stem cells into osteoblasts (Karpiuk et al., 2012).

A

	WT (n=2F)	HET(n=2F)	KO(n=5F)
Torso length	4.2 cm	4.1 cm	3.0±0.2 cm
Femur length	9.14 mm	9.13 mm	6.18±0.33 mm
Vertebra (L5) length	2.010 mm	1.971 mm	1.334±0.161 mm

	WT (n=3M)	HET (n=1M)	KO (n=2M)
Torso length	4.0±0.1 cm	5.0 cm	3.25 cm
Femur length	9.40±0.20 mm	9.70 mm	6.71 mm

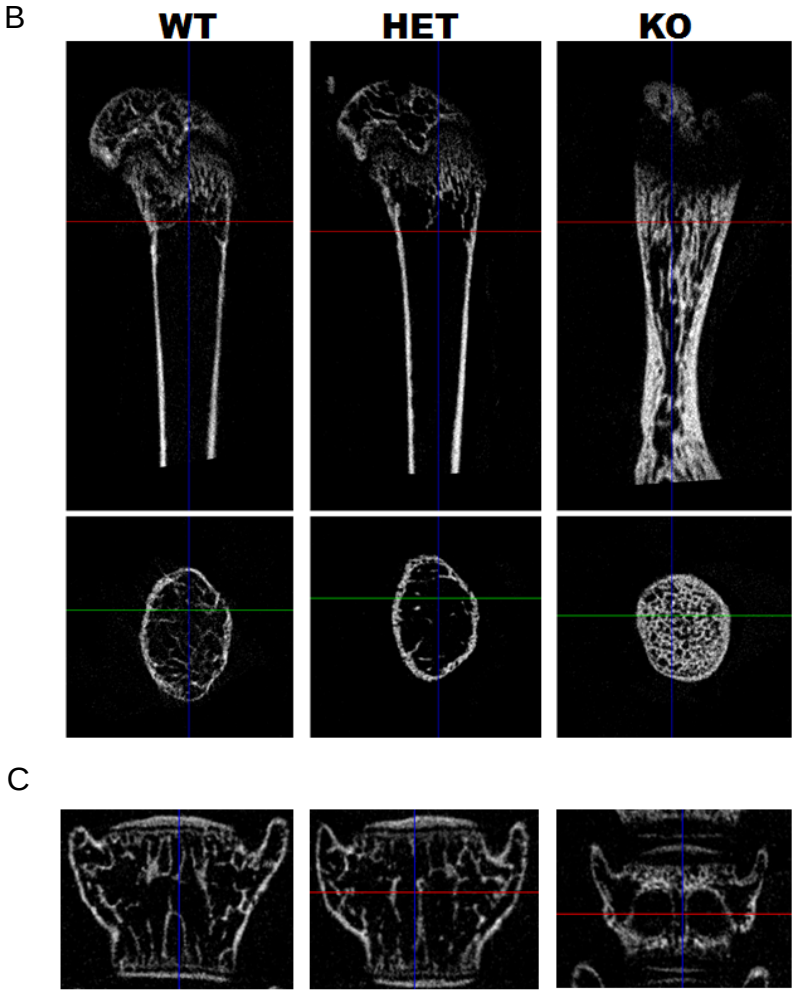

Figure 48*. Conditional Rnf40$^{Runx2\text{-}Cre}$ KO mice show increased bone matrix formation.* **A**. Bone size parameters of bones from Rnf40$^{Runx2\text{-}Cre}$ mice used in the study, shown separately for females (up) and males (below). **B-C**. Representative µ-CT scan pictures of the femur (B) and L5 vertebrae (C) of female mice at age of 3.5-4 weeks. The bones were analyzed using a SkyScan 1176 micro CT (Bruker, Billerica, USA) equipped with an X-ray tube working at 50 kV/100 µA. Resolution was 9 µm, rotation step was fixed at 1°, and a 0.5 mm aluminum filter was used. For reconstruction of femora, region of interest was defined 0.3 mm apart from the distal growth plate into the diaphysis spanning 1.8 mm.

Interestingly, the KO mice also lacked the teeth which implies either defects in the function of osteoblasts or perhaps incomplete functional activity of osteoclasts (through possible perturbation of osteoblast-osteoclast communication) which are important regulators of tooth eruption through alveolar resorption (Wise et al., 2002).

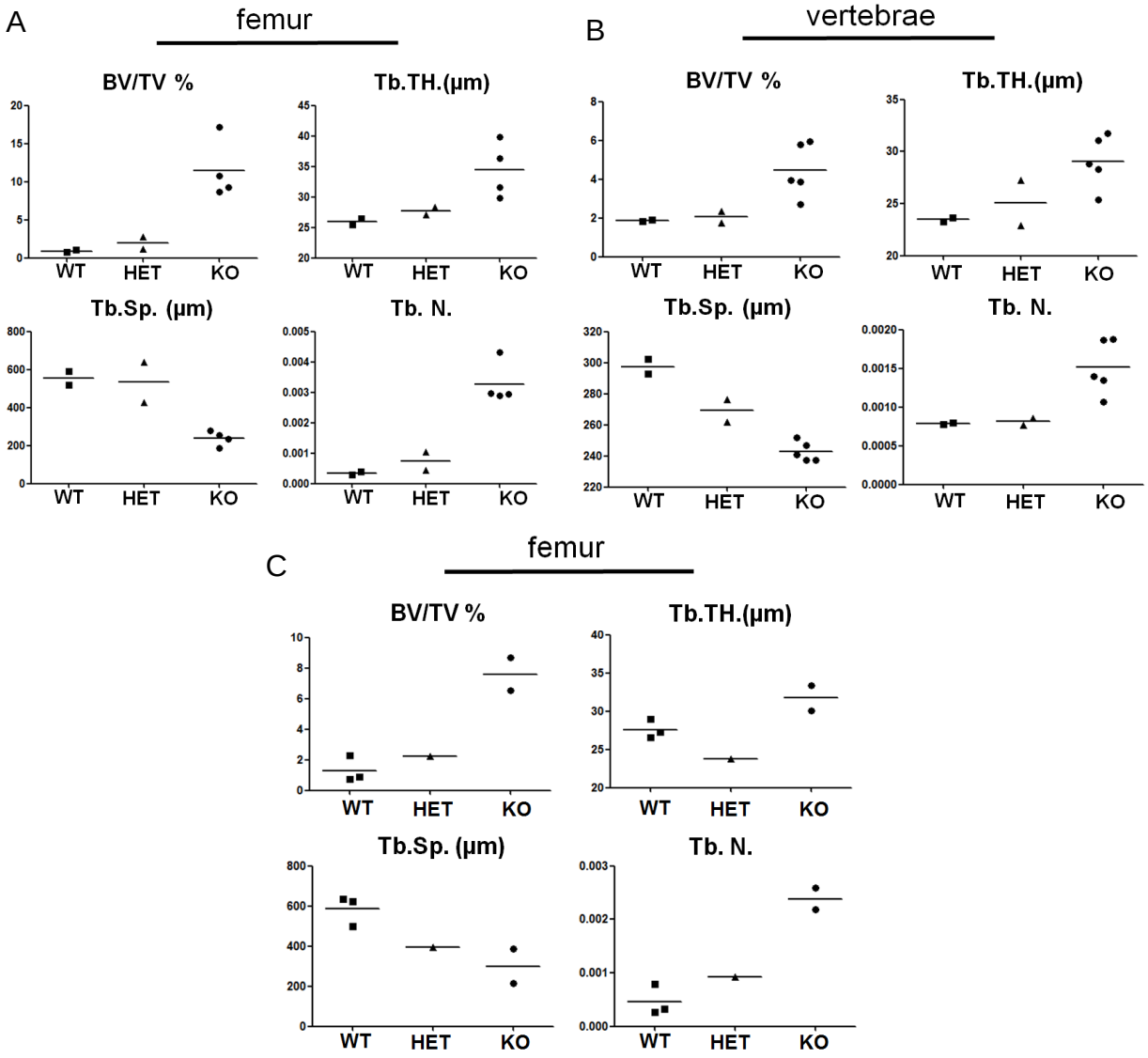

Figure 49. ***Bone histormorphometric parameters in conditional Rnf40$^{Runx2\text{-}Cre}$ mice indicate increased bone mass in knockout animals.*** Trabecular bone volume/tissue volume (BV/TV), trabecular thickness (Tb.Th.), trabecular separation (Tb. Sp.), trabecular number (Tb.N.),) of femora (**A**) and vertabrae (**B**) in female conditional Rnf40$^{Runx2\text{-}Cre}$ mice and in femora of male mice (**C**), respectievely were determined according to guidelines by ASBMR Histomorphometry Nomenclature Committee (Dempster et al., 2013).

Altogether, the Runx2-mediated deletion of Rnf40 in mice resulted in a complex phenotype with signs of osteopetrosis, i.e. increased bone mass and inconsistently shorter bone size characteristic for achdonroplastic mice.

USP22 has no role in bone development *in vivo*

Since Runx2 mediated loss of Rnf40 in mice showed clear defects in skeletal system leading to shorter bone size and increased bone density we questioned whether we could achieve reversed phenotype by deleting Ubiquitin Specific Peptidase 22 (USP22), the enzyme responsible for removal of ubiquitin moieties from H2BK120 (Johnsen, 2012). For that, we crossed the Runx2-Cre with USP22 floxed mouse line (Figure 50). The generated progeny of transgenic mice did not show any phenotypic differences between the genotypes.

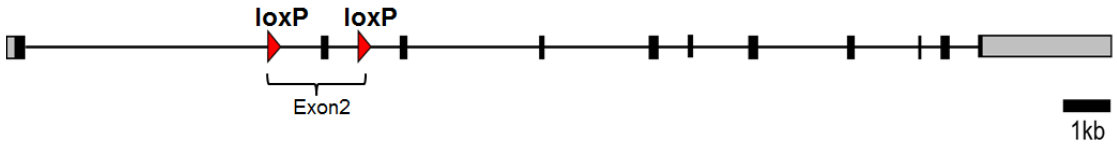

Figure 50. ***The floxed allele of USP22.*** The floxed USP22 mouse line contains loxP sites flanking the exon 2 of USP22 gene.

Moreover, the evaluation of bone histomorphometric parameters through µCT analysis confirmed the absence of differences among the genotypes (Figure 51). This suggested that although the removal of H2Bub1 accounts for defects in skeletal development, the opposite did not have major impact on bone formation.

Table 8. *Conditional USP22$^{Runx2\text{-}Cre}$ mice used in the study for µCT analysis*

Mouse#	Gender	Runx2-Cre	USP22/LoxP	Genotype	Age (weeks)	Weight
1	M	-	+/-	*WT*	6w	17.5
2	M	-	+/+	*WT*	6w	21.9
3	M	-	+/+	*WT*	6w	20.5
4	M	-	+/-	*WT*	6w	19.8
5	M	-	+/+	*WT*	6w	19.4
6	M	+	+/-	*HET*	6w	18.5
7	M	+	+/+	*KO*	6w	22.6
8	M	+	+/+	*KO*	6w	16.5
9	M	+	+/+	*KO*	6w	16.2

A

	WT (n=5)	HET(n=1)	KO(n=3)
Torso length	5.2±0.1 cm	4.9 cm	5.1±0.2 cm
Femur length	10.65±0.53 mm	10.05 mm	10.20±1.22 mm
Vertebra (L5) length	2.598±0.023 mm	2.575 mm	2.567±0.096 mm

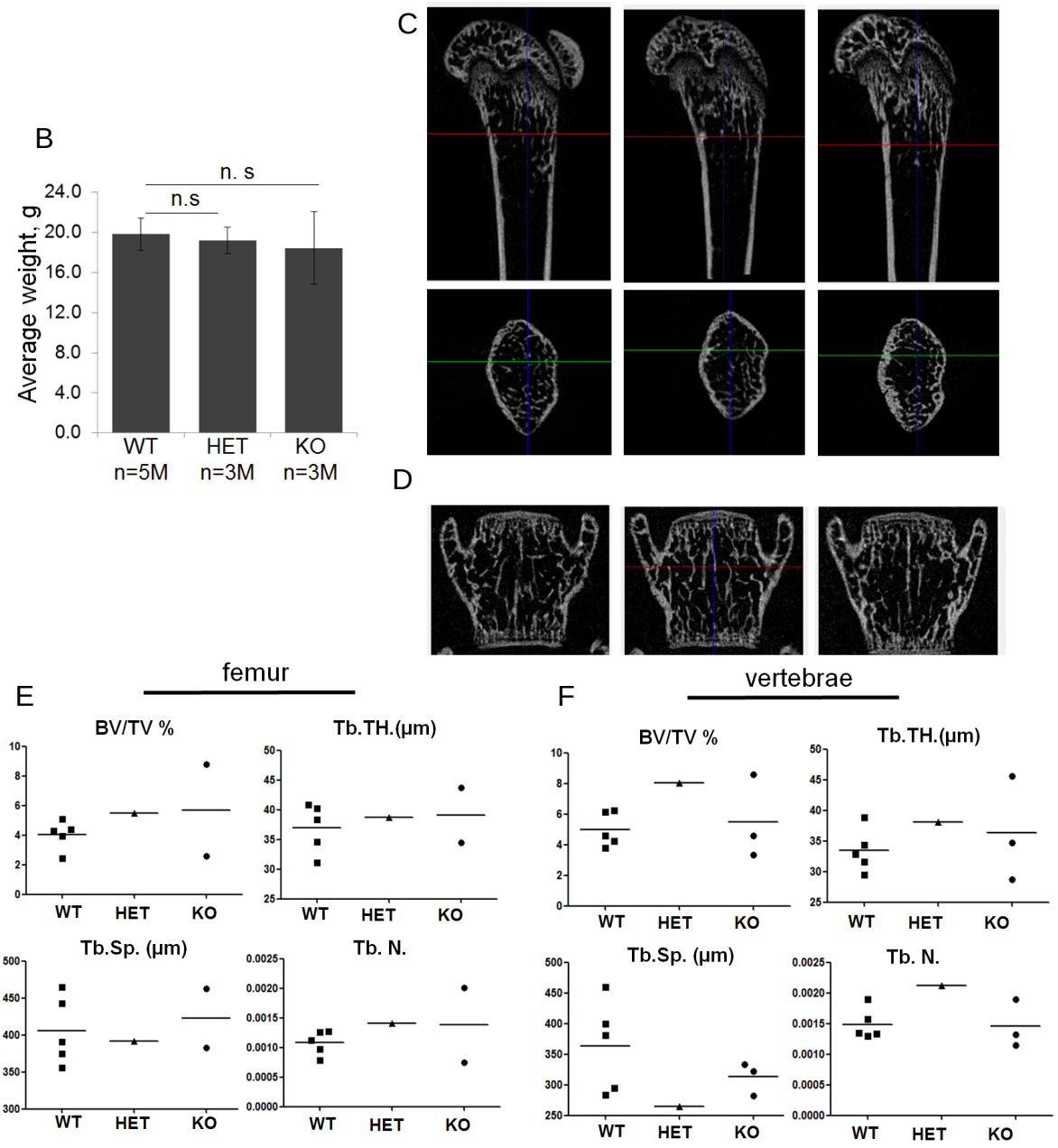

Figure 51. ***Conditional USP22$^{Runx2\text{-}Cre}$ KO mice show no differences in bone parameters.*** **A**. Bone size parameters of bones from USP22$^{Runx2\text{-}Cre}$ mice used in the study. **B.** Average weight of conditional WT, HET and KO mice at 6 weeks of age **C-D**. Representative µ-CT scan pictures of the femur (C) and L5 vertebrae (D). The bones were analyzed using a SkyScan 1176 micro CT (Bruker, Billerica, USA) equipped with an X-ray tube working at 50 kV/100 µA. Resolution was 9 µm, rotation step was fixed at 1°, and a 0.5 mm aluminum filter was used. For reconstruction of femora, region of interest was defined 0.3 mm apart from the distal growth plate into the diaphysis spanning 1.8 mm. **E-F**. Trabecular bone volume/tissue volume (BV/TV), trabecular thickness (Tb.Th.), trabecular separation (Tb. Sp.), trabecular number (Tb.N.),) of femora (E) and vertabrae (F), respectievely were determined according to guidelines by ASBMR Histomorphometry Nomenclature Committee (Dempster et al., 2013).

Bone-specific deletion of Rnf40 leads to osteopetrosis-like phenotype

Since conditional Runx2-specific Rnf40 knockout mice displayed complex phenotype involving both the osteoblasts and most likely the chondrocytes, we decided to further analyze solely osteoblast-specific role of Rnf40 driven H2B monoubiquitination in the context of bone formation. Therefore we used another mouse line bearing Cre-recombinase expression under the control of osteocalcin Bglap promoter (Zhang et al., 2002). Bglap is an extracellular matrix protein expressed by osteoblasts involved in mineralization (Hauschka et al., 1989; Lee et al., 2007). According to Zhang *et al*., Bglap-Cre was exclusively expressed in osteoblasts and osteocytes. Similarly, Bglap-Cre mouse line was crossed with Rnf40 floxed mice to achieve conditional deletion of Rnf40 in the bones from the initial steps of bone formation. Interestingly, unlike the Runx2-specific Rnf40 knockout mice, the conditional osteocalcin-specific Rnf40 knockout mice did not display any visual differences in the appearance or weight when compared to wild-type or heterozygous littermates (Figure 52,Table 9) suggesting absence of achondroplasia-like phenotype.

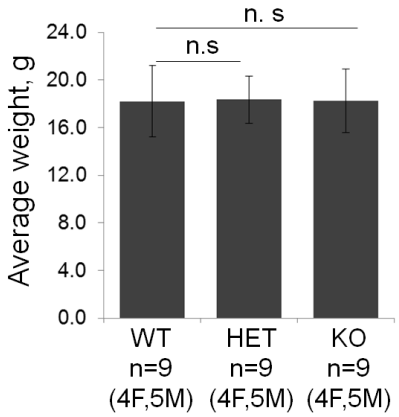

Figure 52. ***Conditional Rnf40$^{Bglap\text{-}Cre}$ KO mice don't show any phenotypic changes*****.** Average weight of conditional WT, HET and KO mice for both genders (F=female, M=male) at 6 weeks of age.

However, despite the fact that Rnf40 is required for the differentiation of hMSCs into osteoblastic lineage (Karpiuk et al., 2012) , the µCT analysis of the mice skeletons revealed increased bone mass similar to $Rnf40^{Runx2\text{-}Cre}$ conditional mice (Figure 53) suggesting increased bone formation and/or decreased bone resorption.

Table 9. *Conditional $Rnf40^{Bglap\text{-}Cre}$ mice used in the study for µCT analysis*

Mouse#	Gender	Bglap-Cre	USP22/LoxP	Genotype	Age (weeks)	Weight
1	F	+	-/-	*WT*	6 w	15.2
2	F	+	-/-	*WT*	6 w	16.5
3	F	-	+/-	*WT*	6 w	14
4	F	-	+/+	*WT*	6 w	16.5
5	F	+	+/+	KO	6 w	16
6	F	+	+/+	KO	6 w	17.5
7	F	+	+/+	KO	6 w	17.5
8	F	+	+/+	KO	6 w	13.4
9	F	+	+/-	HET	6 w	16.2
10	F	+	+/-	HET	6 w	16.3
11	F	+	+/-	HET	6 w	18.4
12	F	+	+/-	HET	6 w	15.4
13	M	+	-/-	*WT*	6 w	18
14	M	+	-/-	*WT*	6 w	21
15	M	+	-/-	*WT*	6 w	22.4
16	M	+	-/-	*WT*	6 w	18.5
17	M	-	+/-	*WT*	6 w	21.8
18	M	+	+/+	KO	6 w	20.8
19	M	+	+/+	KO	6 w	21.3
20	M	+	+/+	KO	6 w	21.3
21	M	+	+/+	KO	6 w	17
22	M	+	+/+	KO	6 w	19.5
23	M	+	+/-	HET	6 w	18.7
24	M	+	+/-	HET	6 w	20.8
25	M	+	+/-	HET	6 w	20.6
26	M	+	+/-	HET	6 w	19.5
27	M	+	+/-	HET	6 w	19.3

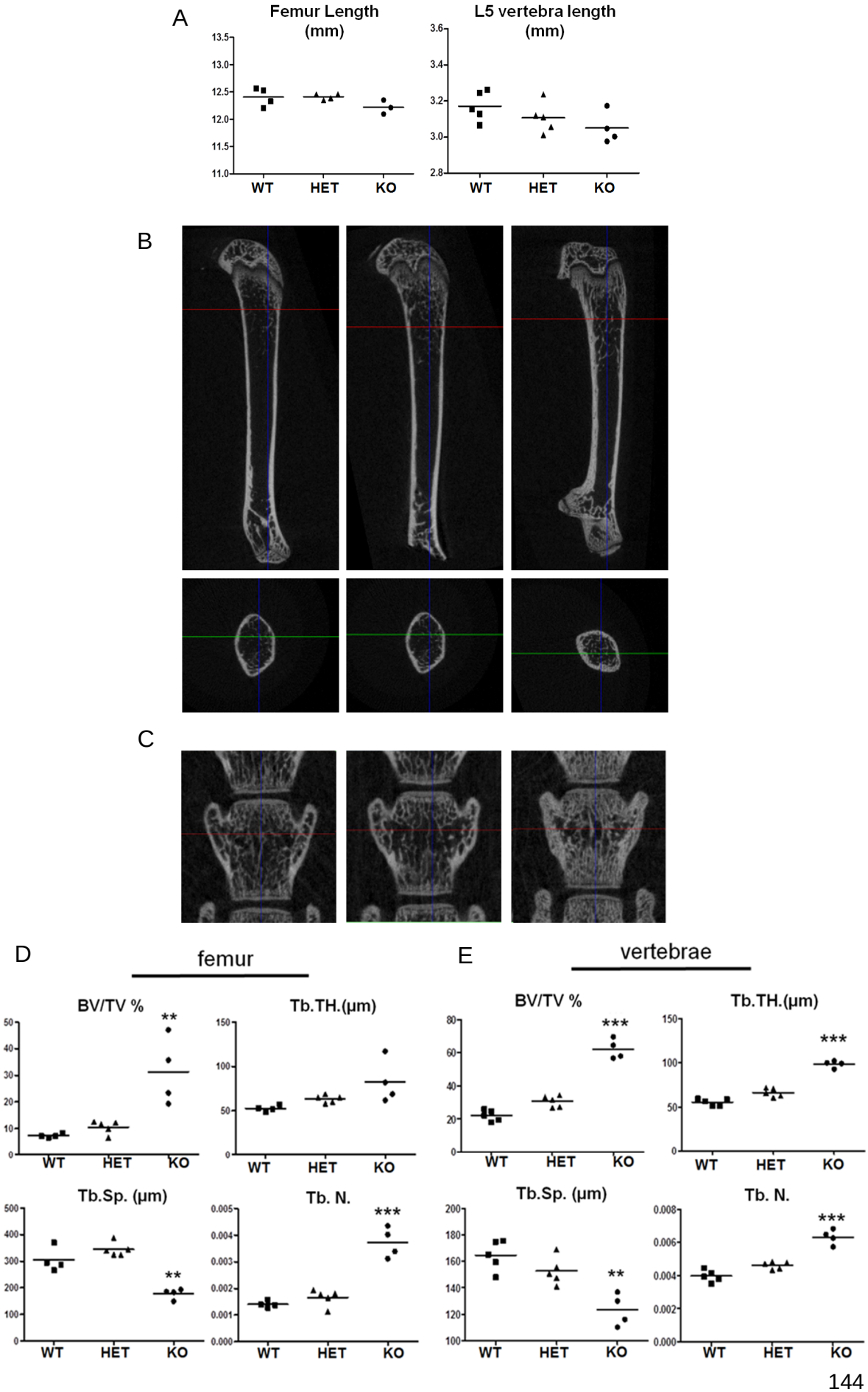
A
Femur Length (mm)
L5 vertebra length (mm)
WT
HET
KO
B
C
D
femur
BV/TV %
Tb.TH.(µm)
Tb.Sp. (µm)
Tb. N.
E
vertebrae
BV/TV %
Tb.TH.(µm)
Tb.Sp. (µm)
Tb. N.

Figure 53. ***Conditional Rnf40$^{Bglap\text{-}Cre}$ KO mice show increased bone mineral density.*** **A**. Bone size parameters of femora (left) and L5 vertabrae (right) from male mice at 6 weeks of age used in the study. **B-C**. Representative µ-CT scan pictures of the femur (B) and L5 vertebrae (C) of male mice. The bones were analyzed using a SkyScan 1176 micro CT (Bruker, Billerica, USA) equipped with an X-ray tube working at 50 kV/100 µA. Resolution was 9 µm, rotation step was fixed at 1°, and a 0.5 mm aluminum filter was used. For reconstruction of femora, region of interest was defined 0.3 mm apart from the distal growth plate into the diaphysis spanning 1.8 mm. **D-E**. Trabecular bone volume/tissue volume (BV/TV), trabecular thickness (Tb.Th.), trabecular separation (Tb. Sp.), trabecular number (Tb.N.),) of femora (D) and vertabrae (E), respectievely were determined according to guidelines by ASBMR Histomorphometry Nomenclature Committee (Dempster et al., 2013). Student's T-test was used for statistical analysis.

Bone is a very dynamic tissue undergoing lifelong process of remodeling comprising two opposite processes of osteoblast mediated bone formation and osteoclast dependent bone resorption. Coupling of both is essential for bone formation, growth and healthy metabolism of bone tissue. To evaluate how bone development could be affected in conditional Rnf40 deficient mice we assessed the bone formation rate in these mice via fluorometric double labeling of newly synthesized mineralizing tissue by calcein (Suzuki and Mathews, 1966)

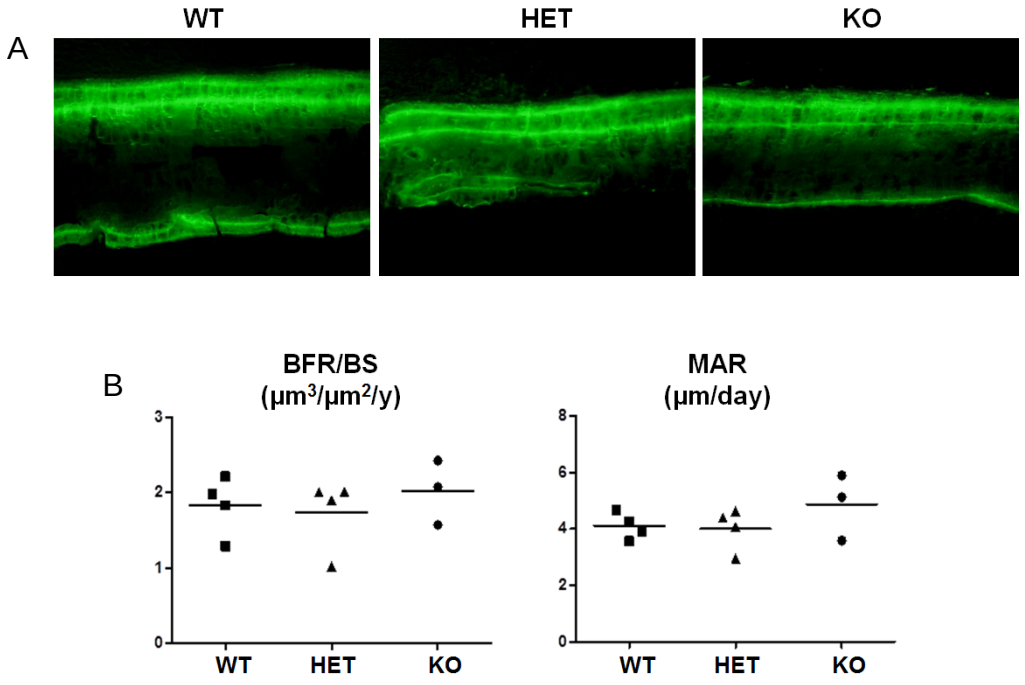

Figure 54. ***Bone formation rate is not affected in conditional Rnf40$^{Oc\text{-}Cre}$ mice*****.** Conditional Rnf40$^{Bglap\text{-}Cre}$ mice were double injected with calcein with a gap of 1 week 2 days prior sacrificing. The femurs were subjected to dynamic bone histomorphometry analysis. **A**. Fluorescent micrographs of femur cortical bone of 6 weeks old male mice showing double calcein labeling. **B**. Bone formation rate per bone surface (BFR/BS) and mineral apposition rate (MAR) were quantified for 4 wildtype (WT),4 heterozygous (HZ) and 3 knockout (KO) mice, respectively.

Interestingly, the bone formation rate (BFR) which is indicative of the actively mineralizing bone surface amount that depends on the number of active osteoblasts, as well as the mineral apposition rate (MAR) that demonstrates the average activity of osteoblasts and the rate at which these cells produce calcifying matrix for a given period of time was not different between the genotypes suggesting absence of functional defects in osteoblasts (Figure 54).

However, the most striking finding was to discover that the number of osteoclasts was significantly decreased in the Rnf40 knockout animals (Figure 55). This, in fact, explains why the conditional Rnf40 knockout mice displayed higher bone matrix density in comparison with wildtype and heterozygous littermates.

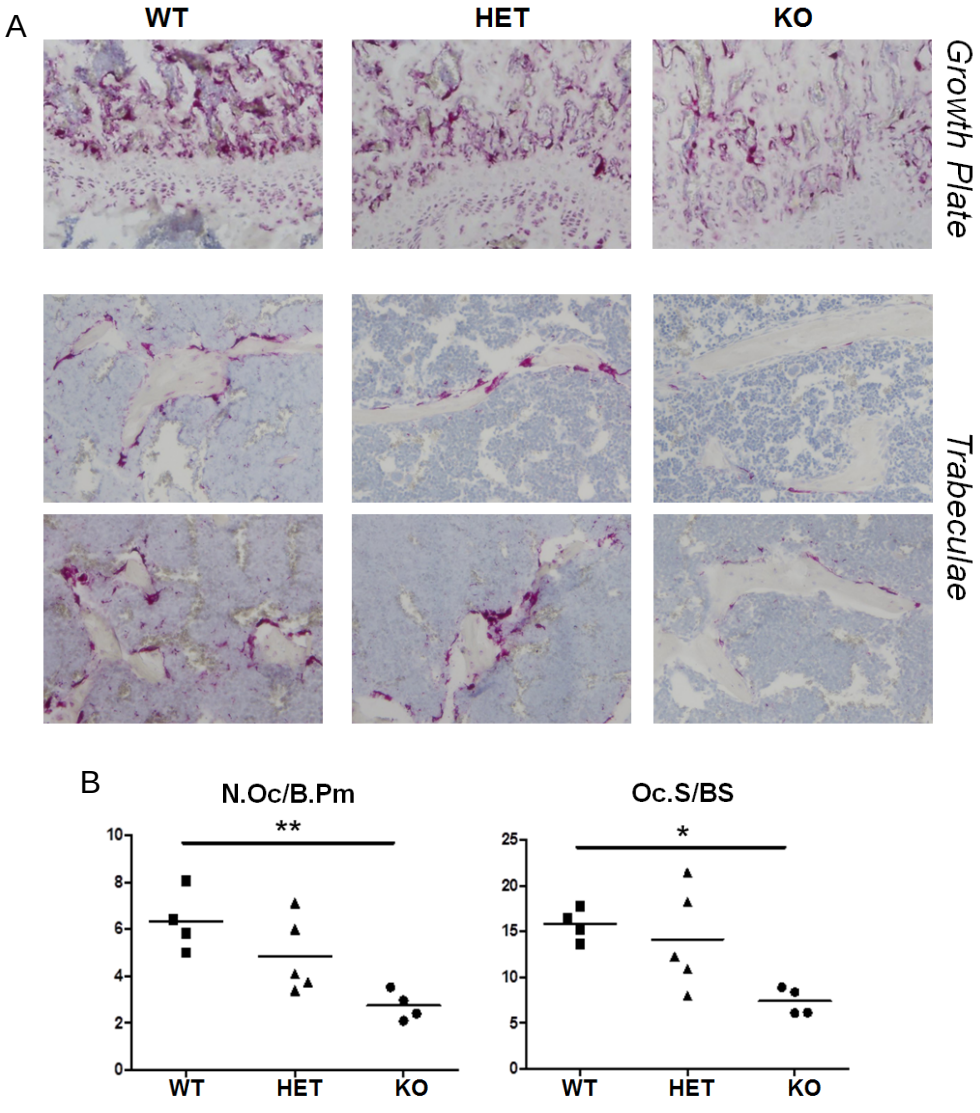

Figure 55. *Conditional Rnf40$^{Bglap\text{-}Cre}$ mice display decreased osteoclast numbers*. The plastic embeded femoral sections were subjected to **A**. TRAP stainings shown for growth plate and trabeculae separately. **B** The number of osteoclasts and the osteoclast surface was definied on "osteomeasure" software and depicted as number of osteoclasts per bone perimeter (N.OC/B.PM) and osteoclast surface per bone surface (Oc.S/BS, %). Student T-test was used for statistics.

The *in vivo* data in mice, altogether, highlighted the importance of Rnf40 mediated H2B monoubiquitination in skeletal development. Although at first sight it seemed that the mice developed morphologically healthy bones in Rnf40 deficient conditions, the increased bone mass due to decreased number of osteoclasts suggested that the osteoblast-osteoclast "communication" in these mice were more likely affected in a negative way. Since Bglap is a solely osteoblast-specific protein and hence the expression of Cre-recombinase was restricted only to osteoblastic lineage, despite unaffected mineral tissue deposition amount and rate the Rnf40 deficient osteoblasts were most likely functionally unable to induce osteoclast differentiation and/or activity.

Rnf40 deficient primary osteoblasts exhibit reduced differentiation capacity

In order to understand how Rnf40 deficiency in osteoblasts contributed to a bone mass change in osteoclast dependent manner we sought to analyze primary molecular effects of Rnf40 loss in osteoblasts *ex vivo*.

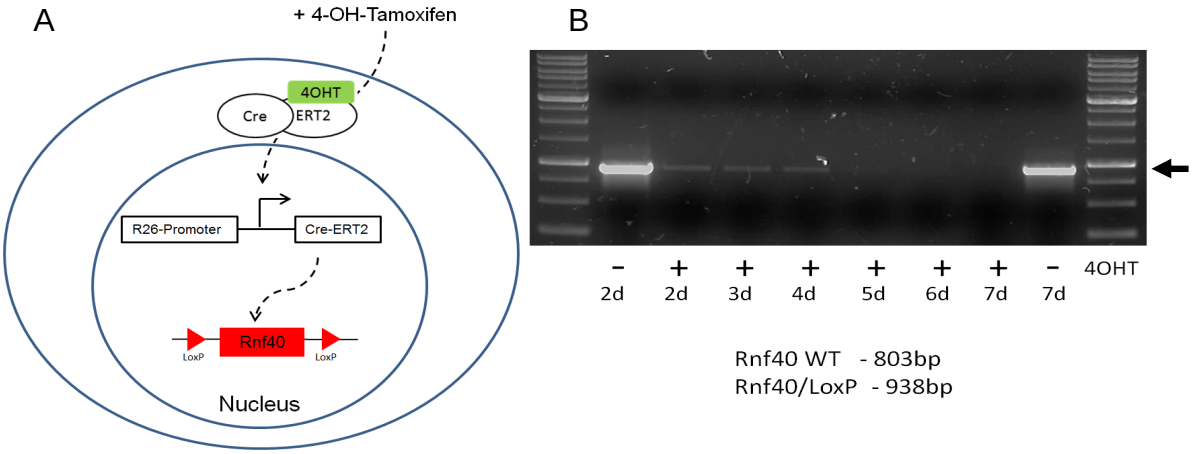

Figure 56. ***Time course 4OHT treatment in primary osteoblasts ex vivo*****. A**. Schematic representation of 4-hydroxy-tamoxifen (4OHT) induced Rnf40 gene deletion. The Cre-recombinase fused with mutated estrogen binding domain (ERT2) is placed under the control of ubiquitously expressed Rosa26 promoter. The fused Cre protein can be translocated into the nucleus once binding with 4OHT ligand where it leads to the deletion of LoxP intervening DNA sequence flanking the exon 3 and 4 of Rnf40 gene. **B.** Time course 4OHT treatments were used to test the efficiency of Rnf40 gene deletion. Agarose gel pictures of Rnf40 wildtype or Rnf40 floxed PCR products performed on DNA from primary long bone cells isolated from $Rnf40^{Rosa\text{-}CreERT2}$ mouse homozygous for Rnf40/LoxP sites after 2-7 days of 4OHT treatment, respectively. The arrow indicates 1000bp.

The primary long or calvarial bone cells were isolated from $Rnf40^{Rosa\text{-}CreERT2}$ mice at age of six weeks or the first three days after birth, respectively. 7 days of 4-hydroxy-tamoxifen (4OHT) treatment was sufficient for almost complete recombination and loss of Rnf40 gene in primary osteoblasts (Figure 56).

We then checked the differentiation potential of the primary osteoblasts *ex vivo* (Figure 57A). Interestingly, Rnf40 deficient cells with significant loss of H2Bub1 (Figure 57B) didn't differentiate well into alkaline phosphatase (ALP) positive cells. Moreover, they failed to mineralize after 21 days of differentiation (Figure 57C).

Since the differentiation potential of the cells was significantly impaired upon Rnf40 knockout, we also analyzed the expression of lineage-specific genes in both the calvarial as well as long bone cells. Loss of Rnf40 lead to reduced expression of the marker genes in both cell types (Figure 58) consistent with the previously reported *in vitro* results from human mesenchymal stem cells (Karpiuk et al., 2012).

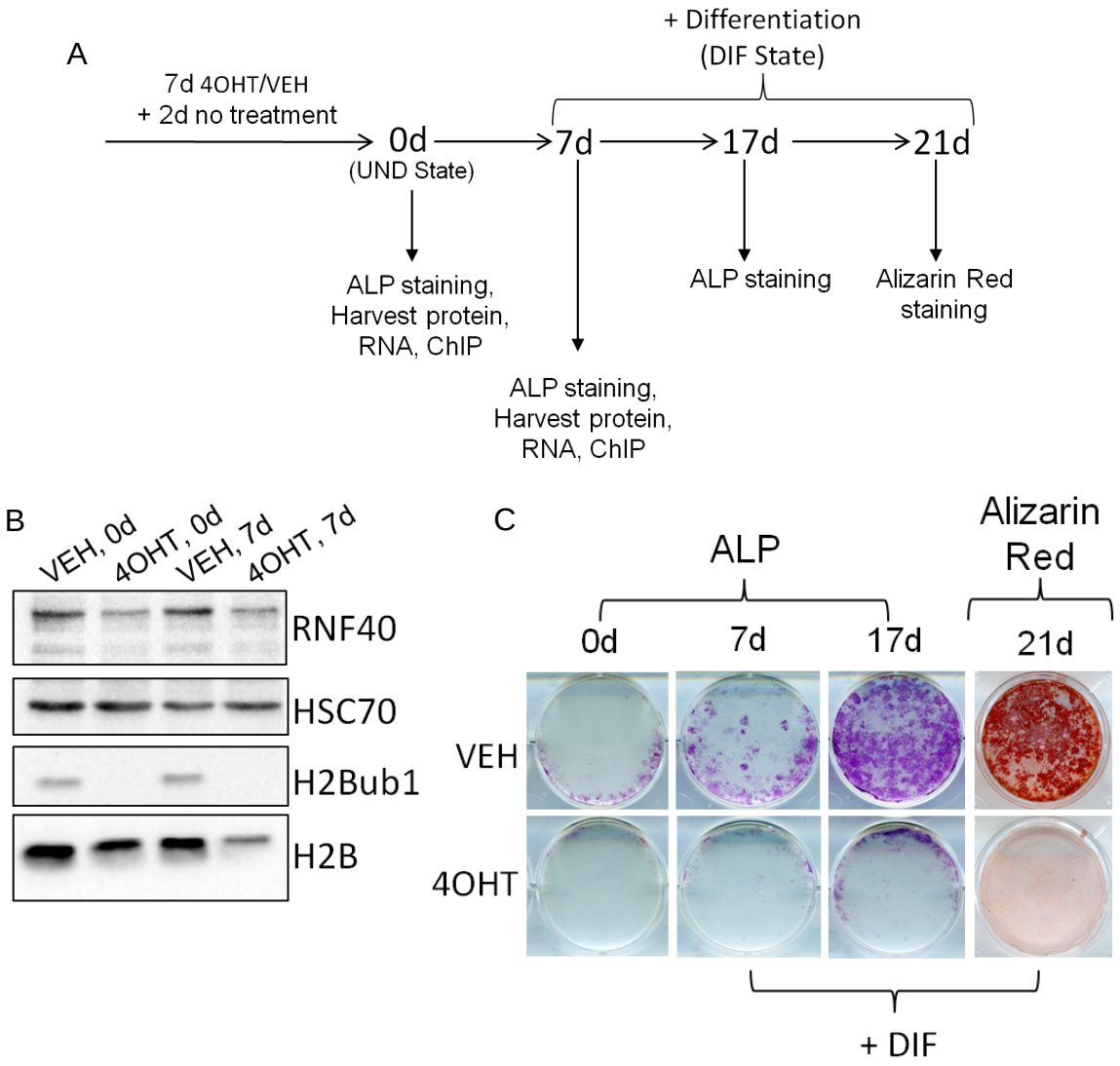

Figure 57. ***Rnf40 knockout primary osteoblasts failed to differentiate*****. A**. Schematic representation of experimental design. Primary osteoblasts were treated 7 days with 250nM 4OHT or equivalent volume of 100% ethanol (VEH), after which the treatments were removed and cells were cultured 2 more days in complete media. Cells were stained for Alkaline phopshotase activity (0d) and protein extracts for undifferentiated state (UND) were harvested at this time point. Then cells were induced do differentiate for 7, 17 and 21 days. At 7 days of differentiation cells were used for alkaline phosphatase staining and protein, RNA and ChIP extracts were harvested. At 17 days following differentiation cells were stained for alkaline phosphatase activity and at 21 days – with alizarin red staining. **B**. Western Blot analysis of Rnf40 and H2Bub1 in whole cell protein lysates harvested at 0 and 7 days of differentiation from primary calvarial osteoblasts. HSC70 and H2B were used as loading controls. **C**. Scanned images of wells with primary calvarial osteoblasts stained for alkaline phosphatase activity at 0d, 7d and 17d and Alizarin Red – at 21 days of differentiation.

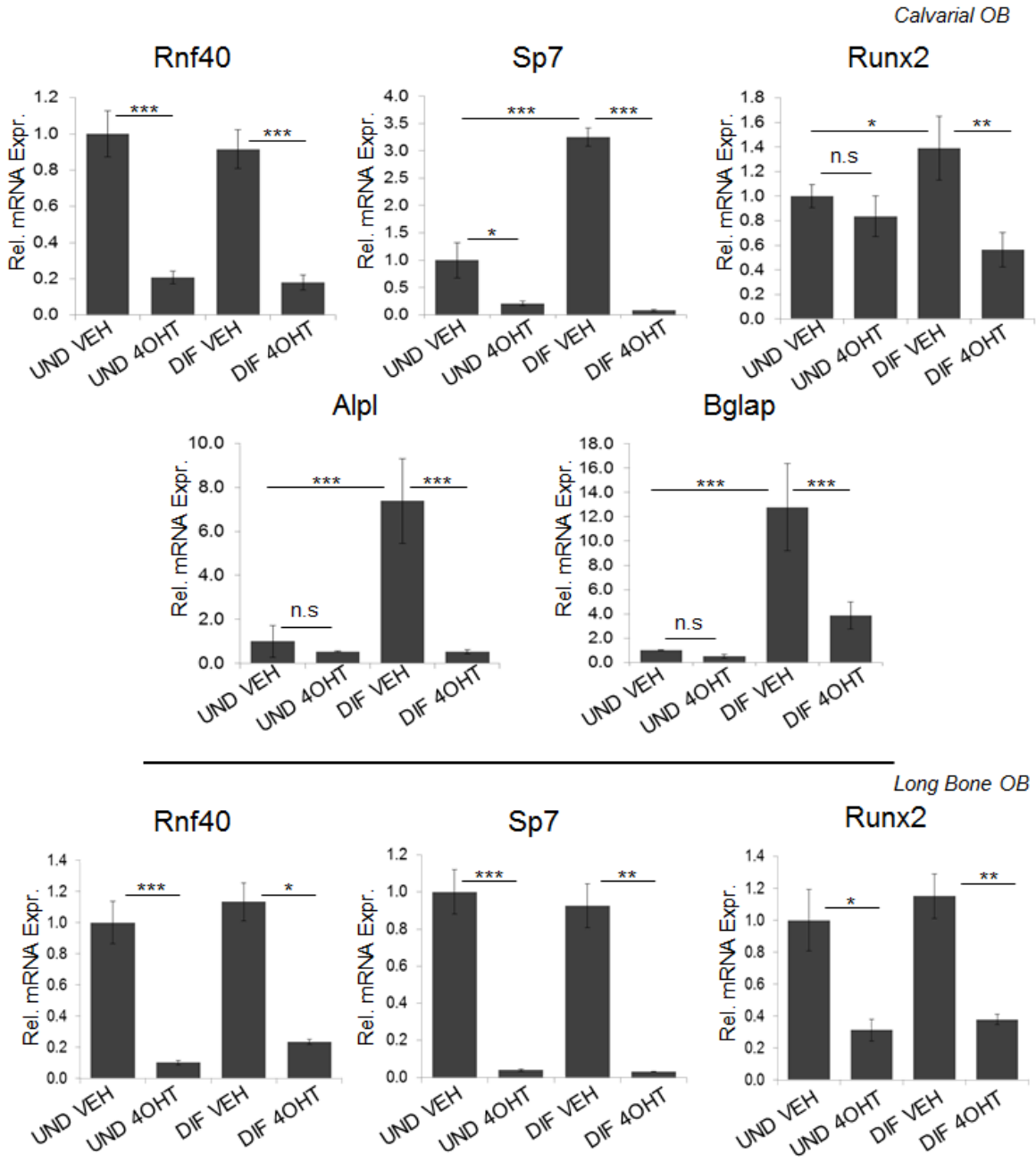

Figure 58. ***Expression of osteoblast-specific genes is reduced in Rnf40 deficient cells***, The primary cells were differentiated as stated in (Figure 57). The relative expression of osteoblast marker genes in calvarial osteoblasts (upper panel) and long bone cells (lower panel) was evaluated via qRT-PCR analysis and normalized to expression level of Gapdh housekeeping gene in undifferentiated vehicle treated state. Mean±SD, n=4. Student t-test was performed for statistical analysis where ***p<0.001, **p<0.01, *p<0.05.

To look for transcriptome wide effects caused by Rnf40 loss in primary osteoblasts the mRNA of these cells was subjected to high-throughput sequencing. The clustering analysis of replicates revealed the similarity between the samples and

conditions (Figure 59A). Interestingly, the differences induced by Rnf40 loss in differentiated state were higher than in undifferentiated state (Figure 59B).

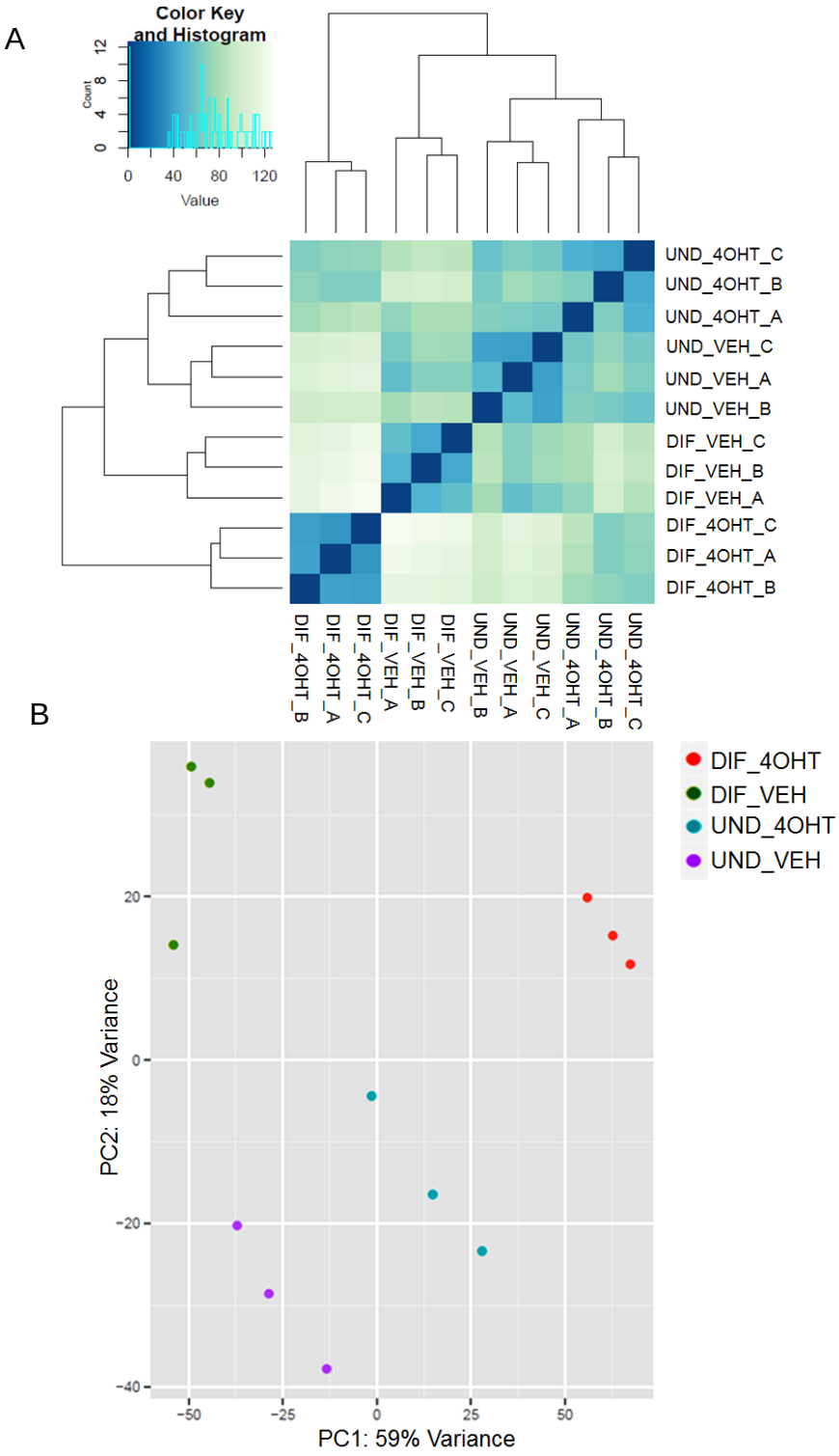

Figure 59. ***Quality diagnostics of RNA-Seq data from primary calvarial osteoblasts*****. A**.Heatmap of hierarchical clustering of Elucidean sample distances and **B**. Principal Component Analysis (PCA) of the mRNA-Seq data after variance stabilized transformation.

Notably, knockout of Rnf40 gene in calvarial osteoblasts almost reverted the differentiation induced gene expression program (Figure 60). Interestingly, already in undifferentiated state Rnf40 loss affected the same set of genes as in differentiated cells where in the latter the effects were further enhanced.

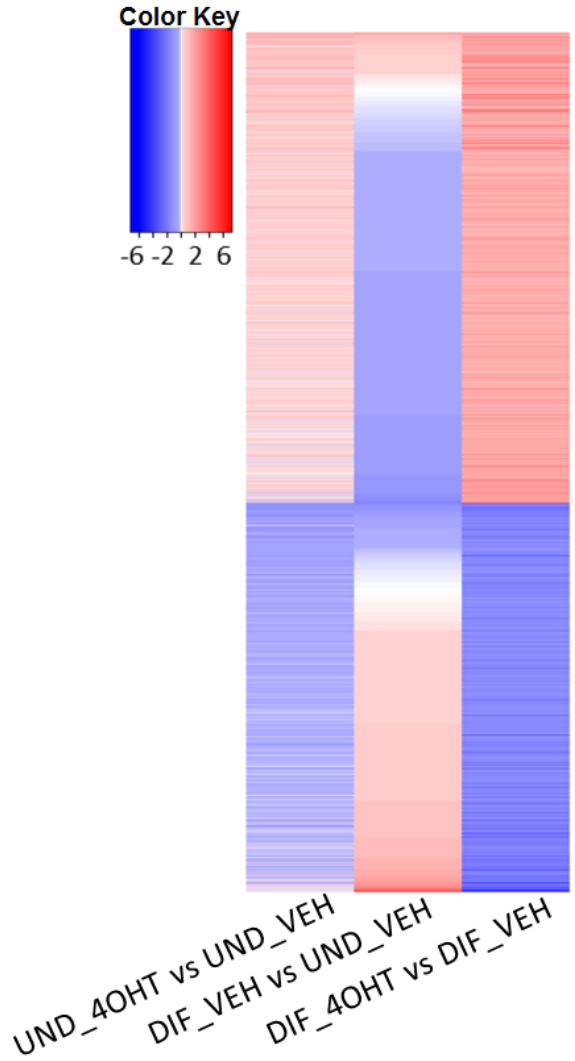

Figure 60. ***Transcriptome wide effects of Rnf40 deficiency in primary osteoblasts.*** Heatmap depicting log2fold change values of mRNA-Seq data from primary calvarial osteoblasts: (left) of 4OHT versus VEH treated cells in undifferentiated state; (middle) of control VEH treated cells in differentiated versus undifferentiated state; (right) of 4OHT treated cells versus VEH in differentiated state. Each row represents single gene. Genes up- (log2fold change value ≥1, padj≤0.05) and downregulated (log2fold change value ≤-1, padj≤0.05) in 4OHT versus VEH treated condition in differentiated state were selected for the heatmap.

The list of Rnf40 dependent genes in undifferentiated state included several hits involved in extracellular matrix organization and endochondral ossification (Figure 61A). In the differentiated state the list was broader involving in general skeletal system and extracellular matrix associated pathways (Figure 61B) .

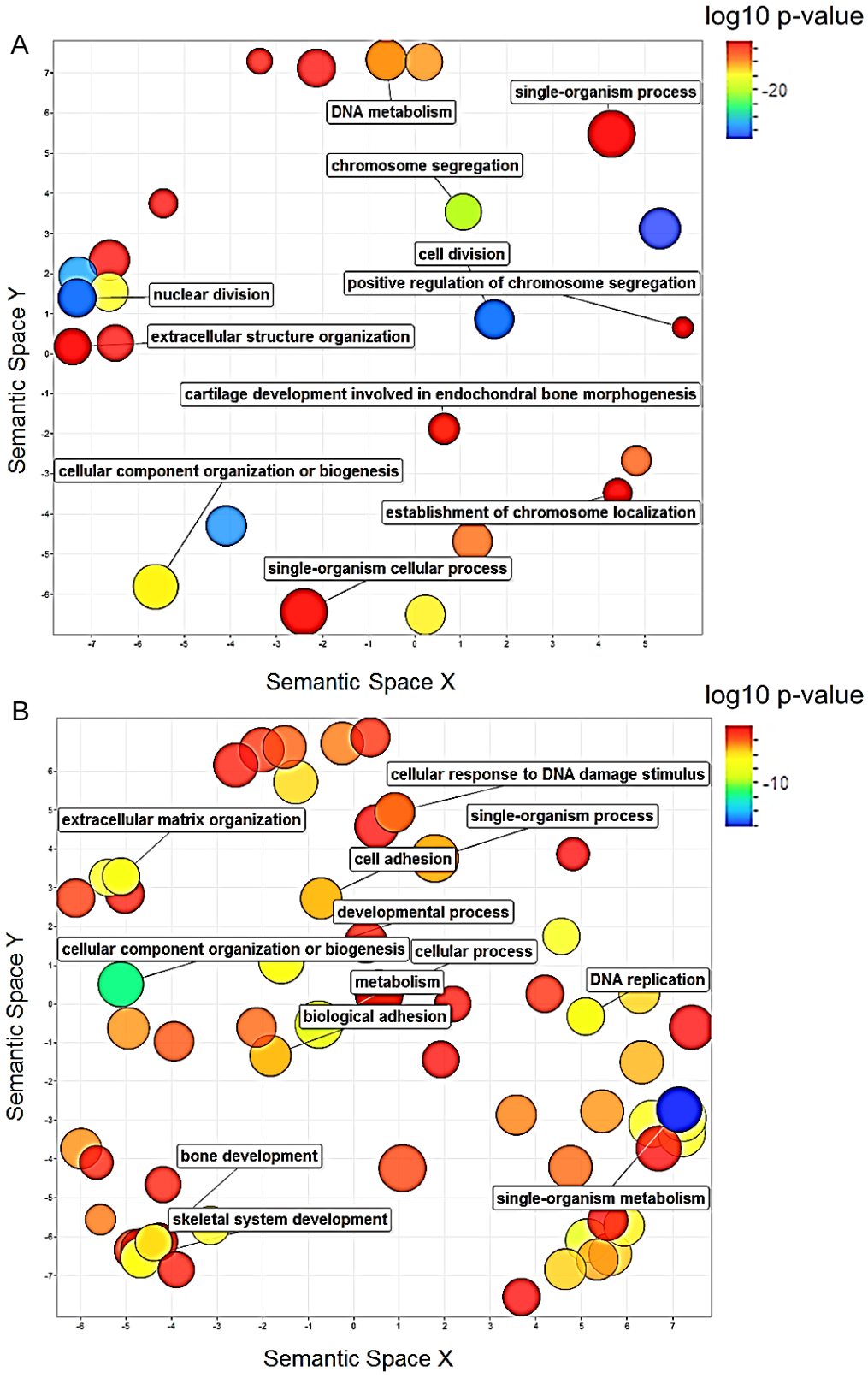

Figure 61. ***Gene Ontology on Rnf40 dependent genes in primary calvarial osteoblasts.*** Functional Classification Summary of GO terms associated with genes downregulated (log2fold change ≤-1, padj≤0.05) with Rnf40 knockout in **A.** undifferentiated and **B**. differentiated calvarial osteoblasts. The bubble plots were created by GO visualization tool REVGO. The color code depicts the log10 p-values of enriched GO term clusters.

As previously mentioned the coupling of osteoblast mediated bone formation and osteoclast driven bone resorption is the leading mechanism of bone mass maintenance. We therefore sought to test whether the Rnf40 deficient osteoblasts would exhibit defects in triggering the activation of osteoclasts that would explain the increased bone mass observed in condtional Rnf40$^{Bglap\text{-}Cre}$ knockout mice. Number of factors produced by osteoblasts and osteocytes are known to coordinate the activation of osteoclasts (Boyce and Xing, 2007). Interestingly, the receptor activator of nuclear factor kappa-B ligand gene (Rankl) expression was significantly reduced in Rnf40 knockout primary osteoblasts whereas the osteoprotegerin (Opg, or Tnfrsf11b) level was not affected much (Figure 62A).

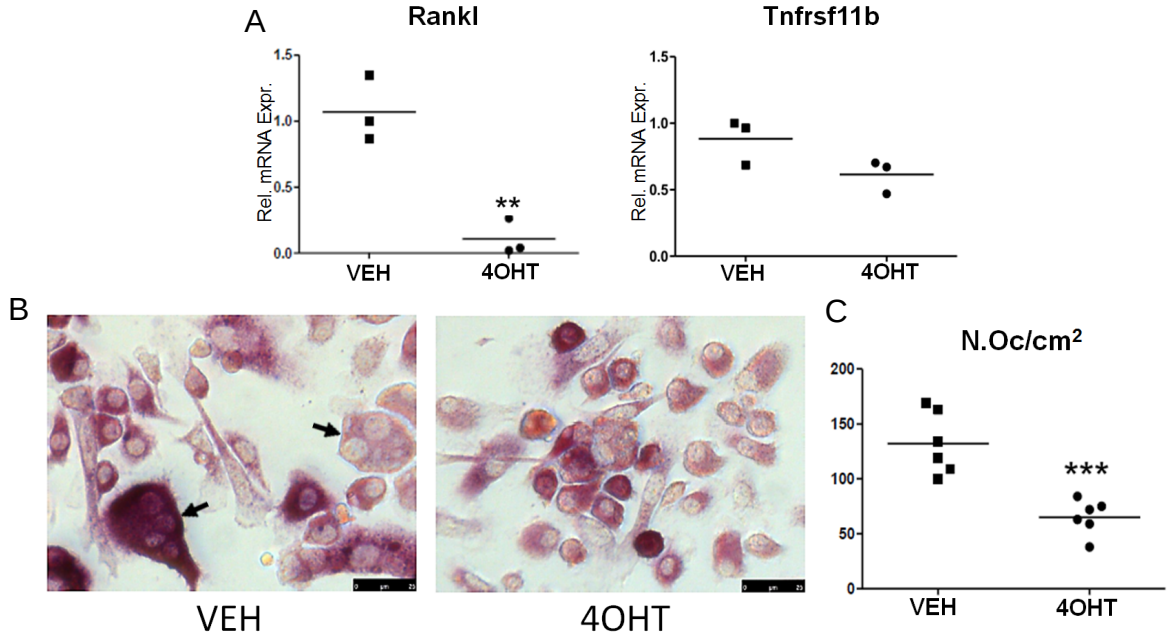

Figure 62. ***Primary Rnf40 deficient calvarial osteoblasts fail to trigger osteoclast formation*****.** Primary Calvarial Osteoblasts from Rosa26-CreERT2 x Rnf40/flox mouse following 7 days of vehicle or 4OHT treatment were co-cultured with primary bone marrow derived macrophages and subjected to 9 days of 10nM vitamin D treatment. **A**. Relative expression of Rankl and Tnfrsf11B gene in control (VEH) or KO (4OHT) osteoblasts used for co-culture experiment. **B**. TRAP staining was used to visualize the osteoclasts. C. Quantification of TRAP positive multinucleated osteoclasts in co-culture with control (VEH) or KO (4OHT) calvarial osteoblasts**.**

Moreover, the co-culture of Rnf40 deficient primary calvarial osteoblasts with wildtype macrophages revealed decreased formation of multinucleated osteoclasts from the latter (Figure 62B).

Altogether these findings revealed the indispensable function of Rnf40 mediated H2Bub1 during the differentiation of osteoblasts. The cells devoid of Rnf40 failed to mineralize *ex vivo*, however these observations were not consistent with the previously mentioned in vivo data where the conditional bone-specific Rnf40 knockout mice developed functionally normal bones. Consistently, the Rnf40 deficient osteoblasts also failed to trigger osteoclast formation *ex vivo* due to reduced RANKL gene expression which more likely explains the increased bone mass phenotype and decrease in osteoclast numbers observed in conditional Rnf40 knockout mice.

DISCUSSION

Bone development is a complex process that is coordinated by a sophisticated network of extra- and intracellular signaling cascades. Growing evidence suggests importance of epigenetic regulators during development and in determination of cell fate. A combination of epigenetic mechanisms allows proper activation of molecular events that control specific cell identity and its maintenance. Perturbation of these epigenetic mechanisms can be the leading cause of development - and differentiation defects, on one side, and can be targeted for therapeutic use, on the other side. In the present study we aimed to elucidate the molecular epigenetic mechanisms governing bone formation which could possibly provide a basis for better understanding and hence development of effective therapies for bone-related diseases.

BRD4 acts independent of H2Bub1 to regulate gene expression

In general, bone formation is achieved through two processes known as intramembranous and endochondral ossification both of which involve the transformation of progenitor mesenchymal stem cells. Indeed, the differentiation of mesenchymal stem cells into bone forming osteoblasts and cartilage forming chondrocytes is the key determining event underlying healthy skeletal development (Bruder et al., 1994; Gilbert, 2000).

Given the positive correlation of H2Bub1 with differentiation induced gene expression in MSCs (Karpiuk et al., 2012) our initial hypothesis suggested BRD4 as upstream component of CDK9-WAC-RNF20/40 axis to regulate osteoblast-specific gene expression program. Although we observed an increase in H2Bub1 levels in hFOBs upon differentiation, consistent with previous finding, the global protein

H2Bub1 levels were not affected by loss or inhibition of BRD4 suggesting H2Bub1 independent function of BRD4 in regulating osteoblast differentiation.

Association of H2Bub1 exclusively with transcribed regions of protein coding genes as revealed by genome wide enrichment analysis, correlation with the transcribing RNAPII implies H2Bub1 as “readout” of transcriptional elongation (this study and Fuchs et al., 2014). Moreover, the bulky structure of H2Bub1 makes it into an important regulator of nucleosome stability and dynamics (Chandrasekharan et al., 2009; Fierz et al., 2011; Jung et al., 2012) and thereby, more likely, hints to “rate limiting” function of H2Bub1 in controlling the “speed” of RNA Polymerase passage and perhaps the proximal RNAPII pause release.

The role of BRD4 in regulation of gene expression is broader. It is involved at several levels of transcriptional regulation, namely facilitating transcription initiation and elongation by promoter- and more importantly, by enhancer-coupled events (Kanno et al., 2014; Liu et al., 2013; Nagarajan et al., 2014; Patel et al., 2013). Functional activity of BRD4 largely relies on the presence of activating histone acetylation marks (Dey et al., 2003; Filippakopoulos et al., 2012; Roe et al., 2015; Zhang et al., 2012). In addition, several reports uncovered the ability of BRD4 to bind also acetylated transcription factors (Brown et al., 2014; Huang et al., 2009; Roe et al., 2015; Shi et al., 2014). However, there is also an increasing amount of evidence pointing to bromodomain-independent functions of BRD4 in regulating gene expression (Rahman et al., 2011; Wu et al., 2013). Furthermore, implication of histone chaperone and acetyltransferase “abilities” of BET proteins (Devaiah et al., 2016; Kanno et al., 2014) also brings in another level of complexity into the understanding of BRD4 dependent transcriptional regulation. Altogether, these facts imply that BRD4 promotes gene expression in a “hierarchical” and context-

dependent manner where action through H2Bub1 pathway would only partially explain the broad effects of BRD4 loss on gene regulation. This can be also supported by the finding that despite the inhibition of BRD4 by JQ1 where JQ1 downregulated genes consistently lost H2Bub1 on the transcribed region, the JQ1 upregulated genes gained it which speaks for dependence of H2Bub1 levels on the outcome of gene expression change rather than BRD4 itself.

BRD4 is indispensable for development and maintenance of osteoblast phenotype

The first hint about the possible relevance of BRD4 for skeletal development came from the study by Houzelstein et al., 2002. Here the authors for the first time discovered that heterozygosity for BRD4 in mice leads to developmental defects including abnormalities in skull bones. Our study further strengthened the role of BRD4 in bone formation. Namely, we uncovered indispensability of BRD4 at earlier as well as later stages of osteoblast differentiation. Although global mRNA or protein levels of BRD4 did not change upon differentiation there was a considerable increase of BRD4 occupancy around the TSS of genes and the change was markedly higher on genes upregulated during differentiation. More importantly, the increase in BRD4 occupancy was observed on the identified osteoblast-specific putative enhancers implying a potential function of BRD4 in controlling osteoblast-specific gene expression

Both JQ1 and siRNA mediated knockdown of BRD4 elicited similar pattern in regulation of osteoblast-specific genes. However, the overlap between these two treatments was not high. Consistent with the fact that JQ1 targets all BET proteins including BRD2, -3 and -4 (Filippakopoulos et al., 2010) and the potential differences

induced by inhibition of bromodomain-mediated protein-protein interactions versus effects observed following a complete loss of BRD4 protein expression, the differences observed between effects of JQ1 and BRD4 knockdown were not surprising. According to RNA-Seq data out of the BET family proteins only BRD4 and BRD3 were expressed in hFOBs. Unlike BRD4 protein, BRD3 lacks the C-terminal P-TEFb interaction domain and there is little evidence about the role of BRD3 in transcriptional regulation (Wang and Filippakopoulos, 2015). BRD3 was shown to interact with acetylated GATA1 to regulate erythroid differentiation (Gamsjaeger et al., 2011; Lamonica et al., 2011). Interestingly, Lamourex *et al*. recently highlighted antiproliferative effects of JQ1 in osteosarcoma cell lines to be mainly mediated through BRD4 but not BRD3 or BRD2 (Lamoureux et al., 2014).

Moreover, the differences in transcriptome-wide effects of BRD4 loss or inhibition by JQ1 might be also explained by the fact that the latter would only expose the bromodomain dependent functions of BRD4. In this case some additional experiments such as JQ1 Chem-Seq or BRD4 ChIP-Seq following the JQ1 treatment would help to address the significance of bromodomain dependent function of BRD4 in regulation of osteoblast-specific gene expression. Nonetheless, the overall increased occupancy of BRD4 around the TSS of genes and putative enhancers during differentiation, enrichment of BRD4 and JQ1 dependent genes with skeletal system associated GO terms clearly support the specific function of BRD4 in regulating osteoblast dependent transcriptional program.

BRD4 and gene expression control

In general, BRD4 was found to positively correlate with gene expression, i.e. more expressed genes were highly marked by BRD4. Surprisingly, however, the intuitive

assumption that highly BRD4 marked genes would be the most sensitive to BRD4 inhibition or loss did not happen to be completely true. In contrast, only a subset of BRD4 dependent genes was highly marked by this protein. Notably, lowly expressed and lowly marked BRD4 genes showed the highest change in expression upon JQ1 treatment. The association of JQ1 unregulated genes with metabolic pathways indicated life maintaining – housekeeping biological functions of these genes where a minor change could potentially have drastic effects on the cellular wellbeing. In general, housekeeping genes are known to show high CGI (CpG island) content at the promoter regions (Larsen et al., 1992; Lercher et al., 2003). Although, most of the highly expressed JQ1 unregulated genes were indeed high CGI genes, the CGI content of JQ1 regulated genes was not significantly lower. The similar pattern was observed with differentiation dependent and unregulated genes suggesting hierarchy of more complex mechanisms involved in the regulation of gene expression control. On the other side, the stability of the nucleosomes flanking the TSS, the DNA sequence of -1 and +1 nucleosomes that defines the specificity of the binding for chromatin remodelers might be the other characteristic factor for differentiating the highly and lowly expressed genes (Kubik et al., 2015). Whether highly expressed BRD4 marked genes also possess “fragile” promoters remains a matter of further investigation. Based on the findings of the current study one could assume that the key factor in controlling gene expression level would be not the “amount” of loss induced by the treatment but rather the “amount” of remaining activating factors/marks left following the treatment. Therefore low marked and hence low expressed genes are more sensitive to be stimuli dependent than the highly “packed” genes.

BRD4 on osteoblast-specific enhancers

The fact that TSS associated BRD4 levels were not predictive of JQ1 sensitivity in the subgroup of JQ1 dependent genes hinted to possible involvement of other mechanisms of gene expression regulation mediated by BRD4. Broad intergenic localization of BRD4 in hFOBs and correlation with RNAPII on these regions suggested involvement of BRD4 in additional regulation of gene expression through enhancer-coupled events. Enhancers can be defined as transcription factor bound regulatory DNA elements distally controlling target gene expression in a spatiotemporal manner. Chromatin interaction analysis revealed partitioning of mammalian genome into topologically associated domains (TAD) where enhancers were shown to form long-range interactions with target promoters within the insulated regions (Dixon et al., 2012; Dowen et al., 2014). In such manner, due to the chromatin “looping” enhancers can be brought to closer proximity to the target promoters. Therefore, the integrity of “looped” structures within the TADs is certainly important for proper gene expression control. On the other hand, increasing amount of evidence suggests transcription of noncoding RNAs from enhancers which similarly can influence target gene expression (De Santa et al., 2010; Hah et al., 2013; Kim et al., 2010) . Characterization of hFOB-specific BRD4 sites uncovered cell-type-specific localization pattern of BRD4 on potential enhancer regions. This suggests that although BRD4 acts as general transcriptional regulator it does so in cell-type-specific manner.

Interestingly, most osteoblast-specific BRD4 bound enhancer regions revealed elevated enrichment of BRD4 along with H3K27ac and RNAPII upon differentiation. More importantly, most of these regions were also associated with osteoblast-specific genes. However, chromatin conformation capture techniques followed by

next-generation sequencing would be required to identify the direct target promoters of each enhancer. Moreover, loss-of-function experiments involving deletion of enhancer containing DNA regions could address the functional relevance and enhancer redundancy in regulating target gene expression.

Context-specific function of BRD4

The tissue-specific function of an enhancer is dictated by the panel of transcription factors bound to it at a given time. The transcription factors define the composition and hence the outcome of enhancer-promoter interactions on gene regulation (van Arensbergen et al., 2014; Matharu and Ahituv, 2015; Nolis et al., 2009). The identification of osteoblast-specific BRD4-bound putative enhancers and transcription factors associated with these regions further strengthens the role of BRD4 in lineage determination. Five candidate transcription factors were computationally predicted to be potentially enriched at BRD4 bound enhancer segments: C/EBPb, AP1 factors JUND and FOSL2, TEAD1 and STAT3. Previous studies already established important functions of C/EBPb, AP1 and STAT3 transcription factors in regulating osteoblast differentiation (Gutierrez et al., 2002; Nicolaidou et al., 2012; Sabatakos et al., 2000; Zhou et al., 2011). Although the specific role of TEAD1 in the context of bone formation has not yet been studied, its importance can be implied based on its interaction and dependence on the TAZ transcriptional co-activators (Stein et al., 2015). Specifically, TAZ was shown to regulate osteoblast differentiation and mediate the effects of canonical Wnt signaling, a central regulator of osteoblast differentiation (Byun et al., 2014; Hong et al., 2005). One of the main transcription factors involved in the osteoblast differentiation is the Runt-related transcription factor 2 (RUNX2) (Otto et al., 1997). Although the RUNX2 motifs were not specifically identified by motif discovery tool, analysis of RUNX2 in

NHOST cells suggested its co-localization on osteoblast-specific BRD4-enriched regions. Consistently, RUNX2 was previously reported to interact with both AP1 factors as well as C/EBPb (D'Alonzo et al., 2002; Gutierrez et al., 2002; Meyer et al., 2014a) to regulate osteoblast differentiation. Moreover, C/EBPb along with RUNX2 were shown to localize to epigentically active enhancers during differentiation of osteoblasts (Meyer et al., 2014b) .Thus, it is very likely that BRD4 localization to "Segment 3+4" is mediated by functional cooperation between RUNX2 and other DNA binding transcription factors . In general, the distinct binding pattern of the identified TFs suggests that each plays a specific role in coordinating BRD4 function during the establishment of osteoblast-specific transcriptional programs. Whether these TFs directly interact with BRD4 in bromodomain-dependent manner or indirectly by means of additional co-factors needs further analysis. The strong association of p300 with BRD4 specifically on enhancers as well as with C/EBPb, AP1, TEAD1 and STAT proteins suggests a possible model where the identified transcription factors could utilize p300 to recruit BRD4 onto tissue-specific enhancers (Arias et al., 1994; Mink et al., 1997; Paulson et al., 1999; Schwartz et al., 2003; Stein et al., 2015). Moreover, some of the transcription factors may themselves serve as acetylation targets for p300 (Ni et al., 2014; Roe et al., 2015), offering an additional, more direct mode of mediating BRD4 recruitment to enhancers.

Although BRD4 is a ubiquitously expressed protein that serves as a general facilitator of transcriptional activation, an increasing body of evidence indicates that it regulates gene expression in a context-specific manner where the specificity is defined by the repertoire of transcription factors and co-factors expressed. Together, our findings support the role of BRD4 as a central intermediary of the induction of gene expression in response to external signaling via its recruitment to both the

promoter and enhancer regions bound by a subset of transcription factors. Thus, these findings begin to provide an explanation of the intricacies and diversity of BETi-mediated transcriptional effects elicited in different tissues and cell lines. A further understanding of the context-dependent functions of BET proteins will be essential for the efficient and correct clinical application of BET inhibitors in various diseases.

The complex phenotype of Rnf40Runx2-Cre conditional knockout mouse

The early knowledge about importance of histone H2B monoubiquitination (H2Bub1) in developmental regulation came initially from yeast studies (Fleming et al., 2008; Hwang et al., 2003; Tanny et al., 2007; Wood et al., 2005). In addition, several reports had indicated the crucial role of H2Bub1 for the maintenance of germ line stem cells in *Drosophila* (Buszczak et al., 2009; Wright et al., 2011). However, many questions remain unanswered regarding the functional relevance of this modification for the mammalian development.

To confirm the biological significance of H2Bub1 signaling *in vivo* we sought to determine how modulating RNF40 expression would affect normal bone development in mice. By using the conditional knockout approach we generated mouse line bearing osteoblast-specific loss of Rnf40 under the control of Runx2 promoter.

RUNX2 is the initial transcription factor required for osteoblastic commitment of mesenchymal stem cells. RUNX2 deficient mice display complete absence of bone formation and die shortly after birth (Komori et al., 1997). RUNX2 is similarly essential for maturation of chondrocytes which implies its role in endochondral

ossification in addition to intramembranous bone formation (Chen et al., 2014). RUNX2 expressing cells are therefore referred as bipotential with ability to differentiate into osteoblasts or chondrocytes. And only the expression of downstream transcription factor *Osterix* (*SP7*) that negatively regulates SOX9, the determinant of chondrocyte phenotype, further directs the fate of the mesenchymal cells into functional osteoblasts (Nakashima and de Crombrugghe, 2003).

The Runx2-Cre mouse line used in this study was reported to show efficient recombination in long bones and calvaria, and consistently some partial recombination events were observed in the cartilage (Rauch et al., 2010). This most likely explains the “dwarfism” of conditional Rnf40$^{Runx2\text{-}Cre}$ knockout mice suggesting the defects in both osteoblast as well as chondrocytes lacking functional Rnf40 gene. However, this assumption needs further validation and use of cartilage-specific Rnf40 mutant mouse would enlighten the specific function of this protein in chondrocytes.

Moreover, the defects in intramembranous ossification most likely contributed to smaller skull size in the knockout mice. Perhaps, this was the main reason why mice were developing hydrocephalus. Hydrocephalus is known to be very common also aduring achondroplastic abnormalities observed in humans (Steinbok et al., 1989). Therefore, early termination of the experiment was required to reduce the suffering of animals mainly shortly after weaning.

Furthermore, the mice also lacked the teeth. RUNX2 is equally important for the differentiation of odontoblasts, the cells responsible for dentin formation (Chen et al., 2009). Additionally, osteoclasts are similarly relevant during tooth eruption (Wang and McCauley, 2011) and whether the absence of teeth were due to direct defects in

osteoblasts and/or odontoblasts, or due indirect functional insufficiency of osteoclasts needs further investigation.

Altogether, the combination of phenotypic changes observed in conditional $Rnf40^{Runx2\text{-}Cre}$ suggested both osteopetrotic- as well as achondroplastic-like phenotypes. Further analysis, involving estimation of bone formation rate to address the defects in bone remodeling and osteoblast-osteoclast coupling, quantification of osteoblast and osteoclast numbers, histological assessment of the growth plates to address the defects in chondrocytes and, in general, in endochondral ossification are required to delineate the functional significance of RNF40 in different cellular compartments involved in bone formation.

USP22 in developing bone

To date most of the knowledge about biological function of USP22 come from tumor based studies. In fact, USP22 has been reported to be one of 11 genes associated with cancer stem-cell signature and essentially leads to poor outcome and decreased survival rate in patients with different types of cancer (Glinsky et al., 2005; He et al., 2015; Zhang et al., 2011b).

USP22 is a ubiquitously expressed protein and has been implicated in regulation of stem cell differentiation (Sussman et al., 2013). Loss of USP22 leads to embryonic lethality (Lin et al., 2012) whereas significant reduction of USP22 was associated with growth retardation and differentiation defects especially in highly proliferating tissues like intestine (Kosinsky et al., 2015). As a member of the deubiquitination module (DUB) of the SAGA complex, USP22 is considered one of the important regulators of H2B K120 monoubiquitination (Henry et al., 2003; Lang et al., 2011). Furthermore, USP22 was reported to have additional target proteins such as SIRT1,

COX-2 and RCAN1 (Ao et al., 2014; Hong et al., 2015; Xiao et al., 2015). However, in contrast to our expectations, the conditional deletion of Usp22 in mouse osteoblasts did not reveal any significant phenotypic or morphological changes in the skeletal system of the mice.

It has been shown before that association of USP22 with ATXN7L3 and ENY2 and additionally with ATXN7 that anchors DUB module within the SAGA complex is in fact important for the enzymatic activity of the complex as a whole (Lan et al., 2015; Lang et al., 2011; Samara et al., 2010). Moreover, several reports had indicated that USP22 loss alone was not sufficient to affect H2B monoubiquitination and interestingly, depletion of ATXN7L3 or ENY2 greatly increased H2Bub1 levels (Atanassov et al., 2016; Lang et al., 2011). Characterization of two additional deubiquitinating enzymes USP27X and USP51 based on high homology to USP22 protein, could explain the redundant function of H2Bub1 specific DUBs (Atanassov et al., 2016). Moreover, USP44, was demonstrated to show enzymatic activity towards monoubiquitinated at K120 H2B (Fuchs et al., 2012). Consistently, differentiation defects observed in the intestines of $Usp22^{LacZ}$ were also shown to be not associated with changes in H2Bub1 levels (Kosinsky et al., 2015).

Altogether, in the view of all the above mentioned facts, the absence of bone-specific function of USP22 was in fact not surprising. However, one could assume that USP22 deficient bones would show impaired regenerative potential and fracture-healing experiments would be additionally required to test this hypothesis. Moreover, given the fact that USP22 acts as a co-activator during estrogen- and glucocorticoid-receptor mediated transactivation (Zhao et al., 2008), one could analyze the role of USP22 during menopause- and steroid-induced osteoporosis, respectively.

The osteopetrotic-like phenotype of Rnf40 deficient mice

Use of Rnf40$^{Runx2\text{-}Cre}$ conditional mouse line with the complex phenotype restricted our understanding of the osteoblast-specific function of Rnf40. Therefore we utilized another bone-specific mouse line bearing Cre expression under the *Bglap* (osteocalcin) promoter. Osteocalcin is a secreted protein involved in matrix mineralization produced mainly by osteoblasts and osteocytes (Hauschka et al., 1989; Lee et al., 2007). The expression of *Bglap* is regulated by Runx2 and Sp7 transcription factors (Lee et al., 2007; Nakashima and de Crombrugghe, 2003). Interestingly, the conditional Rnf40$^{Bglap\text{-}Cre}$ knockout mice displayed mainly osteopetrotic-like phenotype with no signs of growth retardation confirming the previously observed "dwarfism" in Rnf40$^{Runx2\text{-}Cre}$ to be mainly associated with potential defects in chondrocytes. However, the absence of changes in bone formation rate and fully developed skeleton in these mice suggested intact function of osteoblasts. Interestingly, this was not consistent with the observed reduction in differentiation capacity of Rnf40 deficient primary osteoblasts. Since BGLAP is a relatively late expressed gene, one could assume that function of RNF40 is more relevant at earlier stages of osteoblast commitment. In that case, the smaller skull, absence of the teeth and shorter bone size observed in conditional Runx2-specific Rnf40 knockout mice, could in fact support the stage-specific function of RNF40 in regulation of osteoblast differentiation. Positive regulation of RUNX2 and SP7 master transcription factors by RNF40 further strengthens the relatively earlier contribution of RNF40 in regulating the osteoblast lineage commitment. However, further confirmation of changes in osteoblast number and bone formation rate in Rnf40$^{Runx2\text{-}Cre}$ mice would be required to support this statement. Furthermore, additional *ex vivo* studies with subsequent knockout of Rnf40 in primary mouse osteoblasts at different

time points following differentiation induction would uncover the requirement of more committed osteoblasts in Rnf40. Additionally, a similar approach could be performed in the another inducible $Rnf40^{Sp7\text{-}CreERT2}$ mouse model with postnatal 4-hydroxytamoxifen injections to confirm the stage specificity of H2Bub1 signaling in developing bone.

The reduction in osteoclast number was most likely the main reason leading to increased bone density in $Rnf40^{Bglap\text{-}Cre}$ knockout mice. Further *ex vivo* analysis of Rnf40 deficient osteoblasts with significant reduction in *Rankl* expression supported the potential contribution of perturbed osteoblast-osteoclast “interaction” as underlying mechanism of osteopetrotic-like phenotype observed in Rnf40 knockout mouse. Moreover, several reports had outlined the role of osteocalcin in recruitment and differentiation of osteoclasts (Glowacki and Lian, 1987; Hauschka et al., 1989) and given the fact that Bglap is positively regulated by Rnf40 could additionally explain the decrease in osteoclasts numbers in Rnf40 deficient mice.

Consistent with the role of osteocalcin in energy metabolism (Lee et al., 2007) one could also expect differences in the glucose tolerance and fat deposition of conditional $Rnf40^{Bglap\text{-}Cre}$ knockout mice. However, another experimental setup involving high-fat diet and glucose tolerance test would be required to address this assumption.

Implications of Rnf40 in lineage-specific gene expression regulation

Altogether, the conditional knockout approach with bone-specific deletion of Rnf40 gene in mice strengthened the functional relevance of H2Bub1 signaling for bone formation and development. However, further investigation and follow-up studies are

required to fully uncover the RNF40-H2Bub1 dependent molecular mechanisms involved in the regulation of osteoblast-specific gene expression pattern.

Despite the universal feature of H2Bub1 association with actively transcribed genes, the overall decrease in the levels of this modification upon RNF20/40 loss results in selective regulation of genes (this study, Fuchs et al., 2012; Karpiuk et al., 2012; Prenzel et al., 2011; Shema et al., 2008). A number of factors may define the specificity of H2Bub1 in gene regulation. However, noteworthy is to mention the transcription factor circuits that are the key determinants of specific cellular phenotype. In fact, the osteoblastic differentiation is tightly controlled by the nuclear-hormone receptor signaling. Of specific importance is the vitamin D for the healthy bone development and functioning. Following the ligand induction, vitamin D receptor (VDR) dimerizes with the retinoid X receptor (RXR) and binds to regulatory DNA elements this way facilitating target gene expression (Imai et al., 2013). Interestingly, BGLAP was identified as a first gene to be regulated by VDR and more importantly it harbors vitamin D response element (VDRE) in its promoter region (Ozono et al., 1990). Moreover, several line of evidence suggests interaction of RUNX2 with VDR to promote osteoblast-specific gene expression (Marcellini et al., 2010; Paredes et al., 2004). Importantly, RANKL has been reported to be one of the vitamin D most responsive genes. Consistently, several VDR binding sites were identified upstream of RANKL promoter (Pike et al., 2014).

Despite the adverse effects of clinically used glucocorticoids on bone, glucocorticoid receptor (GR) signaling was shown to be equally important for triggering osteoblast differentiation and matrix mineralization (Eijken et al., 2006). Glucocorticoid response elements (GRE) were found within the promoter regions of BGLAP and COL1A1 genes (Heinrichs et al., 1993; Peterkofsky et al., 1999).

It is also noteworthy to mention the positive role of sex hormones estrogen and androgen receptor signaling in bone physiology (Almeida et al., 2013; Määttä et al., 2013; Russell et al., 2015). Notably, both estrogen and androgen receptor mediated signaling were shown to be dependent on RNF20 and RNF40 for target gene expression in breast and prostate cancer cell lines, respectively (Jääskeläinen et al., 2012; Prenzel et al., 2011). Moreover, AR mediated transactivation involved direct interaction with USP22 (Zhao et al., 2008).

The fact that RANKL expression can be regulated both by VDR and RNF40 suggests relevance of H2Bub1 signaling in mediating VDR dependent transcriptional regulation. However, further validation by ChIP-Seq of VDR and RNF40 to find the co-localization pattern on the target genes would be required. Additionally, the overall contribution of RNF40 to hormonal regulation of osteoblast differentiation can be identified by Co-IP and ChIP studies of RNF40 with the nuclear hormone receptors implicated in the bone physiology.

Concluding remarks

Over past years development and characterization of small molecule inhibitors targeting specific groups of epigenetic enzymes has been shown efficient in the treatment of several disorders. An important breakthrough was the discovery of highly specific BET protein inhibitors that efficiently blocked the oncogene dependent transcriptional programs responsible for cancer development and progression (Cheng et al., 2013; Coudé et al., 2015; Filippakopoulos et al., 2010; Lamoureux et al., 2014; Lockwood et al., 2012; Roe et al., 2015). Importantly, pharmacological inhibition of BET proteins exhibited positive role in osteosarcoma as well (Lamoureux et al., 2014). The authors identified BRD4 inhibition as an important mechanism in

controlling bone cancer growth and proliferation, and remarkably by blocking the differentiation of both the osteoblasts and osteoclasts. BETi hampered the osteosarcoma associated vicious cycle involved in the development of osteolytic lesions and metastasis. Interestingly, the BET inhibition displayed more prominent effects in the osteoclasts than in the osteoblasts leading to reduced bone resorption in mice (Park-Min et al., 2014). This most likely explains the absence of phenotypic changes in healthy mice upon BETi injections and only the induced challenge on the bones such as cancer, inflammation or osteoporosis would reveal the effects of BET inhibition in osteoblasts. Interestingly, our study also revealed the anti-resorptive function of RNF40 loss through modulation of RANKL expression. This suggests inhibition of H2Bub1 signaling as a potential strategy to be used in osteoporosis or cancer associated osteolysis as well. However, so far no inhibitors targeting the RNF20 and RNF40 protein complex have been developed. Given the crosstalk between H2B monoubiquitination and H3K4 and H3K79 methylations (Nakanishi et al., 2009; Vlaming et al., 2014), the use of histone methyltransferase inhibitors could potentially exhibit the same effects as RNF40 loss. However, this assumption requires further careful investigation. Given the positive role of HDAC inhibitors in the bone formation (Bradley et al., 2011) and their synergistic effects to BET inhibition (Bhadury et al., 2014; Heinemann et al., 2015; Mazur et al., 2015) combined therapy of osteoporosis by BET and HDAC inhibitors could be suggested in addition to bisphonates.

In the current study we identified two epigenetic regulators to be involved in the osteoblast lineage determination. The initial role of RNF40 mediated H2Bub1 in osteoblast specialization of mesenchymal progenitors was already reported (Karpiuk et al., 2012). We further confirmed the biological significance of this finding *in vivo*. Despite its H2Bub1 independent function, BRD4 similarly regulated the osteoblast-specific gene expression involving different mechanisms of gene expression control.

In summary, our work provides deeper insights into the regulatory mechanisms controlling cell fate determination. Our findings support the notion that epigenetic changes and regulators may carry a universal feature in transcriptional control however the specificity to this control is dictated by the transcription factor circuits. This is of great importance especially when considering the outcomes of specific therapies targeting the epigenetic networks.

Altogether, based on the previous and obtained knowledge, the following model of transcriptional regulation of osteoblast lineage determination can be suggested (Figure 63).

In the undifferentiated precursor cells, upon differentiation-inducing signal, the extra- and intracellular cascades activate the recruitment of early (pioneer) transcriptional factors that facilitate the early events of chromatin de-condensation through recruitment of chromatin remodeling and modifying enzymes such as histonemethyl- and acetyltransferases (HMT and HAT, respectively).

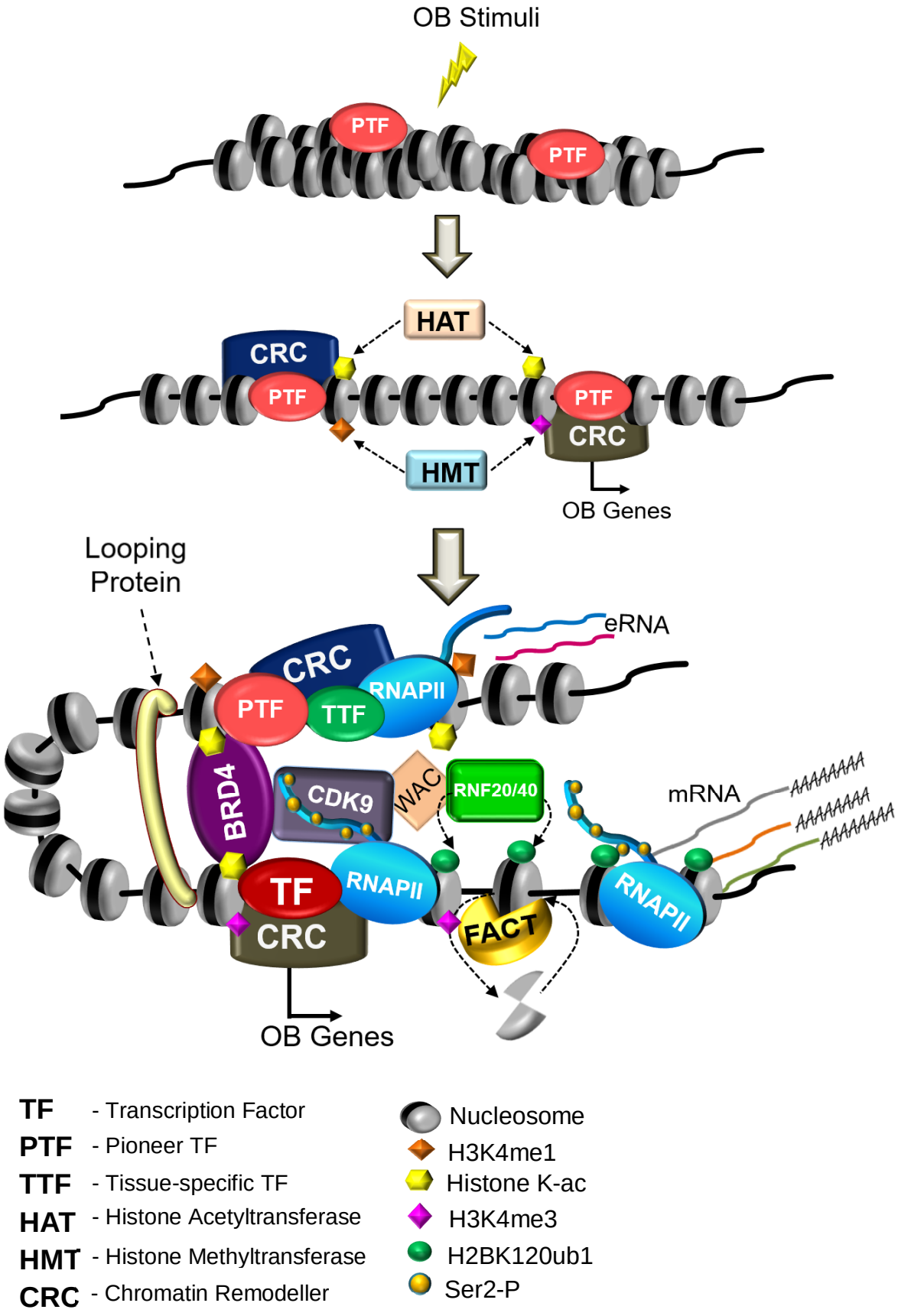

Figure 63. ***Model for transcriptional regulation of osteoblast-specific gene expression.*** The explanation is given within the text.

These transcription factors, hence, prime the chromatin for subsequent binding of tissue-specific transcription factors (TTF) to target osteoblast-specific genes and enhancers. The histone modifiers, in turn, catalyze subsequent methylation (for instance H3K4me3 at promoter regions, and H3K4me1 at enhancer) and acetylation of histone tails within the nucleosomes flanking the promoter and enhancer regions. At the same time transcription factors along with looping proteins facilitate the "bridging" of enhancers with target promoters through chromatin looping. The histone modifications serve as a recruitment signal for various proteins involved in the assembly of general transcriptional machinery followed by recruitment or RNA Polymerase II to promoter and/or enhancers. The epigenetic reader BRD4 by binding to acetylated histones and/or to acetylated TFs on promoter and enhancer regions facilitates activation and release of P-TEFb (CDK9). Presumably, non-coding enhancer RNAs (eRNA) stabilize the enhancer-promoter looping and assist in P-TEFb activation. CDK9 mediated phosphorylation of Ser2 residues within heptapeptide repeats of C-terminal tail of promoter-associated RNA Polymerase II (RNAPII) are recognized by WAC adaptor protein which then enables recruitment of E3 ligase complex RNF20/40 to transcribed region of the given gene. Monoubiquitination of histone H2B at K120 (H2Bub1) facilitates further decompaction of the chromatin. Moreover, histone chaperones such as Facilitates Chromatin Transcription (FACT) complex trigger destabilization of H2Bub1 marked nucleosomes through histone dimer exchange. Altogether, the sequential development of these events leads to efficient transcriptional elongation of osteoblast-specific genes.

References

Almeida, M., Iyer, S., Martin-Millan, M., Bartell, S.M., Han, L., Ambrogini, E., Onal, M., Xiong, J., Weinstein, R.S., Jilka, R.L., et al. (2013). Estrogen receptor-α signaling in osteoblast progenitors stimulates cortical bone accrual. J. Clin. Invest. *123*, 394–404.

Anders, S., Pyl, P.T., and Huber, W. (2015). HTSeq—a Python framework to work with high-throughput sequencing data. Bioinformatics *31*, 166–169.

Ao, N., Liu, Y., Feng, H., Bian, X., Li, Z., Gu, B., Zhao, X., and Liu, Y. (2014). Ubiquitin-Specific Peptidase USP22 Negatively Regulates the STAT Signaling Pathway by Deubiquitinating SIRT1. Cell. Physiol. Biochem. *33*, 1863–1875.

van Arensbergen, J., van Steensel, B., and Bussemaker, H.J. (2014). In search of the determinants of enhancer–promoter interaction specificity. Trends Cell Biol. *24*, 695–702.

Arias, J., Alberts, A.S., Brindle, P., Claret, F.X., Smeal, T., Karin, M., Feramisco, J., and Montminy, M. (1994). Activation of cAMP and mitogen responsive genes relies on a common nuclear factor. Nature *370*, 226–229.

Asangani, I.A., Dommeti, V.L., Wang, X., Malik, R., Cieslik, M., Yang, R., Escara-Wilke, J., Wilder-Romans, K., Dhanireddy, S., Engelke, C., et al. (2014). Therapeutic Targeting of BET Bromodomain Proteins in Castration-Resistant Prostate Cancer. Nature *510*, 278–282.

Atanassov, B.S., Mohan, R.D., Lan, X., Kuang, X., Lu, Y., Lin, K., McIvor, E., Li, W., Zhang, Y., Florens, L., et al. (2016). ATXN7L3 and ENY2 Coordinate Activity of Multiple H2B Deubiquitinases Important for Cellular Proliferation and Tumor Growth. Mol. Cell *62*, 558–571.

Baratta, M.G., Schinzel, A.C., Zwang, Y., Bandopadhayay, P., Bowman-Colin, C., Kutt, J., Curtis, J., Piao, H., Wong, L.C., Kung, A.L., et al. (2015). An in-tumor genetic screen reveals that the BET bromodomain protein, BRD4, is a potential therapeutic target in ovarian carcinoma. Proc. Natl. Acad. Sci. *112*, 232–237.

Baron, R., and Kneissel, M. (2013). WNT signaling in bone homeostasis and disease: from human mutations to treatments. Nat. Med. *19*, 179–192.

Becker, P.B., and Workman, J.L. (2013). Nucleosome Remodeling and Epigenetics. Cold Spring Harb. Perspect. Biol. *5*.

Bhadury, J., Nilsson, L.M., Veppil Muralidharan, S., Green, L.C., Li, Z., Gesner, E.M., Hansen, H.C., Keller, U.B., McLure, K.G., and Nilsson, J.A. (2014). BET and HDAC inhibitors induce similar genes and biological effects and synergize to kill in Myc-induced murine lymphoma. Proc. Natl. Acad. Sci. U. S. A. *111*, E2721–E2730.

Bihani, T., Ezell, S.A., Ladd, B., Grosskurth, S.E., Mazzola, A.M., Pietras, M., Reimer, C., Zinda, M., Fawell, S., D'Cruz, C.M., et al. (2014). Resistance to

everolimus driven by epigenetic regulation of MYC in ER+ breast cancers. Oncotarget *6*, 2407–2420.

Blankenberg, D., Von Kuster, G., Coraor, N., Ananda, G., Lazarus, R., Mangan, M., Nekrutenko, A., and Taylor, J. (2010). Galaxy, a web-based genome analysis tool for experimentalists. Curr. Protoc. Mol. Biol. Ed. Frederick M Ausubel Al *0 19*, Unit-19.1021.

Blee, A.M., Liu, S., Wang, L., and Huang, H. (2016). BET bromodomain-mediated interaction between ERG and BRD4 promotes prostate cancer cell invasion. Oncotarget.

Boyce, B.F., and Xing, L. (2007). Biology of RANK, RANKL, and osteoprotegerin. Arthritis Res. Ther. *9*, 1–7.

Boyce, B.F., and Xing, L. (2008). Functions of RANKL/RANK/OPG in bone modeling and remodeling. Arch. Biochem. Biophys. *473*, 139–146.

Bradley, E.W., McGee-Lawrence, M.E., and Westendorf, J.J. (2011). Hdac-Mediated Control of Endochondral and Intramembranous Ossification. Crit. Rev. Eukaryot. Gene Expr. *21*, 101–113.

Brown, J.D., Lin, C.Y., Duan, Q., Griffin, G., Federation, A., Paranal, R.M., Bair, S., Newton, G., Lichtman, A., Kung, A., et al. (2014). NF-kB directs dynamic super enhancer formation in inflammation and atherogenesis. Mol. Cell *56*, 219–231.

Bruder, S.P., Fink, D.J., and Caplan, A.I. (1994). Mesenchymal stem cells in bone development, bone repair, and skeletal regenaration therapy. J. Cell. Biochem. *56*, 283–294.

Brunelle, M., Nordell Markovits, A., Rodrigue, S., Lupien, M., Jacques, P.-É., and Gévry, N. (2015). The histone variant H2A.Z is an important regulator of enhancer activity. Nucleic Acids Res. *43*, 9742–9756.

Buck, D.W., and Dumanian, G.A. (2012). Bone biology and physiology: Part I. The fundamentals. Plast. Reconstr. Surg. *129*, 1314–1320.

Buckwalter, J.A., Glimcher, M.J., Cooper, R.R., and Recker, R. (1995). Bone Biology. J Bone Jt. Surg Am *77*, 1256–1275.

Buszczak, M., Paterno, S., and Spradling, A.C. (2009). Drosophila stem cells share a common requirement for the histone H2B ubiquitin protease Scrawny. Science *323*, 248–251.

Byun, M.R., Hwang, J.-H., Kim, A.R., Kim, K.M., Hwang, E.S., Yaffe, M.B., and Hong, J.-H. (2014). Canonical Wnt signalling activates TAZ through PP1A during osteogenic differentiation. Cell Death Differ. *21*, 854–863.

Cao, J., and Yan, Q. (2012). Histone Ubiquitination and Deubiquitination in Transcription, DNA Damage Response, and Cancer. Front. Oncol. *2*.

Case, N., and Rubin, J. (2010). β-Catenin—A Supporting Role in the Skeleton. J. Cell. Biochem. *110*, 545–553.

Chandrasekharan, M.B., Huang, F., and Sun, Z.-W. (2009). Ubiquitination of histone H2B regulates chromatin dynamics by enhancing nucleosome stability. Proc. Natl. Acad. Sci. U. S. A. *106*, 16686–16691.

Chen, H., and Boutros, P.C. (2011). VennDiagram: a package for the generation of highly-customizable Venn and Euler diagrams in R. BMC Bioinformatics *12*, 35.

Chen, D.-M., Zhong, X.-Q., and Jiang, K.W. and Y.-Z. (2015). SWI/SNF Chromatin Remodeling Complex in Regulating Mesenchymal Stem Cell Lineage Specification. J. Tissue Sci. Eng. *2015*.

Chen, H., Ghori-Javed, F.Y., Rashid, H., Adhami, M.D., Serra, R., Gutierrez, S.E., and Javed, A. (2014). Runx2 Regulates Endochondral Ossification Through Control of Chondrocyte Proliferation and Differentiation. J. Bone Miner. Res. *29*, 2653–2665.

Chen, P., Zhao, J., Wang, Y., Wang, M., Long, H., Liang, D., Huang, L., Wen, Z., Li, W., Li, X., et al. (2013). H3.3 actively marks enhancers and primes gene transcription via opening higher-ordered chromatin. Genes Dev.

Cheng, Z., Gong, Y., Ma, Y., Lu, K., Lu, X., Pierce, L.A., Thompson, R.C., Muller, S., Knapp, S., and Wang, J. (2013). Inhibition of BET Bromodomain Targets Genetically Diverse Glioblastoma. Clin. Cancer Res. *19*, 1748–1759.

Cho, H.H., Park, H.T., Kim, Y.J., Bae, Y.C., Suh, K.T., and Jung, J.S. (2005). Induction of osteogenic differentiation of human mesenchymal stem cells by histone deacetylase inhibitors. J. Cell. Biochem. *96*, 533–542.

Cirillo, L.A., Lin, F.R., Cuesta, I., Friedman, D., Jarnik, M., and Zaret, K.S. (2002). Opening of Compacted Chromatin by Early Developmental Transcription Factors HNF3 (FoxA) and GATA-4. Mol. Cell *9*, 279–289.

Clapier, C.R., and Cairns, B.R. (2009). The Biology of Chromatin Remodeling Complexes. Annu. Rev. Biochem. *78*, 273–304.

Clarke, B. (2008). Normal bone anatomy and physiology. Clin. J. Am. Soc. Nephrol. CJASN *3 Suppl 3*, S131-139.

Consortium, T.E.P. (2012). An integrated encyclopedia of DNA elements in the human genome. Nature *489*, 57–74.

Coudé, M.-M., Braun, T., Berrou, J., Dupont, M., Bertrand, S., Masse, A., Raffoux, E., Itzykson, R., Delord, M., Riveiro, M.E., et al. (2015). BET inhibitor OTX015 targets BRD2 and BRD4 and decreases c-MYC in acute leukemia cells. Oncotarget *6*, 17698–17712.

de Crombrugghe, B., Lefebvre, V., and Nakashima, K. (2001). Regulatory mechanisms in the pathways of cartilage and bone formation. Curr. Opin. Cell Biol. *13*, 721–727.

D'Alonzo, R.C., Selvamurugan, N., Karsenty, G., and Partridge, N.C. (2002). Physical Interaction of the Activator Protein-1 Factors c-Fos and c-Jun with Cbfa1 for Collagenase-3 Promoter Activation. J. Biol. Chem. *277*, 816–822.

Dansranjavin, T., Krehl, S., Mueller, T., Mueller, L.P., Schmoll, H.-J., and Dammann, R.H. (2009). The role of promoter CpG methylation in the epigenetic control of stem cell related genes during differentiation. Cell Cycle *8*, 916–924.

De Santa, F., Barozzi, I., Mietton, F., Ghisletti, S., Polletti, S., Tusi, B.K., Muller, H., Ragoussis, J., Wei, C.-L., and Natoli, G. (2010). A Large Fraction of Extragenic RNA Pol II Transcription Sites Overlap Enhancers. PLoS Biol *8*, e1000384.

Delaissé, J.-M., Andersen, T.L., Engsig, M.T., Henriksen, K., Troen, T., and Blavier, L. (2003). Matrix metalloproteinases (MMP) and cathepsin K contribute differently to osteoclastic activities. Microsc. Res. Tech. *61*, 504–513.

Delgado-Calle, J., Sañudo, C., Bolado, A., Fernández, A.F., Arozamena, J., Pascual-Carra, M.A., Rodriguez-Rey, J.C., Fraga, M.F., Bonewald, L., and Riancho, J.A. (2012a). DNA methylation contributes to the regulation of sclerostin expression in human osteocytes. J. Bone Miner. Res. Off. J. Am. Soc. Bone Miner. Res. *27*, 926–937.

Delgado-Calle, J., Sañudo, C., Fernández, A.F., García-Renedo, R., Fraga, M.F., and Riancho, J.A. (2012b). Role of DNA methylation in the regulation of the RANKL-OPG system in human bone. Epigenetics *7*, 83–91.

Dempster, D.W., Compston, J.E., Drezner, M.K., Glorieux, F.H., Kanis, J.A., Malluche, H., Meunier, P.J., Ott, S.M., Recker, R.R., and Parfitt, A.M. (2013). Standardized Nomenclature, Symbols, and Units for Bone Histomorphometry: A 2012 Update of the Report of the ASBMR Histomorphometry Nomenclature Committee. J. Bone Miner. Res. Off. J. Am. Soc. Bone Miner. Res. *28*, 2–17.

Denis, G.V., Vaziri, C., Guo, N., and Faller, D.V. (2000). RING3 Kinase Transactivates Promoters of Cell Cycle Regulatory Genes through E2F. Cell Growth Differ. *11*, 417–424.

Devaiah, B.N., Case-Borden, C., Gegonne, A., Hsu, C.H., Chen, Q., Meerzaman, D., Dey, A., Ozato, K., and Singer, D.S. (2016). BRD4 is a histone acetyltransferase that evicts nucleosomes from chromatin. Nat. Struct. Mol. Biol.

Dey, A., Chitsaz, F., Abbasi, A., Misteli, T., and Ozato, K. (2003). The double bromodomain protein Brd4 binds to acetylated chromatin during interphase and mitosis. Proc. Natl. Acad. Sci. U. S. A. *100*, 8758–8763.

Di Micco, R., Fontanals-Cirera, B., Low, V., Ntziachristos, P., Yuen, S.K., Lovell, C.D., Dolgalev, I., Yonekubo, Y., Zhang, G., Rusinova, E., et al. (2014). Control of Embryonic Stem Cell Identity by BRD4-Dependent Transcriptional Elongation of Super-Enhancer-Associated Pluripotency Genes. Cell Rep. *9*, 234–247.

Dixon, J.R., Selvaraj, S., Yue, F., Kim, A., Li, Y., Shen, Y., Hu, M., Liu, J.S., and Ren, B. (2012). Topological domains in mammalian genomes identified by analysis of chromatin interactions. Nature *485*, 376–380.

Dowen, J.M., Fan, Z.P., Hnisz, D., Ren, G., Abraham, B.J., Zhang, L.N., Weintraub, A.S., Schujiers, J., Lee, T.I., Zhao, K., et al. (2014). Control of cell identity genes occurs in insulated neighborhoods in mammalian chromosomes. Cell *159*, 374–387.

Drouin, J. (2014). Minireview: Pioneer Transcription Factors in Cell Fate Specification. Mol. Endocrinol. *28*, 989–998.

Dwek, J.R. (2010). The periosteum: what is it, where is it, and what mimics it in its absence? Skeletal Radiol. *39*, 319–323.

Eijken, M., Koedam, M., van Driel, M., Buurman, C.J., Pols, H. a. P., and van Leeuwen, J.P.T.M. (2006). The essential role of glucocorticoids for proper human osteoblast differentiation and matrix mineralization. Mol. Cell. Endocrinol. *248*, 87–93.

Eulalio, A., Huntzinger, E., Nishihara, T., Rehwinkel, J., Fauser, M., and Izaurralde, E. (2009). Deadenylation is a widespread effect of miRNA regulation. RNA *15*, 21–32.

Farley, F.W., Soriano, P., Steffen, L.S., and Dymecki, S.M. (2000). Widespread recombinase expression using FLPeR (Flipper) mice. Genesis *28*, 106–110.

Fierz, B., Chatterjee, C., McGinty, R.K., Bar-Dagan, M., Raleigh, D.P., and Muir, T.W. (2011). Histone H2B ubiquitylation disrupts local and higher order chromatin compaction. Nat. Chem. Biol. *7*, 113–119.

Filippakopoulos, P., Qi, J., Picaud, S., Shen, Y., Smith, W.B., Fedorov, O., Morse, E.M., Keates, T., Hickman, T.T., Felletar, I., et al. (2010). Selective inhibition of BET bromodomains. Nature *468*, 1067–1073.

Filippakopoulos, P., Picaud, S., Mangos, M., Keates, T., Lambert, J.-P., Barsyte-Lovejoy, D., Felletar, I., Volkmer, R., Müller, S., Pawson, T., et al. (2012). Histone Recognition and Large-Scale Structural Analysis of the Human Bromodomain Family. Cell *149*, 214–231.

Fleming, A.B., Kao, C.-F., Hillyer, C., Pikaart, M., and Osley, M.A. (2008). H2B Ubiquitylation Plays a Role in Nucleosome Dynamics during Transcription Elongation. Mol. Cell *31*, 57–66.

Fritah, A., Saucier, C., Mester, J., Redeuilh, G., and Sabbah, M. (2005). p21WAF1/CIP1 Selectively Controls the Transcriptional Activity of Estrogen Receptor α. Mol. Cell. Biol. *25*, 2419–2430.

Fuchs, G., Shema, E., Vesterman, R., Kotler, E., Wolchinsky, Z., Wilder, S., Golomb, L., Pribluda, A., Zhang, F., Haj-Yahya, M., et al. (2012). RNF20 and USP44 Regulate Stem Cell Differentiation by Modulating H2B Monoubiquitylation. Mol. Cell *46*, 662–673.

Funato, N., Ohtani, K., Ohyama, K., Kuroda, T., and Nakamura, M. (2001). Common Regulation of Growth Arrest and Differentiation of Osteoblasts by Helix-Loop-Helix Factors. Mol. Cell. Biol. *21*, 7416–7428.

Gamsjaeger, R., Webb, S.R., Lamonica, J.M., Billin, A., Blobel, G.A., and Mackay, J.P. (2011). Structural Basis and Specificity of Acetylated Transcription Factor GATA1 Recognition by BET Family Bromodomain Protein Brd3. Mol. Cell. Biol. *31*, 2632–2640.

Gaucher, J., Boussouar, F., Montellier, E., Curtet, S., Buchou, T., Bertrand, S., Hery, P., Jounier, S., Depaux, A., Vitte, A.-L., et al. (2012). Bromodomain-dependent stage-specific male genome programming by Brdt: Brdt: a master regulator of spermatogenesis. EMBO J. *31*, 3809–3820.

Ge, W., Shi, L., Zhou, Y., Liu, Y., Ma, G., Jiang, Y., Xu, Y., Zhang, X., and Feng, H. (2011). Inhibition of Osteogenic Differentiation of Human Adipose-Derived Stromal Cells by Retinoblastoma Binding Protein 2 Repression of RUNX2-Activated Transcription. STEM CELLS *29*, 1112–1125.

Ge, W., Liu, Y., Chen, T., Zhang, X., Lv, L., Jin, C., Jiang, Y., Shi, L., and Zhou, Y. (2014). The epigenetic promotion of osteogenic differentiation of human adipose-derived stem cells by the genetic and chemical blockade of histone demethylase LSD1. Biomaterials *35*, 6015–6025.

Giardine, B., Riemer, C., Hardison, R.C., Burhans, R., Elnitski, L., Shah, P., Zhang, Y., Blankenberg, D., Albert, I., Taylor, J., et al. (2005). Galaxy: A platform for interactive large-scale genome analysis. Genome Res. *15*, 1451–1455.

Gilbert, S.F. (2000). Osteogenesis: The Development of Bones. In Developmental Biology, (Sunderland (MA): Sinauer Associates), p.

Gingery, A., Subramaniam, M., Pitel, K.S., Reese, J.M., Cicek, M., Lindenmaier, L.B., Ingle, J.N., Goetz, M.P., Turner, R.T., Iwaniec, U.T., et al. (2014). The Effects of a Novel Hormonal Breast Cancer Therapy, Endoxifen, on the Mouse Skeleton. PLOS ONE *9*, e98219.

Glinsky, G.V., Berezovska, O., and Glinskii, A.B. (2005). Microarray analysis identifies a death-from-cancer signature predicting therapy failure in patients with multiple types of cancer. J. Clin. Invest. *115*, 1503–1521.

Glowacki, J., and Lian, J.B. (1987). Impaired recruitment and differentiation of osteoclast progenitors by osteocalcin-deplete bone implants. Cell Differ. *21*, 247–254.

Goecks, J., Nekrutenko, A., and Taylor, J. (2010). Galaxy: a comprehensive approach for supporting accessible, reproducible, and transparent computational research in the life sciences. Genome Biol. *11*, R86.

Gomes, N.P., and Espinosa, J.M. (2010). Gene-specific repression of the p53 target gene PUMA via intragenic CTCF-Cohesin binding. Genes Dev. *24*, 1022–1034.

Gomes, N.P., Bjerke, G., Llorente, B., Szostek, S.A., Emerson, B.M., and Espinosa, J.M. (2006). Gene-specific requirement for P-TEFb activity and RNA polymerase II phosphorylation within the p53 transcriptional program. Genes Dev. *20*, 601–612.

Gordon, J.A.R., Stein, J.L., Westendorf, J.J., and van Wijnen, A.J. (2015). Chromatin modifiers and histone modifications in bone formation, regeneration, and therapeutic intervention for bone-related disease. Bone *81*, 739–745.

Griffon, A., Barbier, Q., Dalino, J., van Helden, J., Spicuglia, S., and Ballester, B. (2015). Integrative analysis of public ChIP-seq experiments reveals a complex multi-cell regulatory landscape. Nucleic Acids Res. *43*, e27–e27.

Gursoy-Yuzugullu, O., Ayrapetov, M.K., and Price, B.D. (2015). Histone chaperone Anp32e removes H2A.Z from DNA double-strand breaks and promotes nucleosome reorganization and DNA repair. Proc. Natl. Acad. Sci. *112*, 7507–7512.

Gutierrez, S., Javed, A., Tennant, D.K., Rees, M. van, Montecino, M., Stein, G.S., Stein, J.L., and Lian, J.B. (2002). CCAAT/Enhancer-binding Proteins (C/EBP) β and δ Activate Osteocalcin Gene Transcription and Synergize with Runx2 at the C/EBP Element to Regulate Bone-specific Expression. J. Biol. Chem. *277*, 1316–1323.

Haberland, M., Mokalled, M.H., Montgomery, R.L., and Olson, E.N. (2009). Epigenetic control of skull morphogenesis by histone deacetylase 8. Genes Dev. *23*, 1625–1630.

Hah, N., Murakami, S., Nagari, A., Danko, C.G., and Kraus, W.L. (2013). Enhancer transcripts mark active estrogen receptor binding sites. Genome Res. *23*, 1210–1223.

Hargreaves, D.C., and Crabtree, G.R. (2011). ATP-dependent chromatin remodeling: genetics, genomics and mechanisms. Cell Res. *21*, 396–420.

Harris, S.A., Enger, R.J., Riggs, B.L., and Spelsberg, T.C. (1995). Development and characterization of a conditionally immortalized human fetal osteoblastic cell line. J. Bone Miner. Res. Off. J. Am. Soc. Bone Miner. Res. *10*, 178–186.

Hassan, M.Q., Maeda, Y., Taipaleenmaki, H., Zhang, W., Jafferji, M., Gordon, J.A.R., Li, Z., Croce, C.M., van Wijnen, A.J., Stein, J.L., et al. (2012). miR-218 directs a Wnt signaling circuit to promote differentiation of osteoblasts and osteomimicry of metastatic cancer cells. J. Biol. Chem. *287*, 42084–42092.

Hassan, M.Q., Tye, C.E., Stein, G.S., and Lian, J.B. (2015). Non-coding RNAs: Epigenetic regulators of bone development and homeostasis. Bone *81*, 746–756.

Hauschka, P.V., Lian, J.B., Cole, D.E., and Gundberg, C.M. (1989). Osteocalcin and matrix Gla protein: vitamin K-dependent proteins in bone. Physiol. Rev. *69*, 990–1047.

He, N., Jahchan, N.S., Hong, E., Li, Q., Bayfield, M.A., Maraia, R.J., Luo, K., and Zhou, Q. (2008). A La-Related Protein Modulates 7SK snRNP Integrity to Suppress P-TEFb-Dependent Transcriptional Elongation and Tumorigenesis. Mol. Cell *29*, 588–599.

He, Y., Jin, Y.-J., Zhang, Y.-H., Meng, H.-X., Zhao, B.-S., Jiang, Y., Zhu, J.-W., Liang, G.-Y., Kong, D., and Jin, X.-M. (2015). Ubiquitin-specific peptidase 22

overexpression may promote cancer progression and poor prognosis in human gastric carcinoma. Transl. Res. *165*, 407–416.

Heinemann, A., Cullinane, C., De Paoli-Iseppi, R., Wilmott, J.S., Gunatilake, D., Madore, J., Strbenac, D., Yang, J.Y., Gowrishankar, K., Tiffen, J.C., et al. (2015). Combining BET and HDAC inhibitors synergistically induces apoptosis of melanoma and suppresses AKT and YAP signaling. Oncotarget *6*, 21507–21521.

Heinrichs, A.A., Bortell, R., Rahman, S., Stein, J.L., Alnemri, E.S., Litwack, G., Lian, J.B., and Stein, G.S. (1993). Identification of multiple glucocorticoid receptor binding sites in the rat osteocalcin gene promoter. Biochemistry (Mosc.) *32*, 11436–11444.

Hemming, S., Cakouros, D., Isenmann, S., Cooper, L., Menicanin, D., Zannettino, A., and Gronthos, S. (2014). EZH2 and KDM6A act as an epigenetic switch to regulate mesenchymal stem cell lineage specification. Stem Cells Dayt. Ohio *32*, 802–815.

Henry, K.W., Wyce, A., Lo, W.-S., Duggan, L.J., Emre, N.C.T., Kao, C.-F., Pillus, L., Shilatifard, A., Osley, M.A., and Berger, S.L. (2003). Transcriptional activation via sequential histone H2B ubiquitylation and deubiquitylation, mediated by SAGA-associated Ubp8. Genes Dev. *17*, 2648–2663.

Hesse, E., Saito, H., Kiviranta, R., Correa, D., Yamana, K., Neff, L., Toben, D., Duda, G., Atfi, A., Geoffroy, V., et al. (2010). Zfp521 controls bone mass by HDAC3-dependent attenuation of Runx2 activity. J. Cell Biol. *191*, 1271–1283.

Hojo, H., Ohba, S., Yano, F., Saito, T., Ikeda, T., Nakajima, K., Komiyama, Y., Nakagata, N., Suzuki, K., Takato, T., et al. (2012). Gli1 Protein Participates in Hedgehog-mediated Specification of Osteoblast Lineage during Endochondral Ossification. J. Biol. Chem. *287*, 17860–17869.

Hojo, H., Ohba, S., and Chung, U. (2015). Signaling pathways regulating the specification and differentiation of the osteoblast lineage. Regen. Ther. *1*, 57–62.

Holoch, D., and Moazed, D. (2015). RNA-mediated epigenetic regulation of gene expression. Nat. Rev. Genet. *16*, 71–84.

Hong, A., Lee, J.E., and Chung, K.C. (2015). Ubiquitin-specific protease 22 (USP22) positively regulates RCAN1 protein levels through RCAN1 de-ubiquitination. J. Cell. Physiol. *230*, 1651–1660.

Hong, J.-H., Hwang, E.S., McManus, M.T., Amsterdam, A., Tian, Y., Kalmukova, R., Mueller, E., Benjamin, T., Spiegelman, B.M., Sharp, P.A., et al. (2005). TAZ, a Transcriptional Modulator of Mesenchymal Stem Cell Differentiation. Science *309*, 1074–1078.

Hossan, T., Nagarajan, S., Baumgart, S.J., Xie, W., Magallanes, R.T., Hernandez, C., Chiaroni, P.-M., Indenbirken, D., Spitzner, M., Thomas-Chollier, M., et al. (2016). Histone Chaperone SSRP1 is Essential for Wnt Signaling Pathway Activity During Osteoblast Differentiation. Stem Cells Dayt. Ohio *34*, 1369–1376.

Houzelstein, D., Bullock, S.L., Lynch, D.E., Grigorieva, E.F., Wilson, V.A., and Beddington, R.S.P. (2002). Growth and Early Postimplantation Defects in Mice

Deficient for the Bromodomain-Containing Protein Brd4†. Mol. Cell. Biol. *22*, 3794–3802.

Hsieh, C.-L., Fei, T., Chen, Y., Li, T., Gao, Y., Wang, X., Sun, T., Sweeney, C.J., Lee, G.-S.M., Chen, S., et al. (2014). Enhancer RNAs participate in androgen receptor-driven looping that selectively enhances gene activation. Proc. Natl. Acad. Sci. *111*, 7319–7324.

Hu, H., Hilton, M.J., Tu, X., Yu, K., Ornitz, D.M., and Long, F. (2005). Sequential roles of Hedgehog and Wnt signaling in osteoblast development. Development *132*, 49–60.

Huang, B., Yang, X.-D., Zhou, M.-M., Ozato, K., and Chen, L.-F. (2009). Brd4 Coactivates Transcriptional Activation of NF-κB via Specific Binding to Acetylated RelA. Mol. Cell. Biol. *29*, 1375–1387.

Hwang, W.W., Venkatasubrahmanyam, S., Ianculescu, A.G., Tong, A., Boone, C., and Madhani, H.D. (2003). A Conserved RING Finger Protein Required for Histone H2B Monoubiquitination and Cell Size Control. Mol. Cell *11*, 261–266.

Imai, Y., Youn, M.-Y., Inoue, K., Takada, I., Kouzmenko, A., and Kato, S. (2013). Nuclear Receptors in Bone Physiology and Diseases. Physiol. Rev. *93*, 481–523.

Jääskeläinen, T., Makkonen, H., Visakorpi, T., Kim, J., Roeder, R.G., and Palvimo, J.J. (2012). Histone H2B ubiquitin ligases RNF20 and RNF40 in androgen signaling and prostate cancer cell growth. Mol. Cell. Endocrinol. *350*, 87–98.

Jang, M.K., Mochizuki, K., Zhou, M., Jeong, H.-S., Brady, J.N., and Ozato, K. (2005). The Bromodomain Protein Brd4 Is a Positive Regulatory Component of P-TEFb and Stimulates RNA Polymerase II-Dependent Transcription. Mol. Cell *19*, 523–534.

Jeltsch, A. (2011). Handbook of Epigenetics: The New Molecular and Medical Genetics. Edited by Trygve Tollefsbol. ChemBioChem *12*, 970–970.

Jeon, E.-J., Lee, K.-Y., Choi, N.-S., Lee, M.-H., Kim, H.-N., Jin, Y.-H., Ryoo, H.-M., Choi, J.-Y., Yoshida, M., Nishino, N., et al. (2006). Bone Morphogenetic Protein-2 Stimulates Runx2 Acetylation. J. Biol. Chem. *281*, 16502–16511.

Johnsen, S.A. (2012). The enigmatic role of H2Bub1 in cancer. FEBS Lett. *586*, 1592–1601.

Jung, I., Kim, S.-K., Kim, M., Han, Y.-M., Kim, Y.S., Kim, D., and Lee, D. (2012). H2B monoubiquitylation is a 5′-enriched active transcription mark and correlates with exon–intron structure in human cells. Genome Res. *22*, 1026–1035.

Kalashnikova, A.A., Porter-Goff, M.E., Muthurajan, U.M., Luger, K., and Hansen, J.C. (2013). The role of the nucleosome acidic patch in modulating higher order chromatin structure. J. R. Soc. Interface *10*.

Kanno, T., Kanno, Y., LeRoy, G., Campos, E., Sun, H.-W., Brooks, S.R., Vahedi, G., Heightman, T.D., Garcia, B.A., Reinberg, D., et al. (2014). BRD4 assists elongation

of both coding and enhancer RNAs by interacting with acetylated histones. Nat. Struct. Mol. Biol. *21*, 1047–1057.

Karaplis, A.C., Luz, A., Glowacki, J., Bronson, R.T., Tybulewicz, V.L., Kronenberg, H.M., and Mulligan, R.C. (1994). Lethal skeletal dysplasia from targeted disruption of the parathyroid hormone-related peptide gene. Genes Dev. *8*, 277–289.

Karolchik, D., Hinrichs, A.S., Furey, T.S., Roskin, K.M., Sugnet, C.W., Haussler, D., and Kent, W.J. (2004). The UCSC Table Browser data retrieval tool. Nucleic Acids Res. *32*, D493–D496.

Karpiuk, O., Najafova, Z., Kramer, F., Hennion, M., Galonska, C., König, A., Snaidero, N., Vogel, T., Shchebet, A., Begus-Nahrmann, Y., et al. (2012). The Histone H2B Monoubiquitination Regulatory Pathway Is Required for Differentiation of Multipotent Stem Cells. Mol. Cell *46*, 705–713.

Kawai, S., Yamauchi, M., Wakisaka, S., Ooshima, T., and Amano, A. (2007). Zinc-Finger Transcription Factor Odd-Skipped Related 2 Is One of the Regulators in Osteoblast Proliferation and Bone Formation. J. Bone Miner. Res. *22*, 1362–1372.

Khalid, A.B., and Krum, S.A. (2016). Estrogen receptors alpha and beta in bone. Bone *87*, 130–135.

Kim, J.H., and Kim, N. (2016). Signaling Pathways in Osteoclast Differentiation. Chonnam Med. J. *52*, 12–17.

Kim, D., Pertea, G., Trapnell, C., Pimentel, H., Kelley, R., and Salzberg, S.L. (2013a). TopHat2: accurate alignment of transcriptomes in the presence of insertions, deletions and gene fusions. Genome Biol. *14*, R36.

Kim, J., Hake, S.B., and Roeder, R.G. (2005). The Human Homolog of Yeast BRE1 Functions as a Transcriptional Coactivator through Direct Activator Interactions. Mol. Cell *20*, 759–770.

Kim, J.H., Liu, X., Wang, J., Chen, X., Zhang, H., Kim, S.H., Cui, J., Li, R., Zhang, W., Kong, Y., et al. (2013b). Wnt signaling in bone formation and its therapeutic potential for bone diseases. Ther. Adv. Musculoskelet. Dis. *5*, 13–31.

Kim, T.-K., Hemberg, M., Gray, J.M., Costa, A.M., Bear, D.M., Wu, J., Harmin, D.A., Laptewicz, M., Barbara-Haley, K., Kuersten, S., et al. (2010). Widespread transcription at neuronal activity-regulated enhancers. Nature *465*, 182–187.

Kini, U., and Nandeesh, B.N. (2012). Physiology of Bone Formation, Remodeling, and Metabolism. In Radionuclide and Hybrid Bone Imaging, I. Fogelman, G. Gnanasegaran, and H. van der Wall, eds. (Springer Berlin Heidelberg), pp. 29–57.

Kitazawa, R., and Kitazawa, S. (2007). Methylation Status of a Single CpG Locus 3 Bases Upstream of TATA-Box of Receptor Activator of Nuclear Factor-κB Ligand (RANKL) Gene Promoter Modulates Cell- and Tissue-Specific RANKL Expression and Osteoclastogenesis. Mol. Endocrinol. *21*, 148–158.

Komori, T. (2009). Regulation of bone development and extracellular matrix protein genes by RUNX2. Cell Tissue Res. *339*, 189–195.

Komori, T., Yagi, H., Nomura, S., Yamaguchi, A., Sasaki, K., Deguchi, K., Shimizu, Y., Bronson, R.T., Gao, Y.-H., Inada, M., et al. (1997). Targeted Disruption of Cbfa1 Results in a Complete Lack of Bone Formation owing to Maturational Arrest of Osteoblasts. Cell *89*, 755–764.

Kordowich, S., Serup, P., Collombat, P., and Mansouri, A. (2012). Generation of animals allowing the conditional inactivation of the Pax4 gene. Transgenic Res. *21*, 1215–1220.

Kosinsky, R.L., Wegwitz, F., Hellbach, N., Dobbelstein, M., Mansouri, A., Vogel, T., Begus-Nahrmann, Y., Johnsen, S.A., Kosinsky, R.L., Wegwitz, F., et al. (2015). Usp22 deficiency impairs intestinal epithelial lineage specification in vivo. Oncotarget *6*, 37906–37918.

Kousteni, S., Bellido, T., Plotkin, L.I., O'Brien, C.A., Bodenner, D.L., Han, L., Han, K., DiGregorio, G.B., Katzenellenbogen, J.A., Katzenellenbogen, B.S., et al. (2001). Nongenotropic, Sex-Nonspecific Signaling through the Estrogen or Androgen Receptors: Dissociation from Transcriptional Activity. Cell *104*, 719–730.

Koziel, L., Wuelling, M., Schneider, S., and Vortkamp, A. (2005). Gli3 acts as a repressor downstream of Ihh in regulating two distinct steps of chondrocyte differentiation. Development *132*, 5249–5260.

Kubik, S., Bruzzone, M.J., Jacquet, P., Falcone, J.-L., Rougemont, J., and Shore, D. (2015). Nucleosome Stability Distinguishes Two Different Promoter Types at All Protein-Coding Genes in Yeast. Mol. Cell *60*, 422–434.

Lagger, G., O'Carroll, D., Rembold, M., Khier, H., Tischler, J., Weitzer, G., Schuettengruber, B., Hauser, C., Brunmeir, R., Jenuwein, T., et al. (2002). Essential function of histone deacetylase 1 in proliferation control and CDK inhibitor repression. EMBO J. *21*, 2672–2681.

Lamonica, J.M., Deng, W., Kadauke, S., Campbell, A.E., Gamsjaeger, R., Wang, H., Cheng, Y., Billin, A.N., Hardison, R.C., Mackay, J.P., et al. (2011). Bromodomain protein Brd3 associates with acetylated GATA1 to promote its chromatin occupancy at erythroid target genes. Proc. Natl. Acad. Sci. U. S. A. *108*, E159–E168.

Lamoureux, F., Baud'huin, M., Rodriguez Calleja, L., Jacques, C., Berreur, M., Rédini, F., Lecanda, F., Bradner, J.E., Heymann, D., and Ory, B. (2014). Selective inhibition of BET bromodomain epigenetic signalling interferes with the bone-associated tumour vicious cycle. Nat. Commun. *5*, 3511.

Lan, X., Koutelou, E., Schibler, A.C., Chen, Y.C., Grant, P.A., and Dent, S.Y.R. (2015). Poly(Q) Expansions in ATXN7 Affect Solubility but Not Activity of the SAGA Deubiquitinating Module. Mol. Cell. Biol. *35*, 1777–1787.

Lang, G., Bonnet, J., Umlauf, D., Karmodiya, K., Koffler, J., Stierle, M., Devys, D., and Tora, L. (2011). The Tightly Controlled Deubiquitination Activity of the Human

SAGA Complex Differentially Modifies Distinct Gene Regulatory Elements. Mol. Cell. Biol. *31*, 3734–3744.

Langmead, B., and Salzberg, S.L. (2012). Fast gapped-read alignment with Bowtie 2. Nat. Methods *9*, 357–359.

Larsen, F., Gundersen, G., Lopez, R., and Prydz, H. (1992). CpG islands as gene markers in the human genome. Genomics *13*, 1095–1107.

Lau, P.N.I., and Cheung, P. (2011). Histone code pathway involving H3 S28 phosphorylation and K27 acetylation activates transcription and antagonizes polycomb silencing. Proc. Natl. Acad. Sci. U. S. A. *108*, 2801–2806.

Lawson, K.A., Teteak, C.J., Gao, J., Li, N., Hacquebord, J., Ghatan, A., Zielinska-Kwiatkowska, A., Song, G., Chansky, H.A., and Yang, L. (2013). ESET histone methyltransferase regulates osteoblastic differentiation of mesenchymal stem cells during postnatal bone development. FEBS Lett. *587*, 3961–3967.

Lee, M., and Partridge, N.C. (2010). Parathyroid Hormone Activation of Matrix Metalloproteinase-13 Transcription Requires the Histone Acetyltransferase Activity of p300 and PCAF and p300-dependent Acetylation of PCAF. J. Biol. Chem. *285*, 38014–38022.

Lee, H.W., Suh, J.H., Kim, A.Y., Lee, Y.S., Park, S.Y., and Kim, J.B. (2006). Histone Deacetylase 1-Mediated Histone Modification Regulates Osteoblast Differentiation. Mol. Endocrinol. *20*, 2432–2443.

Lee, N.K., Sowa, H., Hinoi, E., Ferron, M., Ahn, J.D., Confavreux, C., Dacquin, R., Mee, P.J., McKee, M.D., Jung, D.Y., et al. (2007). Endocrine Regulation of Energy Metabolism by the Skeleton. Cell *130*, 456–469.

Lee, S., Park, J.-R., Seo, M.-S., Roh, K.-H., Park, S.-B., Hwang, J.-W., Sun, B., Seo, K., Lee, Y.-S., Kang, S.-K., et al. (2009). Histone deacetylase inhibitors decrease proliferation potential and multilineage differentiation capability of human mesenchymal stem cells. Cell Prolif. *42*, 711–720.

Lee, Y.F., Nimura, K., Lo, W.N., Saga, K., and Kaneda, Y. (2014). Histone H3 Lysine 36 Methyltransferase Whsc1 Promotes the Association of Runx2 and p300 in the Activation of Bone-Related Genes. PLOS ONE *9*, e106661.

Lefebvre, V., and Bhattaram, P. (2010). Vertebrate skeletogenesis. Curr. Top. Dev. Biol. *90*, 291–317.

Lercher, M.J., Urrutia, A.O., Pavlíček, A., and Hurst, L.D. (2003). A unification of mosaic structures in the human genome. Hum. Mol. Genet. *12*, 2411–2415.

Li, H. (2011). A statistical framework for SNP calling, mutation discovery, association mapping and population genetical parameter estimation from sequencing data. Bioinforma. Oxf. Engl. *27*, 2987–2993.

Li, H., Handsaker, B., Wysoker, A., Fennell, T., Ruan, J., Homer, N., Marth, G., Abecasis, G., Durbin, R., and 1000 Genome Project Data Processing Subgroup

(2009). The Sequence Alignment/Map format and SAMtools. Bioinforma. Oxf. Engl. *25*, 2078–2079.

Li, Q., Price, J.P., Byers, S.A., Cheng, D., Peng, J., and Price, D.H. (2005). Analysis of the Large Inactive P-TEFb Complex Indicates That It Contains One 7SK Molecule, a Dimer of HEXIM1 or HEXIM2, and Two P-TEFb Molecules Containing Cdk9 Phosphorylated at Threonine 186. J. Biol. Chem. *280*, 28819–28826.

Li, W., Notani, D., Ma, Q., Tanasa, B., Nunez, E., Chen, A.Y., Merkurjev, D., Zhang, J., Ohgi, K., Song, X., et al. (2013). Functional roles of enhancer RNAs for oestrogen-dependent transcriptional activation. Nature *498*, 516–520.

Li, Z., Liu, C., Xie, Z., Song, P., Zhao, R.C.H., Guo, L., Liu, Z., and Wu, Y. (2011). Epigenetic Dysregulation in Mesenchymal Stem Cell Aging and Spontaneous Differentiation. PLoS ONE *6*.

Lin, Z., Yang, H., Kong, Q., Li, J., Lee, S.-M., Gao, B., Dong, H., Wei, J., Song, J., Zhang, D.D., et al. (2012). USP22 Antagonizes p53 Transcriptional Activation by Deubiquitinating Sirt1 to Suppress Cell Apoptosis and Is Required for Mouse Embryonic Development. Mol. Cell *46*, 484–494.

Liu, T., Gao, Y., Sakamoto, K., Minamizato, T., Furukawa, K., Tsukazaki, T., Shibata, Y., Bessho, K., Komori, T., and Yamaguchi, A. (2007). BMP-2 promotes differentiation of osteoblasts and chondroblasts in Runx2-deficient cell lines. J. Cell. Physiol. *211*, 728–735.

Liu, T., Ortiz, J.A., Taing, L., Meyer, C.A., Lee, B., Zhang, Y., Shin, H., Wong, S.S., Ma, J., Lei, Y., et al. (2011). Cistrome: an integrative platform for transcriptional regulation studies. Genome Biol. *12*, R83–R83.

Liu, W., Ma, Q., Wong, K., Li, W., Ohgi, K., Zhang, J., Aggarwal, A., and Rosenfeld, M.G. (2013). Brd4 and JMJD6-associated Anti-pause Enhancers in Regulation of Transcriptional Pause Release. Cell *155*, 1581–1595.

Lockwood, W.W., Zejnullahu, K., Bradner, J.E., and Varmus, H. (2012). Sensitivity of human lung adenocarcinoma cell lines to targeted inhibition of BET epigenetic signaling proteins. Proc. Natl. Acad. Sci. U. S. A. *109*, 19408–19413.

Love, M.I., Huber, W., and Anders, S. (2014). Moderated estimation of fold change and dispersion for RNA-seq data with DESeq2. Genome Biol. *15*, 550.

Määttä, J.A., Büki, K.G., Ivaska, K.K., Nieminen-Pihala, V., Elo, T.D., Kähkönen, T., Poutanen, M., Härkönen, P., and Väänänen, K. (2013). Inactivation of the androgen receptor in bone-forming cells leads to trabecular bone loss in adult female mice. BoneKEy Rep. *2*, 440.

Mahoney, W.M., Hong, J.-H., Yaffe, M.B., and Farrance, I.K.G. (2005). The transcriptional co-activator TAZ interacts differentially with transcriptional enhancer factor-1 (TEF-1) family members. Biochem. J. *388*, 217–225.

Mammana, A., and Chung, H.-R. (2015). Chromatin segmentation based on a probabilistic model for read counts explains a large portion of the epigenome. Genome Biol. *16*, 151.

Marcellini, S., Bruna, C., Henríquez, J.P., Albistur, M., Reyes, A.E., Barriga, E.H., Henríquez, B., and Montecino, M. (2010). Evolution of the interaction between Runx2 and VDR, two transcription factors involved in osteoblastogenesis. BMC Evol. Biol. *10*, 78.

Matharu, N., and Ahituv, N. (2015). Minor Loops in Major Folds: Enhancer–Promoter Looping, Chromatin Restructuring, and Their Association with Transcriptional Regulation and Disease. PLoS Genet. *11*.

Mazur, P.K., Herner, A., Mello, S.S., Wirth, M., Hausmann, S., Sánchez-Rivera, F.J., Lofgren, S.M., Kuschma, T., Hahn, S.A., Vangala, D., et al. (2015). Combined inhibition of BET family proteins and histone deacetylases as a potential epigenetics-based therapy for pancreatic ductal adenocarcinoma. Nat. Med. *21*, 1163–1171.

McLean, C.Y., Bristor, D., Hiller, M., Clarke, S.L., Schaar, B.T., Lowe, C.B., Wenger, A.M., and Bejerano, G. (2010). GREAT improves functional interpretation of cis-regulatory regions. Nat. Biotechnol. *28*, 495–501.

Medina-Rivera, A., Defrance, M., Sand, O., Herrmann, C., Castro-Mondragon, J.A., Delerce, J., Jaeger, S., Blanchet, C., Vincens, P., Caron, C., et al. (2015). RSAT 2015: Regulatory Sequence Analysis Tools. Nucleic Acids Res. *43*, W50–W56.

Mertz, J.A., Conery, A.R., Bryant, B.M., Sandy, P., Balasubramanian, S., Mele, D.A., Bergeron, L., and Sims, R.J. (2011). Targeting MYC dependence in cancer by inhibiting BET bromodomains. Proc. Natl. Acad. Sci. *108*, 16669–16674.

Meyer, M.B., Benkusky, N.A., and Pike, J.W. (2014a). The RUNX2 Cistrome in Osteoblasts CHARACTERIZATION, DOWN-REGULATION FOLLOWING DIFFERENTIATION, AND RELATIONSHIP TO GENE EXPRESSION. J. Biol. Chem. *289*, 16016–16031.

Meyer, M.B., Benkusky, N.A., Lee, C.-H., and Pike, J.W. (2014b). Genomic Determinants of Gene Regulation by 1,25-Dihydroxyvitamin D3 during Osteoblast-lineage Cell Differentiation. J. Biol. Chem. *289*, 19539–19554.

Mikami, Y., Asano, M., Honda, M.J., and Takagi, M. (2010). Bone morphogenetic protein 2 and dexamethasone synergistically increase alkaline phosphatase levels through JAK/STAT signaling in C3H10T1/2 cells. J. Cell. Physiol. *223*, 123–133.

Minarovits, J., Banati, F., Szenthe, K., and Niller, H.H. (2016). Epigenetic Regulation. Adv. Exp. Med. Biol. *879*, 1–25.

Mink, S., Haenig, B., and Klempnauer, K.H. (1997). Interaction and functional collaboration of p300 and C/EBPbeta. Mol. Cell. Biol. *17*, 6609–6617.

Minsky, N., Shema, E., Field, Y., Schuster, M., Segal, E., and Oren, M. (2008). Monoubiquitinated H2B is associated with the transcribed region of highly expressed genes in human cells. Nat. Cell Biol. *10*, 483–488.

Miranda-Carboni, G.A., Guemes, M., Bailey, S., Anaya, E., Corselli, M., Peault, B., and Krum, S.A. (2011). GATA4 Regulates Estrogen Receptor-α-Mediated Osteoblast Transcription. Mol. Endocrinol. *25*, 1126–1136.

Mootha, V.K., Lindgren, C.M., Eriksson, K.-F., Subramanian, A., Sihag, S., Lehar, J., Puigserver, P., Carlsson, E., Ridderstråle, M., Laurila, E., et al. (2003). PGC-1α-responsive genes involved in oxidative phosphorylation are coordinately downregulated in human diabetes. Nat. Genet. *34*, 267–273.

Mousavi, K., Zare, H., Dell'Orso, S., Grontved, L., Gutierrez-Cruz, G., Derfoul, A., Hager, G.L., and Sartorelli, V. (2013). eRNAs Promote Transcription by Establishing Chromatin Accessibility at Defined Genomic Loci. Mol. Cell *51*, 606–617.

Movérare-Skrtic, S., Henning, P., Liu, X., Nagano, K., Saito, H., Börjesson, A.E., Sjögren, K., Windahl, S.H., Farman, H., Kindlund, B., et al. (2014). Osteoblast-derived WNT16 represses osteoclastogenesis and prevents cortical bone fragility fractures. Nat. Med. *20*, 1279–1288.

Nagarajan, S., Hossan, T., Alawi, M., Najafova, Z., Indenbirken, D., Bedi, U., Taipaleenmäki, H., Ben-Batalla, I., Scheller, M., Loges, S., et al. (2014). Bromodomain Protein BRD4 Is Required for Estrogen Receptor-Dependent Enhancer Activation and Gene Transcription. Cell Rep. *8*, 460–469.

Nagarajan, S., Benito, E., Fischer, A., Johnsen, S.A., Nagarajan, S., Benito, E., Fischer, A., and Johnsen, S.A. (2015). H4K12ac is regulated by estrogen receptor-alpha and is associated with BRD4 function and inducible transcription. Oncotarget *6*, 7305–7317.

Nakanishi, S., Lee, J.S., Gardner, K.E., Gardner, J.M., Takahashi, Y., Chandrasekharan, M.B., Sun, Z.-W., Osley, M.A., Strahl, B.D., Jaspersen, S.L., et al. (2009). Histone H2BK123 monoubiquitination is the critical determinant for H3K4 and H3K79 trimethylation by COMPASS and Dot1. J. Cell Biol. *186*, 371–377.

Nakashima, K., and de Crombrugghe, B. (2003). Transcriptional mechanisms in osteoblast differentiation and bone formation. Trends Genet. *19*, 458–466.

Ni, J., Shen, Y., Wang, Z., Shao, D., Liu, J., Kong, Y., Fu, L., Zhou, L., Xue, H., Huang, Y., et al. (2014). P300-dependent STAT3 acetylation is necessary for angiotensin II-induced pro-fibrotic responses in renal tubular epithelial cells. Acta Pharmacol. Sin. *35*, 1157–1166.

Nicolaidou, V., Wong, M.M., Redpath, A.N., Ersek, A., Baban, D.F., Williams, L.M., Cope, A.P., and Horwood, N.J. (2012). Monocytes Induce STAT3 Activation in Human Mesenchymal Stem Cells to Promote Osteoblast Formation. PLoS ONE *7*.

Nolis, I.K., McKay, D.J., Mantouvalou, E., Lomvardas, S., Merika, M., and Thanos, D. (2009). Transcription factors mediate long-range enhancer–promoter interactions. Proc. Natl. Acad. Sci. U. S. A. *106*, 20222–20227.

Orimo, H. (2010). The Mechanism of Mineralization and the Role of Alkaline Phosphatase in Health and Disease. J. Nippon Med. Sch. *77*, 4–12.

Otto, F., Thornell, A.P., Crompton, T., Denzel, A., Gilmour, K.C., Rosewell, I.R., Stamp, G.W.H., Beddington, R.S.P., Mundlos, S., Olsen, B.R., et al. (1997). Cbfa1, a Candidate Gene for Cleidocranial Dysplasia Syndrome, Is Essential for Osteoblast Differentiation and Bone Development. Cell *89*, 765–771.

Oury, F. (2012). A crosstalk between bone and gonads. Ann. N. Y. Acad. Sci. *1260*, 1–7.

Ozono, K., Liao, J., Kerner, S.A., Scott, R.A., and Pike, J.W. (1990). The vitamin D-responsive element in the human osteocalcin gene. Association with a nuclear proto-oncogene enhancer. J. Biol. Chem. *265*, 21881–21888.

Paredes, R., Arriagada, G., Cruzat, F., Villagra, A., Olate, J., Zaidi, K., van Wijnen, A., Lian, J.B., Stein, G.S., Stein, J.L., et al. (2004). Bone-Specific Transcription Factor Runx2 Interacts with the 1α,25-Dihydroxyvitamin D3 Receptor To Up-Regulate Rat Osteocalcin Gene Expression in Osteoblastic Cells. Mol. Cell. Biol. *24*, 8847–8861.

Park-Min, K.-H., Lim, E., Lee, M.J., Park, S.H., Giannopoulou, E., Yarilina, A., van der Meulen, M., Zhao, B., Smithers, N., Witherington, J., et al. (2014). Inhibition of osteoclastogenesis and inflammatory bone resorption by targeting BET proteins and epigenetic regulation. Nat. Commun. *5*, 5418.

Patel, M.C., Debrosse, M., Smith, M., Dey, A., Huynh, W., Sarai, N., Heightman, T.D., Tamura, T., and Ozato, K. (2013). BRD4 Coordinates Recruitment of Pause Release Factor P-TEFb and the Pausing Complex NELF/DSIF To Regulate Transcription Elongation of Interferon-Stimulated Genes. Mol. Cell. Biol. *33*, 2497–2507.

Paulson, M., Pisharody, S., Pan, L., Guadagno, S., Mui, A.L., and Levy, D.E. (1999). Stat Protein Transactivation Domains Recruit p300/CBP through Widely Divergent Sequences. J. Biol. Chem. *274*, 25343–25349.

Pavri, R., Zhu, B., Li, G., Trojer, P., Mandal, S., Shilatifard, A., and Reinberg, D. (2006). Histone H2B Monoubiquitination Functions Cooperatively with FACT to Regulate Elongation by RNA Polymerase II. Cell *125*, 703–717.

Peterkofsky, B., Gosiewska, A., Singh, K., Pearlman, S., and Mahmoodian, F. (1999). Species differences in cis-elements of the proalpha1(I) procollagen promoter and their binding proteins. J. Cell. Biochem. *73*, 408–422.

Pike, J.W., Lee, S.M., and Meyer, M.B. (2014). Regulation of gene expression by 1,25-dihydroxyvitamin D3 in bone cells: exploiting new approaches and defining new mechanisms. BoneKEy Rep. *3*, 482.

Pike, J.W., Meyer, M.B., St. John, H.C., and Benkusky, N.A. (2015). Epigenetic histone modifications and master regulators as determinants of context dependent nuclear receptor activity in bone cells. Bone *81*, 757–764.

Pirngruber, J., and Johnsen, S.A. (2010). Induced G1 cell-cycle arrest controls replication-dependent histone mRNA 3′ end processing through p21, NPAT and CDK9. Oncogene *29*, 2853–2863.

Pirngruber, J., Shchebet, A., Schreiber, L., Shema, E., Minsky, N., Chapman, R.D., Eick, D., Aylon, Y., Oren, M., and Johnsen, S.A. (2009). CDK9 directs H2B monoubiquitination and controls replication-dependent histone mRNA 3′-end processing. EMBO Rep. *10*, 894–900.

Prenzel, T., Begus-Nahrmann, Y., Kramer, F., Hennion, M., Hsu, C., Gorsler, T., Hintermair, C., Eick, D., Kremmer, E., Simons, M., et al. (2011). Estrogen-dependent gene transcription in human breast cancer cells relies upon proteasome-dependent monoubiquitination of histone H2B. Cancer Res. *71*, 5739–5753.

Prideaux, M., Findlay, D.M., and Atkins, G.J. (2016). Osteocytes: The master cells in bone remodelling. Curr. Opin. Pharmacol. *28*, 24–30.

Quinlan, A.R., and Hall, I.M. (2010). BEDTools: a flexible suite of utilities for comparing genomic features. Bioinformatics *26*, 841–842.

Raggatt, L.J., and Partridge, N.C. (2010). Cellular and Molecular Mechanisms of Bone Remodeling. J. Biol. Chem. *285*, 25103–25108.

Rahman, M.S., Akhtar, N., Jamil, H.M., Banik, R.S., and Asaduzzaman, S.M. (2015). TGF-β/BMP signaling and other molecular events: regulation of osteoblastogenesis and bone formation. Bone Res. *3*.

Rahman, S., Sowa, M.E., Ottinger, M., Smith, J.A., Shi, Y., Harper, J.W., and Howley, P.M. (2011). The Brd4 Extraterminal Domain Confers Transcription Activation Independent of pTEFb by Recruiting Multiple Proteins, Including NSD3 ▽. Mol. Cell. Biol. *31*, 2641–2652.

Rajagopalan, V., Vaidyanathan, M., Janardhanam, V.A., and Bradner, J.E. (2014). Pre-Clinical Analysis of Changes in Intra-cellular Biochemistry of Glioblastoma Multiforme (GBM) Cells Due to c-Myc Silencing. Cell. Mol. Neurobiol. *34*, 1059–1069.

Ramírez, F., Dündar, F., Diehl, S., Grüning, B.A., and Manke, T. (2014). deepTools: a flexible platform for exploring deep-sequencing data. Nucleic Acids Res. *42*, W187–W191.

Rauch, F. (2005). Bone growth in length and width: the Yin and Yang of bone stability. J. Musculoskelet. Neuronal Interact. *5*, 194–201.

Rauch, A., Seitz, S., Baschant, U., Schilling, A.F., Illing, A., Stride, B., Kirilov, M., Mandic, V., Takacz, A., Schmidt-Ullrich, R., et al. (2010). Glucocorticoids Suppress Bone Formation by Attenuating Osteoblast Differentiation via the Monomeric Glucocorticoid Receptor. Cell Metab. *11*, 517–531.

Robinson, J.T., Thorvaldsdóttir, H., Winckler, W., Guttman, M., Lander, E.S., Getz, G., and Mesirov, J.P. (2011). Integrative genomics viewer. Nat. Biotechnol. *29*, 24–26.

Roe, J.-S., Mercan, F., Rivera, K., Pappin, D.J., and Vakoc, C.R. (2015). BET Bromodomain Inhibition Suppresses the Function of Hematopoietic Transcription Factors in Acute Myeloid Leukemia. Mol. Cell *58*, 1028–1039.

Rossetto, D., Avvakumov, N., and Côté, J. (2012). Histone phosphorylation. Epigenetics *7*, 1098–1108.

Ross-Innes, C.S., Stark, R., Teschendorff, A.E., Holmes, K.A., Ali, H.R., Dunning, M.J., Brown, G.D., Gojis, O., Ellis, I.O., Green, A.R., et al. (2012). Differential oestrogen receptor binding is associated with clinical outcome in breast cancer. Nature *481*, 389–393.

Russell, P.K., Clarke, M.V., Cheong, K., Anderson, P.H., Morris, H.A., Wiren, K.M., Zajac, J.D., and Davey, R.A. (2015). Androgen receptor action in osteoblasts in male mice is dependent on their stage of maturation. J. Bone Miner. Res. Off. J. Am. Soc. Bone Miner. Res. *30*, 809–823.

Sabatakos, G., Sims, N.A., Chen, J., Aoki, K., Kelz, M.B., Amling, M., Bouali, Y., Mukhopadhyay, K., Ford, K., Nestler, E.J., et al. (2000). Overexpression of ΔFosB transcription factor(s) increases bone formation and inhibits adipogenesis. Nat. Med. *6*, 985–990.

Samara, N.L., Datta, A.B., Berndsen, C.E., Zhang, X., Yao, T., Cohen, R.E., and Wolberger, C. (2010). Structural Insights into the Assembly and Function of the SAGA Deubiquitinating Module. Science *328*, 1025–1029.

Samee, N., Geoffroy, V., Marty, C., Schiltz, C., Vieux-Rochas, M., Levi, G., and de Vernejoul, M.-C. (2008). Dlx5, a positive regulator of osteoblastogenesis, is essential for osteoblast-osteoclast coupling. Am. J. Pathol. *173*, 773–780.

Schaukowitch, K., Joo, J.-Y., Liu, X., Watts, J.K., Martinez, C., and Kim, T.-K. (2014). Enhancer RNA Facilitates NELF Release from Immediate Early Genes. Mol. Cell *56*, 29–42.

Schröder, S., Cho, S., Zeng, L., Zhang, Q., Kaehlcke, K., Mak, L., Lau, J., Bisgrove, D., Schnölzer, M., Verdin, E., et al. (2012). Two-pronged Binding with Bromodomain-containing Protein 4 Liberates Positive Transcription Elongation Factor b from Inactive Ribonucleoprotein Complexes. J. Biol. Chem. *287*, 1090–1099.

Schroeder, T.M., Nair, A.K., Staggs, R., Lamblin, A.-F., and Westendorf, J.J. (2007). Gene profile analysis of osteoblast genes differentially regulated by histone deacetylase inhibitors. BMC Genomics *8*, 362.

Schwartz, C., Beck, K., Mink, S., Schmolke, M., Budde, B., Wenning, D., and Klempnauer, K.-H. (2003). Recruitment of p300 by C/EBPβ triggers phosphorylation of p300 and modulates coactivator activity. EMBO J. *22*, 882–892.

Seeman, E. (2009). Bone modeling and remodeling. Crit. Rev. Eukaryot. Gene Expr. *19*, 219–233.

Senn, S.M., Kantor, S., Poulton, I.J., Morris, M.J., Sims, N.A., O'Brien, T.J., and Wark, J.D. (2010). Adverse effects of valproate on bone: defining a model to investigate the pathophysiology. Epilepsia *51*, 984–993.

Shchebet, A., Karpiuk, O., Kremmer, E., Eick, D., and Johnsen, S.A. (2012). Phosphorylation by cyclin-dependent kinase-9 controls ubiquitin-conjugating enzyme-2A function. Cell Cycle *11*, 2122–2127.

Shema, E., Tirosh, I., Aylon, Y., Huang, J., Ye, C., Moskovits, N., Raver-Shapira, N., Minsky, N., Pirngruber, J., Tarcic, G., et al. (2008). The histone H2B-specific ubiquitin ligase RNF20/hBRE1 acts as a putative tumor suppressor through selective regulation of gene expression. Genes Dev. *22*, 2664–2676.

Shi, J., Wang, Y., Zeng, L., Wu, Y., Deng, J., Zhang, Q., Lin, Y., Li, J., Kang, T., Tao, M., et al. (2014). Disrupting the Interaction of BRD4 with Di-acetylated Twist Suppresses Tumorigenesis in Basal-like Breast Cancer. Cancer Cell *25*, 210–225.

Shimizu, E., Selvamurugan, N., Westendorf, J.J., Olson, E.N., and Partridge, N.C. (2010). HDAC4 Represses Matrix Metalloproteinase-13 Transcription in Osteoblastic Cells, and Parathyroid Hormone Controls This Repression. J. Biol. Chem. *285*, 9616–9626.

Shimoyama, A., Wada, M., Ikeda, F., Hata, K., Matsubara, T., Nifuji, A., Noda, M., Amano, K., Yamaguchi, A., Nishimura, R., et al. (2007). Ihh/Gli2 Signaling Promotes Osteoblast Differentiation by Regulating Runx2 Expression and Function. Mol. Biol. Cell *18*, 2411–2418.

Shin, H., Liu, T., Manrai, A.K., and Liu, X.S. (2009). CEAS: cis-regulatory element annotation system. Bioinformatics *25*, 2605–2606.

Siersbæk, R., Nielsen, R., John, S., Sung, M.-H., Baek, S., Loft, A., Hager, G.L., and Mandrup, S. (2011). Extensive chromatin remodelling and establishment of transcription factor ‘hotspots’’ during early adipogenesis.’ EMBO J. *30*, 1459–1472.

Silva, B.C., and Bilezikian, J.P. (2015). Parathyroid hormone: anabolic and catabolic actions on the skeleton. Curr. Opin. Pharmacol. *22*, 41–50.

Simonet, W.S., Lacey, D.L., Dunstan, C.R., Kelley, M., Chang, M.-S., Lüthy, R., Nguyen, H.Q., Wooden, S., Bennett, L., Boone, T., et al. (1997). Osteoprotegerin: A Novel Secreted Protein Involved in the Regulation of Bone Density. Cell *89*, 309–319.

Sims, N.A., and Martin, T.J. (2014). Coupling the activities of bone formation and resorption: a multitude of signals within the basic multicellular unit. BoneKEy Rep. *3*, 481.

Song, T.-Y., Yang, J.-H., Park, J.Y., Song, Y., Han, J.-W., Youn, H.-D., and Cho, E.-J. (2012). The role of histone chaperones in osteoblastic differentiation of C2C12 myoblasts. Biochem. Biophys. Res. Commun. *423*, 726–732.

St John, H.C., Bishop, K.A., Meyer, M.B., Benkusky, N.A., Leng, N., Kendziorski, C., Bonewald, L.F., and Pike, J.W. (2014). The osteoblast to osteocyte transition: epigenetic changes and response to the vitamin D3 hormone. Mol. Endocrinol. Baltim. Md *28*, 1150–1165.

Stein, C., Bardet, A.F., Roma, G., Bergling, S., Clay, I., Ruchti, A., Agarinis, C., Schmelzle, T., Bouwmeester, T., Schübeler, D., et al. (2015). YAP1 Exerts Its Transcriptional Control via TEAD-Mediated Activation of Enhancers. PLoS Genet. *11*.

Steinbok, P., Hall, J., and Flodmark, O. (1989). Hydrocephalus in achondroplasia: the possible role of intracranial venous hypertension. J. Neurosurg. *71*, 42–48.

Stonestrom, A.J., Hsu, S.C., Jahn, K.S., Huang, P., Keller, C.A., Giardine, B.M., Kadauke, S., Campbell, A.E., Evans, P., Hardison, R.C., et al. (2015). Functions of BET proteins in erythroid gene expression. Blood *125*, 2825–2834.

Strahl, B.D., and Allis, C.D. (2000). The language of covalent histone modifications. Nature *403*, 41–45.

Su, W.-X., Li, Q.-Z., Zuo, Y.-C., and Zhang, L.-Q. (2016). Association analysis between the distributions of histone modifications and gene expression in the human embryonic stem cell. Gene *575*, 90–100.

Subramanian, A., Tamayo, P., Mootha, V.K., Mukherjee, S., Ebert, B.L., Gillette, M.A., Paulovich, A., Pomeroy, S.L., Golub, T.R., Lander, E.S., et al. (2005). Gene set enrichment analysis: A knowledge-based approach for interpreting genome-wide expression profiles. Proc. Natl. Acad. Sci. *102*, 15545–15550.

Sugatani, T., and Hruska, K.A. (2013). Down-regulation of miR-21 biogenesis by estrogen action contributes to osteoclastic apoptosis. J. Cell. Biochem. *114*, 1217–1222.

Sugatani, T., Vacher, J., and Hruska, K.A. (2011). A microRNA expression signature of osteoclastogenesis. Blood *117*, 3648–3657.

Supek, F., Bošnjak, M., Škunca, N., and Šmuc, T. (2011). REVIGO Summarizes and Visualizes Long Lists of Gene Ontology Terms. PLoS ONE *6*, e21800.

Sussman, R.T., Stanek, T.J., Esteso, P., Gearhart, J.D., Knudsen, K.E., and McMahon, S.B. (2013). The Epigenetic Modifier Ubiquitin-specific Protease 22 (USP22) Regulates Embryonic Stem Cell Differentiation via Transcriptional Repression of Sex-determining Region Y-box 2 (SOX2). J. Biol. Chem. *288*, 24234–24246.

Suzuki, H.K., and Mathews, A. (1966). Two-Color Fluorescent Labeling of Mineralizing Tissues with Tetracycline and 2,4-Bis[N,N'-Di-(Carbomethyl)Aminomethyl] Fluorescein. Stain Technol. *41*, 57–60.

Syed, F., and Khosla, S. (2005). Mechanisms of sex steroid effects on bone. Biochem. Biophys. Res. Commun. *328*, 688–696.

Szutorisz, H., Canzonetta, C., Georgiou, A., Chow, C.-M., Tora, L., and Dillon, N. (2005). Formation of an Active Tissue-Specific Chromatin Domain Initiated by Epigenetic Marking at the Embryonic Stem Cell Stage. Mol. Cell. Biol. *25*, 1804–1820.

Takada, I., Mihara, M., Suzawa, M., Ohtake, F., Kobayashi, S., Igarashi, M., Youn, M.-Y., Takeyama, K., Nakamura, T., Mezaki, Y., et al. (2007). A histone lysine methyltransferase activated by non-canonical Wnt signalling suppresses PPAR-gamma transactivation. Nat. Cell Biol. *9*, 1273–1285.

Takeuchi, Y., Kodama, Y., and Matsumoto, T. (1994). Bone matrix decorin binds transforming growth factor-beta and enhances its bioactivity. J. Biol. Chem. *269*, 32634–32638.

Tanny, J.C., Erdjument-Bromage, H., Tempst, P., and Allis, C.D. (2007). Ubiquitylation of histone H2B controls RNA polymerase II transcription elongation independently of histone H3 methylation. Genes Dev. *21*, 835–847.

Tarcic, O., Pateras, I.S., Cooks, T., Shema, E., Kanterman, J., Ashkenazi, H., Boocholez, H., Hubert, A., Rotkopf, R., Baniyash, M., et al. (2016). RNF20 Links Histone H2B Ubiquitylation with Inflammation and Inflammation-Associated Cancer. Cell Rep. *14*, 1462–1476.

Thomas-Chollier, M., Herrmann, C., Defrance, M., Sand, O., Thieffry, D., and Helden, J. van (2011). RSAT peak-motifs: motif analysis in full-size ChIP-seq datasets. Nucleic Acids Res. gkr1104.

Thomas-Chollier, M., Darbo, E., Herrmann, C., Defrance, M., Thieffry, D., and van Helden, J. (2012). A complete workflow for the analysis of full-size ChIP-seq (and similar) data sets using peak-motifs. Nat. Protoc. *7*, 1551–1568.

Thorvaldsdóttir, H., Robinson, J.T., and Mesirov, J.P. (2013). Integrative Genomics Viewer (IGV): high-performance genomics data visualization and exploration. Brief. Bioinform. *14*, 178–192.

Tsai, L.-H., Wu, J.-Y., Cheng, Y.-W., Chen, C.-Y., Sheu, G.-T., Wu, T.-C., and Lee, H. (2015). The MZF1/c-MYC axis mediates lung adenocarcinoma progression caused by wild-type lkb1 loss. Oncogene *34*, 1641–1649.

Tu, X., Joeng, K.S., Nakayama, K.I., Nakayama, K., Rajagopal, J., Carroll, T.J., McMahon, A.P., and Long, F. (2007). Noncanonical Wnt Signaling through G Protein-Linked PKCδ Activation Promotes Bone Formation. Dev. Cell *12*, 113–127.

Twine, N.A., Chen, L., Pang, C.N., Wilkins, M.R., and Kassem, M. (2014). Identification of differentiation-stage specific markers that define the ex vivo osteoblastic phenotype. Bone *67*, 23–32.

Väänänen, K. (2005). Mechanism of osteoclast mediated bone resorption—rationale for the design of new therapeutics. Adv. Drug Deliv. Rev. *57*, 959–971.

Venkataraman, S., Alimova, I., Balakrishnan, I., Harris, P., Birks, D.K., Griesinger, A., Amani, V., Cristiano, B., Remke, M., Taylor, M.D., et al. (2014). Inhibition of BRD4 attenuates tumor cell self-renewal and suppresses stem cell signaling in MYC driven medulloblastoma. Oncotarget *5*, 2355–2371.

Ventura, A., Kirsch, D.G., McLaughlin, M.E., Tuveson, D.A., Grimm, J., Lintault, L., Newman, J., Reczek, E.E., Weissleder, R., and Jacks, T. (2007). Restoration of p53 function leads to tumour regression in vivo. Nature *445*, 661–665.

Verdone, L., Caserta, M., and Mauro, E.D. (2005). Role of histone acetylation in the control of gene expression. Biochem. Cell Biol. *83*, 344–353.

Vlaming, H., Welsem, T., Graaf, E.L., Ontoso, D., Altelaar, A.M., San-Segundo, P.A., Heck, A.J., and Leeuwen, F. (2014). Flexibility in crosstalk between H2B ubiquitination and H3 methylation in vivo. EMBO Rep. *15*, 1077–1084.

Vrtačnik, P., Marc, J., and Ostanek, B. (2014). Epigenetic mechanisms in bone. Clin. Chem. Lab. Med. *52*, 589–608.

Wang, C.-Y., and Filippakopoulos, P. (2015). Beating the odds: BETs in disease. Trends Biochem. Sci. *40*, 468–479.

Wang, Z., and McCauley, L.K. (2011). Osteoclasts and odontoclasts: signaling pathways to development and disease. Oral Dis. *17*, 129–142.

Wang, R., Li, Q., Helfer, C.M., Jiao, J., and You, J. (2012). Bromodomain Protein Brd4 Associated with Acetylated Chromatin Is Important for Maintenance of Higher-order Chromatin Structure. J. Biol. Chem. *287*, 10738–10752.

Wang, X., Guo, B., Li, Q., Peng, J., Yang, Z., Wang, A., Li, D., Hou, Z., Lv, K., Kan, G., et al. (2013). miR-214 targets ATF4 to inhibit bone formation. Nat. Med. *19*, 93–100.

Warnes, G.R., Bolker, B., Bonebakker, L., Gentleman, R., Liaw, W.H.A., Lumley, T., Maechler, M., Magnusson, A., Moeller, S., Schwartz, M., et al. (2015). gplots: Various R Programming Tools for Plotting Data.

Wei, Y., Chen, Y.-H., Li, L.-Y., Lang, J., Yeh, S.-P., Shi, B., Yang, C.-C., Yang, J.-Y., Lin, C.-Y., Lai, C.-C., et al. (2011). CDK1-dependent phosphorylation of EZH2 suppresses methylation of H3K27 and promotes osteogenic differentiation of human mesenchymal stem cells. Nat. Cell Biol. *13*, 87–94.

Wickham, H. (2009). ggplot2 - Elegant Graphics for Data Analysis | Hadley Wickham | Springer.

Wise, G.E., Frazier-Bowers, S., and D'Souza, R.N. (2002). Cellular, Molecular, and Genetic Determinants of Tooth Eruption. Crit. Rev. Oral Biol. Med. *13*, 323–335.

Woo, S.M., Rosser, J., Dusevich, V., Kalajzic, I., and Bonewald, L.F. (2011). Cell line IDG-SW3 replicates osteoblast-to-late-osteocyte differentiation in vitro and accelerates bone formation in vivo. J. Bone Miner. Res. Off. J. Am. Soc. Bone Miner. Res. *26*, 2634–2646.

Wood, A., Schneider, J., Dover, J., Johnston, M., and Shilatifard, A. (2005). The Bur1/Bur2 Complex Is Required for Histone H2B Monoubiquitination by Rad6/Bre1 and Histone Methylation by COMPASS. Mol. Cell *20*, 589–599.

Wright, D.E., Wang, C.-Y., and Kao, C.-F. (2011). Flickin' the ubiquitin switch. Epigenetics *6*, 1165–1175.

Wu, H., and Zhang, Y. (2014). Reversing DNA Methylation: Mechanisms, Genomics, and Biological Functions. Cell *156*, 45–68.

Wu, M., Chen, G., and Li, Y.-P. (2016). TGF-β and BMP signaling in osteoblast, skeletal development, and bone formation, homeostasis and disease. Bone Res. *4*.

Wu, S.-Y., Lee, A.-Y., Lai, H.-T., Zhang, H., and Chiang, C.-M. (2013). Phospho Switch Triggers Brd4 Chromatin Binding and Activator Recruitment for Gene-Specific Targeting. Mol. Cell *49*, 843–857.

Xiao, H., Tian, Y., Yang, Y., Hu, F., Xie, X., Mei, J., and Ding, F. (2015). USP22 acts as an oncogene by regulating the stability of cyclooxygenase-2 in non-small cell lung cancer. Biochem. Biophys. Res. Commun. *460*, 703–708.

Xu, C.-R., Cole, P.A., Meyers, D.J., Kormish, J., Dent, S., and Zaret, K.S. (2011). Chromatin "Pre-Pattern" and Histone Modifiers in a Fate Choice for Liver and Pancreas. Science *332*, 963–966.

Xu, Y., Ayrapetov, M.K., Xu, C., Gursoy-Yuzugullu, O., Hu, Y., and Price, B.D. (2012). Histone H2A.Z controls a critical chromatin remodeling step required for DNA double-strand break repair. Mol. Cell *48*, 723–733.

Yamaguchi, Y., Takagi, T., Wada, T., Yano, K., Furuya, A., Sugimoto, S., Hasegawa, J., and Handa, H. (1999). NELF, a Multisubunit Complex Containing RD, Cooperates with DSIF to Repress RNA Polymerase II Elongation. Cell *97*, 41–51.

Yamaguchi, Y., Shibata, H., and Handa, H. (2013). Transcription elongation factors DSIF and NELF: Promoter-proximal pausing and beyond. Biochim. Biophys. Acta BBA - Gene Regul. Mech. *1829*, 98–104.

Yamashita, T., Yao, Z., Li, F., Zhang, Q., Badell, I.R., Schwarz, E.M., Takeshita, S., Wagner, E.F., Noda, M., Matsuo, K., et al. (2007). NF-κB p50 and p52 Regulate Receptor Activator of NF-κB Ligand (RANKL) and Tumor Necrosis Factor-induced Osteoclast Precursor Differentiation by Activating c-Fos and NFATc1. J. Biol. Chem. *282*, 18245–18253.

Yang, Z., Yik, J.H.N., Chen, R., He, N., Jang, M.K., Ozato, K., and Zhou, Q. (2005). Recruitment of P-TEFb for Stimulation of Transcriptional Elongation by the Bromodomain Protein Brd4. Mol. Cell *19*, 535–545.

Ye, J., Coulouris, G., Zaretskaya, I., Cutcutache, I., Rozen, S., and Madden, T.L. (2012a). Primer-BLAST: a tool to design target-specific primers for polymerase chain reaction. BMC Bioinformatics *13*, 134.

Ye, L., Fan, Z., Yu, B., Chang, J., Hezaimi, K.A., Zhou, X., Park, N.-H., and Wang, C.-Y. (2012b). Histone Demethylases KDM4B and KDM6B Promotes Osteogenic Differentiation Of Human MSCs. Cell Stem Cell *11*, 50–61.

Young, M.D., Wakefield, M.J., Smyth, G.K., and Oshlack, A. (2010). Gene ontology analysis for RNA-seq: accounting for selection bias. Genome Biol. *11*, R14.

Zaret, K.S., and Carroll, J.S. (2011). Pioneer transcription factors: establishing competence for gene expression. Genes Dev. *25*, 2227–2241.

Zhang, F., and Yu, X. (2011). WAC, a Functional Partner of RNF20/40, Regulates Histone H2B Ubiquitination and Gene Transcription. Mol. Cell *41*, 384–397.

Zhang, Y., and Reinberg, D. (2001). Transcription regulation by histone methylation: interplay between different covalent modifications of the core histone tails. Genes Dev. *15*, 2343–2360.

Zhang, M., Xuan, S., Bouxsein, M.L., Stechow, D. von, Akeno, N., Faugere, M.C., Malluche, H., Zhao, G., Rosen, C.J., Efstratiadis, A., et al. (2002). Osteoblast-specific Knockout of the Insulin-like Growth Factor (IGF) Receptor Gene Reveals an Essential Role of IGF Signaling in Bone Matrix Mineralization. J. Biol. Chem. *277*, 44005–44012.

Zhang, R., Shao, J., and Xiang, L. (2011a). GADD45A protein plays an essential role in active DNA demethylation during terminal osteogenic differentiation of adipose-derived mesenchymal stem cells. J. Biol. Chem. *286*, 41083–41094.

Zhang, W., Prakash, C., Sum, C., Gong, Y., Li, Y., Kwok, J.J.T., Thiessen, N., Pettersson, S., Jones, S.J.M., Knapp, S., et al. (2012). Bromodomain-containing Protein 4 (BRD4) Regulates RNA Polymerase II Serine 2 Phosphorylation in Human CD4+ T Cells. J. Biol. Chem. *287*, 43137–43155.

Zhang, Y., Liu, T., Meyer, C.A., Eeckhoute, J., Johnson, D.S., Bernstein, B.E., Nusbaum, C., Myers, R.M., Brown, M., Li, W., et al. (2008). Model-based Analysis of ChIP-Seq (MACS). Genome Biol. *9*, R137–R137.

Zhang, Y., Yao, L., Zhang, X., Ji, H., Wang, L., Sun, S., and Pang, D. (2011b). Elevated expression of USP22 in correlation with poor prognosis in patients with invasive breast cancer. J. Cancer Res. Clin. Oncol. *137*, 1245–1253.

Zhao, Y., Lang, G., Ito, S., Bonnet, J., Metzger, E., Sawatsubashi, S., Suzuki, E., Le Guezennec, X., Stunnenberg, H.G., Krasnov, A., et al. (2008). A TFTC/STAGA Module Mediates Histone H2A and H2B Deubiquitination, Coactivates Nuclear Receptors, and Counteracts Heterochromatin Silencing. Mol. Cell *29*, 92–101.

Zhao, Y., Wang, L., Ren, S., Wang, L., Blackburn, P.R., McNulty, M.S., Gao, X., Qiao, M., Vessella, R.L., Kohli, M., et al. (2016). Activation of P-TEFb by Androgen Receptor-Regulated Enhancer RNAs in Castration-Resistant Prostate Cancer. Cell Rep. *15*, 599–610.

Zhou, H., Newnum, A.B., Martin, J.R., Li, P., Nelson, M.T., Moh, A., Fu, X.-Y., Yokota, H., and Li, J. (2011). Osteoblast/osteocyte-specific inactivation of Stat3 decreases load-driven bone formation and accumulates reactive oxygen species. Bone *49*, 404–411.

Zhu, L., and Xu, P.-C. (2013). Downregulated LncRNA-ANCR promotes osteoblast differentiation by targeting EZH2 and regulating Runx2 expression. Biochem. Biophys. Res. Commun. *432*, 612–617.

Zhu, B., Zheng, Y., Pham, A.-D., Mandal, S.S., Erdjument-Bromage, H., Tempst, P., and Reinberg, D. (2005). Monoubiquitination of Human Histone H2B: The Factors Involved and Their Roles in HOX Gene Regulation. Mol. Cell *20*, 601–611.

Zhu, J., He, F., Hu, S., and Yu, J. (2008). On the nature of human housekeeping genes. Trends Genet. *24*, 481–484.

Zuo, C., Wang, Z., Lu, H., Dai, Z., Liu, X., and Cui, L. (2013). Expression profiling of lncRNAs in C3H10T1/2 mesenchymal stem cells undergoing early osteoblast differentiation. Mol. Med. Rep. *8*, 463–467.

Curriculum Vitae

Zeynab Najafova
born on 15.05.1986 in Baku, Azerbaijan

Address: Philipp-Reis-Straße 5, 37075 Göttingen, Germany
Email: zeynab.najafova@gmail.com

Education:

07.2014 – present	Ph.D, Genes and Development, Göttingen Graduate School for Neurosciences, Biophysics, and Molecular Biosciences (GGNB), Georg-August-Universität Göttingen, Germany.
07.2012 – 06.2014	Ph.D, Molecuar Medicine, University Medical Center Hamburg–Eppendorf, Germany
10.2012 – 10.2014	Graduate Program in Molecular Biology, Center for Molecular Neurobiology Hamburg (ZMNH)
10.2010 – 05.2012	M.Sc., Molecular Medicine, University Medical Center Göttingen
09.2004 – 06.2009	Azerbaijan Medical University, Faculty of Medical Biology; Obtained degree, Diploma

Fellowships held:

10.2010 – 04.2012	DAAD – Scholarship for Master Studies
07.2006	DAAD – Scholarship, Summer Language Course in Leipzig
08.2003 – 06.2004	High School Exchange Program Fellowship CCI/Soros Foundation, Houston, TX, USA

Academic experience:

07.2012 – present	Doctoral studies under supervision of Prof. Dr. Steven A. Johnsen. Project: Epigenetic Regulation of Osteoblast Differentiation
· 07.2014 – present	Departement of General, Visceral and Pediatric Surgery, University Medical Center, Göttingen, Germany.

· 06.2012 – 06.2014	Institute for Tumor Biology, University Hospital Hamburg-Eppendorf, Hamburg, Germany
10.2011 – 05.2012	Master thesis project under supervision of Prof. Dr. Steven A. Johnsen Project: Role of H2B monoubiquitination and its upstream regulators in mesenchymal stem cell differentiation. Department of Molecular Oncology, University Medical Center Göttingen, Germany
08.2009 – 07.2010	Internship at Genetical Laboratory of Research Institute of Gynecology and Obstetrics in Baku, Azerbaijan

List of publications:

Zeynab Najafova, Roberto Tirado Magallanes, Malayannan Subramaniam, Tareq Hossan, Sankari Nagarajan, Simon Baumgart, Vivek Kumar Mishra, Geske Schmidt, Upasana Bedi, Eric Hesse, Stefan Knapp, John R. Hawse, Steven A. Johnsen. BRD4 localization to lineage-specific enhancers is associated with a distinct transcription factor repertoire. *Nucleic Acid Research* (under revision).

Anusha Sriraman, Marija Radovanovic, Magdalena Wienken, **Zeynab Najafova**, Yizhu Li and Matthias Dobbelstein. Cooperation of Nutlin-3a and a Wip1 inhibitor to induce p53 activity. *Oncotarget,* 2016 (Epub ahead of print).

Magdalena Wienken, Antje Dickmanns, Alice Nemajerova, Daniela Kramer, **Zeynab Najafova**, Miriam Weiss, Oleksandra Karpiuk, Moustapha Kassem, Yanping Zhang, Guillermina Lozano, Steven A. Johnsen, Ute M. Moll, Xin Zhang, Matthias Dobbelstein. MDM2 Associates with Polycomb Repressor Complex 2 and Enhances Stemness-Promoting Chromatin Modifications Independent of p53. *Molecular Cell,* 2016 Jan 7;61(1):68-83.

Sankari Nagarajan, Tareq Hossan, Malik Alawi, **Zeynab Najafova**, Daniela Indenbirken, Upasana Bedi, Hanna Taipaleenmäki, Isabel Ben-Batalla, Marina Scheller, Sonja Loges, Stefan Knapp, Eric Hesse, Cheng-Ming Chiang, Adam Grundhoff, Steven. A. Johnsen. Bromodomain protein BRD4 is required for estrogen receptor-dependent enhancer activation and gene transcription. *Cell Reports,* 2014 Jul 24;8(2):460-9.

Oleksandra Karpiuk, **Zeynab Najafova**, Frank Kramer, Magali Hennion, Christina Galonska, Annekatrin König, Nicolas Snaidero, Tanja Vogel, Andrei Shchebet, Yvonne Begus-Nahrmann, Moustapha Kassem, Mikael Simons, Halyna Shcherbata, Tim Beissbarth, Steven. A. Johnsen. The Histone H2B Monoubiquitination Regulatory Pathway Is Required for Differentiation of Multipotent Stem Cells. *Molecular Cell*, 2012 Jun 8;46(5):705-13

Meetings and conferences:

Invited speaker for short talk. 2nd International Symposium on Mesenchymal Stem Cell Differentiation. Odense, Denmark. June, 2016. Title: Role of BRD4 in osteoblast differentiation.

Plenary poster presentation. ASBMR 2015 Annual Meeting, Seattle, WA, USA. October, 2015.

EpiGeneSys workshop "Epigenomics as Discovery Tool in Current Biology". Mainz, Germany. September, 2013.

Poster presentation. 10th EMBL conference on Transcription and Chromatin. Heidelberg, Germany. August, 2012.

Laboratory and research skills:

Molecular biology techniques: Conventional PCR, qRT-PCR, gel-electrophoresis, western blotting, chromatin immunoprecipitation from cells and tissue samples, ChIP-seq and RNA-seq library preparation, alkaline phosphatase, alizarin red and Oil Red O stainings, immunofluorescence and immunohistochemical stainings, microscopy.

Bioinformatic analysis: TopHat, Bowtie, HTSeq, GSEA, DAVID, MACS, SAMTools, BEDTools, EpiCSeg, Picard Tools, Galaxy, Cistrome, deepTools, UCSC Genome Browser, IGV, RSAT, ReMap, GREAT, Linux and R tools.

Cell culture: Mammalian S1 and S2 work, transfections, isolation of primary bone cells.

Animal work: FELASA B certificate

Language skills:

Azerbaijani – mother tongue
Russian – very good
English – very good (TOEFL IBT - 105)
German – good (Göthe Certificate B2)
Turkish – good

References:

Prof. Dr. Steven A Johnsen
Department of General, Visceral and Pediatric Surgery
University Medical Center Göttingen
37075 Göttingen, Germany
Email: steven.johnsen@med.uni-goettingen.de

Prof. Dr. Hans Will
Institute for Tumor Biology
University Hospital Hamburg-Eppendorf
20246 Hamburg, Germany
Email: hanskilianwill@gmail.com

Comments

The first part of the Ph.D dissertation related to the function of BRD4 in osteoblasts was later published in the open access journal Nucleic Acids Research (Oxford University Press) as an article:

Zeynab Najafova, Roberto Tirado-Magallanes, Malayannan Subramaniam, Tareq Hossan, Geske Schmidt, Sankari Nagarajan, Simon J. Baumgart, Vivek Kumar Mishra, Upasana Bedi, Eric Hesse, Stefan Knapp, John R. Hawse, Steven A. Johnsen; *BRD4 localization to lineage-specific enhancers is associated with a distinct transcription factor repertoire*. ***Nucleic Acids Research*** 2017; 45 (1): 127-141. DOI:https://doi.org/10.1093/nar/gkw826